USGS Award Number G13AP00065

Factors controlling strong motion in the normal faulting sequence of earthquakes in southern Fukushima, Japan

John G. Anderson

Nevada Seismological Laboratory

University of Nevada
Reno, Nevada 89557

Office: 775-784-1954
Fax: 775-784-4165

email: jga@unr.edu

August 1, 2013 - July 31, 2015

Abstract

A sequence of normal-faulting events in Japan following the 2011 Tohoku earthquake have greatly increased the number of strong-motion records for normal earthquakes. Anderson et al. (2013) found that peak horizontal accelerations (PGA) and velocities (PGV) during the Mw6.7 mainshock were significantly higher than the 2008 NGA ground motion prediction equation. This paper compares PGA and PGV for 16 normal events with Mw>=5 to the 2014 NGA2 West GMPEs. The residual for an individual station, s, in earthquake e is defined as $\delta_{es} = \ln(PGA_{obs}/PGA_{model})$, or the equivalent equation for PGV. Values of δ_{es} are estimated by two alternative approaches. In the first, site-specific estimates of v_{S30} are used in the NGA relations to directly estimate an expected value of PGA_{model} or PGV_{model}. In the second, the site-specific station corrections of Kawase and Matsuo (2004) have been applied, as was done by Anderson et al. (2013), to convert the observations to a common site condition with $v_{S30} = 760m/s$, and these values are compared to the NGA models for that site condition. By either method, for an individual earthquake, the values of δ_{es} increase rapidly with distance for the first 100 km, beyond which the distance dependence is weaker and depends on the model. Event terms, i.e. the average of δ_{es} over multiple stations for a single earthquake e, therefore depend on the distance range used for the average. This study uses the distance range from 0 to 100 km to estimate the event terms, since this is the most significant range of distances for seismic hazards; this range is smaller than the range from 0-300 km over which the NGA2-West relations are intended to apply. The event terms by the two methods differ. Several explanations are possible, and complete resolution requires additional study. One significant, and interesting, result is that the event terms show a fairly systematic dependence on depth, consistent with the idea that deeper earthquakes tend to have a higher stress drop. Regardless of the method, the event terms are greater than zero for 10 of the 14 events, indicating that more research is needed to understand the regional differences in normal faulting ground motions, to assure that they are properly represented in the US National Seismic Hazard Model.

Comparison of 2011 Fukushima-Hamadori Normal-Faulting Earthquakes with NGAW2

John G. Anderson, Hiroshi Kawase, Kevin M. McBean

May 1, 2016

Abstract

A sequence of normal-faulting events in Japan following the 2011 Tohoku earthquake have greatly increased the number of strong-motion records for normal earthquakes. Anderson et al. (2013) found that peak horizontal accelerations (PGA) and velocities (PGV) during the Mw6.7 mainshock were significantly higher than the 2008 NGA ground motion prediction equation. This paper compares PGA and PGV for 14 normal events with $M_W \geq 5$ to the 2014 NGA2 West GMPEs. The residual for an individual station, s, in earthquake e is defined as $\delta_{es} = \ln(PGA_{obs}/PGA_{model})$, or the equivalent equation for PGV. Values of δ_{es} are estimated by two alternative approaches. In the first, the "NGA method", site-specific estimates of v_{S30} are used in the NGA relations to directly estimate an expected value of PGA_{model} or PGV_{model}. In the second, the "KM method", the site-specific station corrections of Kawase and Matsuo (2004) have been applied, as was done by Anderson et al. (2013), to convert the observations to a common site condition with $v_{S30} = 760m/s$, and these values are compared to the NGA models for that site condition. By either method, for an individual earthquake, the values of δ_{es} increase rapidly with distance for the first 100 km, beyond which the distance dependence is weaker and depends on the model. The average of δ_{es} over multiple stations for a single earthquake e, therefore depends on the distance range used for the average. This study uses the distance range from 0 to 100 km to estimate the average "event terms", since this is the most significant range of distances for seismic hazards; this range is smaller than the range from 0-300 km over which the NGA2-West relations are intended to apply. The event terms by the NGA and KM methods differ. Several explanations are possible, and complete resolution requires additional study. The event terms show a fairly systematic dependence on depth, consistent with the idea that deeper earthquakes tend to have a higher stress drop, even over the limited shallow depth range spanned by these earthquakes. Regardless of the method, the event terms are greater than zero for 10 of the 14 events, indicating that more research is needed to understand the regional differences in normal faulting ground motions, to assure that they are properly represented in the US National Seismic Hazard Model.

Introduction

In the global database of strong earthquake ground motions, there is considerably less data for large normal faulting events in the shallow crust than for events with strike-slip and reverse mechanisms. Beginning on March 18, 2011, a sequence of very well recorded normal faulting earthquakes with magnitudes up to M_W 6.7 occurred near the city of Iwaki in eastern Tohoku, Japan. The general region can be described as the Ibaraki- Fukushima border region (e.g. Imanishi et al., 2012 [15]), while the main shock has been called the Fukushima Hamadori earthquake. The K-Net and Kik-Net records from these events have greatly expanded the global set of strong-motion data for earthquakes with normal mechanisms.

Table 1 gives the magnitude, location, and time of 18 events considered for this paper. The map in Figure 1 indicates the location of the events. Of these events, 14 are analyzed.

This sequence was not included in the 2014 updates (NGAW2) of the NGA ground motion prediction equations (GMPEs) of Abrahamson et al., 2014[2, 1], Boore et al., 2014[8, 7], Campbell and Bozorgnia, 2014[12, 11], and Chiou and Youngs, 2014[14, 13]. Anderson et al. (2013)[3] found that peak ground acceleration (PGA) and peak ground velocity (PGA) from the M_W 6.7 mainshock were up to 3.7 times higher than the 2008 NGA relations predict. In this paper, we compare PGA and PGV for 14 earthquakes to the updated 2014 NGA2W relations. A paper in preparation will compare response spectra, but PGA and PGV represent to some extent the high and low frequency range present in the data.

Methods

Table 1 was constructed from a search of the JMA catalog for shallow earthquakes with $M_{JMA} \geq 5.0$ within the boundaries between latitudes 36.4N to 37.4N and longitudes 140.3E to 141.2E, and depth shallower than 25 km. Subsequently, the F-net catalog was consulted to obtain focal mechanisms. Event 11 has a strike-slip mechanism, so it was not considered. Event 2 is an immediate foreshock of Event 3, and was found to have $M_W < 5$. The time interval between events 5 and 6 is so short that the records for those two events are not always separable, so since Event 5 has the larger magnitude, we associate the peaks on those seismograms with Event 5. Similarly, Event 7 is a foreshock of Event 8, so the peaks on the records containing that pair of events are associated with Event 8. With those adjustments, this study focuses on 14 earthquakes.

We constructed fault geometry models for each event using aftershocks to define the rupture area. The fault models are necessary to calculate the various site-source distances used by the NGAW2 equations. The procedure to do this starts with the detailed earthquake catalog provided by JMA. The focal mecha-

EQ #	Mw	Mo (Nm)	Date	Time	Latitude	Longitude	Depth (km)	# Stations
1	5.1	5.30E+16	3/18/11	23:49	36.737	140.605	4.95	195
2	<5.0	6.05E+17	3/19/11	9:56	36.782	140.574	5.76	-
3	5.8	6.35E+17	3/19/11	9:56	36.784	140.572	5.37	519
4	5.3	9.64E+16	3/20/11	1:30	37.082	140.793	6.03	346
5	5.7	4.26E+17	3/22/11	22:12	37.085	140.788	7.60	395
6	5.2	7.01E+16	3/22/11	22:13	37.035	140.769	0.93	-
7	5.0	3.40E+16	3/22/11	22:34	37.098	140.796	6.69	-
8	5.4	1.32E+17	3/22/11	22:36	37.063	140.771	7.30	417
9	6.6	9.58E+18	4/11/11	8:16	36.946	140.673	6.42	733
10	5.5	1.72E+17	4/11/11	11:42	36.966	140.635	10.57	455
11	5.9	7.05E+17	4/12/11	5:07	37.053	140.644	15.08	-
12	5.4	1.36E+17	4/13/11	1:07	36.915	140.710	4.00	351
13	5.0	3.80E+16	4/14/11	3:08	36.984	140.773	10.75	259
14	5.1	5.81E+16	9/21/11	13:30	36.737	140.577	8.64	321
15	5.1	5.67E+16	9/29/11	10:05	37.133	140.870	8.84	245
16	5.0	3.78E+16	11/20/11	1:23	36.711	140.588	8.99	276
17	5.2	6.52E+16	3/9/12	17:25	36.718	140.613	6.52	311
18	5.0	3.89E+16	12/31/13	1:03	36.692	140.629	6.63	265

Table 1: Earthquake parameters.

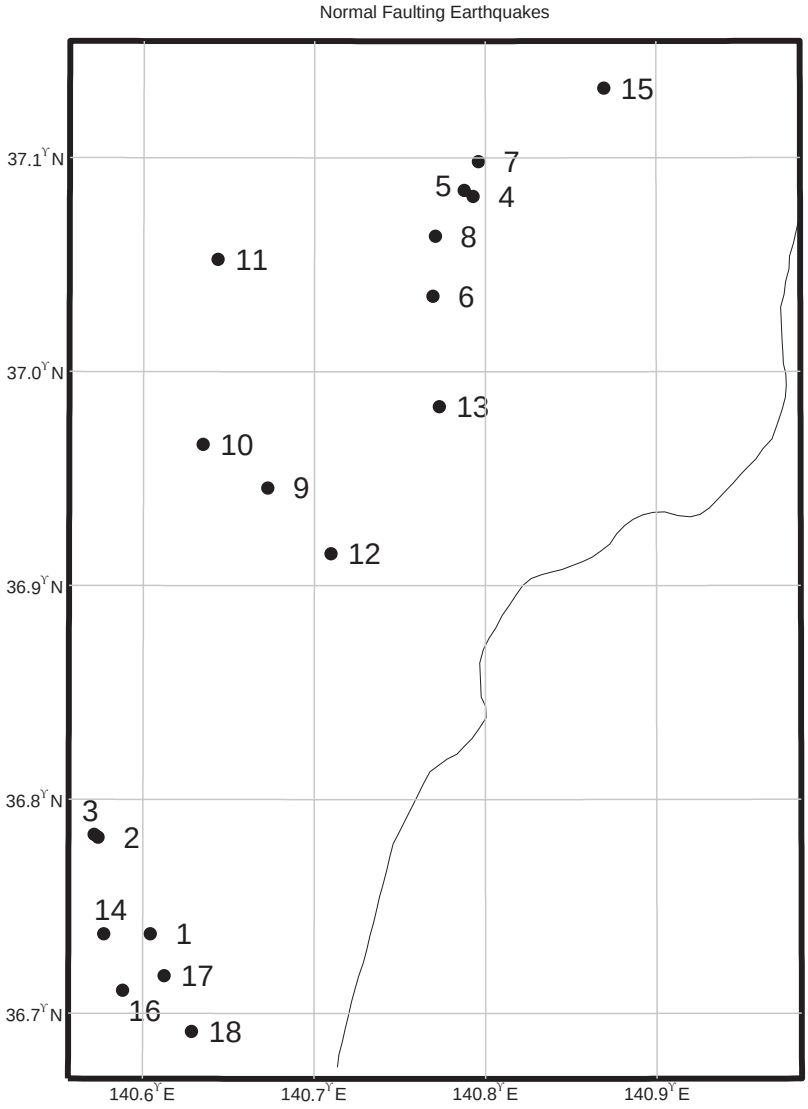

Figure 1: Locations of earthquakes in Table 1.

nisms from F-NET were found for each event with $M_W \geq 5$. These mechanisms are of course ambiguous with two alternative fault planes. The main shock and aftershocks were plotted in both cross sections, and also in each of the two fault planes. The solution that gave the most reasonable alignment of aftershocks was selected. We note that for the smaller events it was often ambiguous, but because they are small, the distances from the finite fault to the stations are not affected significantly in these cases. For the smaller events, to find an estimate of the fault dimension, we found the fault radius consistent with the Brune (1970) [10] model relating fault dimension and magnitude for a 3 MPa (30 bar) stress drop. See Appendix 1 (Supplemental online material) for cross sections and map views with aftershock and rupture areas for each event. These fault geometries were used to find r_{flt} and r_{JB} for each station.

Accelerograms were downloaded from the K-NET and KiK-net web sites of NIED. All records were high-pass filtered using a Butterworth filter (2 poles) applied only in the forward direction, so the filtered record is a causal record. "Raw" peak accelerations and velocities were found on a component-by-component basis as recorded. The records were not processed to find RotD-50 (Boore, 2010) [6] , but considering Boore et al (2006) [9] and Boore (2010) [6] , the difference is expected to be less than 2-3 % for the considered parameters. Figures 2 and 3 show those "raw" peak values for Event 9. Similar plots for all 14 events are shown in Appendix 1.

Next, Vs30 was collected for each station. For KiK-net stations, Vs30 is based on velocity profiles to over 30 meters. For K-NET stations, velocity profiles are generally available to 20 m depth, and the velocity at the base of the profile was assumed to extend to 30 m. NGA-West2 relations for peak acceleration and peak velocity, accounting for each VS30, were used to estimate PGA and PGV, and residuals were calculated. Examples of these residuals for Event 9 are shown in Figure 4. Residuals for all four GMPEs, and for all 14 events, are shown in Appendix 1 (supplemental online material). As observed by Anderson et al (2013) [3] for NGA-West relations, these data are substantially higher than the NGA West 2 relations.

Kawase and Matsuo (2004) [16] found empirical factors for each K-Net and Kik-Net station that adjust peak acceleration and peak velocity in the direct S-wave to a common site condition. We used their results to adjust the PGA and PGV values to a reference V_{S30} of 760 m/s. The adjusted data were then compared to the NGA2W models evaluated at $V_{S30} = 760$ m/s. For brevity, this is subsequently called the KM approach. These results are shown in Figures 5 and 6. In addition, Figure 7 shows an example of the residuals from the GMPEs for distances smaller than 100 km. Residuals for all four GMPEs, and for all 14 events, are shown in Appendix 1. The average residual for PGA and PGV over the distance range 0-100 km is given as μ in the legend in these figures. These average residuals are designated here as the "event terms" for this earthquake. Figure 7 and the figures in Appendix 1 (Digital online supplement) also show that on average, the residuals increase with distance from 0 to 100 km. This is an indication that the NGA-W2 GMPEs predict ground motion to decrease more rapidly with distance than what is seen in this part of Japan. The GMPEs do

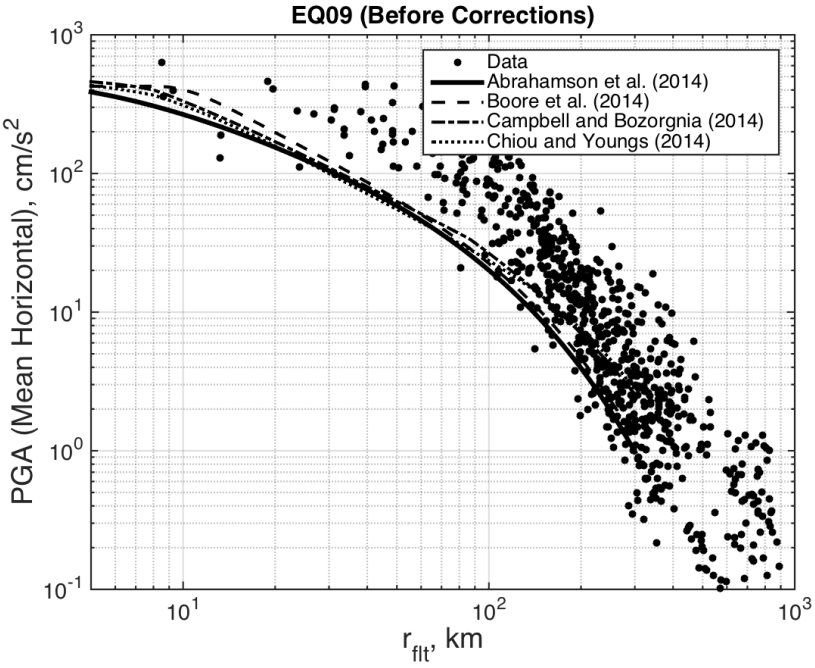

Figure 2: Raw values of peak horizontal acceleration for the main shock (EQ09, MW=6.7). For reference, the NGA-West models show median peak acceleation for the case where Vs30=400 m/s. This may be a reasonable average value, but the data are not adjusted to this value.

use Japanese data, but not from this region. Regional differences in attenuation have been observed in Japan (e.g. Kawase and Matsuo, 2004 [16]; Nakano et al., 2015 [17]). Comparing Figures 4 and 7, note that the the standard deviation σ is significantly reduced for the KM adjustment approach. This shows the advantage of obtaining site-specific data for prediction of ground motions, as has been noted by others (e.g. Atkinson, 2006 [4]; Rodriguez-Marek, Montalvo et al., 2011 [18]; Rogriguez-Marek, Rathje, et al., 2014 [19]).

Event terms are calculated in a manner similar to that in Figures 4 and 7 for each of the four considered NGA2W models and for all events in Table 1. The results are summarized as a function of magnitude in Figures 8 and 9. As an approximation, the event terms for each of the GMPEs and each adjustment for site condition tend to fall in triangular area, with a relatively constant upper bound, but a decreasing lower bound as magnitude decreases. There are very few instances where a smaller event has an event term that exceeds the event term for the main shock. This is consistent with results of Nakano et al. (2015) [17], who suggested that the stress drop of earthquakes in a sequence may be more scattered for smaller magnitudes. Figures 8 and 9 also show the mean

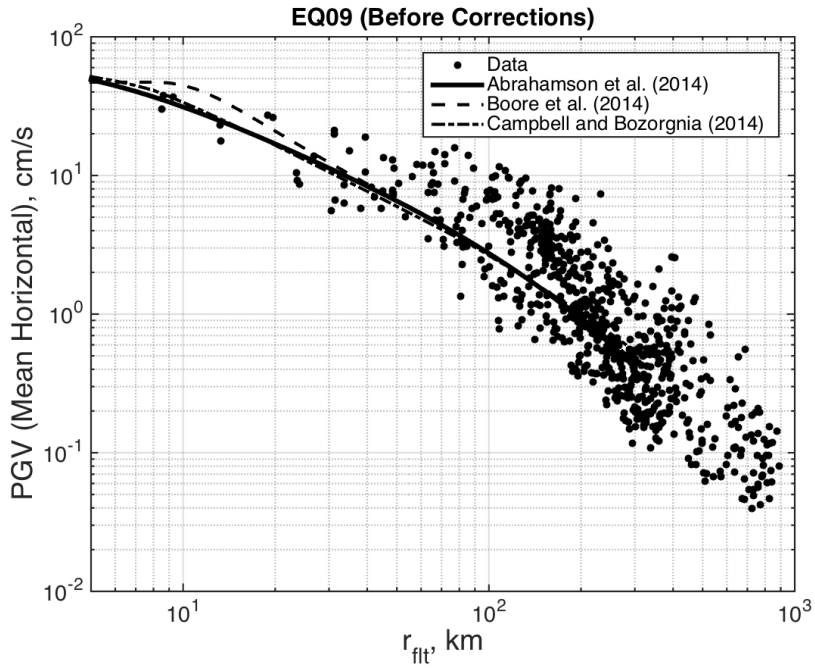

Figure 3: Raw values of PGV. See Figure 2 for details.

Event #	Date	Time (UT)	Magnitude (Mw)	Moment (dyne-cm)	Strike	Dip	Rake	Total Fault Length	Total Fault Width	Fault Area (km^2)	Shallowest depth of faulting	Maximum depth of faulting	Mean Slip (cm)	Stress Drop (bars)
EQ #1	3/18/11	23:49	5.1	5.62E+23	195	59	-85	4.0	4.0	16.0	5.0	8.4	11.7	24.2
EQ #3	3/19/11	9:56	5.8	6.31E+24	141	46	-95	8.9	8.9	79.2	3.0	9.4	26.6	24.6
EQ #4	3/20/11	1:30	5.3	1.12E+24	69	52	-60	4.0	4.5	18.0	4.0	7.5	20.8	40.3
EQ #5	3/22/11	22:12	5.7	4.47E+24	191	64	-94	9.0	6.5	58.5	3.8	9.6	25.5	27.1
EQ #6	3/22/11	22:13											#DIV/0!	#DIV/0!
EQ #7	3/22/11	22:34											#DIV/0!	#DIV/0!
EQ #8	3/22/11	22:36	5.4	1.58E+24	179	55	-90	5.4	6.0	32.4	4.0	8.9	16.3	23.6
EQ #9	4/11/11	8:16	6.7	1.22E+26	162	66	270	13.4	20.0	268.0	0.0	18.3	151.3	74.7
	4/11/11	8:16	6.7	1.36E+26	128	66	270	15.3	15.0	229.5	0.0	13.7	198.2	107.9
EQ #10	4/11/11	11:42	5.5	2.24E+24	264	62	-92	6.0	5.9	35.4	6.0	11.2	21.1	29.2
EQ #11	4/12/11	5:07	5.9	8.91E+24	167	51	2	13.0	9.4	122.2	0.0	7.3	24.3	17.9
EQ #12	4/13/11	1:07	5.9	8.91E+24	180	57	-89	9.0	9.0	81.0	4.0	11.5	36.7	33.6
EQ #13	4/14/11	3:08	5.0	3.98E+23	79	46	-66	5.0	5.0	25.0	9.0	12.6	5.3	8.8
EQ #14	9/21/11	13:30	5.1	5.62E+23	163	58	-88	4.0	4.1	16.4	7.0	10.5	11.4	23.3
EQ #15	9/29/11	10:05	5.1	5.62E+23	224	63	-92	4.0	4.0	16.0	5.3	8.9	11.7	24.2
EQ #16	11/20/11	1:23	5.0	3.98E+23	307	66	-122	4.5	3.5	15.8	7.0	10.2	8.4	17.4
EQ #17	3/9/12	17:25	5.2	7.94E+23	155	53	-93	6.0	3.0	18.0	5.9	8.3	14.7	27.0
EQ #18	12/31/13	1:03	5.1	5.62E+23	292	50	-135	4.0	4.0	16.0	5.0	8.1	11.7	24.2

Table 2: Fault Geometry Parameters. Note that EQ #11 is not a normal event and that EQ #9, the mainshock, has two fault models, one for each of the two faults that ruptured during the mainshock.

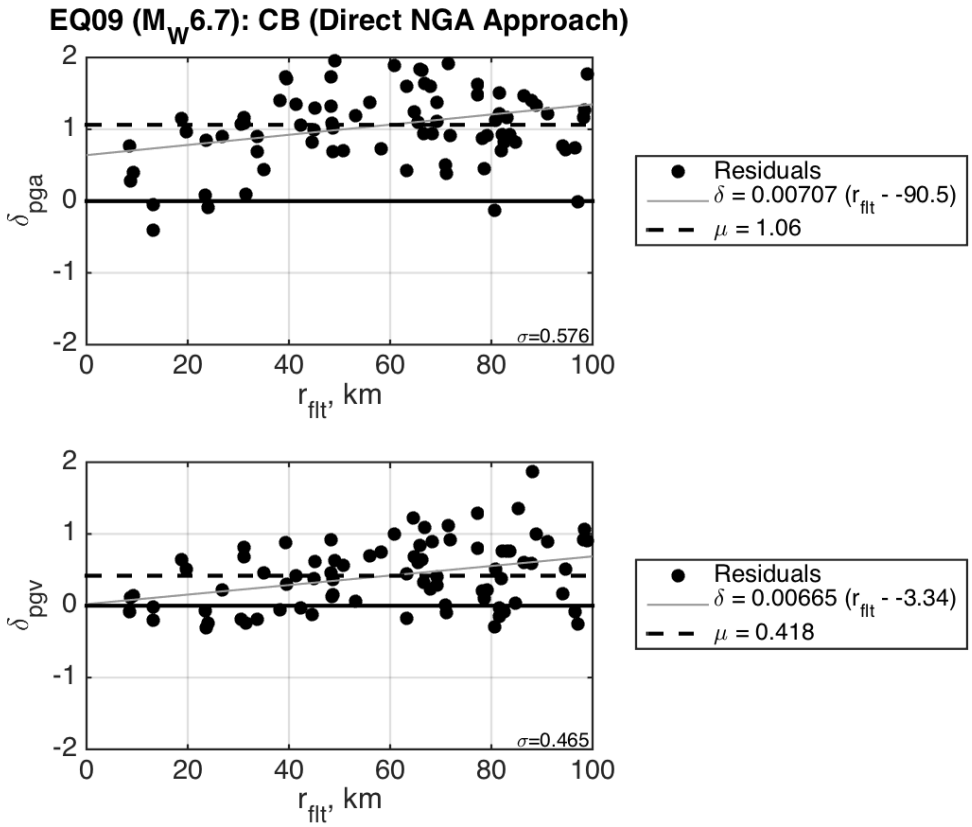

Figure 4: Residuals for for the main shock (EQ09, MW=6.7), based on the direct NGA approach that uses Vs30 appropriate to each station as a predictive parameter. The residual is defined al $\delta_{PGA} = \ln[PGA(data)] - \ln[PGA(GMPE)]$-, or the equivalent for PGV. Thus positive residuals indicate that the model underestimates the observed amplitude. A few residuals are too large to display on this scale. The model, for this figure, is by Campbell and Bozorgnia (2014) [12], using the adjustment for Japan attenuation and using estimates of Vs30 for each station, as explained in the text. The horizontal dashed line is the average residual ($\mu = \bar{\delta_i}$) for distances from 0-100 km, and the standard deviation σ shown on the plot is found as $\sigma^2 = \frac{1}{N}\sum(\delta_i - \mu)^2$ for the N observations in the range. This paper uses the average over this distance range as an estimate of the event term. The solid, gray line is a linear least-squares best fit estimate to the residuals over the distance range shown in this figure. This fit cannot be extrapolated to larger distances.

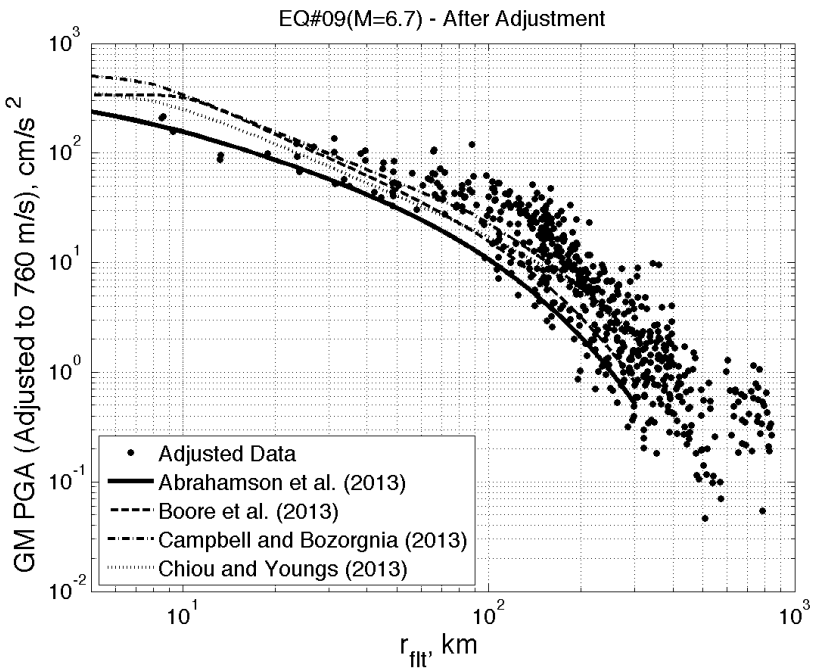

Figure 5: Adjusted values of peak horizontal acceleration for the main shock (EQ09, MW=6.7). These points use the adjustment of Kawase and Matsuo (2004) [16] to 760 m/s. For reference, the NGA-West models show median peak acceleation for the case where Vs30=760 m/s.

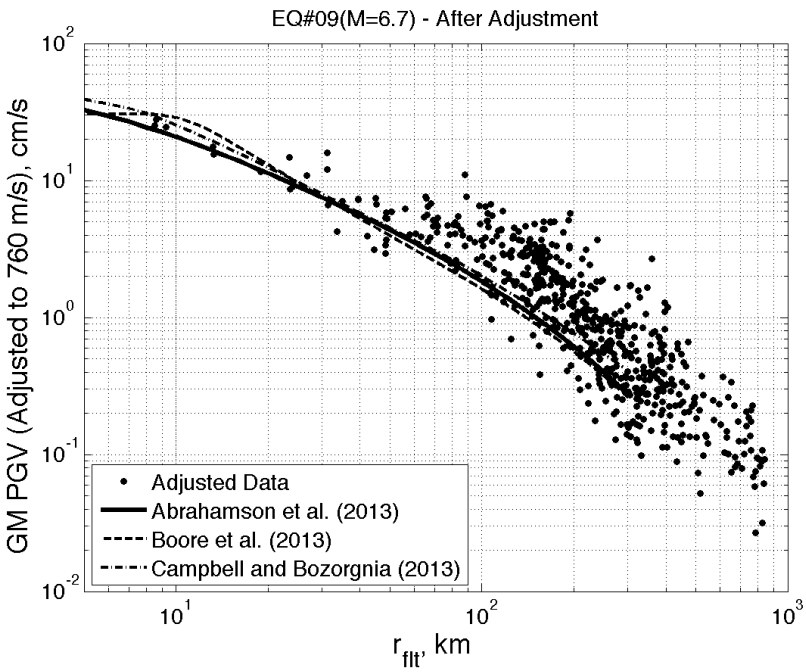

Figure 6: Adjusted values of PGV. See Figure 5 for details.

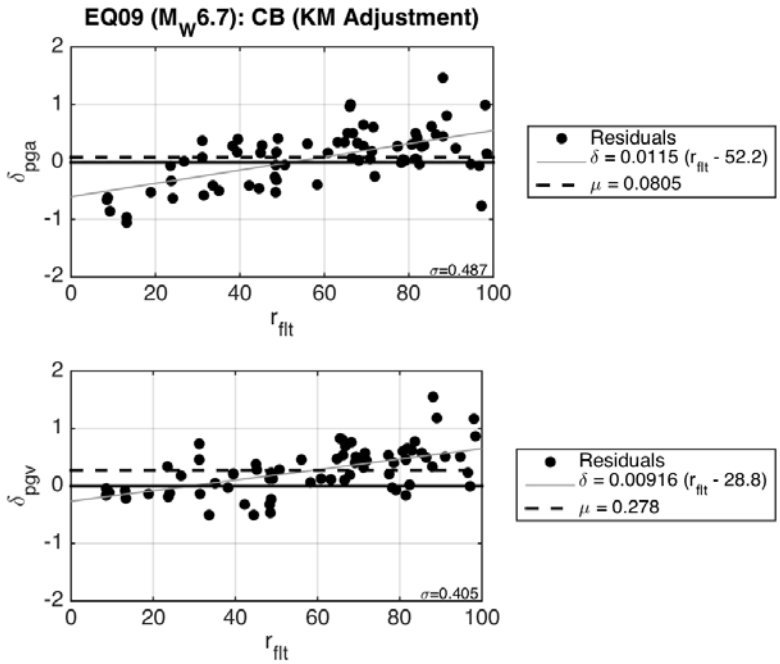

Figure 7: Residuals of adjusted PGA and PGV from the Campbell and Bozorgnia (2014) [12] GMPE for peak horizontal acceleration and peak horizontal velocity for the main shock (EQ09, MW=6.7). These points use the results of Kawase and Matsuo (2004) [16] to adjust all peak values to a station with Vs30 = 760 m/s. Thus, the Campbell and Bozorgnia (2014) [12] model uses Vs30=760 m/s for all stations to find the model estimate. Other features of this figure are the same as in Figure 4.

slope of the residuals obtained using the KM adjustments. One can see that the slopes are all positive and relatively consistent from event to event, with no conspicuous magnitude dependence.

The event terms do show an indication of a dependence on depth. This is demonstrated in Figure 10. Nakano et al. (2015) [17] similarly found a depth dependence in the stress drop parameters.

Finally, Figures 11 and 12 show the mean residuals over longer distance ranges, for the two methods. These show, first, that the distance dependence of the residuals is complex, and depends on the adjustment method as well as on the GMPE. From 0-100 km, every case shows a distance dependence on average, as seen in Figures 4 and 7 and in Appendix 1 (Online supplement). However the roughly linear trend seen at those short distances does not extrapolate to larger distances. The two methods for site adjustment differ most at short distances for PGA, and tend to converge for distances greater than 100 km. In contrast, for PGV, the two methods differ least at short distances, and tend to diverge beyond 100 km. While there is much in this pattern that is difficult to explain, some comments are in order. The KM approach is based on amplitudes of the direct S-wave, while at larger distances the velocity, in particular, is dominated by surface waves. Thus at large distances, especially for PGV, the KM approach might not be optimal. For PGA, the same might apply to some extent, since even though direst S-waves tend to dominate the seismograms their frequency content is increasingly depleted in high frequencies. For PGA, however, the distance range used by Kawase and Matsuo (2004) [16] to determine these factors would control the distance range over which they are optimized. It is clear, from the reduced uncertainties, that for short distances these factors offer a greater predictive value than an average adjustment based on Vs30 as used in the direct NGA approach.

Results and Discussion

A central question is on the relevance of the data from the Fukushima-Hamadori earthquake sequence to estimation of strong ground motion amplitudes in the United States, and in particular for the NGA2W models that are used in the US National Seismic Hazard Model for the western US. This will undoubtedly be a judgmental decision for future GMPE developers. The earthquake sequence has been described as "unusual" (Imanishi et al., 2012 [15]), and as "remarkable", "unique", and "anomalous" (Yoshida et al., 2012 [21]) as this region of Japan is considered to be a compressional regime. The normal faulting was almost certainly triggered by the release of horizontal stress, and perhaps rotation of the principal stress directions (Yoshida et al., 2012 [21]), as a result of the elastic rebound from the March 11, 2011 Tohoku earthquake. Under these circumstances, one might wonder if this sequence is representative of the physics of fault rupture in normal faulting earthquakes.

There is a reasonable case that these earthquakes should be considered rep-

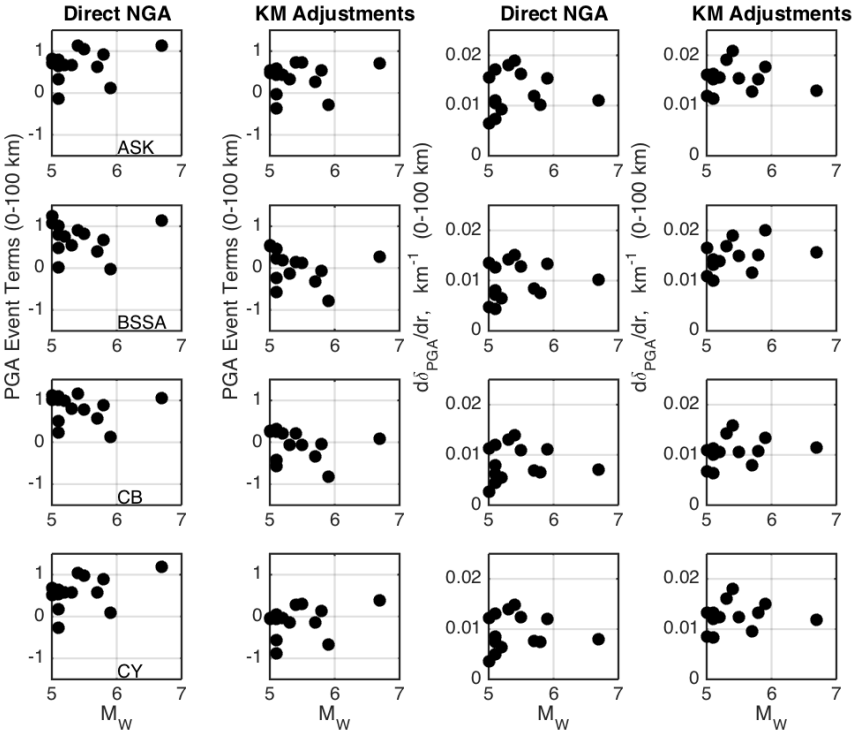

Figure 8: PGA event terms versus magnitude. Because the ordinate axis is the natural log of the ratio of data to model, a perfect match between data and model plots at zero.

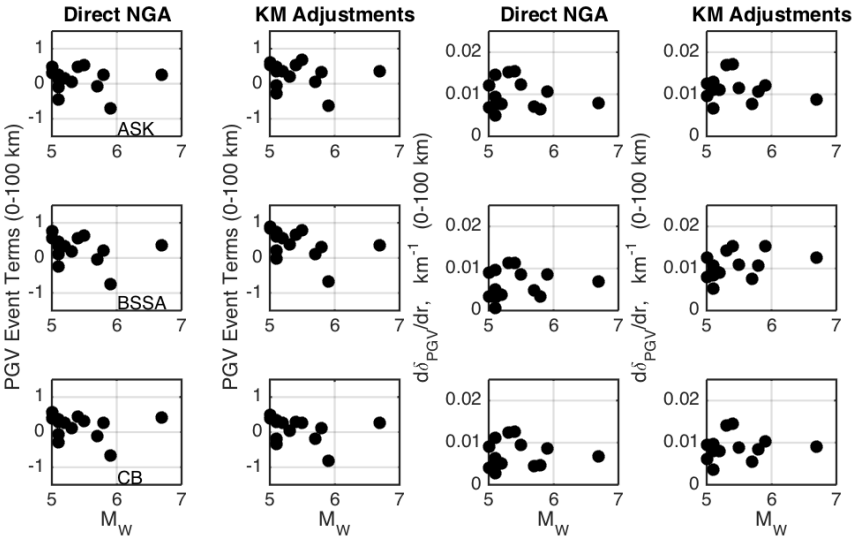

Figure 9: Mean event term is the mean of the three and four NGA2W models for PGA and PGV, respectively. Mean event terms increase with depth up to 7.5 km before leveling off for all but two of the events.

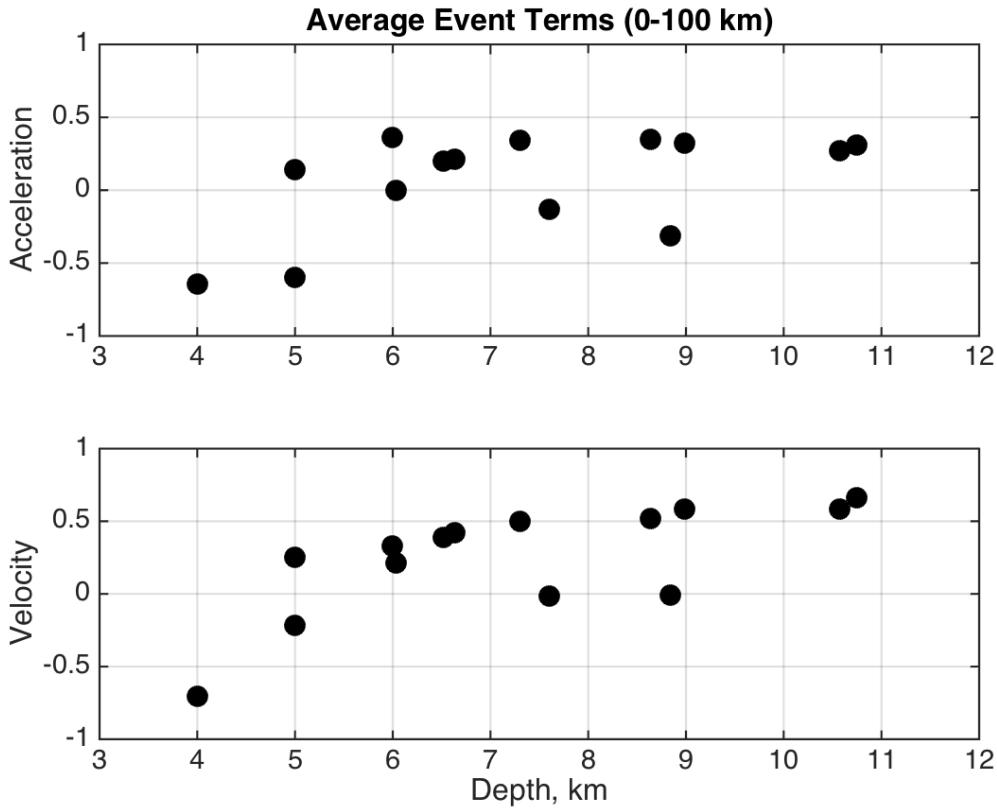

Figure 10: Average residuals for peak acceleration (top) and peak velocity (bottom), determined by the KM method, for each event, plotted as a function of the hypocentral depth. Averages are over all stations at rupture distances under 100 km.

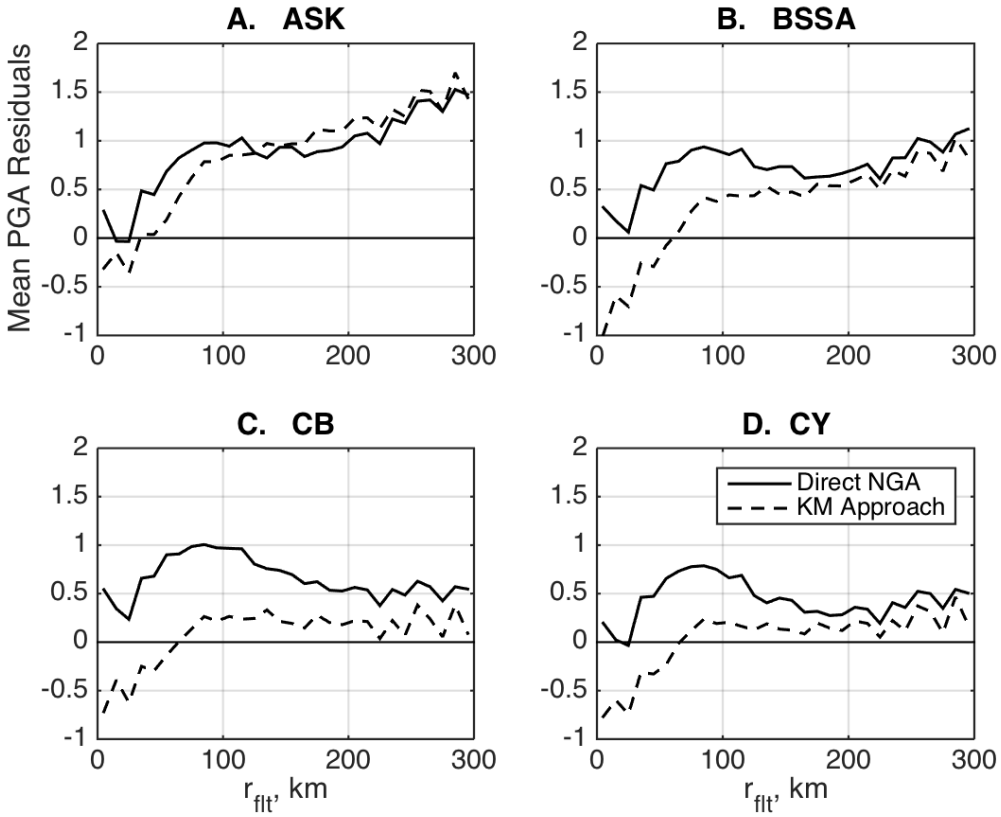

Figure 11: PGA Residuals as a function of distance, for each of the four GMPEs and both methods of adjusting for site condition. All residuals from all earthquakes were combined to generate this plot. These combined residuals were averaged over 10 km distance ranges, 0-10 km, 10-20 km, etc., with each average plotted at the midpoint of its range. For clarity, range midpoints are connected with straight lines. Solid lines are used to connect points using the direct NGA method, while dashed lines are used for the KM approach.

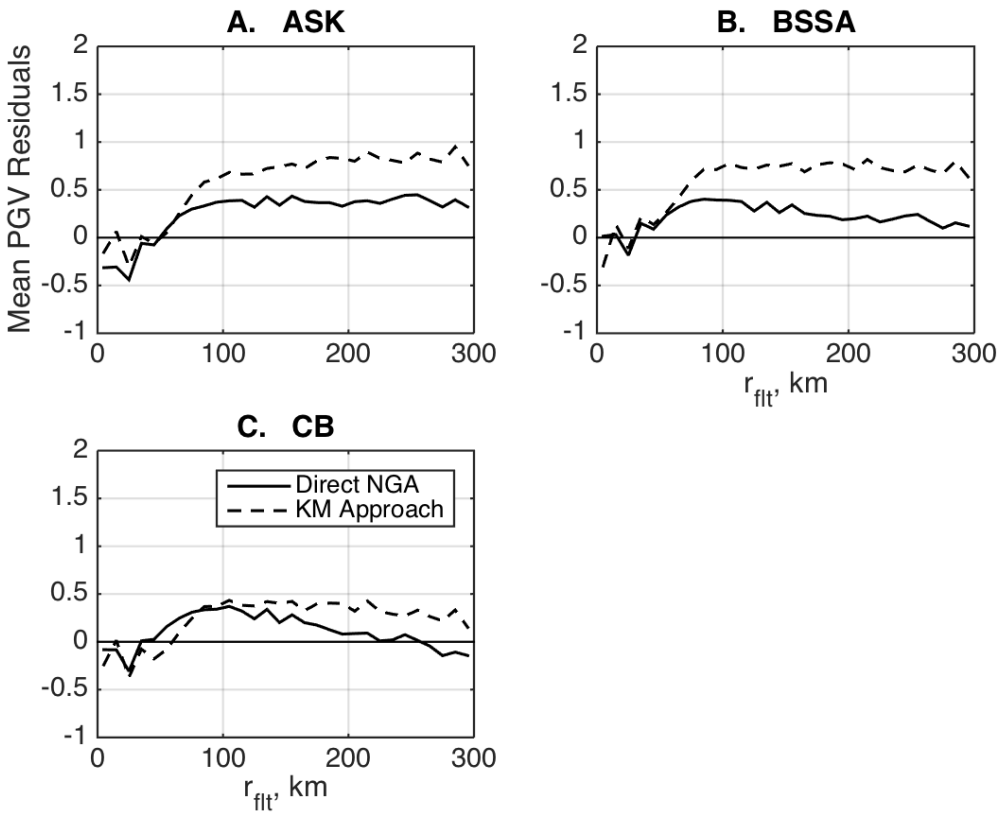

Figure 12: PGV Residuals as a function of distance

resentative of normal faulting processes. Both Imanishi et al., 2012 [15] and Yoshida et al., 2012 [21] estimate that the stress change in the study area due to the Tohoku earthquake was about 1 MPa. Imanishi et al. (2012) point out that this is too small to transform an area dominated by reverse faulting to an area dominated by normal faulting. Anderson et al. (2013) [3] extimated average stress drop on each of the two subparallel faults to be in the range of 3-4 MPa, consistent with the hypothesis that the ~1 MPa stress change was sufficient to trigger the event but that release of pre-existing extensional stress was also involved. Nakano et al. (2015) [17] also find high stress drops for the main shock and many of the smaller events. Imanishi et al. (2012) [15] find that the small region where these events occurred had normal faulting mechanisms in small earthquake prior to the 2011 Tohoku main shock.

The tectonic reasons for a small extensional region to exist within an otherwise compressional environment are not resolved. Imanishi et al. (2012) [15] show evidence for an additional fault dipping from the Fukushima Hamadori region eastwards to the subduction thrust. We suggest that it may also be productive to consider the effects of the Phillipine Sea plate, which is subducted northwards into the mantle above the Pacific plate in this region (e.g. Wu et al., 2007 [20]). Whatever the cause of the perturbation, Imanishi et al. (2012) [15] conclude, and we concur, that the Tohoku main shock perturbed a pre-existing extensional stress field to trigger the Fukushima-Hamadori sequence. In a situation like this, where stress changes due to one earthquake advance the timing of another earthquake, we see no reason to believe that the physics of the triggered earthquake is different.

Accepting that this sequence of earthquakes in the Ibaraki - Fukushima prefecture border region can be considered representative of normal faulting implies that the mean bias revealed by the event terms over the distance range from 0-100 km needs to be reconciled with the GMPEs. From Figures 8 and 9, it appears that the event terms for the KM approach show less scatter and are more consistent from one GMPE to the next than for the NGA direct approach. Average event terms over the considered GMPEs are seen as a function of depth in Figure 10. The main point here is that for most events, the average residual is greater than zero, implying that the event had stronger shaking than implied by the GMPEs. Since these are very well recorded events, including them in future GMPEs might result in adjusting the factor that reduces the overall amplitude of normal faulting motions.

The distance dependence of residuals is present for both methods of handling site effects, and for all four NGA2W models, as seen in Figures 8 and 9. From 0-100 km, the station residuals increase with distance at all magnitudes. Nonlinearity at short distances is not a likely cause since the trend is similar for large and small events. The flattening of the curve from 50-100 km resembles the shape caused by the Moho bounce in the eastern United States (Atkinson and Boore, 2006) [5]. Waveform modeling in realistic crustal structures for this region of Japan and for the appropriate regions of the US will be necessary to resolve the cause of this difference between the NGA2W models and the Japanese attenuation at short distances.

The Event terms increase with the depth of the earthquake, with only two events interrupting a relatively steady increase. This result is consistent with observations of stress drop increasing with depth (Nakano et al, 2015) [17].

The Kawase and Matsuo (2004) [16] corrections significantly reduce scatter in PGA and PGV data, and shift the mean towards the NGA models. This demonstrates the value of recordings of small earthquakes to improve seismic hazard estimates.

Inconsistencies between the Ibaraki - Fukushima border region earthquake ground motions and the NGA2W GMPEs can be explained by at least four different hypotheses:

1. Differences in bulk crustal structure can cause differences in geometrical spreading.

2. Differences in average site response might introduce some systematic biases.

3. Differences in average stress drop between the average in the Fukushima-Hamadori area and the NGA2W data set could introduce systematic bias, particularly at high frequencies.

4. The NGA2W GMPEs might, due to scarcity of data or regional bias introduced by the predominant location of the utilized normal-faulting earthquakes, be mis-calibrated for normal faulting earthquakes.

The results of this study do not resolved the relative importance of each of these possibilities. Additional studies in progress will involve modeling that should help to bring additional clarity to the situation.

Data and Resources

Strong motions records used in this study were obtained from Japan's National Research Institute for Earth Science and Disaster Prevention (NIED). Accelerograms can be obtained from the NIED website at http://www.kyoshin.bosai.go.jp (last accessed January 2014). The earthquake catalog used to determine fault geometry was obtained on CD-ROM from the Japan Meterological Agency. Focal mechanisms were obtained from the F-NET web site of NIED.

Acknowledgements

The authors wish to thank the Japan Meterological Agency and the National Research Institute for Earth Science and Disaster Prevention (NIED), for providing the earthquake catalog and strong motion records of these earthquakes. Research supported by the U.S. Geological Survey (USGS), Department of the Interior, under USGS award number G13AP00065. The views and conclusions contained in this document are those of the authors and should not be interpreted as necessarily representing the official policies, either expressed or implied, of the U.S. Government.

References

[1] Abrahamson, N., Silva, W., and Kamai, R. Update of the as08 ground-motion prediction equations based on the nga-west2 data set. Tech. Rep. PEER 2013/04, Pacific Earthquake Engineering Research Center, 2013.

[2] Abrahamson, N. A., Silva, W. J., and Kamai, R. Summary of the ask14 ground motion relation for active crustal regions. *Earthquake Spectra 30*, 3 (2014), 1025–1055.

[3] Anderson, J. G., Kawase, H., Biasi, G. P., Brune, J. N., and Aoi, S. Ground Motions in the Fukushima Hamadori, Japan, Normal-Faulting Earthquake. *Bulletin of the Seismological Society of America 103*, 3 (JUN 2013), 1935–1951.

[4] Atkinson, G. M. Single-station sigma. *Bulletin of the Seismological Society of America 96*, 2 (2006), 446–455.

[5] Atkinson, G. M., and Boore, D. M. Earthquake ground-motion prediction equations for eastern North America. *Bulletin of the Seismological Society of America 96*, 6 (DEC 2006), 2181–2205.

[6] Boore, D. M. Orientation-Independent, Nongeometric-Mean Measures of Seismic Intensity from Two Horizontal Components of Motion. *BULLETIN OF THE SEISMOLOGICAL SOCIETY OF AMERICA 100*, 4 (AUG 1 2010), 1830–1835.

[7] Boore, D. M., Stewart, J. P., Seyhan, E., and Atkinson, G. M. Nga-west2 equations for predicting response spectral accelerations for shallow crustal earthquakes. Tech. Rep. PEER 2013/05, Pacific Earthquake Engineering Research Center, 2013.

[8] Boore, D. M., Stewart, J. P., Seyhan, E., and Atkinson, G. M. Nga-west2 equations for predicting pga, pgv, and 5% damped psa for shallow crustal earthquakes. *Earthquake Spectra 30*, 3 (2014), 1057–1085.

[9] Boore, D. M., Watson-Lamprey, J., and Abrahamson, N. A. Orientation-independent measures of ground motion. *BULLETIN OF THE SEISMOLOGICAL SOCIETY OF AMERICA 96*, 4 (AUG 2006), 1502–1511.

[10] Brune, J. N. Tectonic stress and spectra of seismic shear waves from earthquakes. *Journal of Geophysical Research 75*, 26 (1970), 4997–&.

[11] Campbell, K. W., and Bozorgnia, Y. Nga-west2 campbell-bozorgnia ground motion model for the horizontal components of pga, pgv, and 5spectra for periods ranging from 0.01 to 10 sec. Tech. Rep. PEER 2013/06, Pacific Earthquake Engineering Research Center, 2013.

[12] Campbell, K. W., and Bozorgnia, Y. Nga-west2 ground motion model for the average horizontal components of pga, pgv, and 5% damped linear acceleration response spectra. *Earthquake Spectra 30*, 3 (2014), 1087–1115.

[13] Chiou, B., and Youngs, R. Update of the chiou and youngs nga ground motion model for average horizontal component of peak ground motion and response spectra. Tech. Rep. PEER 2013/07, Pacific Earthquake Engineering Research Center, 2013.

[14] Chiou, B. S.-J., and Youngs, R. R. Update of the chiou and youngs nga model for the average horizontal component of peak ground motion and response spectra. *Earthquake Spectra 30*, 3 (2014), 1117–1153.

[15] Imanishi, K., Ando, R., and Kuwahara, Y. Unusual shallow normal-faulting earthquake sequence in compressional northeast japan activated after the 2011 off the pacific coast of tohoku earthquake. *GEOPHYSICAL RESEARCH LETTERS 39* (2012), L09306, doi:10.1029/2012GL051491.

[16] Kawase, H., and Matsuo, H. Amplification characteristics of k-net, kik-net, and jma shindokei network sites based on the spectral inversion technique. In *13th World Conference on Earthquake Engineering* (Vancouver, Canada, 2004), p. Paper No. 454.

[17] Nakano, K., Matsushima, S., and Kawase, H. Statistical Properties of Strong Ground Motions from the Generalized Spectral Inversion of Data Observed by K-NET, KiK-net, and the JMA Shindokei Network in Japan. *Bulletin of the Seismological Society of America 105*, 5 (OCT 2015), 2662–2680.

[18] Rodriguez-Marek, A., Montalva, G. A., Cotton, F., and Bonilla, F. Analysis of single-station standard deviation using the kik-net data. *Bulletin of the Seismological Society of America 101*, 3 (2011), 1242–1258.

[19] Rodriguez-Marek, A., Rathje, E. M., Bommer, J. J., Scherbaum, F., and Stafford, P. J. Application of single-station sigma and site-response characterization in a probabilistic seismic-hazard analysis for a new nuclear site. *Bulletin of the Seismological Society of America 104*, 4 (2014), 1601–1619.

[20] Wu, F., Okaya, D., Sato, H., and Hirata, N. Interaction between two subducting plates under tokyo and its possible effects on seismic hazards. *GEOPHYSICAL RESEARCH LETTERS 34* (2007), L18301, doi:10.1029/2007GL030763.

[21] Yoshida, K., Hasegawa, A., Okada, T., Iinuma, T., Ito, Y., and Asano, Y. Stress before and after the 2011 great tohoku-oki earthquake and induced earthquakes in inland areas of eastern japan. *GEOPHYSICAL RESEARCH LETTERS 39* (2012), L03302, doi:10.1029/2011GL049729.

Appendix 1. Plots of Fault Models and Data

1 Earthquake 1. 2011 03 19, 08:49 Mw5.1

Figure 13 shows four frames illustrating the geometry of this earthquake.

Figure 14 shows the uncorrected values of peak acceleration as a funciton of distance, and Figure 16 shows the uncorrected values of peak velocity. For comparison, both of these figures show the NGA-West 2 models for Vs30=400 m/s, which is considered to be a reasonable estimate for the network average. Figure 15 shows the adjusted peak accelerations and Figure 17 shows adjusted peak velocities, where the adjustments to the data use Kawase factors and are adjusted to Vs30=760 m/s. Therefore, the NGA curves on these two firgures are for Vs30-760 m/s.

Residuals are shown in Figures 18-25. Raw and adjusted residuals are paired for ease in comparison. To obtain the "raw" residuals, a station-by-station estimate of Vs30 has been used within the NGA models. Since the adjustments are to a common value of vs30, station-by-station adjustments are not needed.

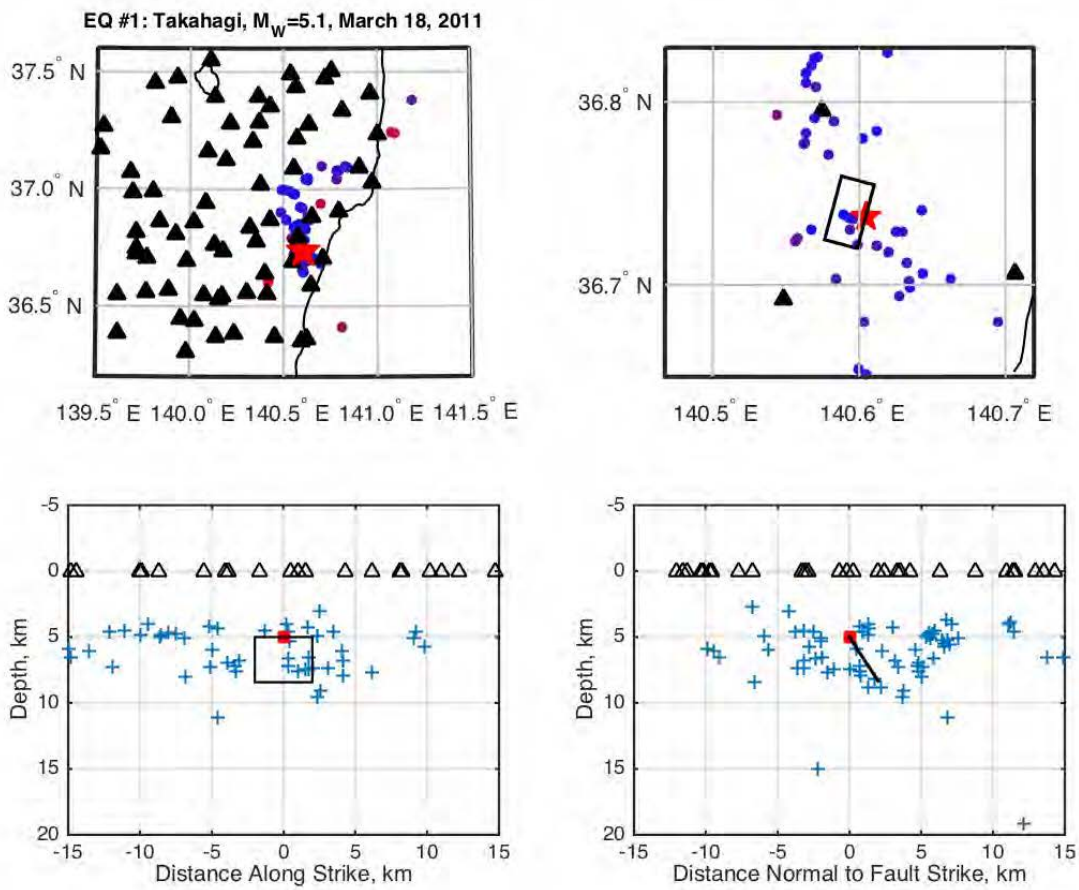

Figure 13: Location and cross section

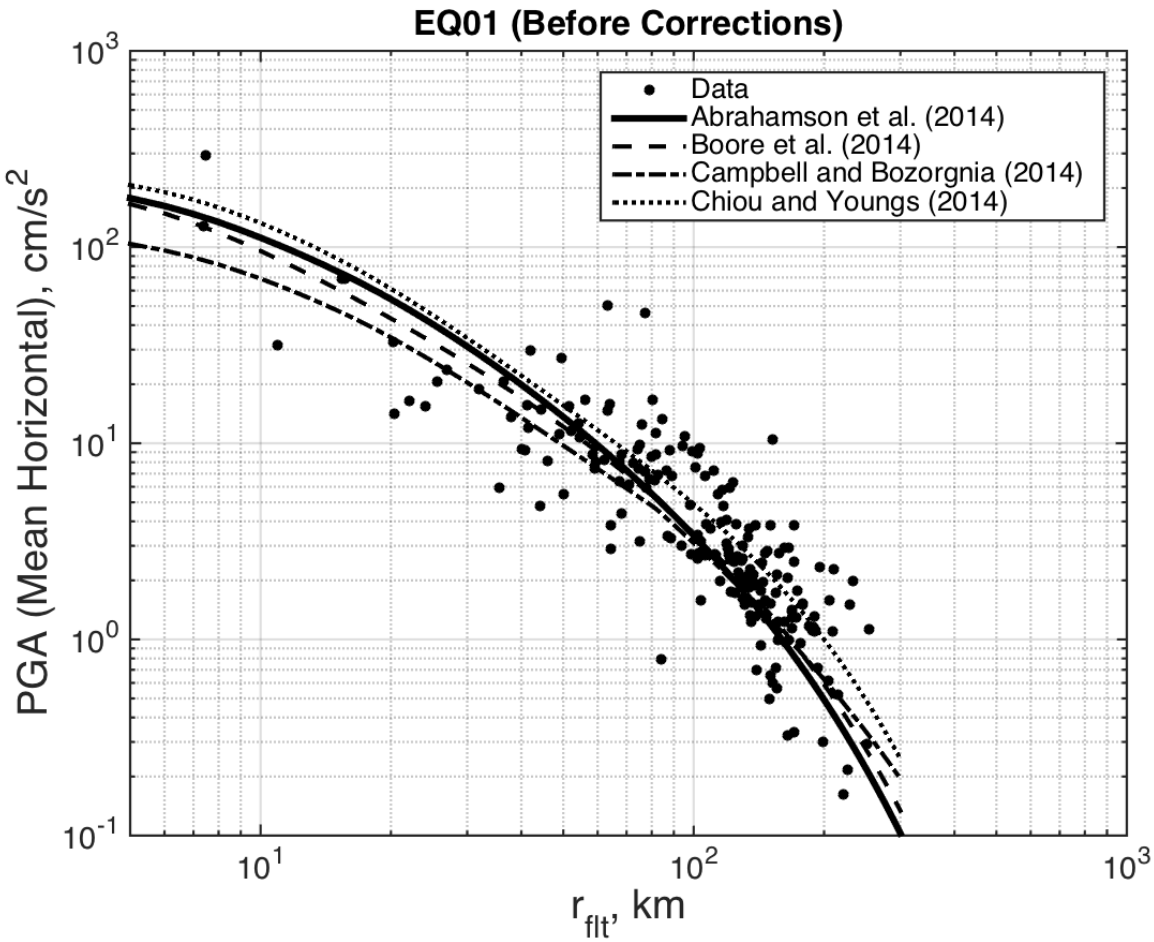

Figure 14: Raw accelerations

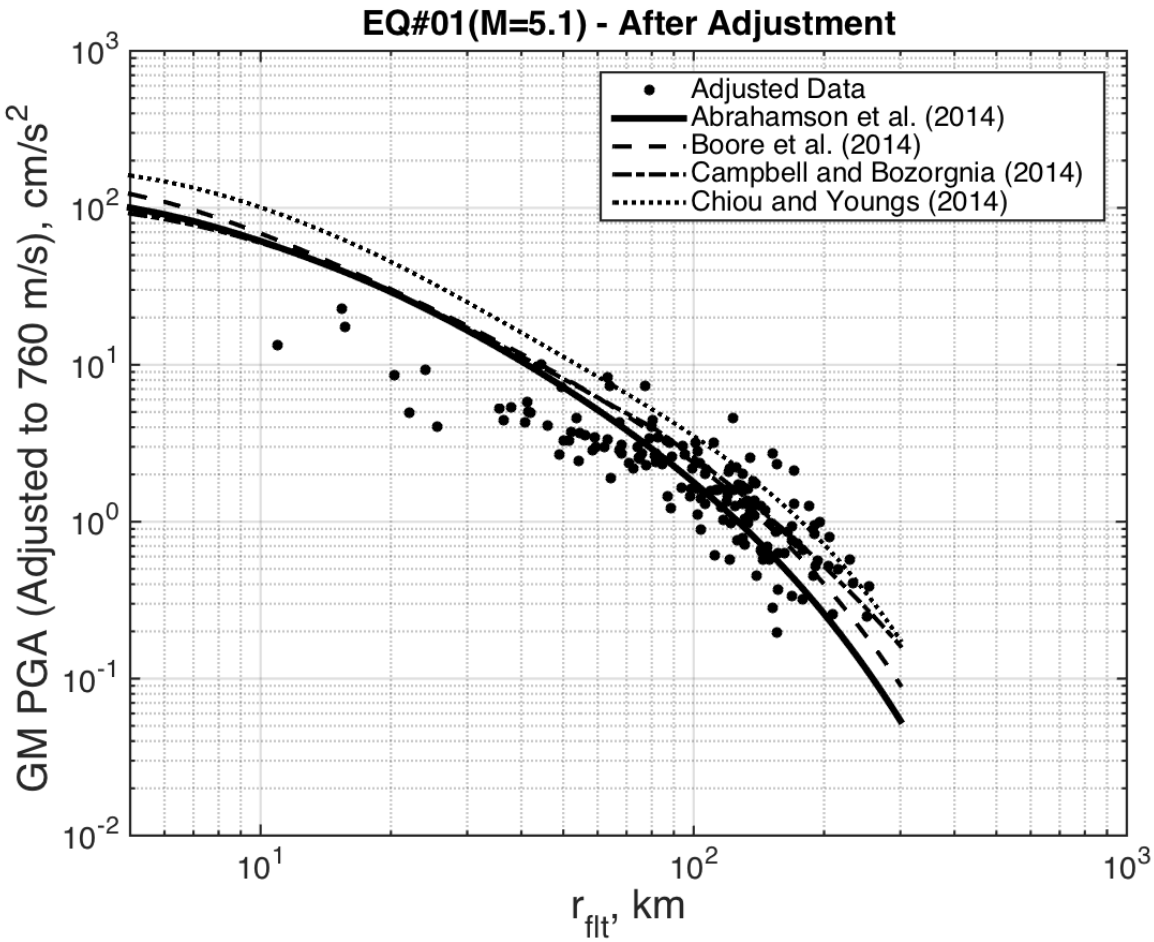

Figure 15: Adjusted accelerations

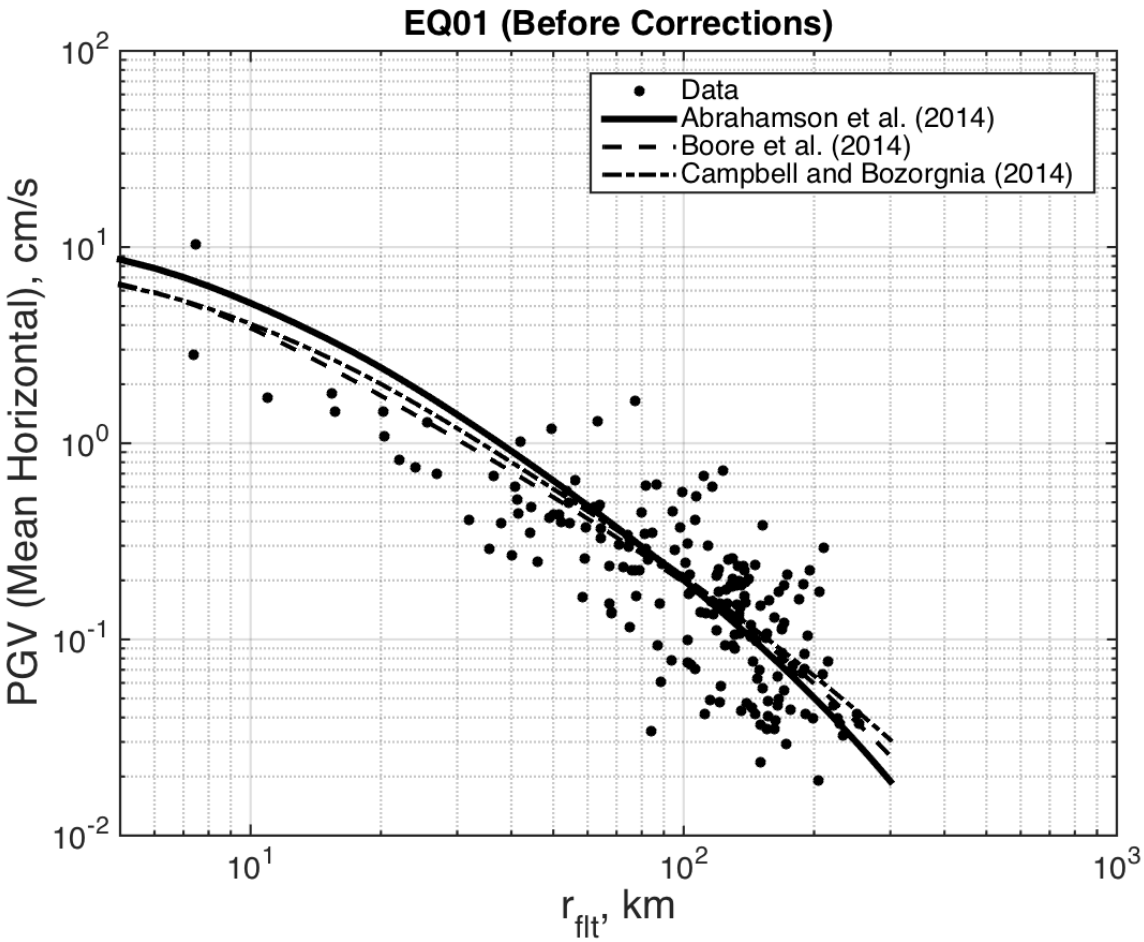

Figure 16: Raw velocities

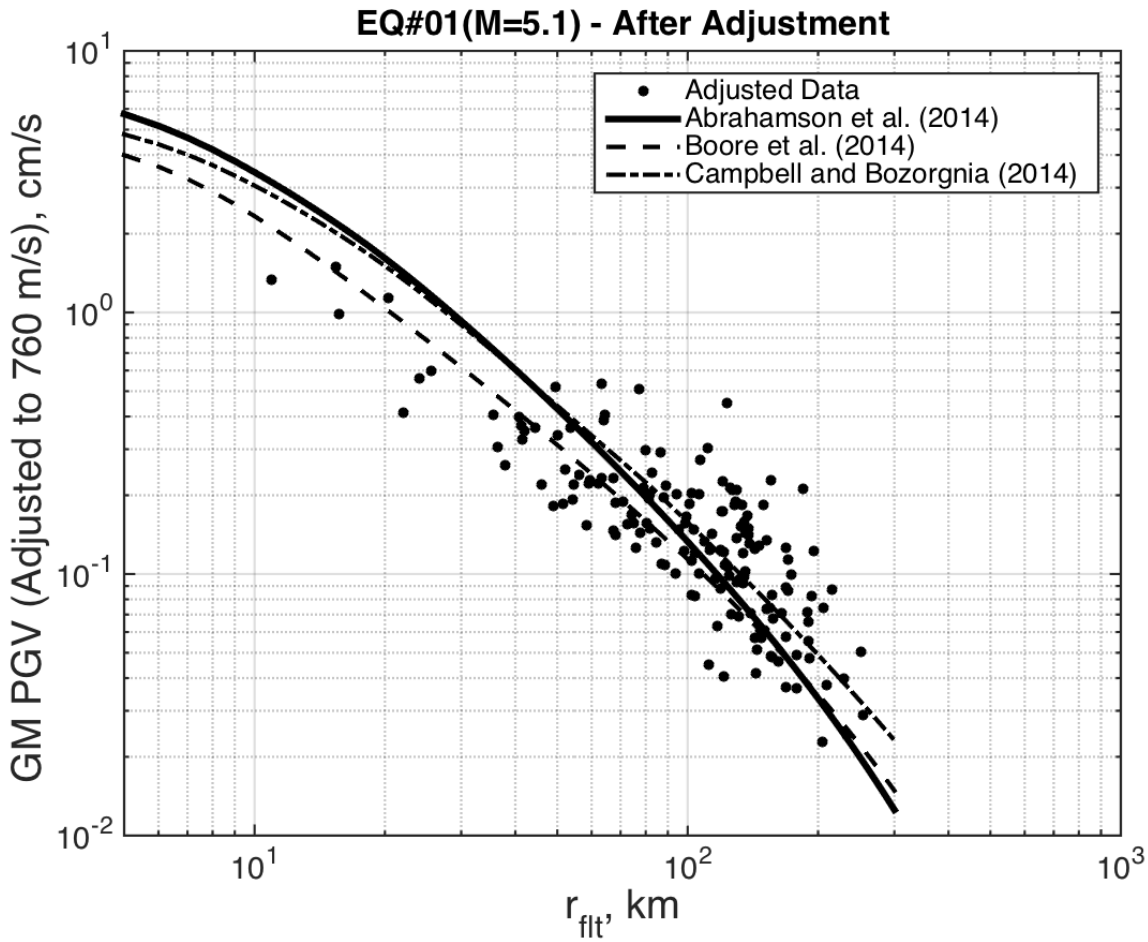

Figure 17: Adjusted velocity

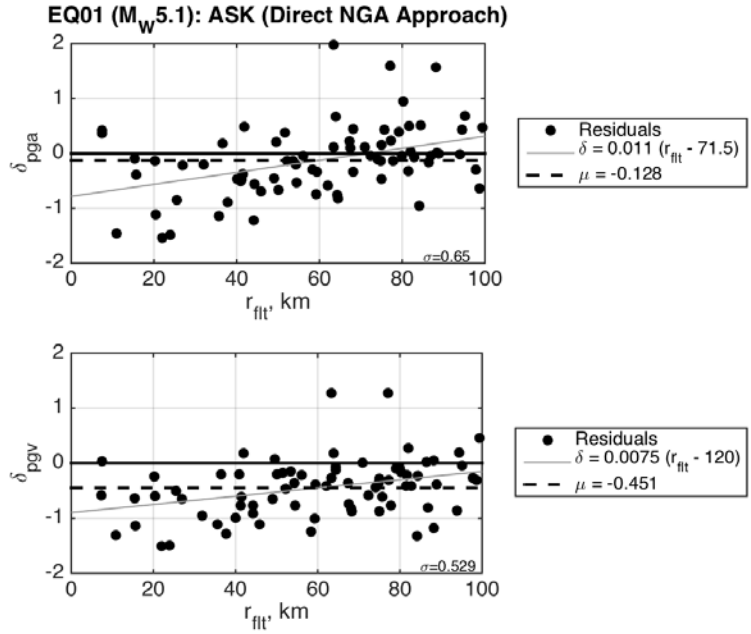

Figure 18: Raw delta ASK

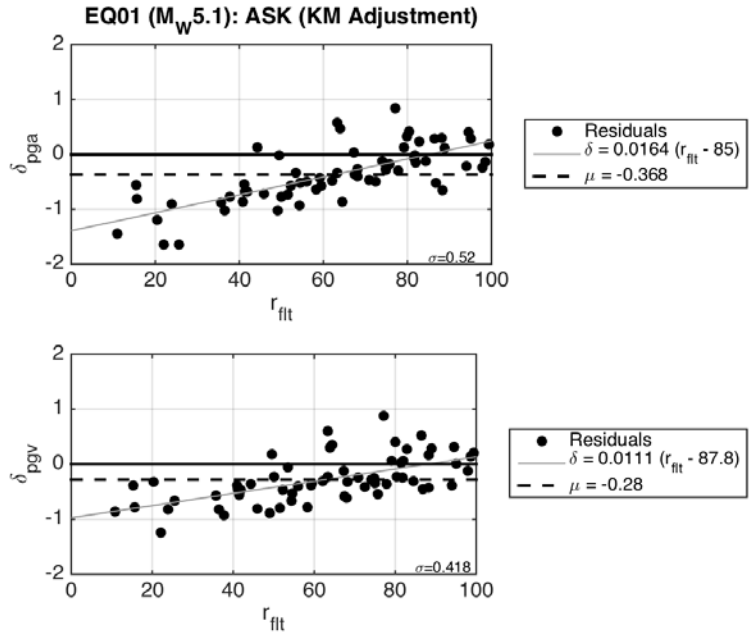

Figure 19: Adjusted delta ASK

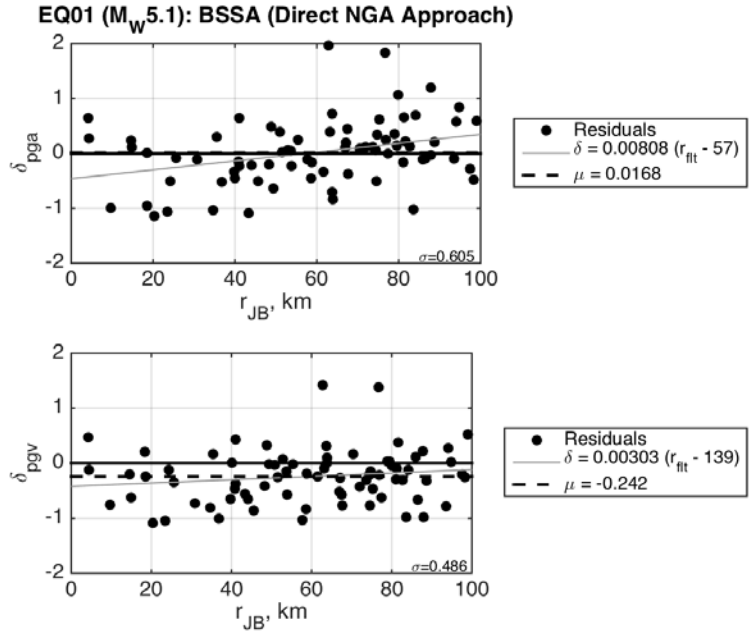

Figure 20: Raw delta BSSA

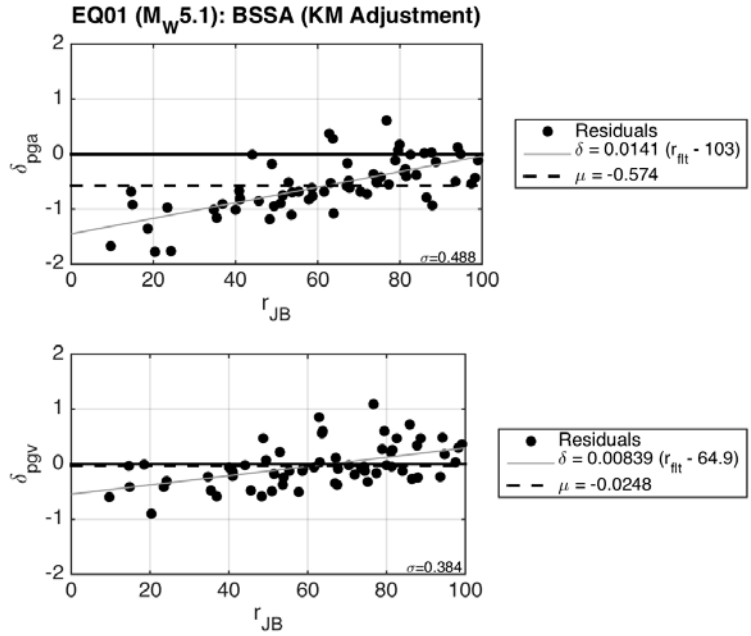

Figure 21: Adjusted delta BSSA

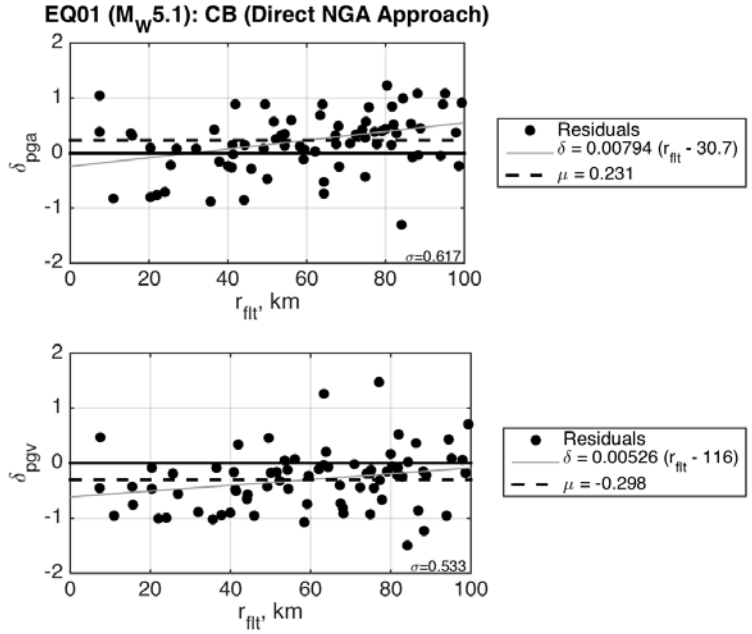

Figure 22: Raw delta CB

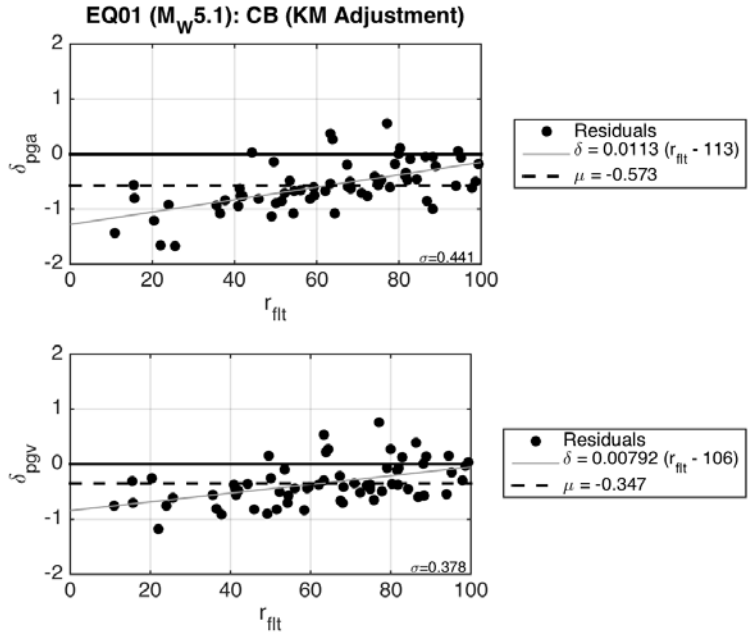

Figure 23: Adjusted delta CB

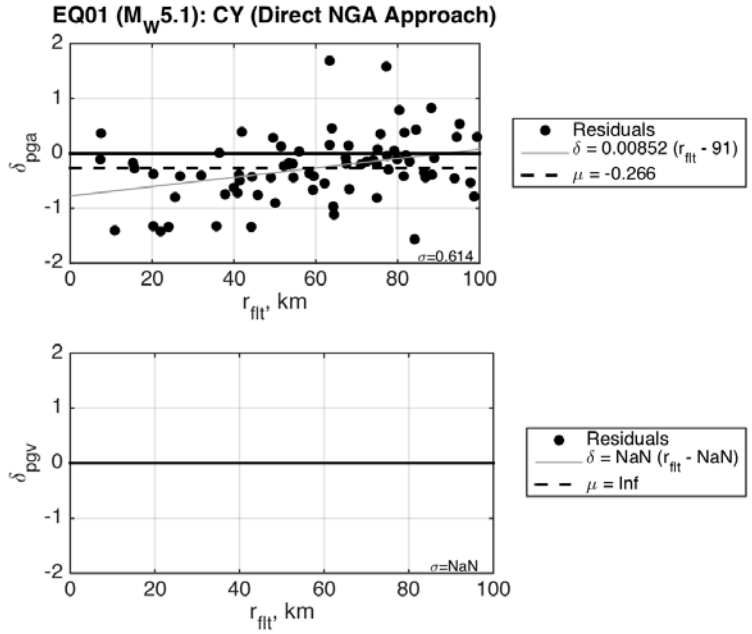

Figure 24: Raw delta CY

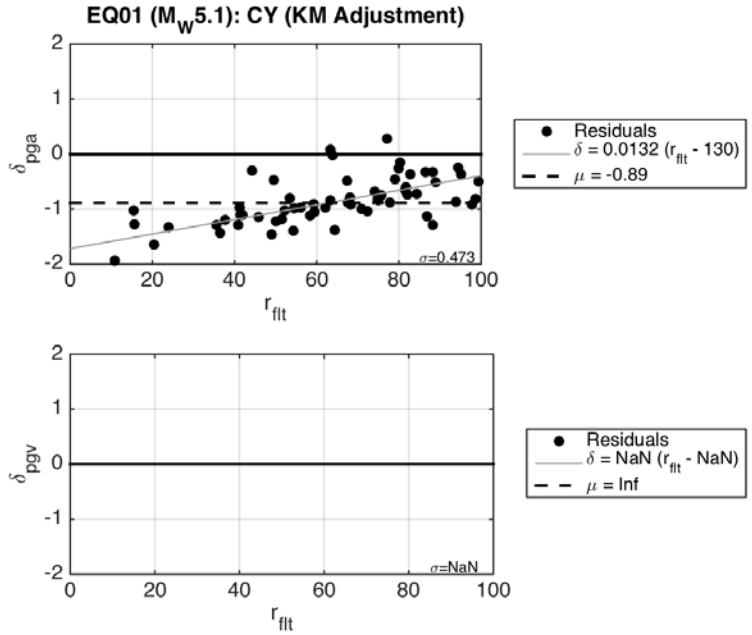

Figure 25: Adjusted delta CY

2 Earthquake 3. 2011 03 19, 18:56 Mw5.8

Figure 26 shows four frames illustrating the geometry of this earthquake.

Figure 27 shows the uncorrected values of peak acceleration as a funciton of distance, and Figure 29 shows the uncorrected values of peak velocity. For comparison, both of these figures show the NGA-West 2 models for Vs30=400 m/s, which is considered to be a reasonable estimate for the network average. Figure 28 shows the adjusted peak accelerations and Figure 30 shows adjusted peak velocities, where the adjustments to the data use Kawase factors and are adjusted to Vs30=760 m/s. Therefore, the NGA curves on these two firgures are for Vs30-760 m/s.

Residuals are shown in Figures 31-38. Raw and adjusted residuals are paired for ease in comparison. To obtain the "raw" residuals, a station-by-station estimate of Vs30 has been used within the NGA models. Since the adjustments are to a common value of vs30, station-by-station adjustments are not needed.

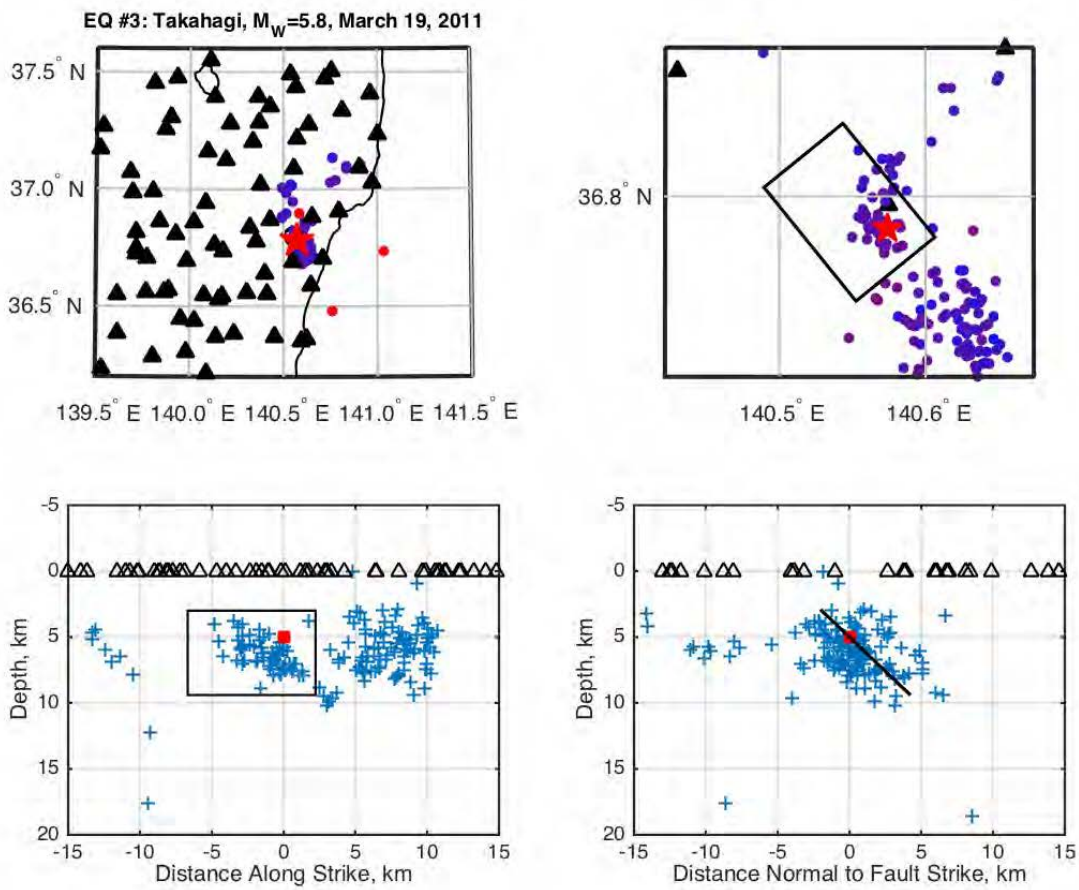

Figure 26: Location and cross section

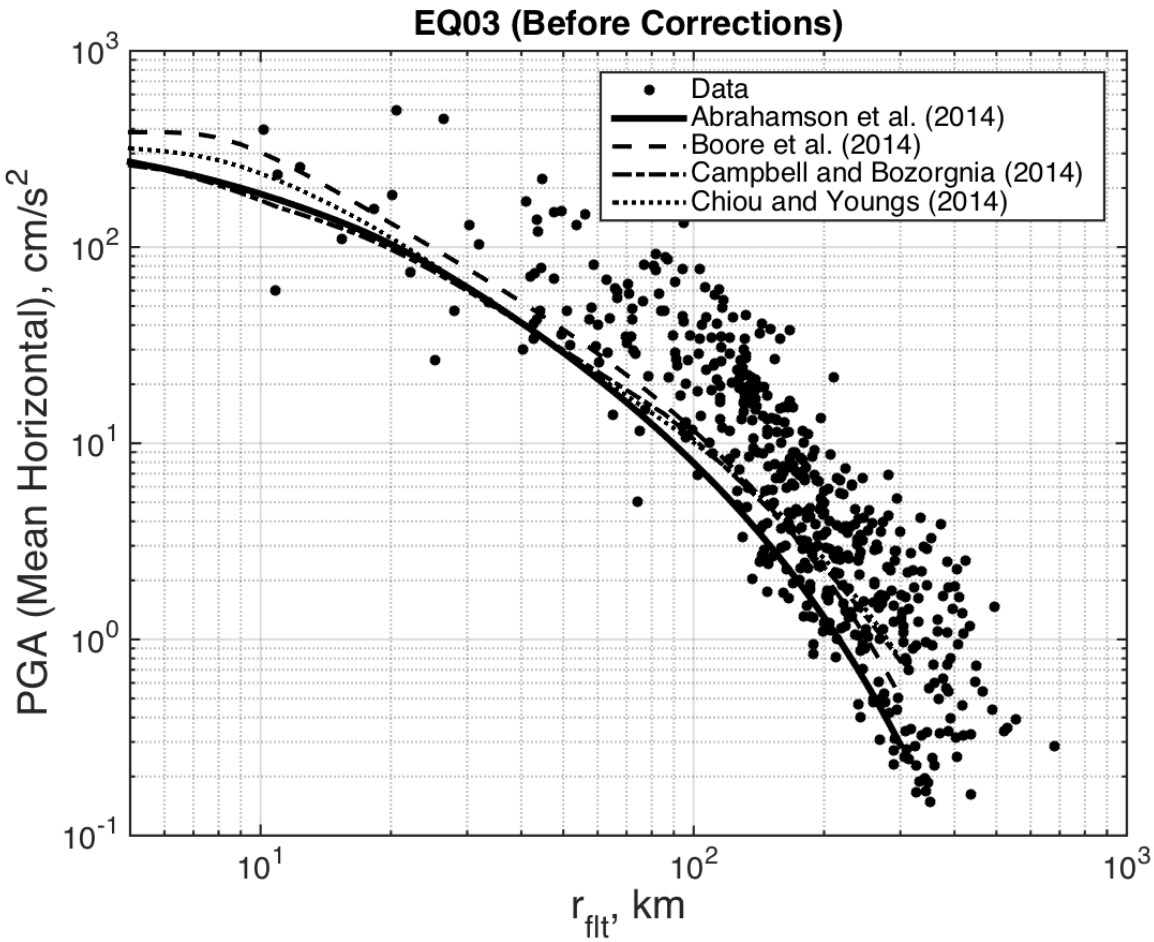

Figure 27: Raw accelerations

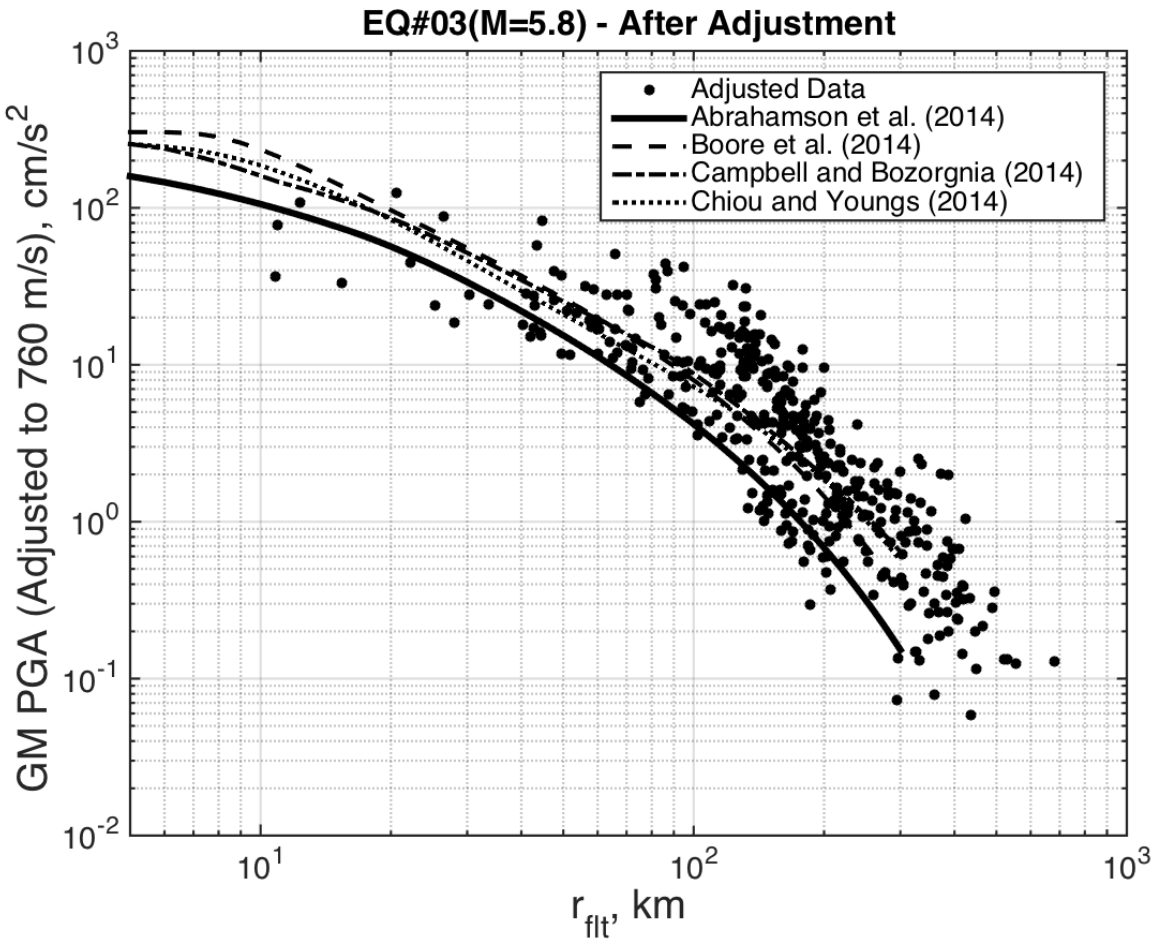

Figure 28: Adjusted accelerations

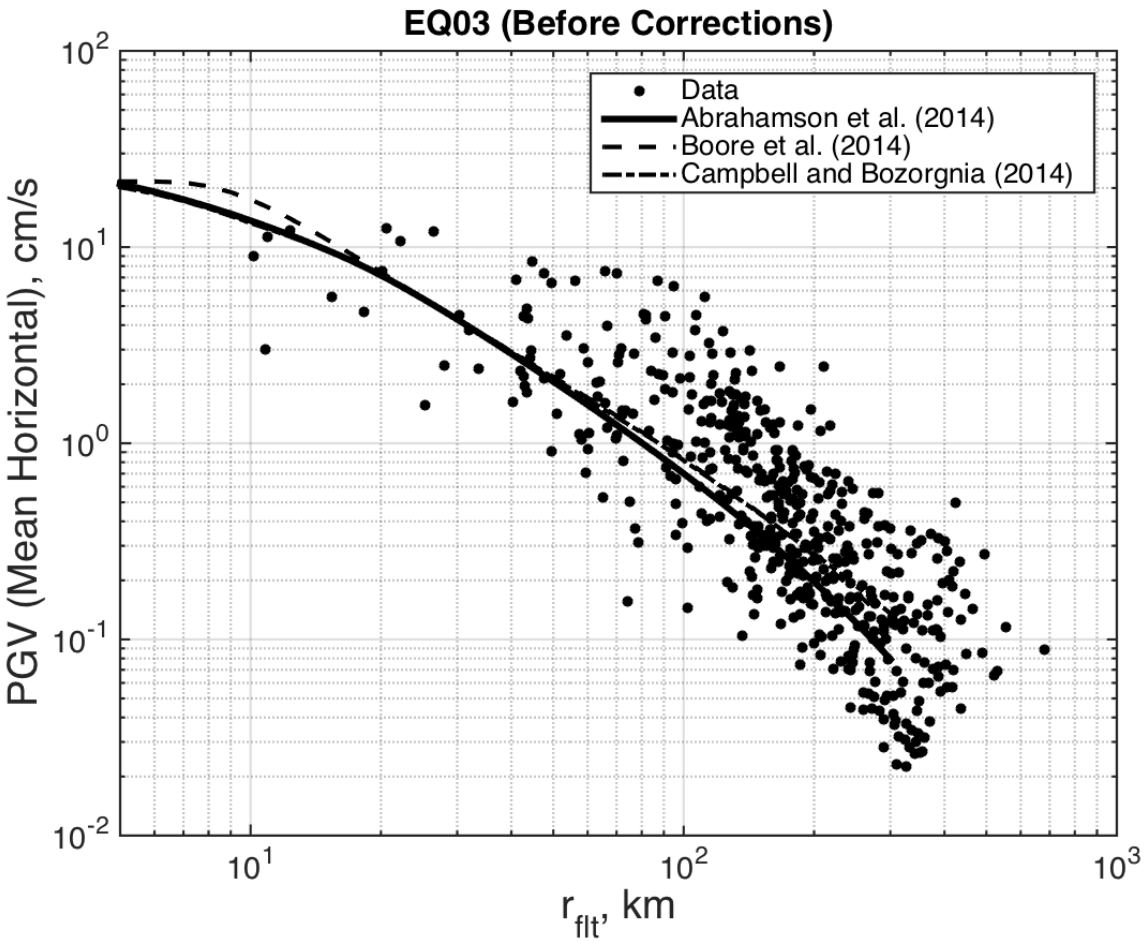

Figure 29: Raw velocities

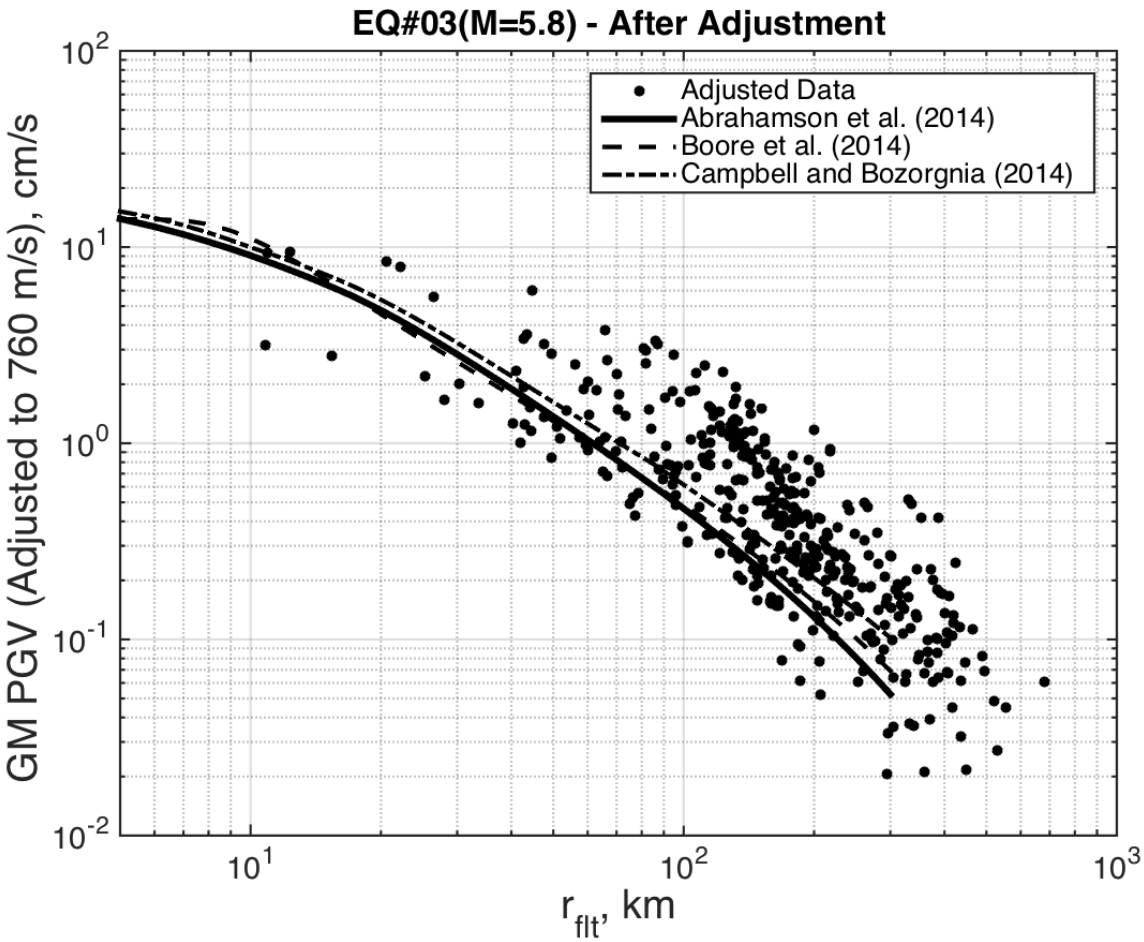

Figure 30: Adjusted velocity

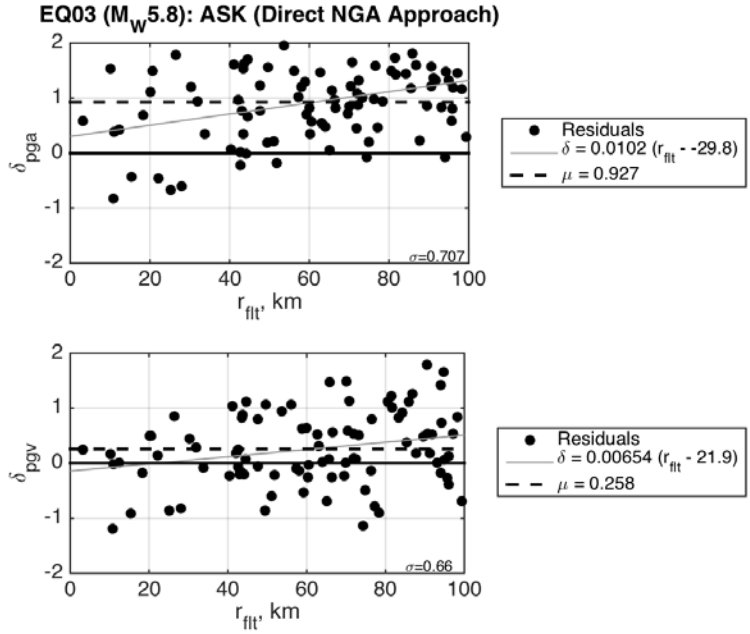

Figure 31: Raw delta ASK

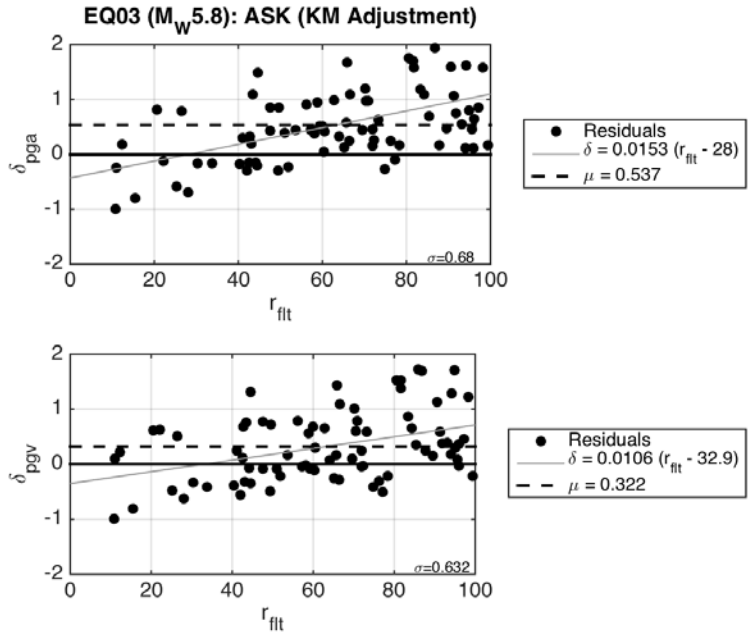

Figure 32: Adjusted delta ASK

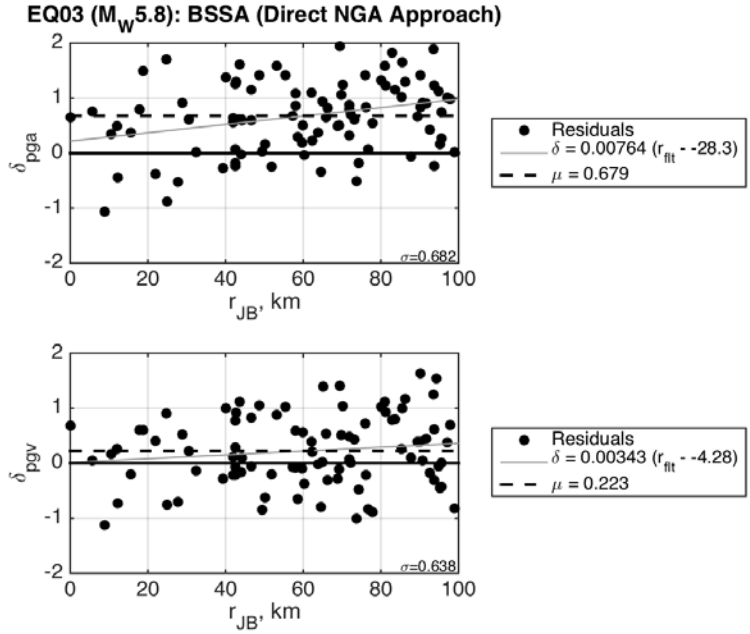

Figure 33: Raw delta BSSA

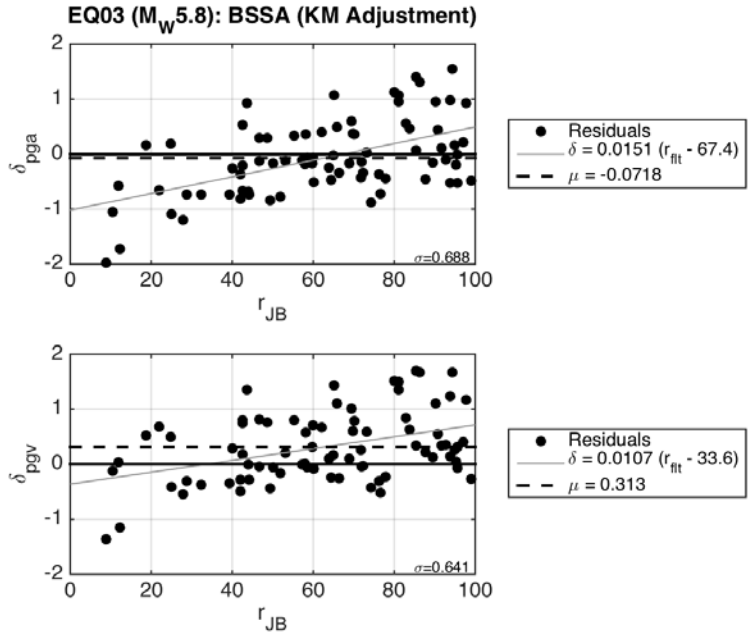

Figure 34: Adjusted delta BSSA

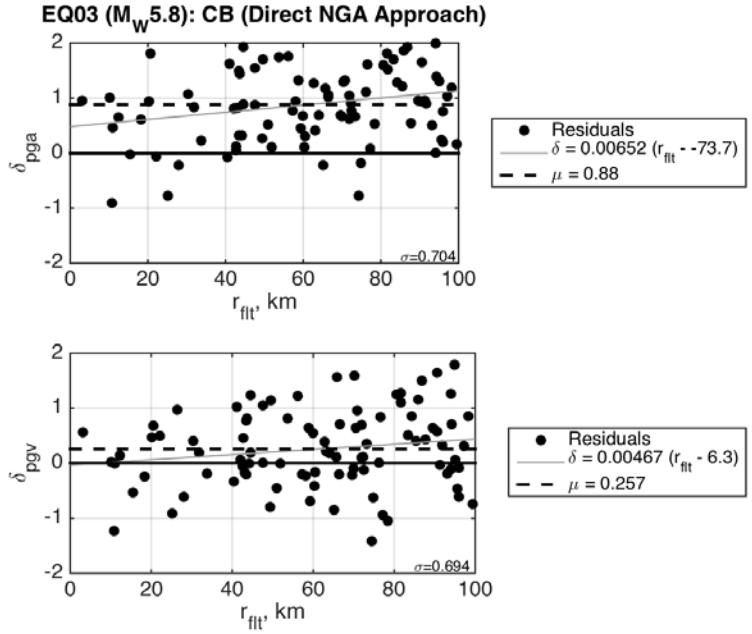

Figure 35: Raw delta CB

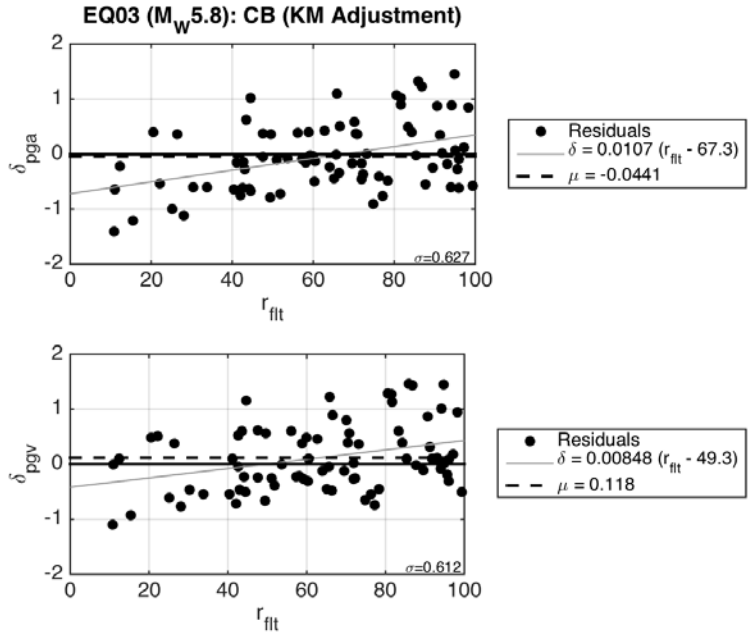

Figure 36: Adjusted delta CB

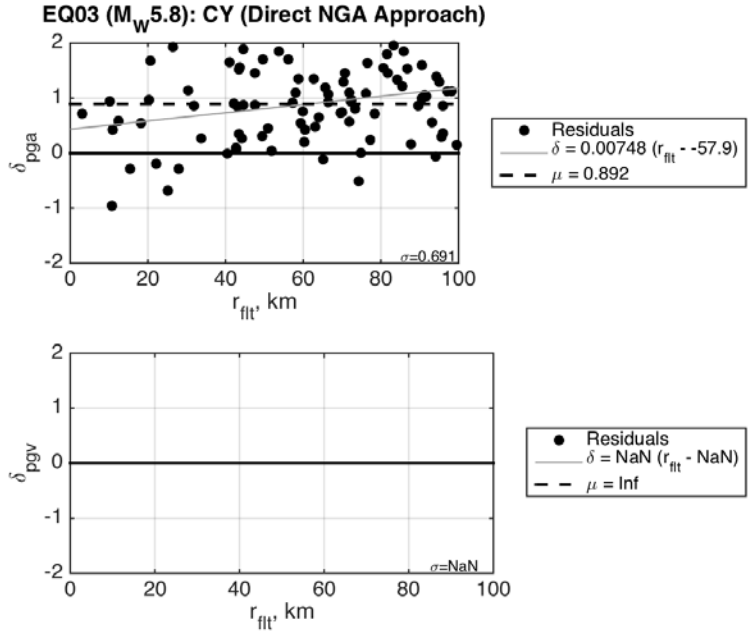

Figure 37: Raw delta CY

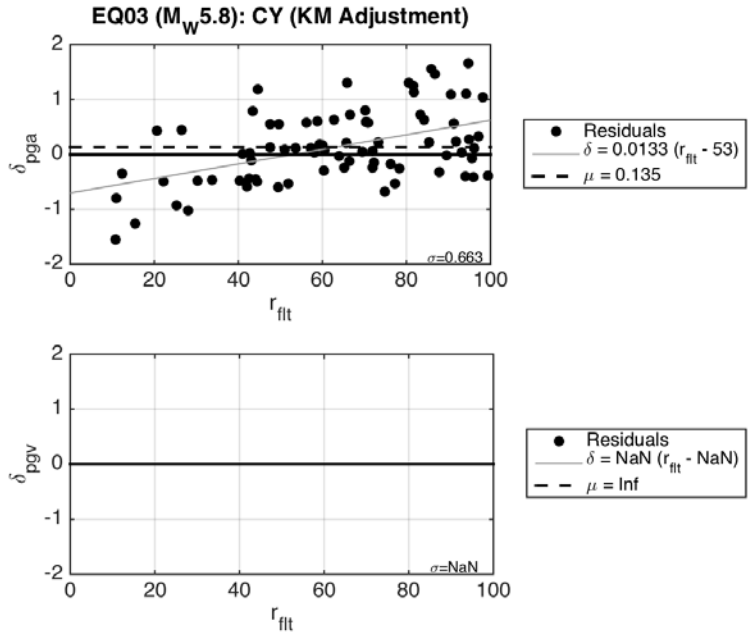

Figure 38: Adjusted delta CY

3 Earthquake 4. 2011 03 20, 10:30 Mw5.3

Figure 39 shows four frames illustrating the geometry of this earthquake.

Figure 40 shows the uncorrected values of peak acceleration as a funciton of distance, and Figure 42 shows the uncorrected values of peak velocity. For comparison, both of these figures show the NGA-West 2 models for Vs30=400 m/s, which is considered to be a reasonable estimate for the network average. Figure 41 shows the adjusted peak accelerations and Figure 42 shows adjusted peak velocities, where the adjustments to the data use Kawase factors and are adjusted to Vs30=760 m/s. Therefore, the NGA curves on these two firgures are for Vs30-760 m/s.

Residuals are shown in Figures 46-51. Raw and adjusted residuals are paired for ease in comparison. To obtain the "raw" residuals, a station-by-station estimate of Vs30 has been used within the NGA models. Since the adjustments are to a common value of vs30, station-by-station adjustments are not needed.

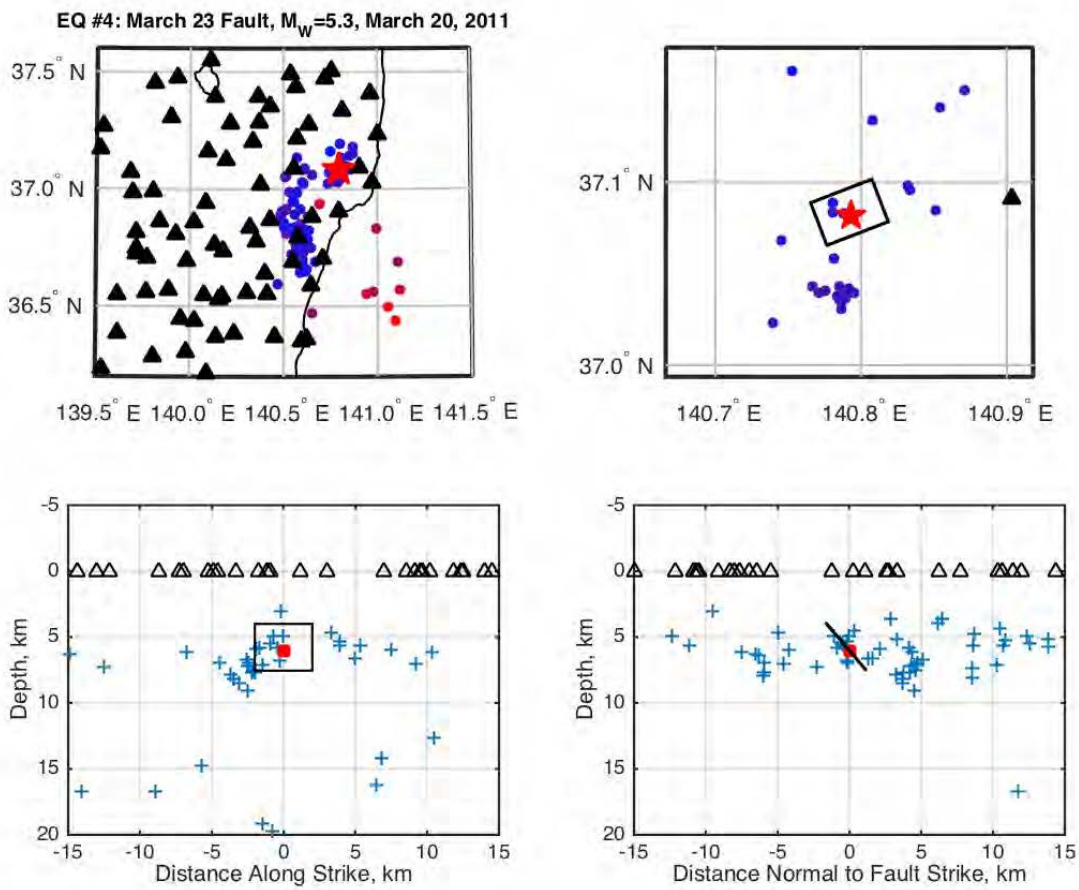

Figure 39: Location and cross section

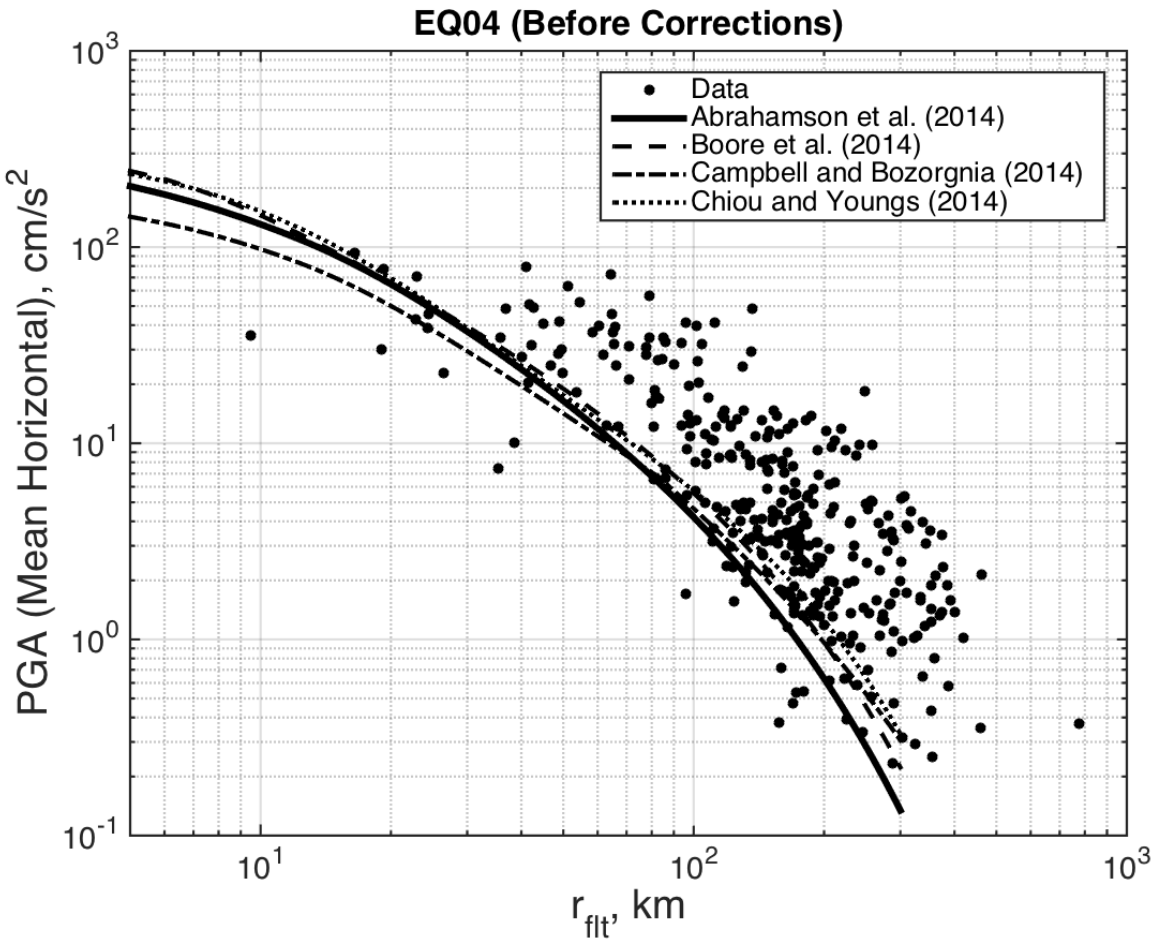

Figure 40: Raw accelerations

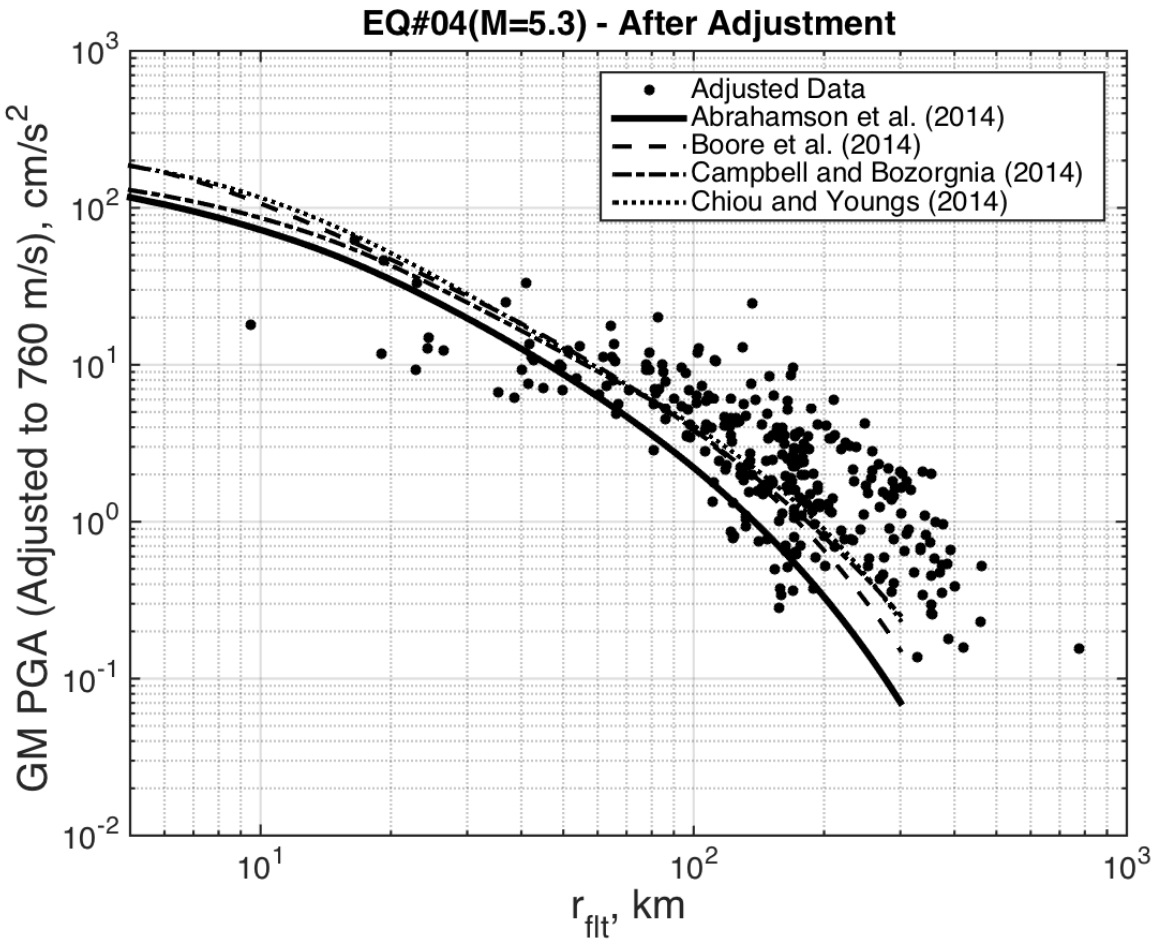

Figure 41: Adjusted accelerations

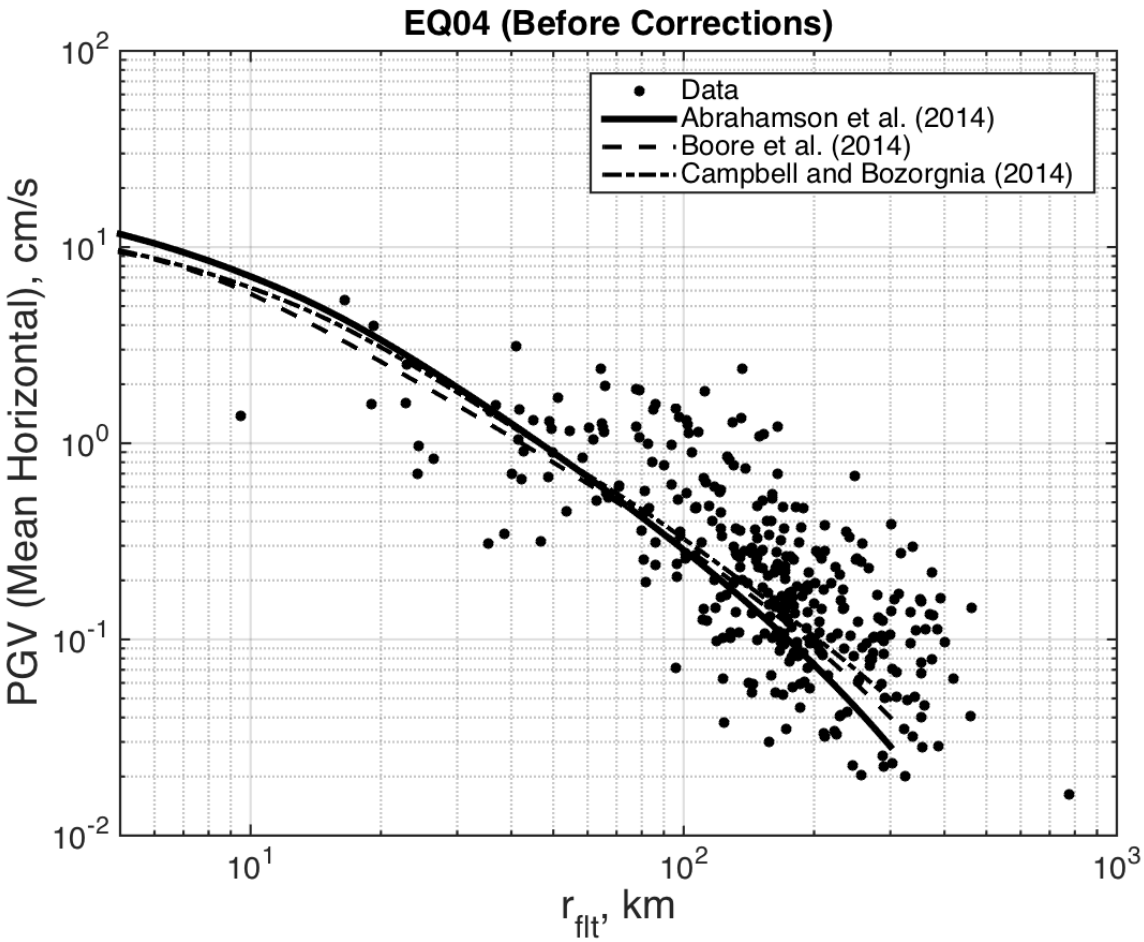

Figure 42: Raw velocities

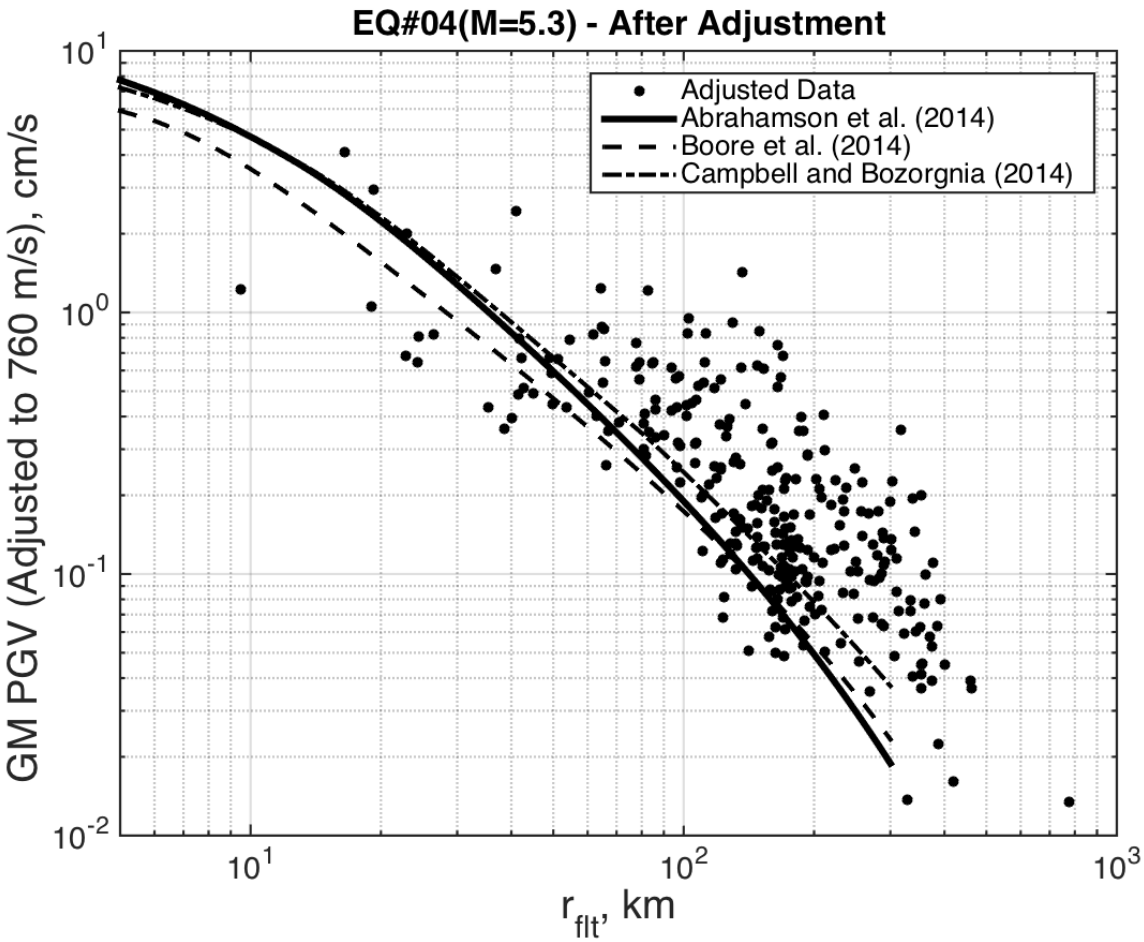

Figure 43: Adjusted velocity

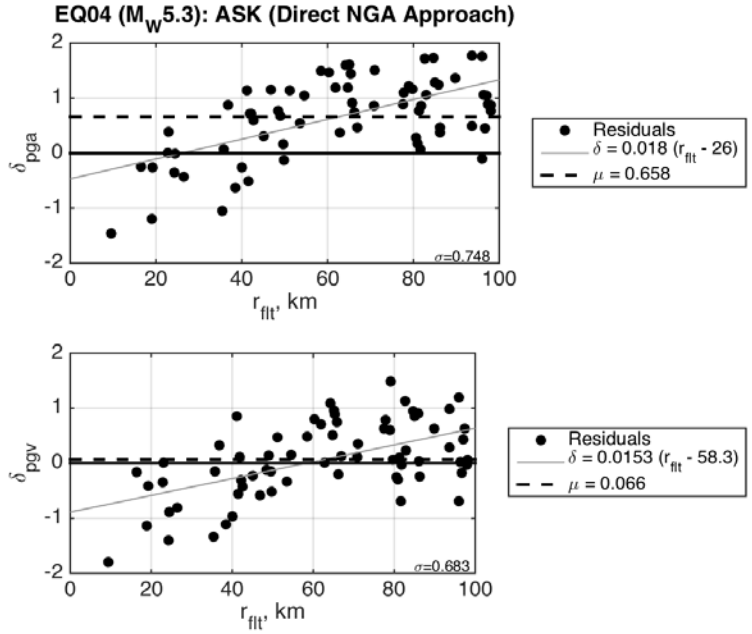

Figure 44: Raw delta ASK

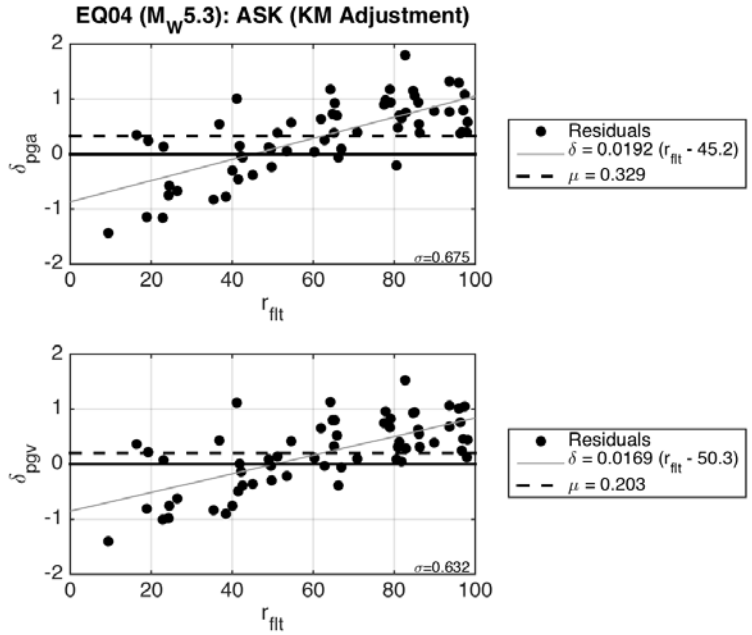

Figure 45: Adjusted delta ASK

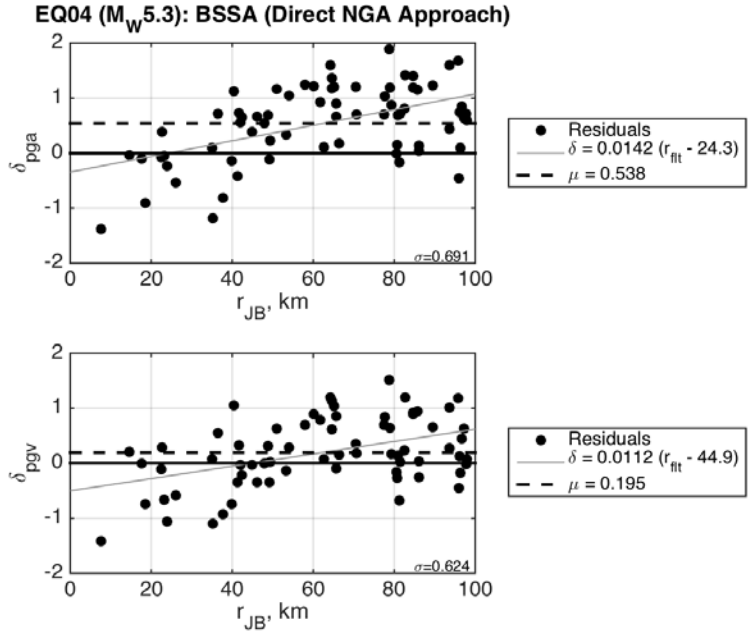

Figure 46: Raw delta BSSA

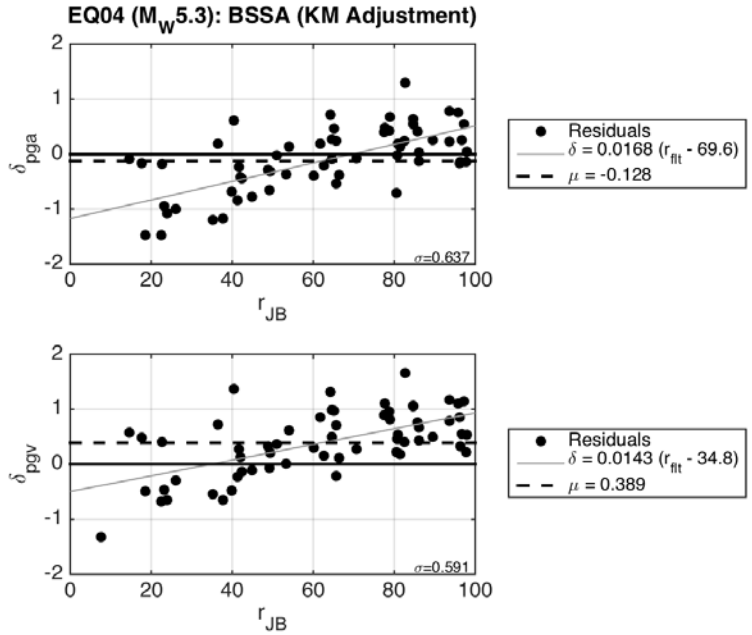

Figure 47: Adjusted delta BSSA

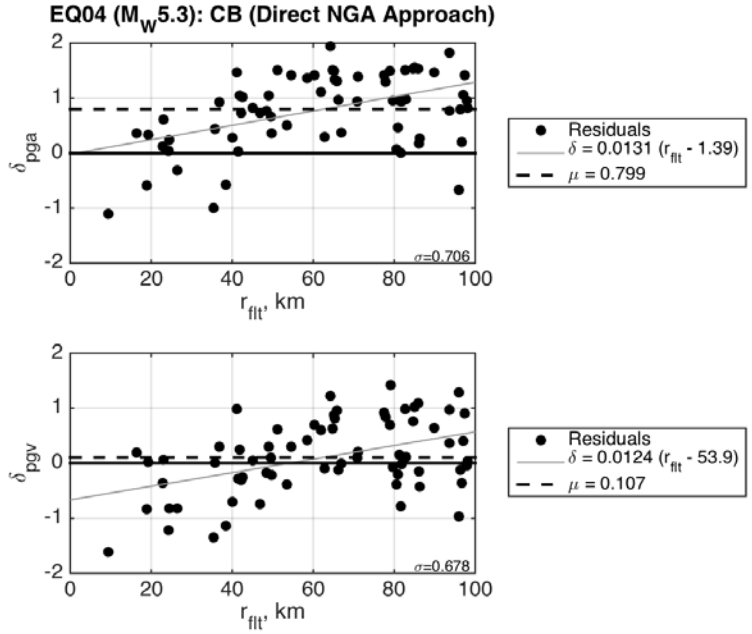

Figure 48: Raw delta CB

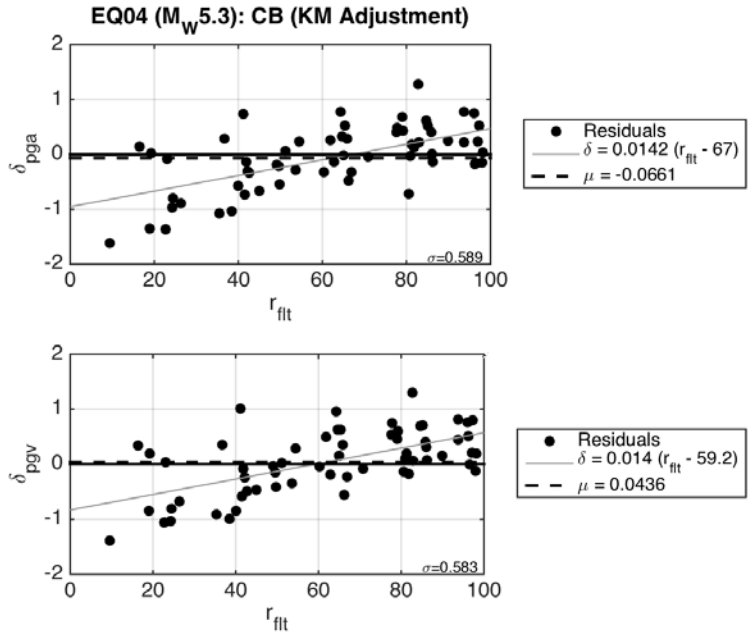

Figure 49: Adjusted delta CB

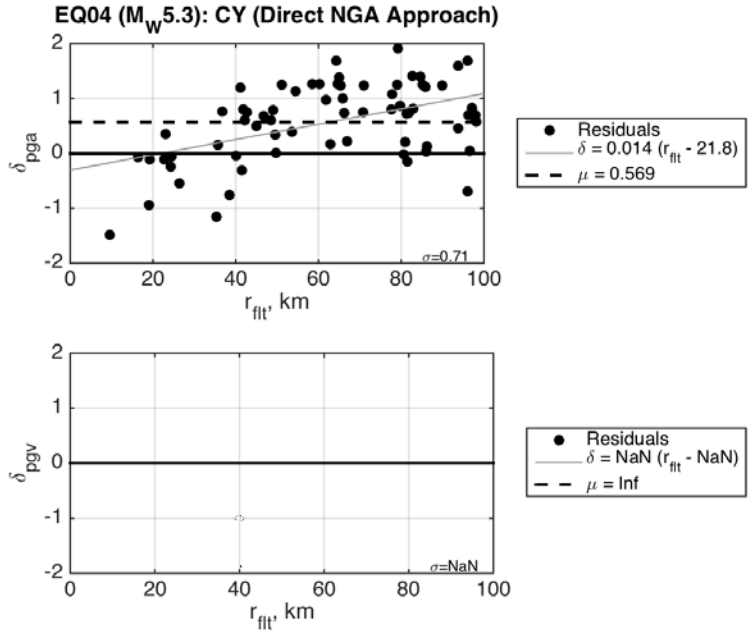

Figure 50: Raw delta CY

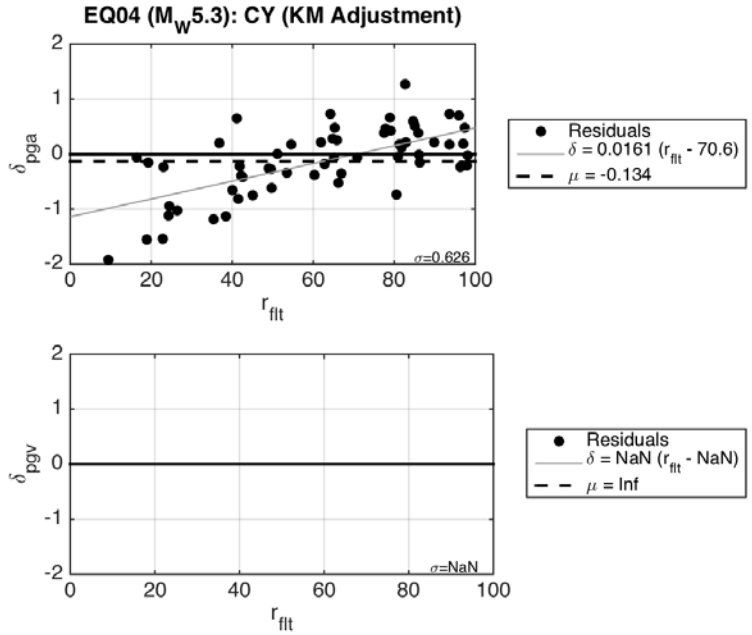

Figure 51: Adjusted delta CY

4 Earthquake 5. 2011 03 23, 07:12 Mw5.7

Figure 52 shows four frames illustrating the geometry of this earthquake.

Figure 53 shows the uncorrected values of peak acceleration as a funciton of distance, and Figure 55 shows the uncorrected values of peak velocity. For comparison, both of these figures show the NGA-West 2 models for Vs30=400 m/s, which is considered to be a reasonable estimate for the network average. Figure 54 shows the adjusted peak accelerations and Figure 56 shows adjusted peak velocities, where the adjustments to the data use Kawase factors and are adjusted to Vs30=760 m/s. Therefore, the NGA curves on these two firgures are for Vs30-760 m/s.

Residuals are shown in Figures 57-64. Raw and adjusted residuals are paired for ease in comparison. To obtain the "raw" residuals, a station-by-station estimate of Vs30 has been used within the NGA models. Since the adjustments are to a common value of vs30, station-by-station adjustments are not needed.

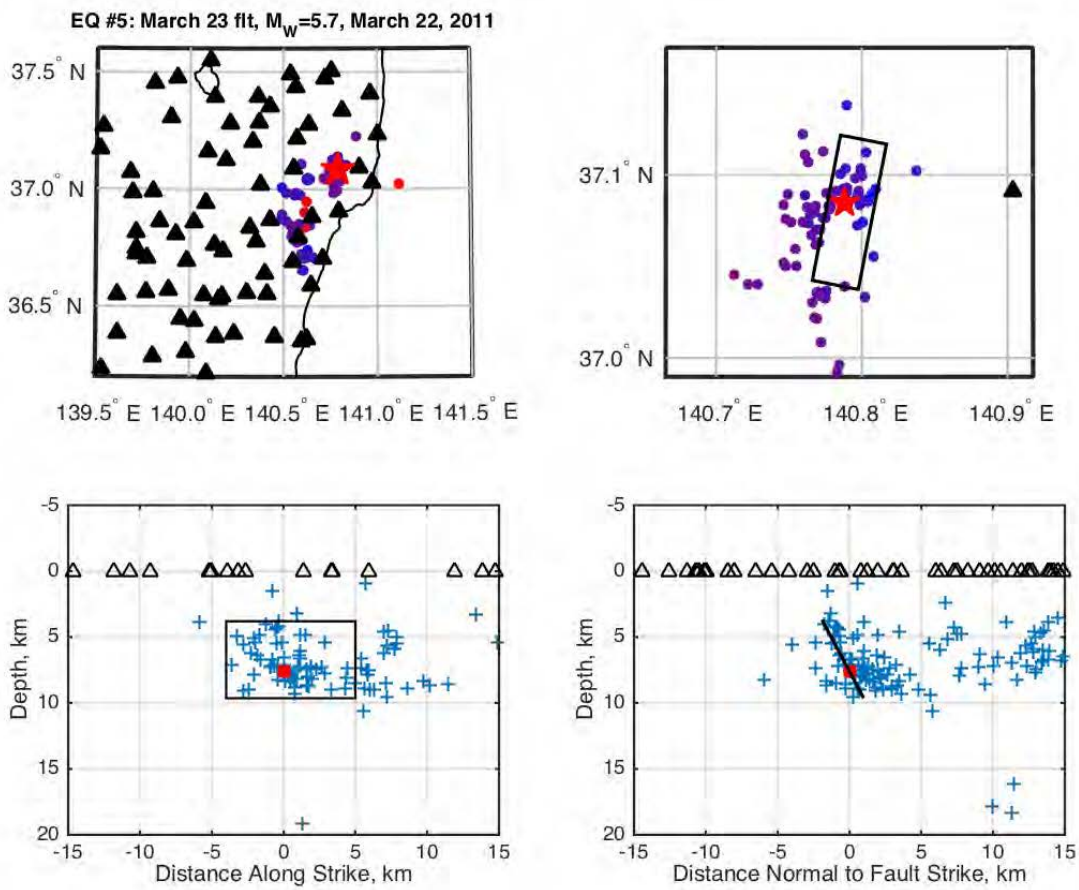

Figure 52: Location and cross section

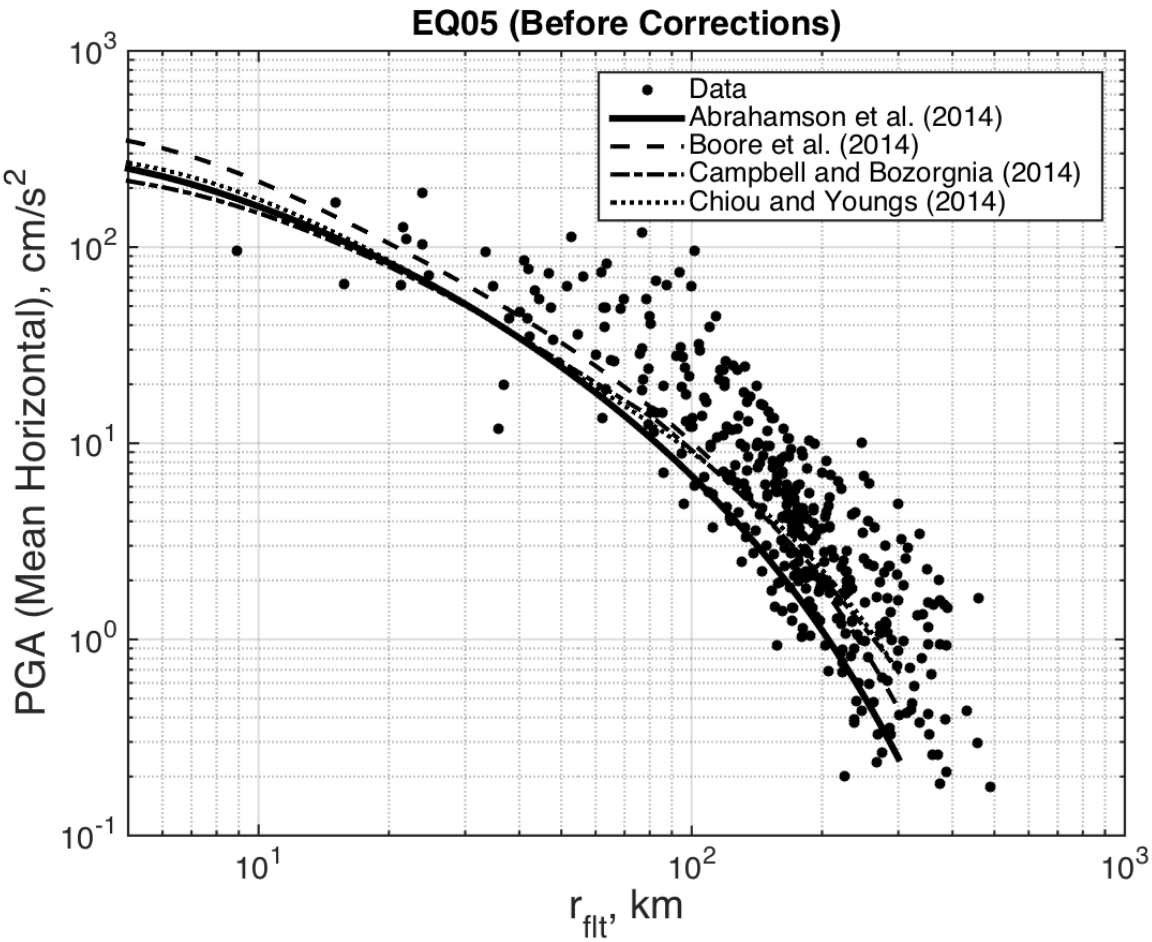

Figure 53: Raw accelerations

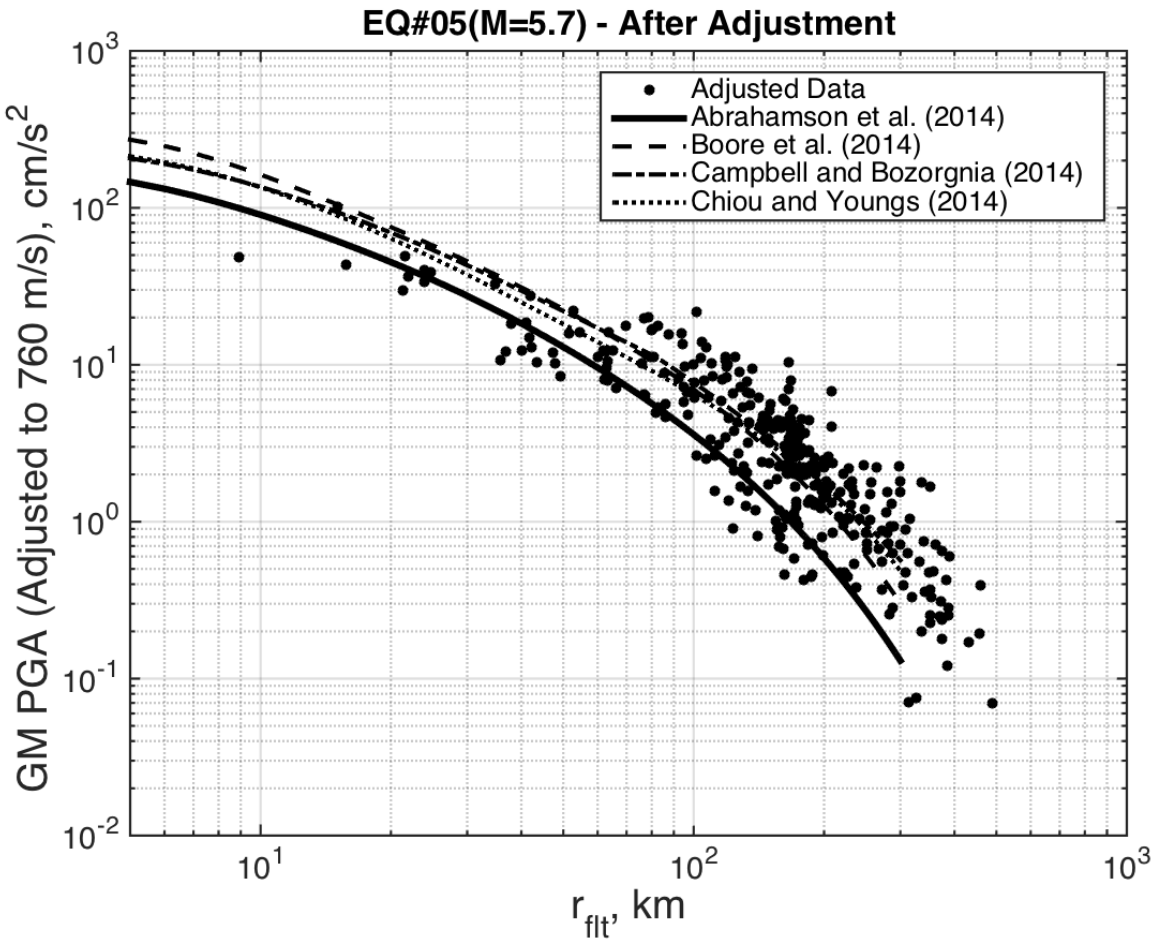

Figure 54: Adjusted accelerations

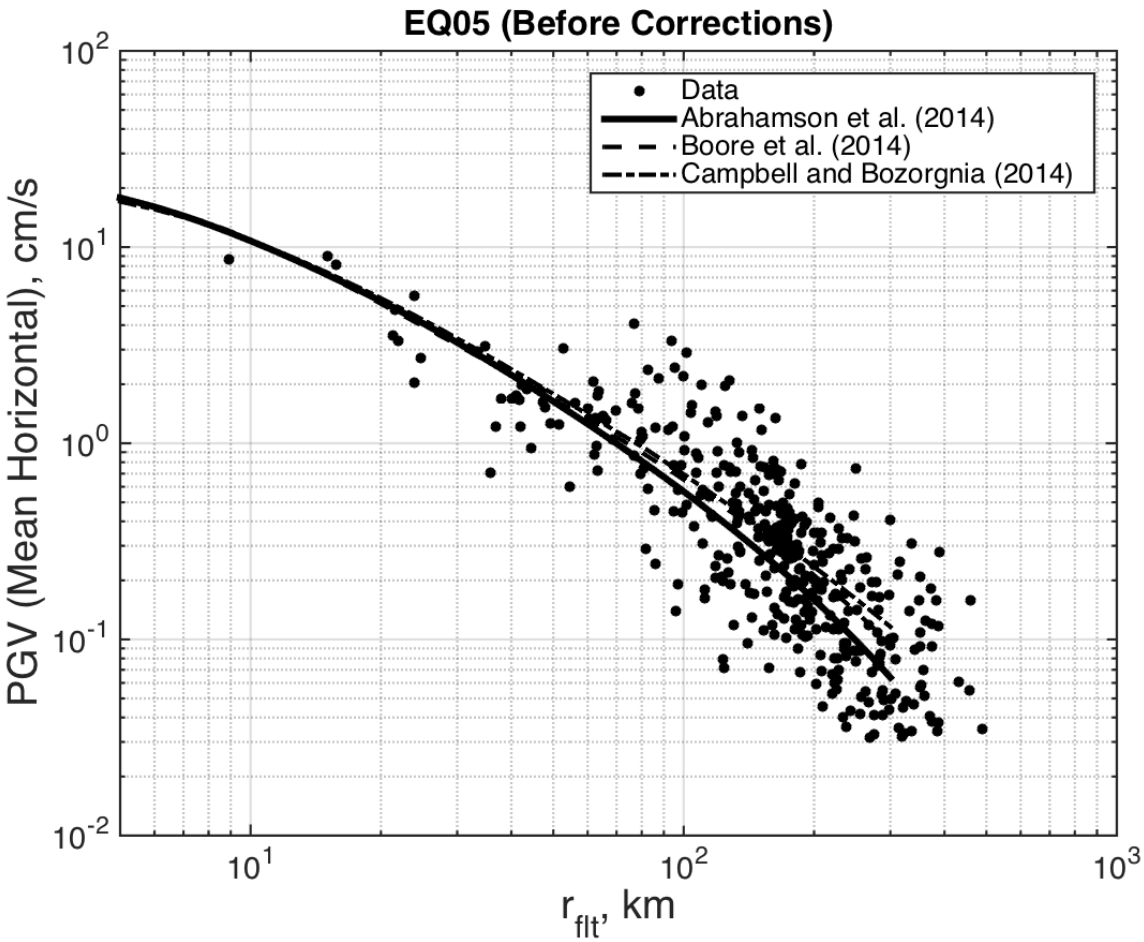

Figure 55: Raw velocities

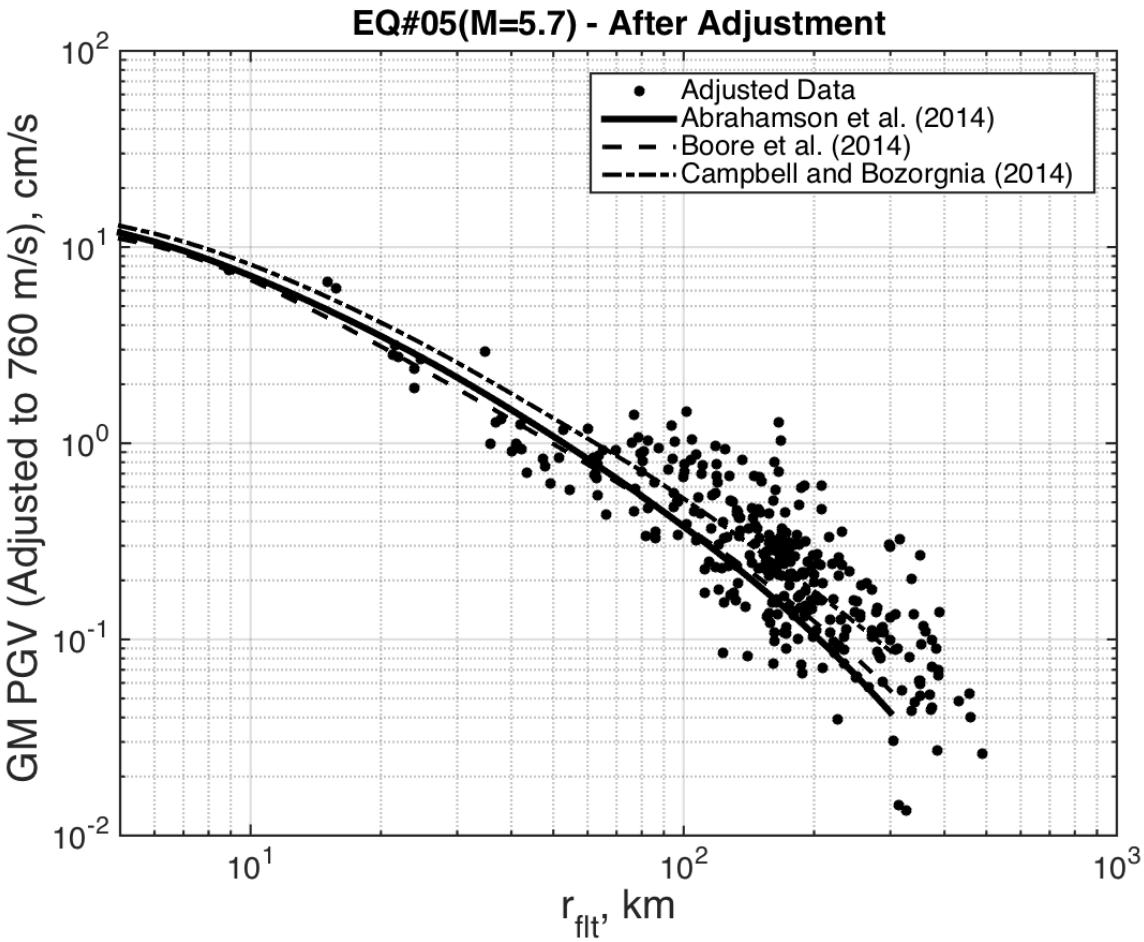

Figure 56: Adjusted velocity

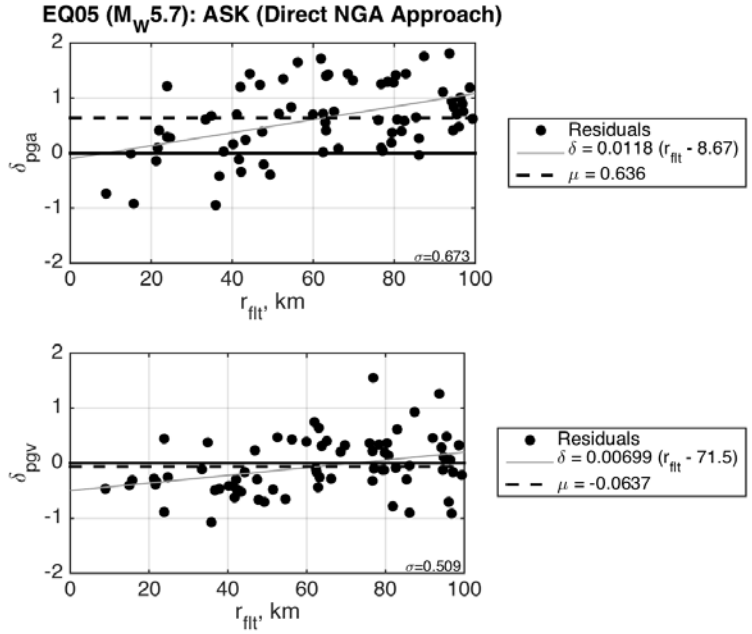

Figure 57: Raw delta ASK

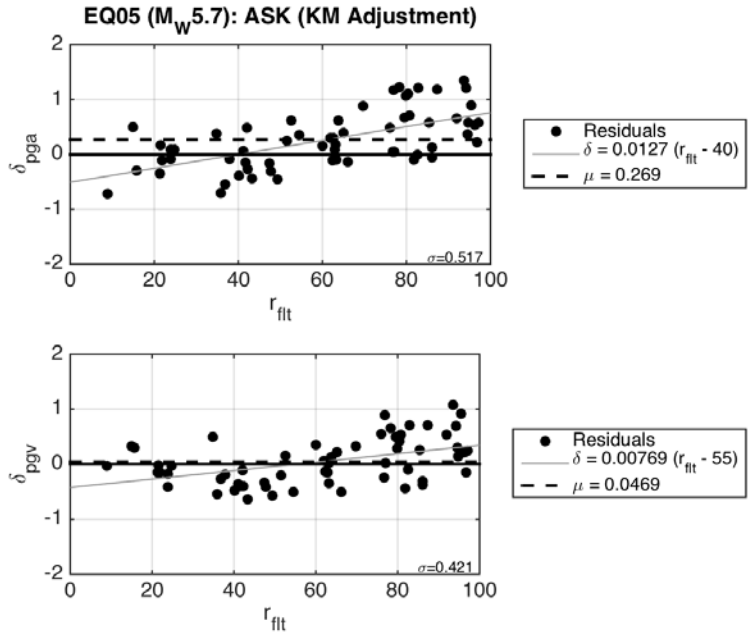

Figure 58: Adjusted delta ASK

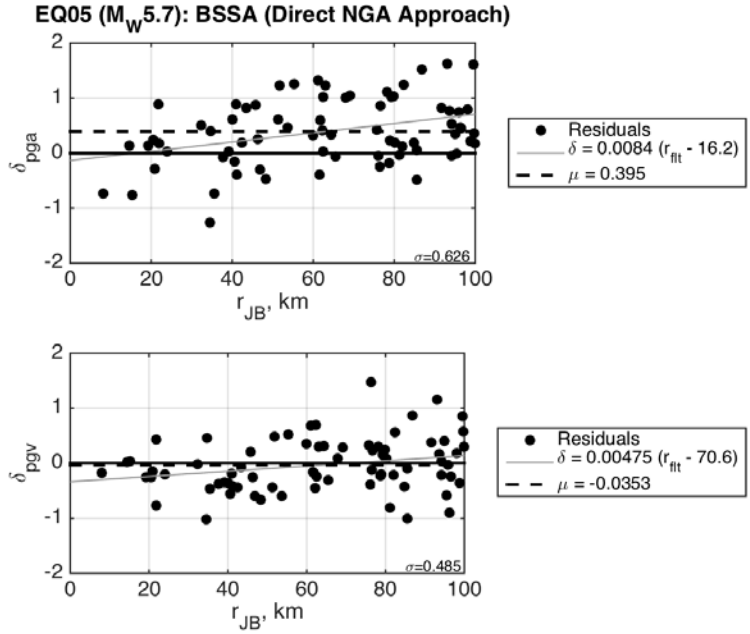

Figure 59: Raw delta BSSA

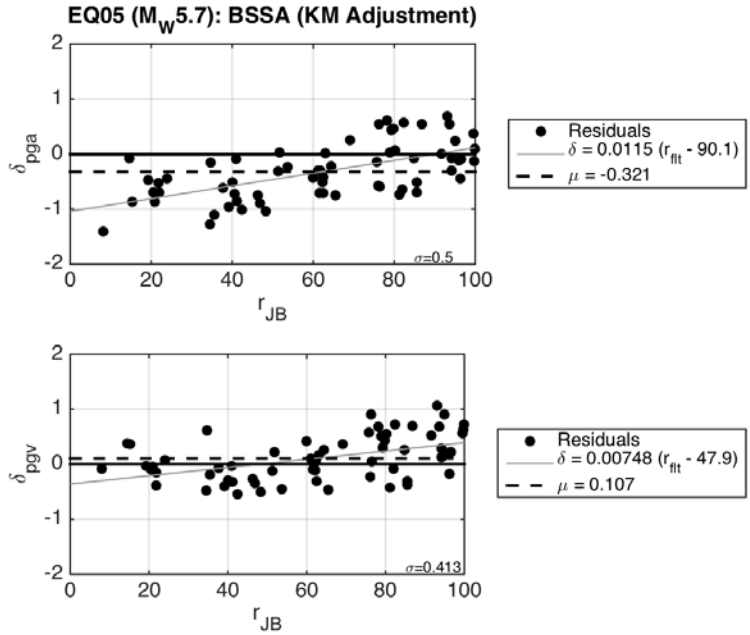

Figure 60: Adjusted delta BSSA

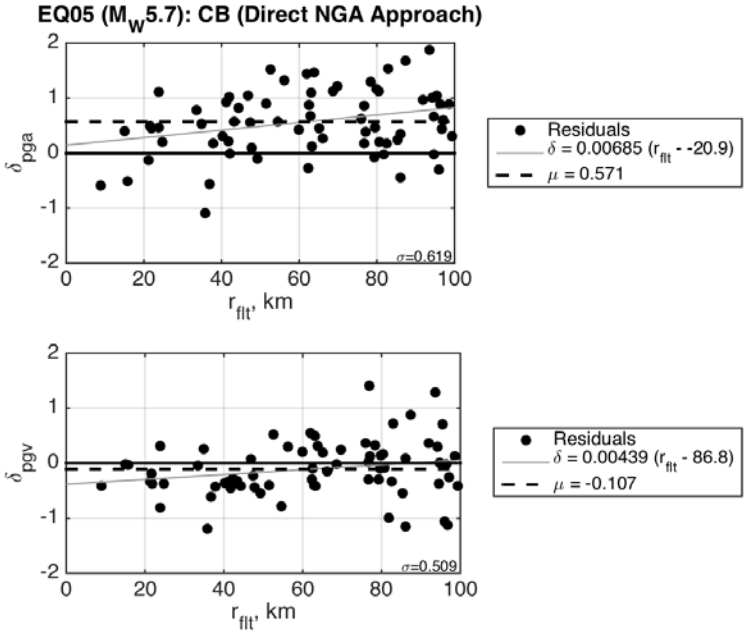

Figure 61: Raw delta CB

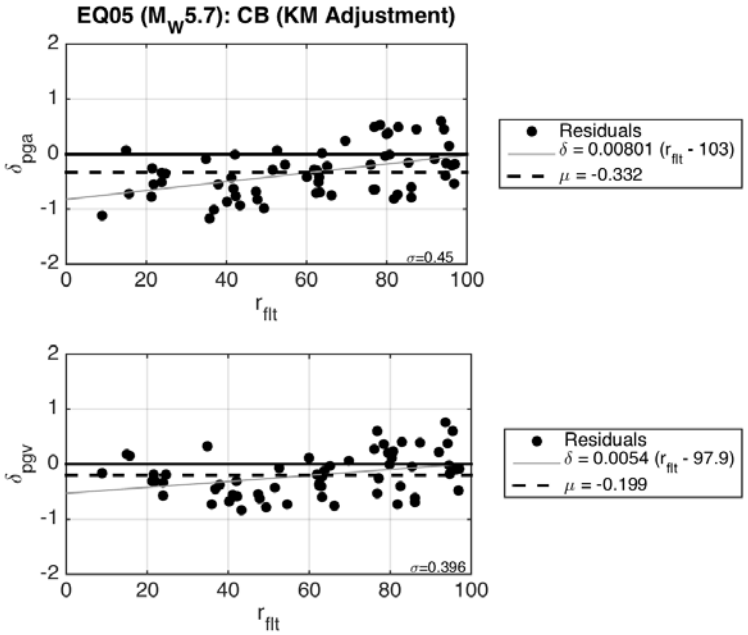

Figure 62: Adjusted delta CB

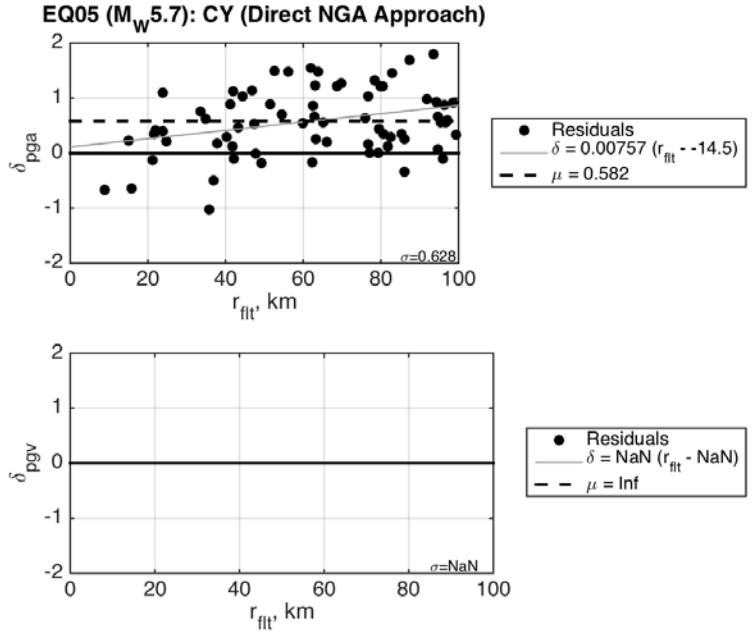

Figure 63: Raw delta CY

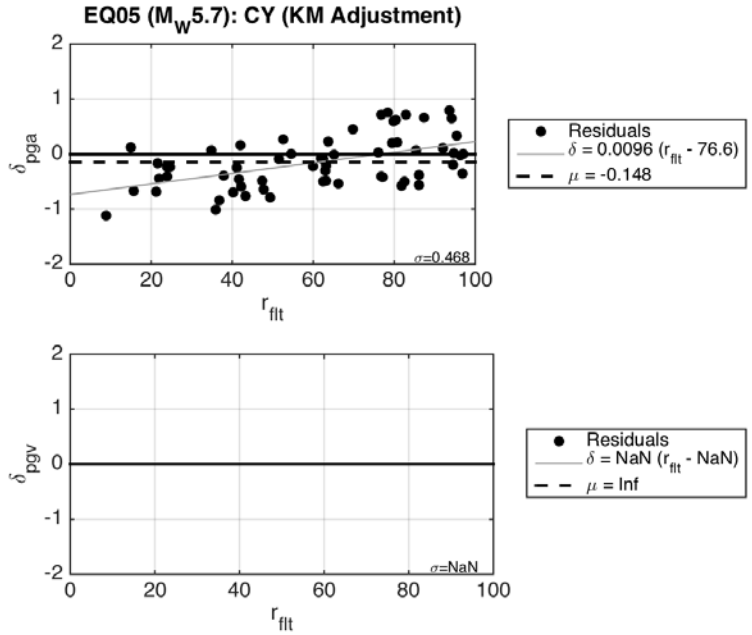

Figure 64: Adjusted delta CY

5 Earthquake 8. 2011 03 23, 07:36 Mw5.4

Figure 65 shows four frames illustrating the geometry of this earthquake.

Figure 66 shows the uncorrected values of peak acceleration as a funciton of distance, and Figure 68 shows the uncorrected values of peak velocity. For comparison, both of these figures show the NGA-West 2 models for Vs30=400 m/s, which is considered to be a reasonable estimate for the network average. Figure 67 shows the adjusted peak accelerations and Figure 69 shows adjusted peak velocities, where the adjustments to the data use Kawase factors and are adjusted to Vs30=760 m/s. Therefore, the NGA curves on these two firgures are for Vs30-760 m/s.

Residuals are shown in Figures 70-77. Raw and adjusted residuals are paired for ease in comparison. To obtain the "raw" residuals, a station-by-station estimate of Vs30 has been used within the NGA models. Since the adjustments are to a common value of vs30, station-by-station adjustments are not needed.

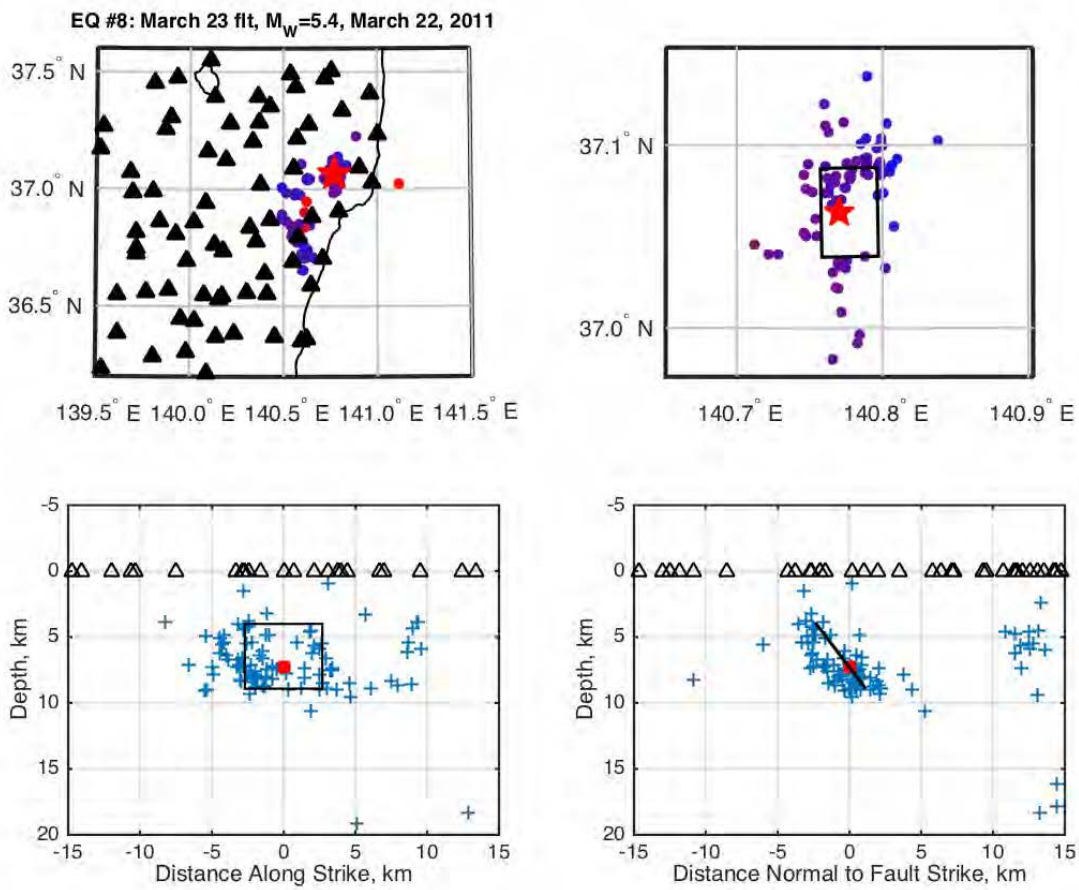

Figure 65: Location and cross section

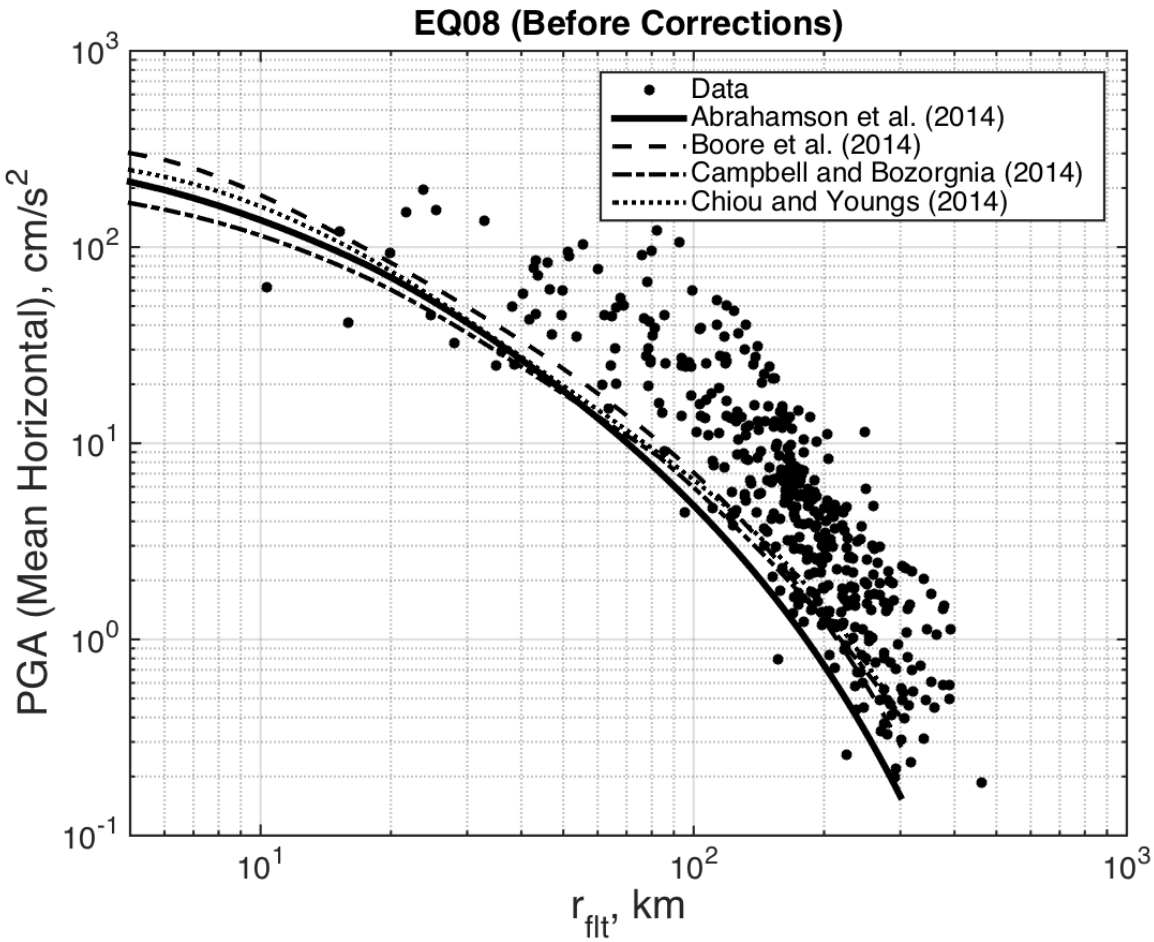

Figure 66: Raw accelerations

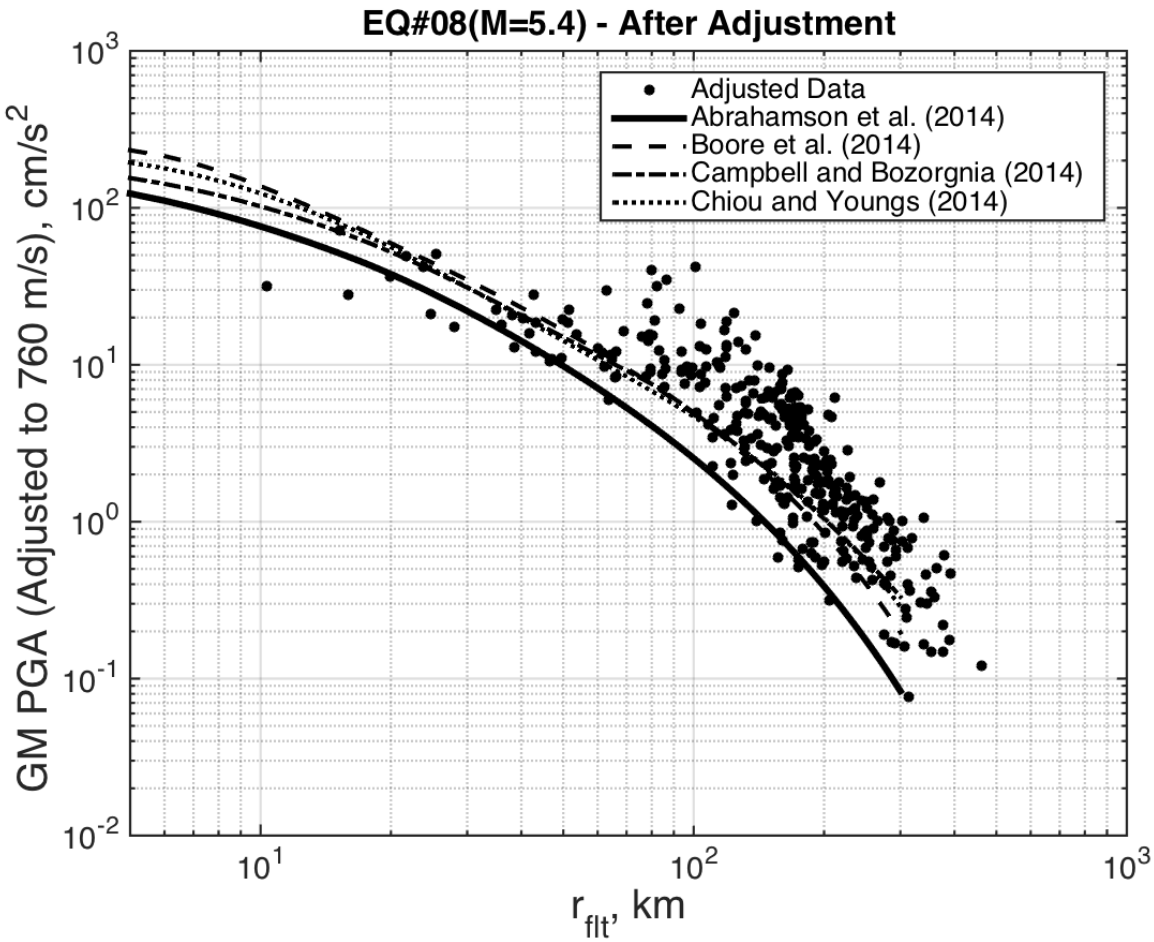

Figure 67: Adjusted accelerations

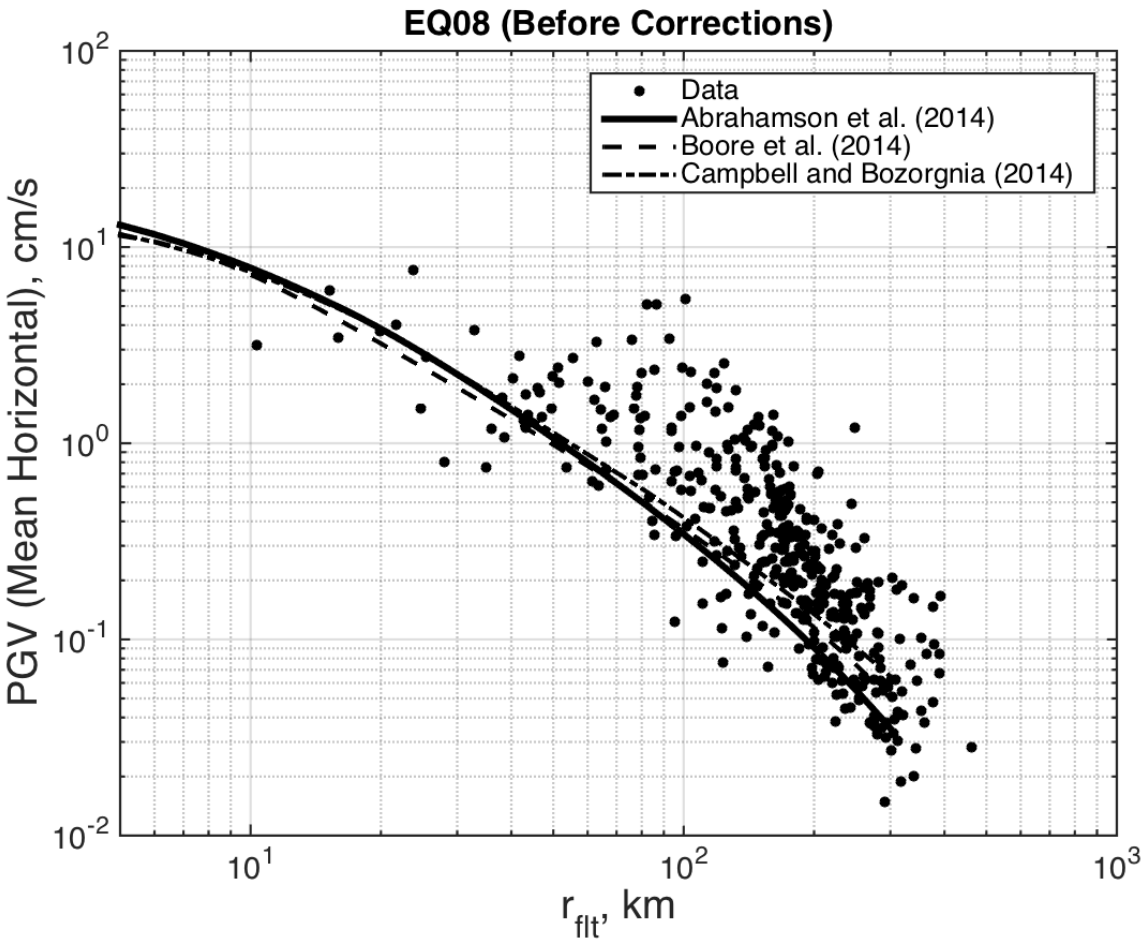

Figure 68: Raw velocities

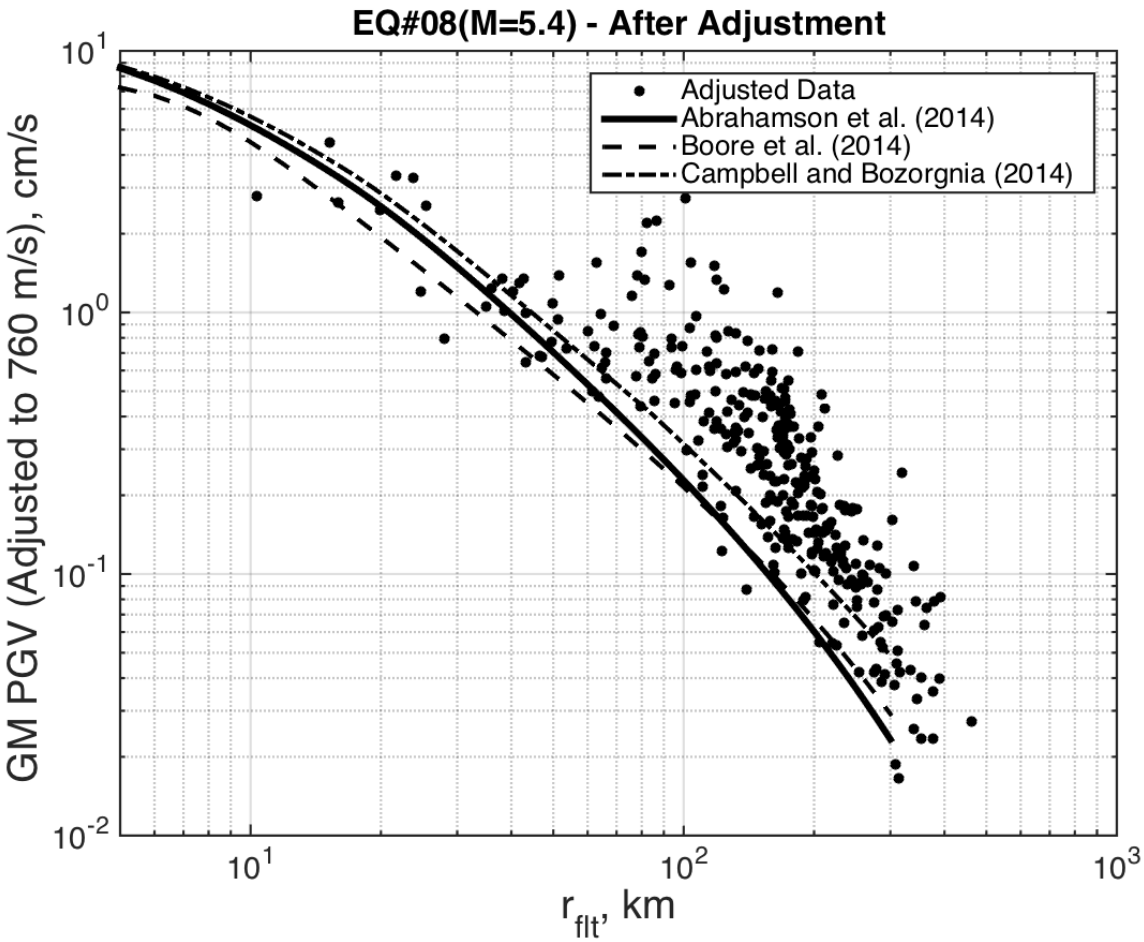

Figure 69: Adjusted velocity

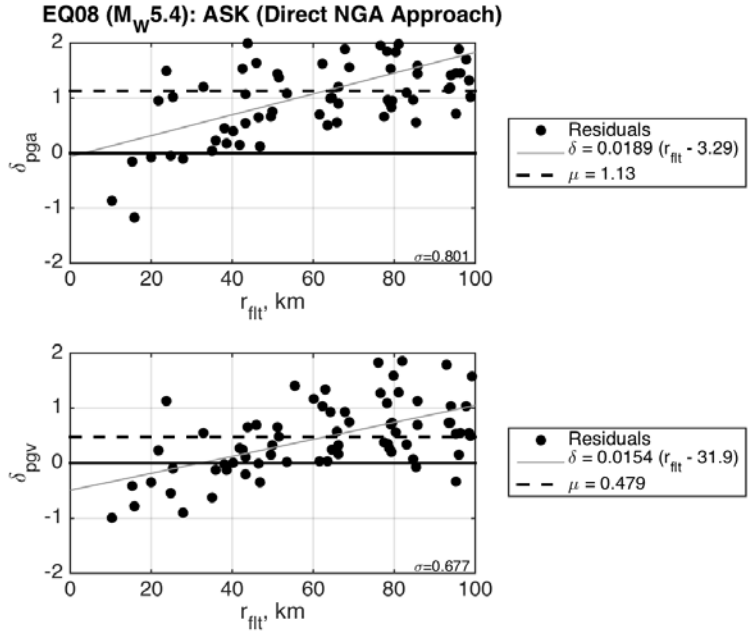

Figure 70: Raw delta ASK

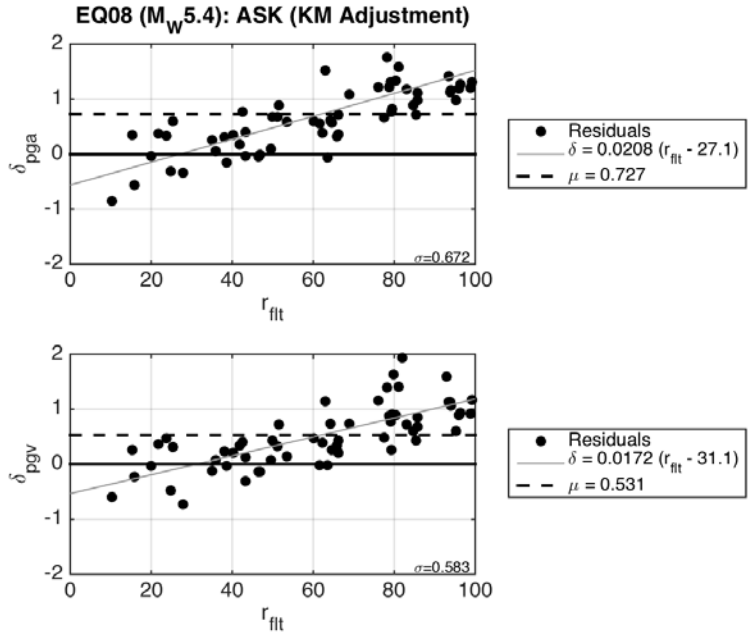

Figure 71: Adjusted delta ASK

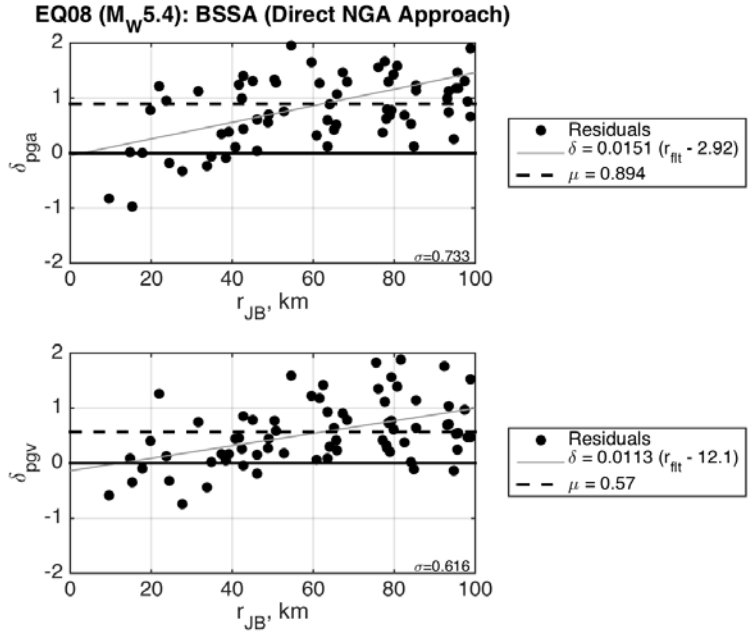

Figure 72: Raw delta BSSA

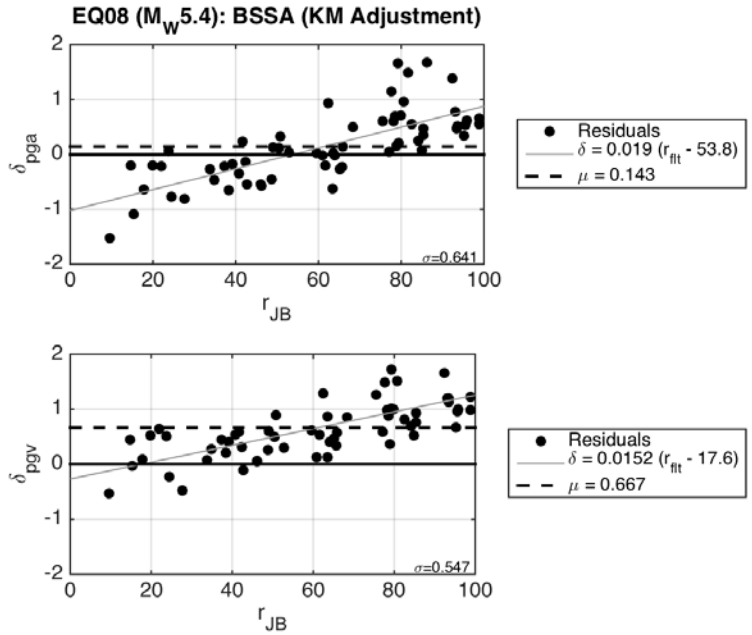

Figure 73: Adjusted delta BSSA

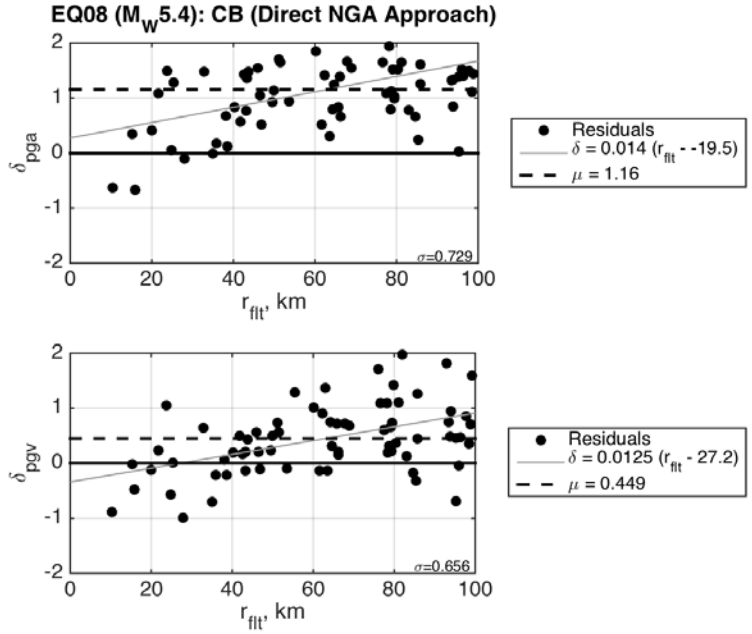

Figure 74: Raw delta CB

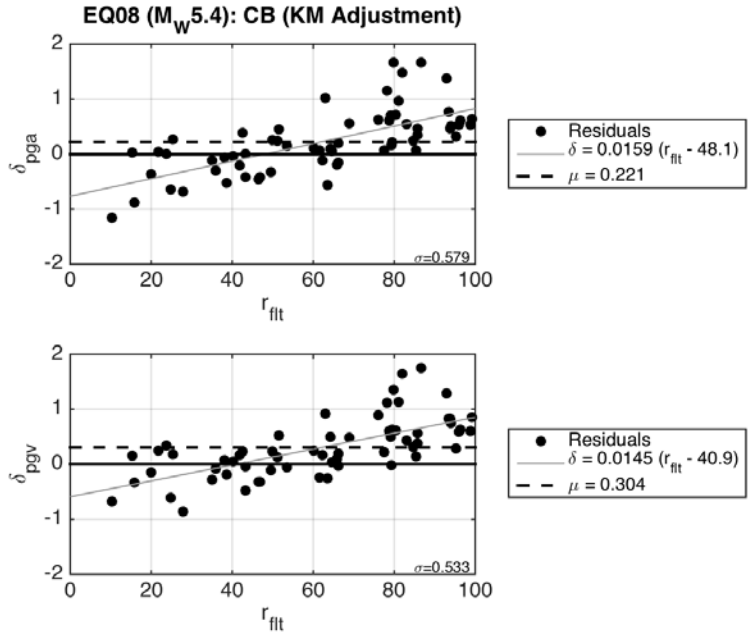

Figure 75: Adjusted delta CB

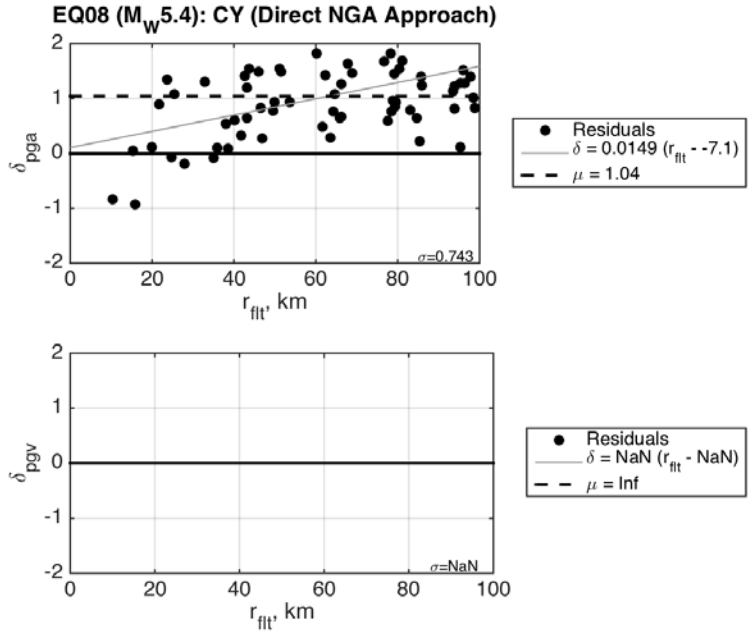

Figure 76: Raw delta CY

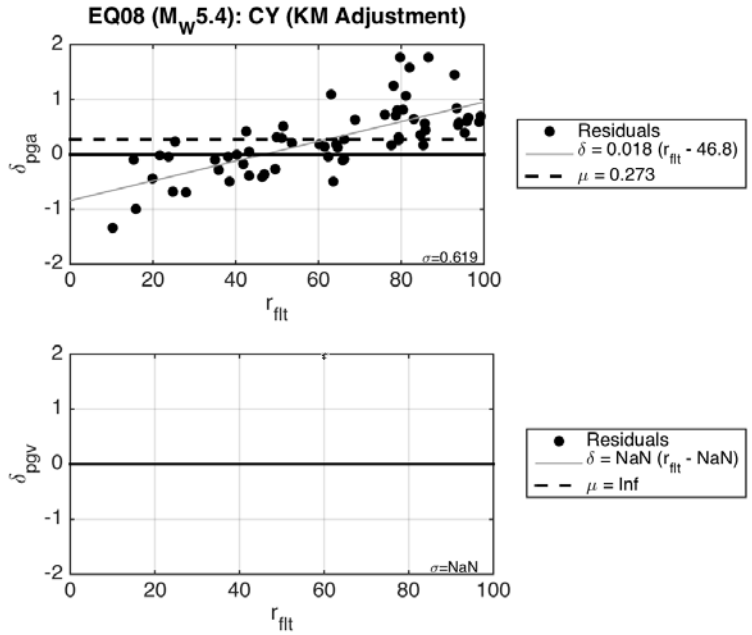

Figure 77: Adjusted delta CY

6 Earthquake 9. 2011 04 11, 17:16 Mw6.7

Figure 78 shows four frames illustrating the geometry of this earthquake.

Figure 79 shows the uncorrected values of peak acceleration as a funciton of distance, and Figure 81 shows the uncorrected values of peak velocity. For comparison, both of these figures show the NGA-West 2 models for Vs30=400 m/s, which is considered to be a reasonable estimate for the network average. Figure 80 shows the adjusted peak accelerations and Figure 82 shows adjusted peak velocities, where the adjustments to the data use Kawase factors and are adjusted to Vs30=760 m/s. Therefore, the NGA curves on these two firgures are for Vs30-760 m/s.

Residuals are shown in Figures 83-90. Raw and adjusted residuals are paired for ease in comparison. To obtain the "raw" residuals, a station-by-station estimate of Vs30 has been used within the NGA models. Since the adjustments are to a common value of vs30, station-by-station adjustments are not needed.

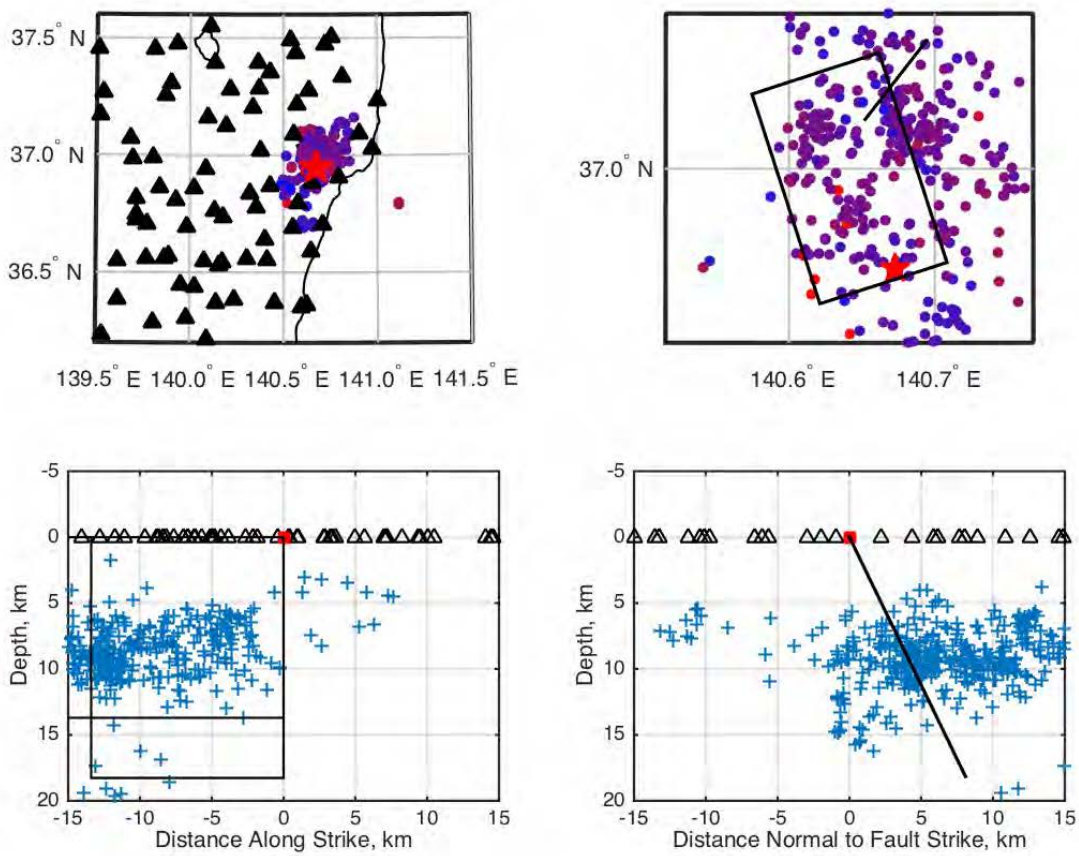

Figure 78: Location and cross section

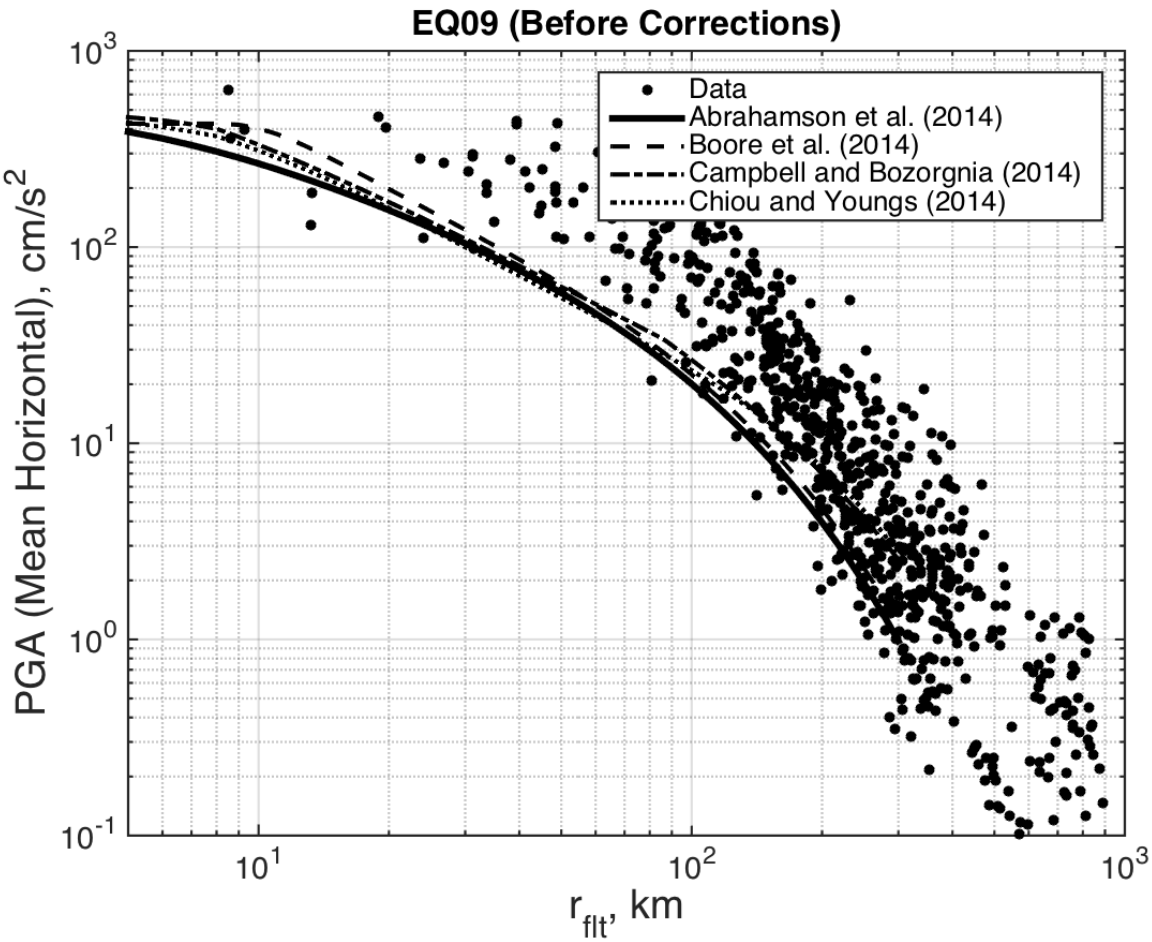

Figure 79: Raw accelerations

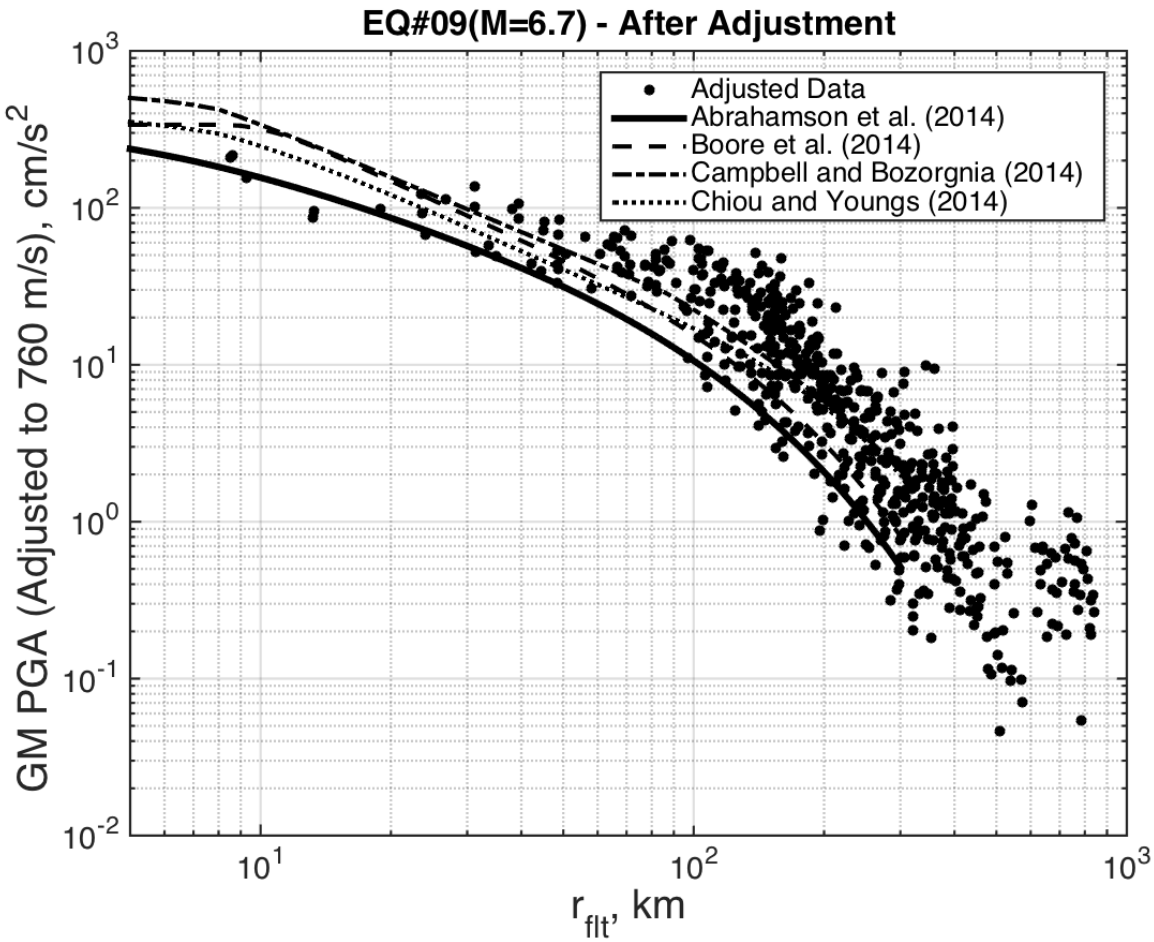

Figure 80: Adjusted accelerations

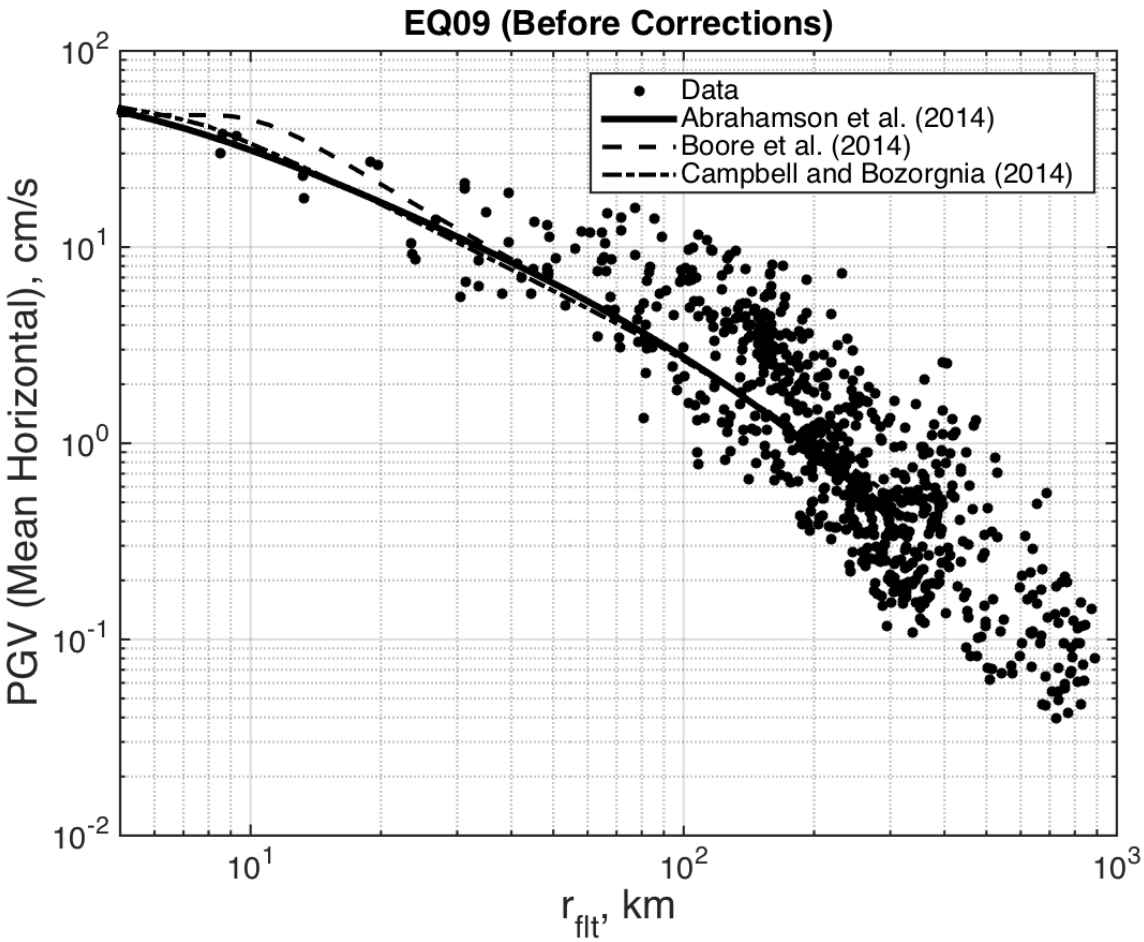

Figure 81: Raw velocities

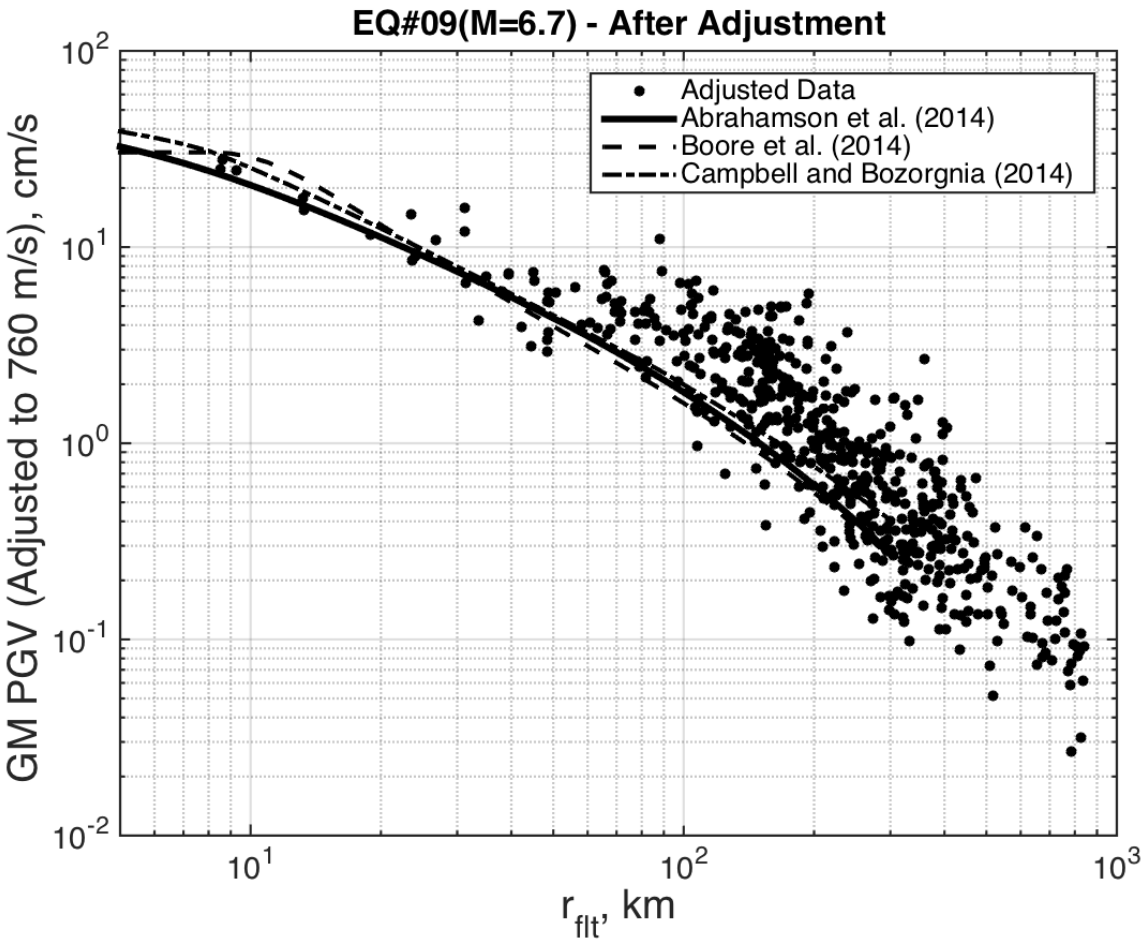

Figure 82: Adjusted velocity

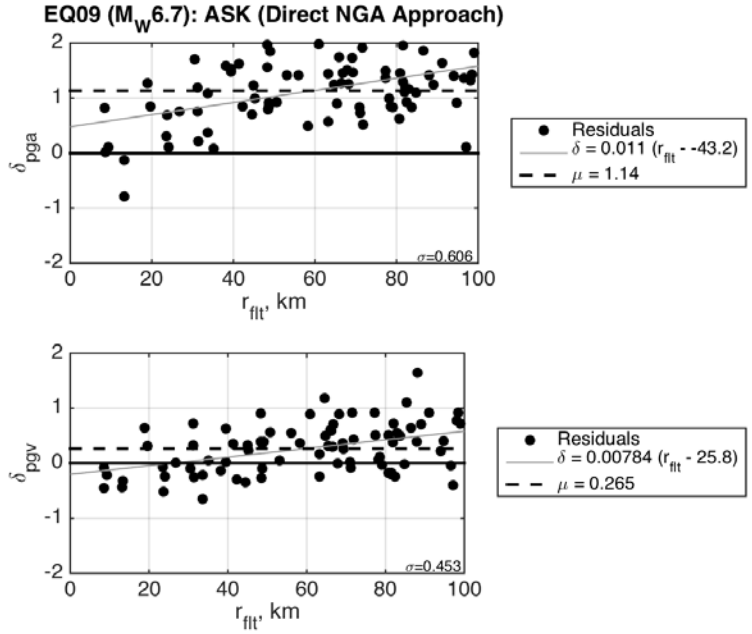

Figure 83: Raw delta ASK

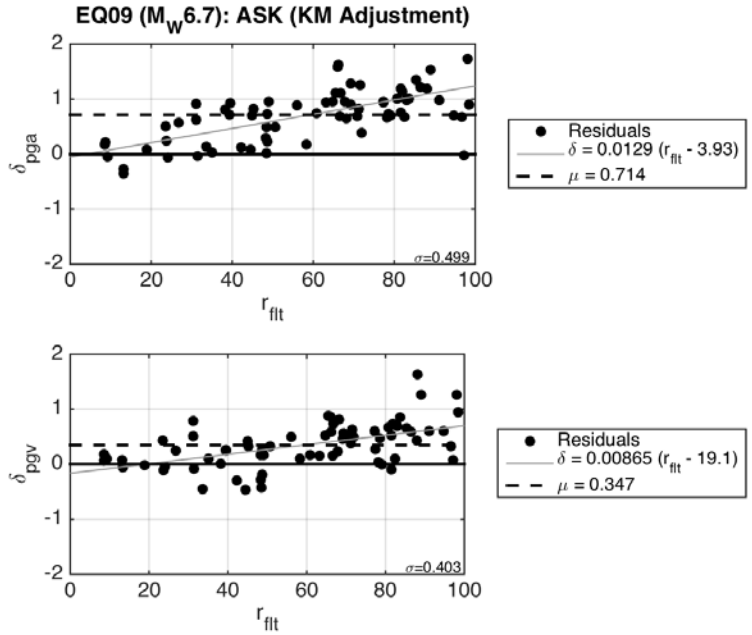

Figure 84: Adjusted delta ASK

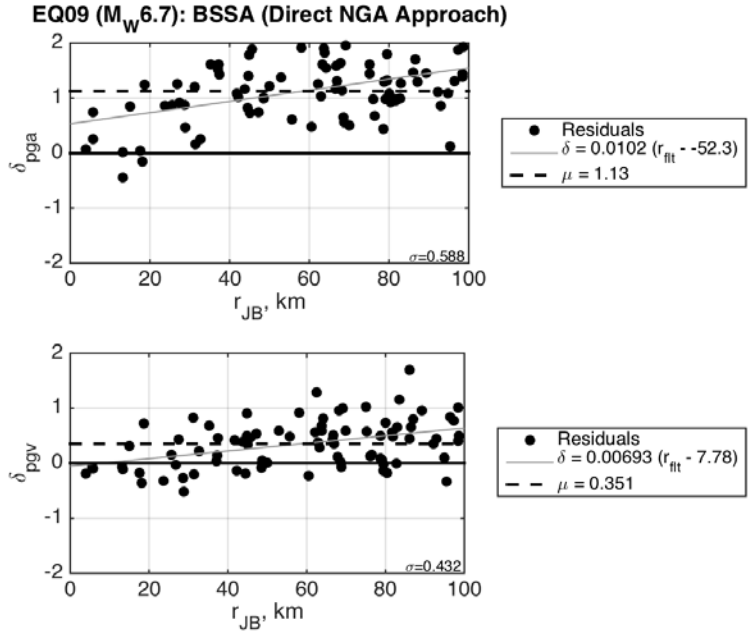

Figure 85: Raw delta BSSA

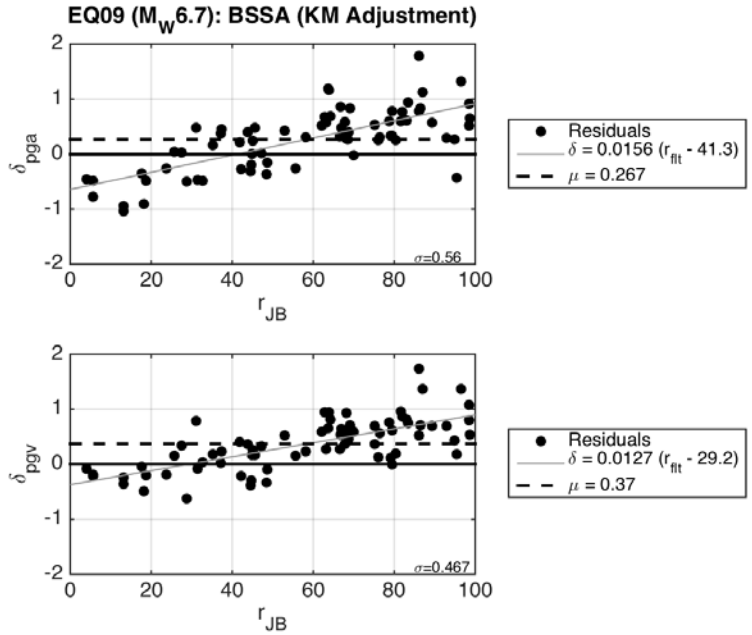

Figure 86: Adjusted delta BSSA

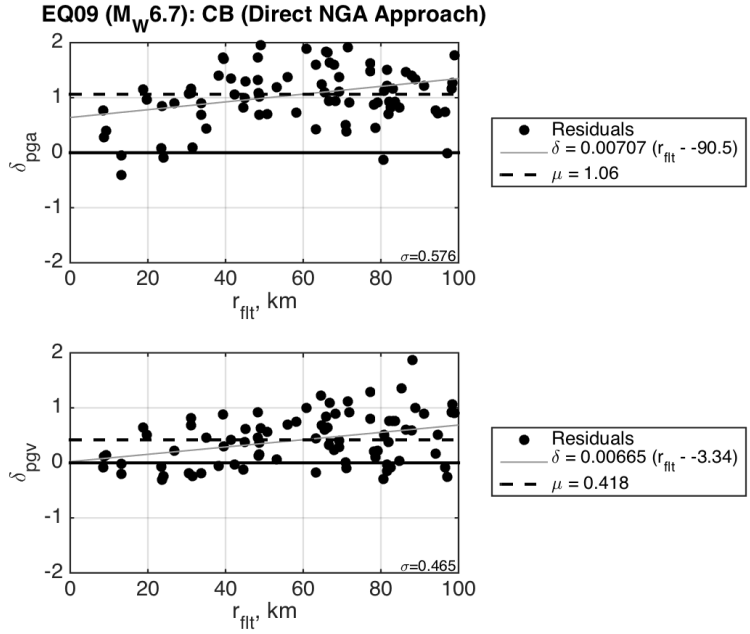

Figure 87: Raw delta CB

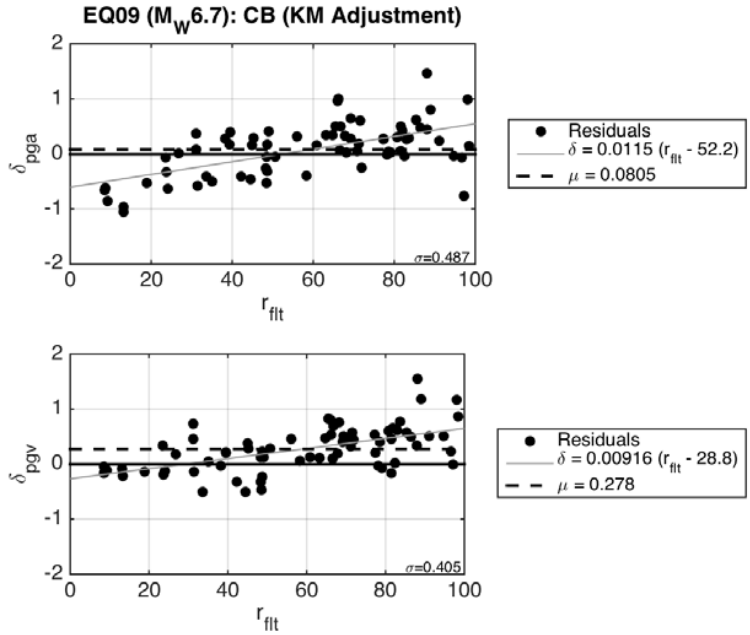

Figure 88: Adjusted delta CB

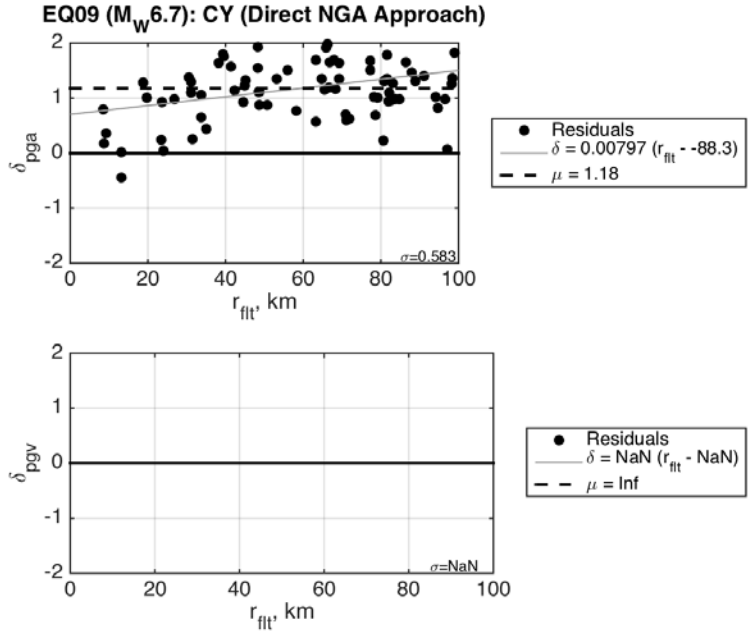

Figure 89: Raw delta CY

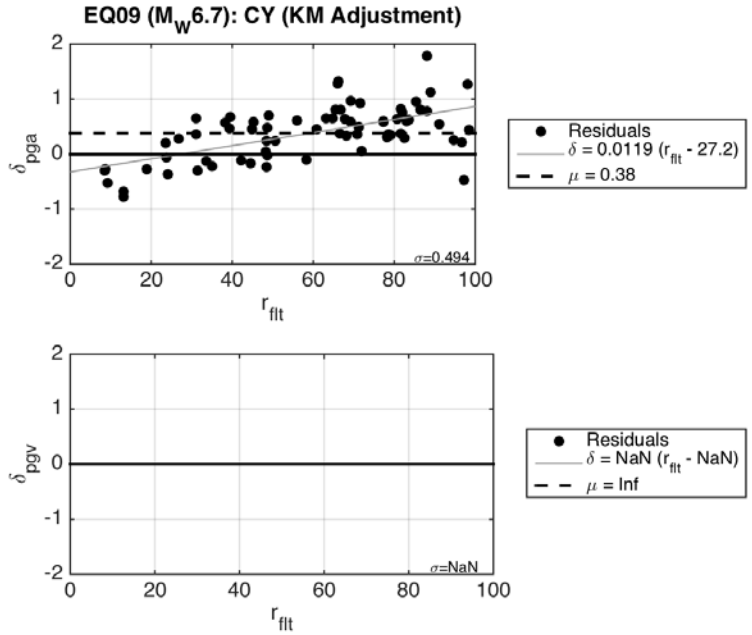

Figure 90: Adjusted delta CY

7 Earthquake 10. 2011 04 11, 20:42 Mw5.5

Figure 91 shows four frames illustrating the geometry of this earthquake.

Figure 92 shows the uncorrected values of peak acceleration as a funciton of distance, and Figure 94 shows the uncorrected values of peak velocity. For comparison, both of these figures show the NGA-West 2 models for Vs30=400 m/s, which is considered to be a reasonable estimate for the network average. Figure 93 shows the adjusted peak accelerations and Figure 95 shows adjusted peak velocities, where the adjustments to the data use Kawase factors and are adjusted to Vs30=760 m/s. Therefore, the NGA curves on these two firgures are for Vs30-760 m/s.

Residuals are shown in Figures 96-103. Raw and adjusted residuals are paired for ease in comparison. To obtain the "raw" residuals, a station-by-station estimate of Vs30 has been used within the NGA models. Since the adjustments are to a common value of vs30, station-by-station adjustments are not needed.

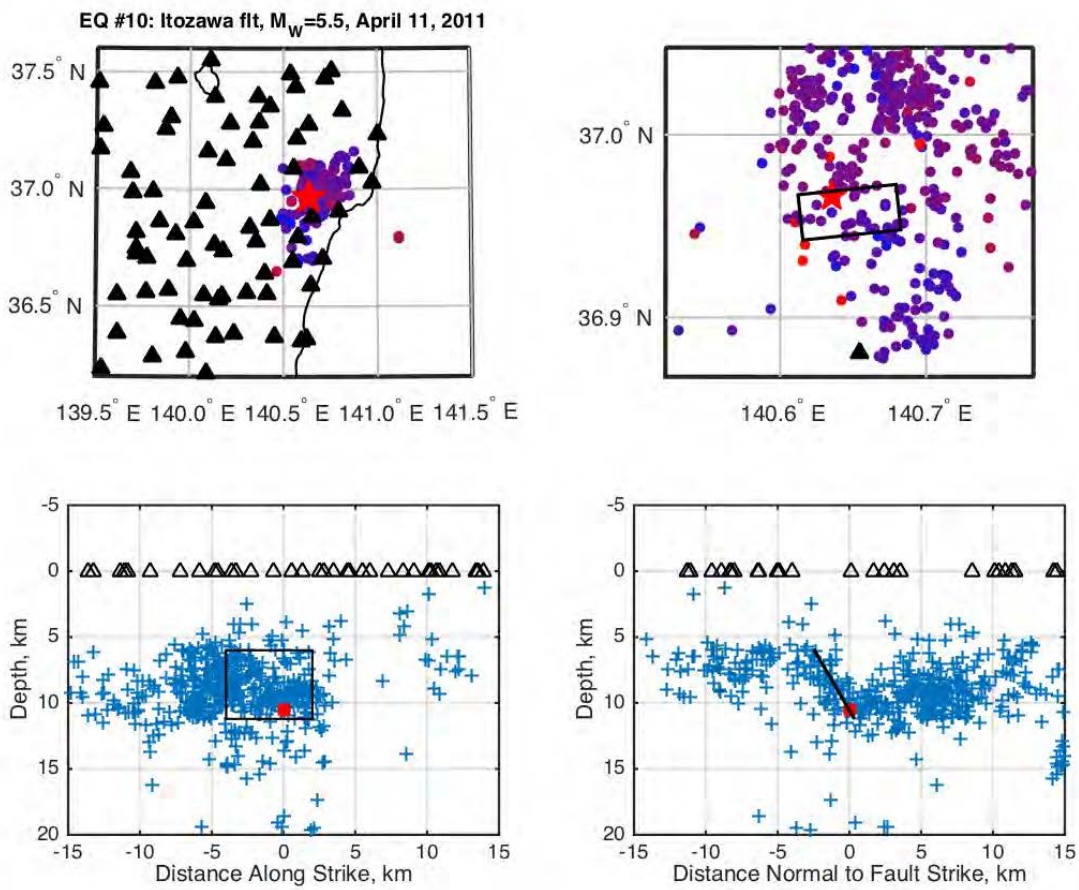

Figure 91: Location and cross section

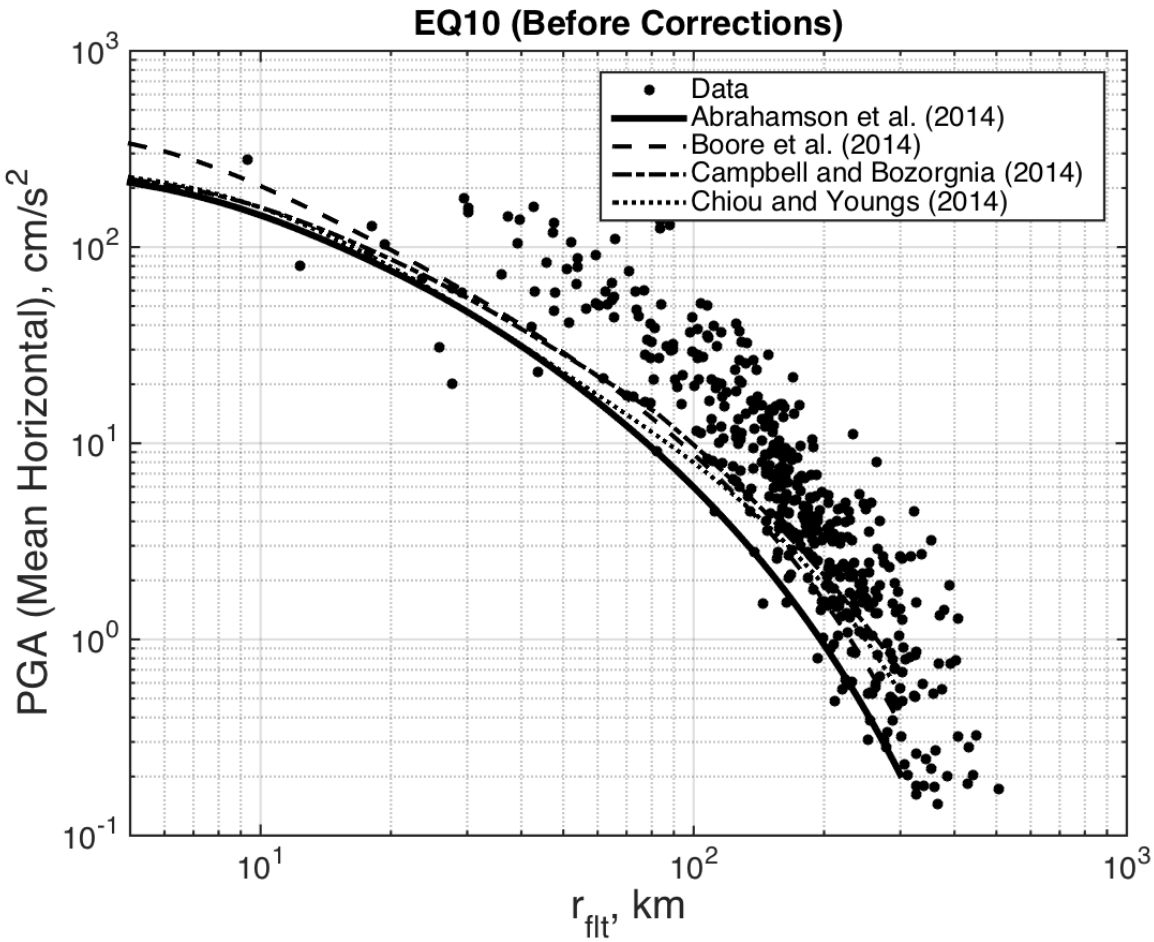

Figure 92: Raw accelerations

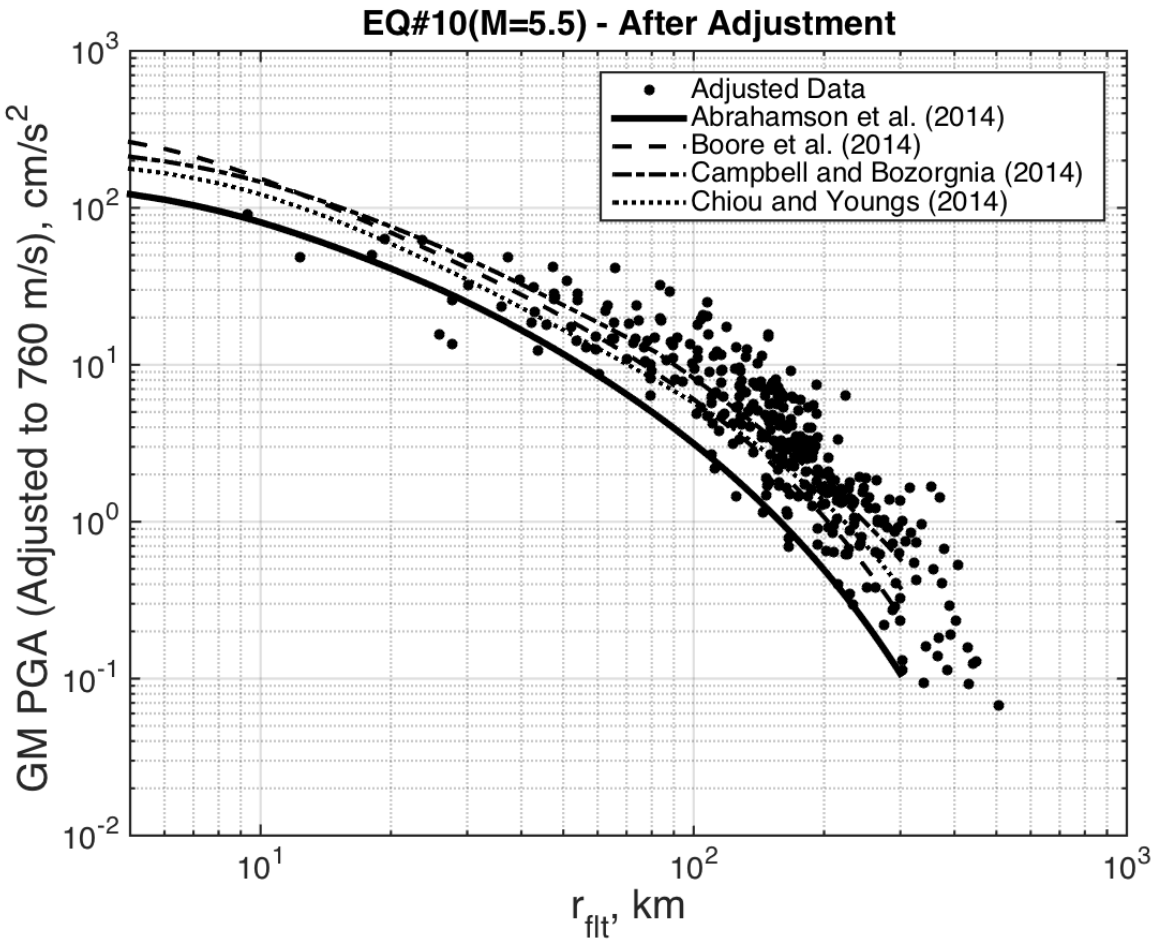

Figure 93: Adjusted accelerations

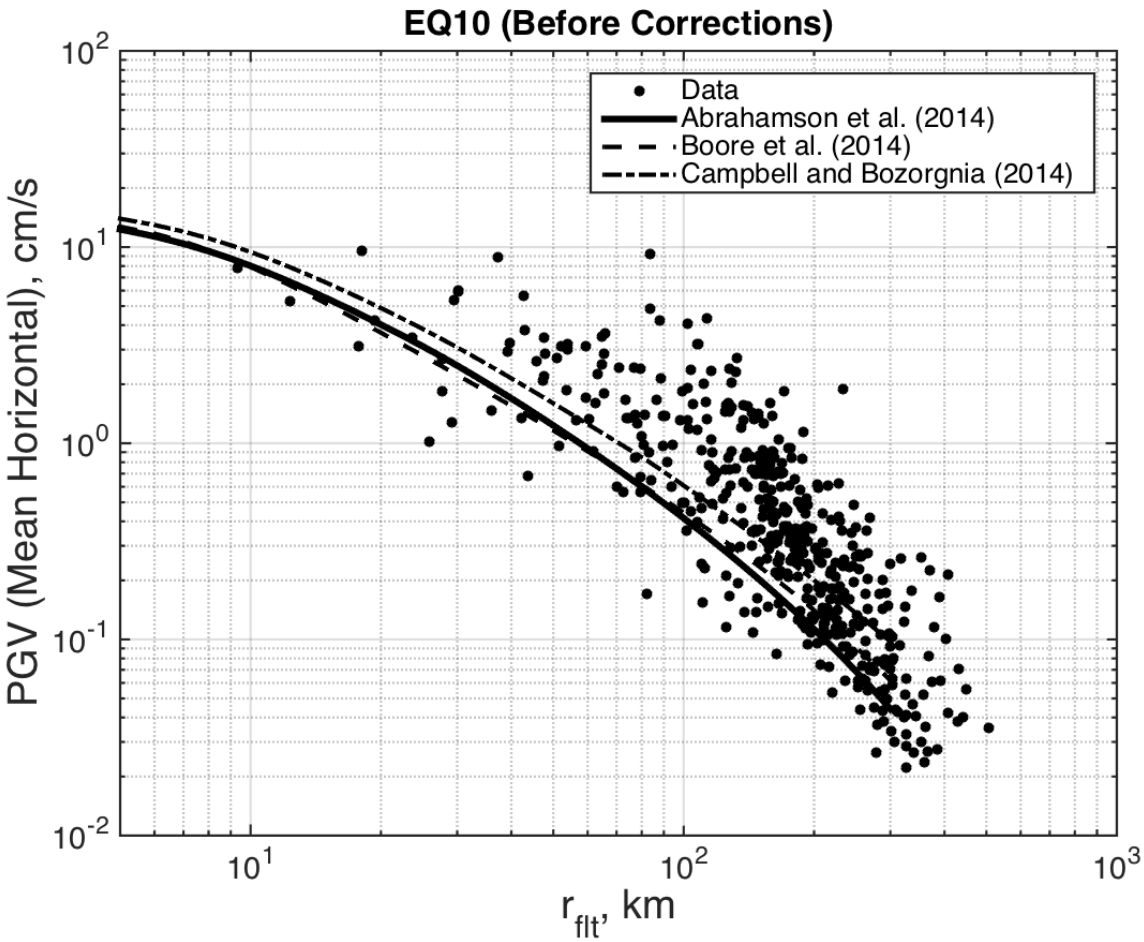

Figure 94: Raw velocities

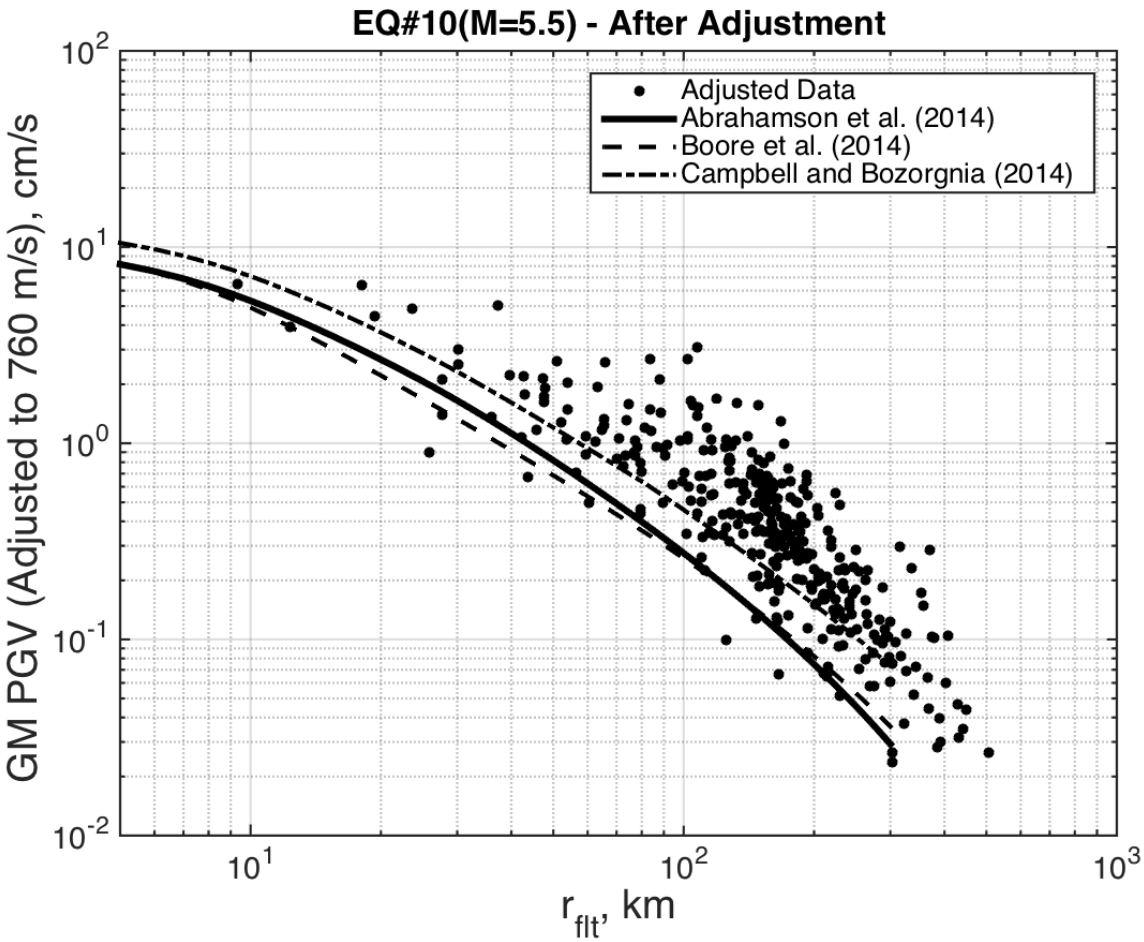

Figure 95: Adjusted velocity

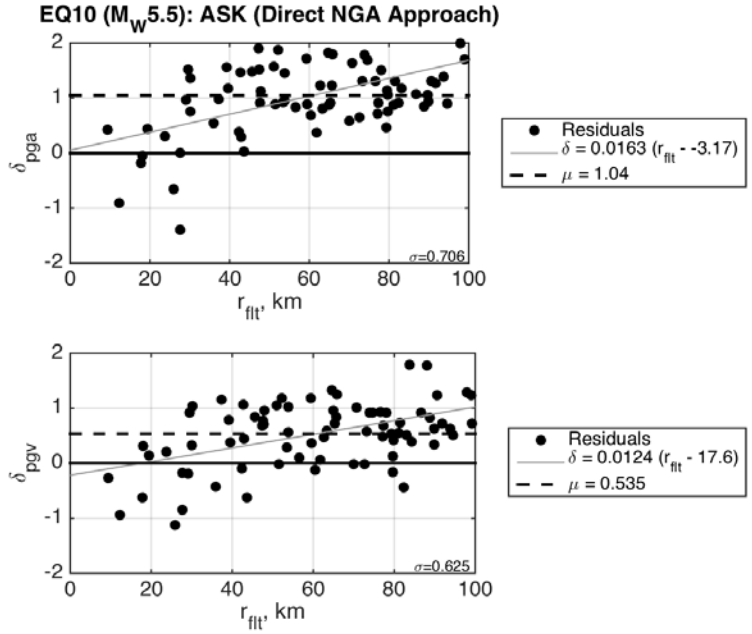

Figure 96: Raw delta ASK

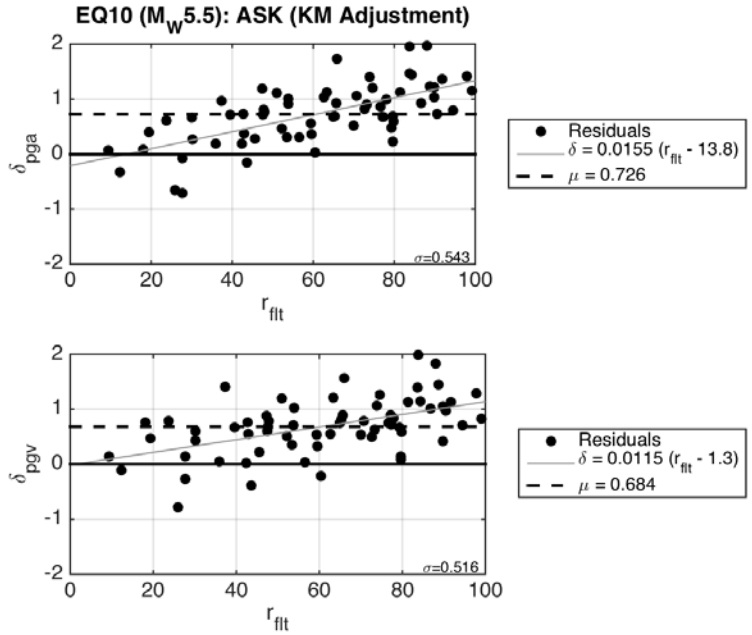

Figure 97: Adjusted delta ASK

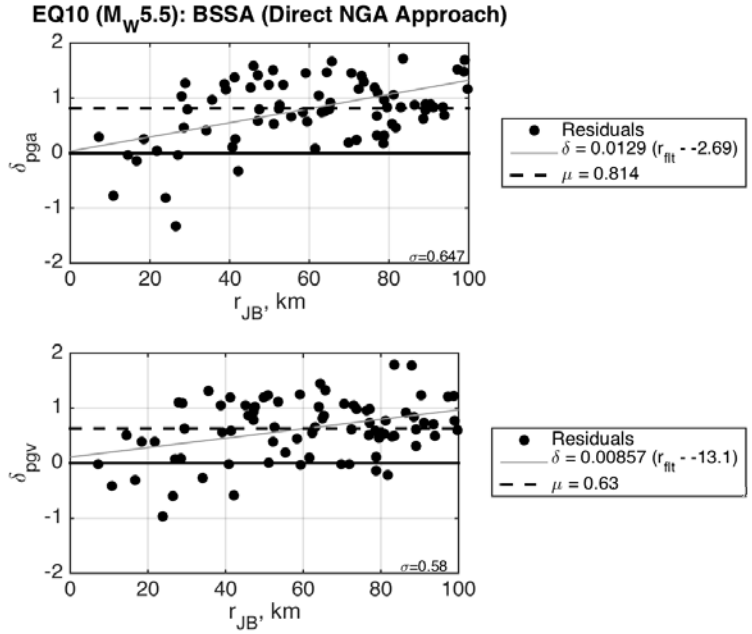

Figure 98: Raw delta BSSA

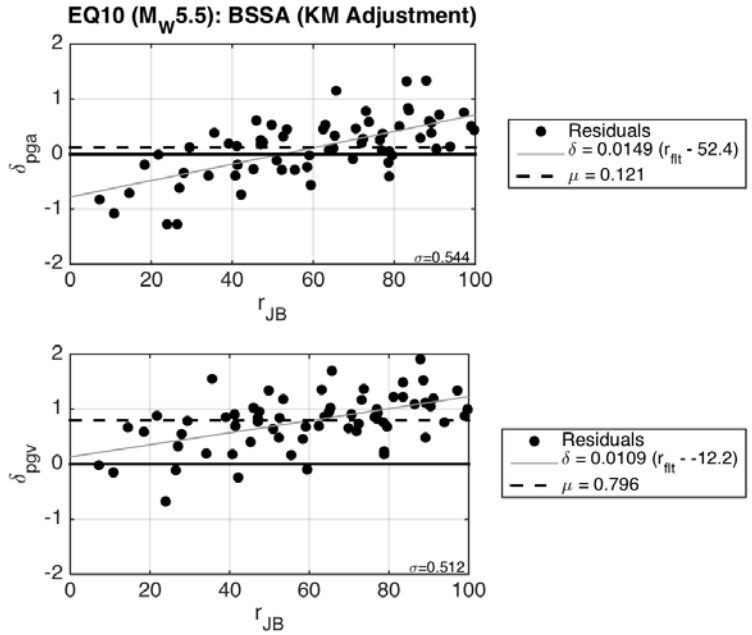

Figure 99: Adjusted delta BSSA

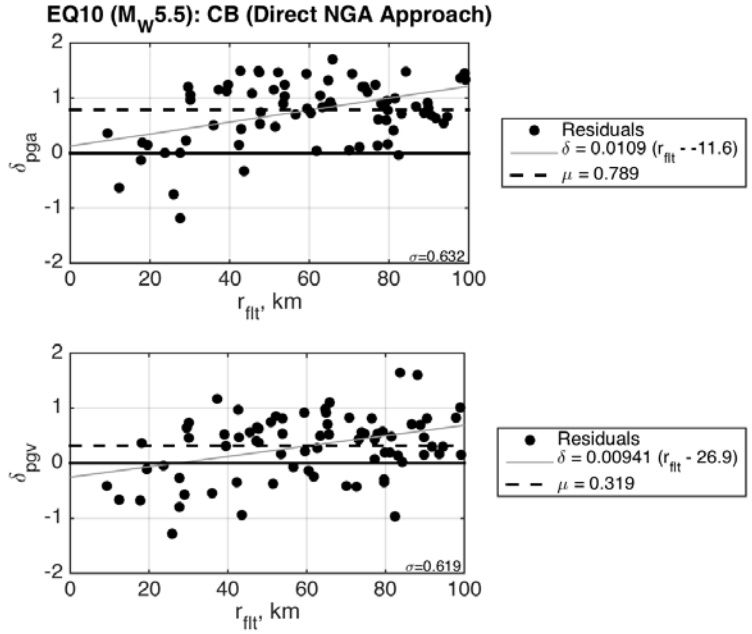

Figure 100: Raw delta CB

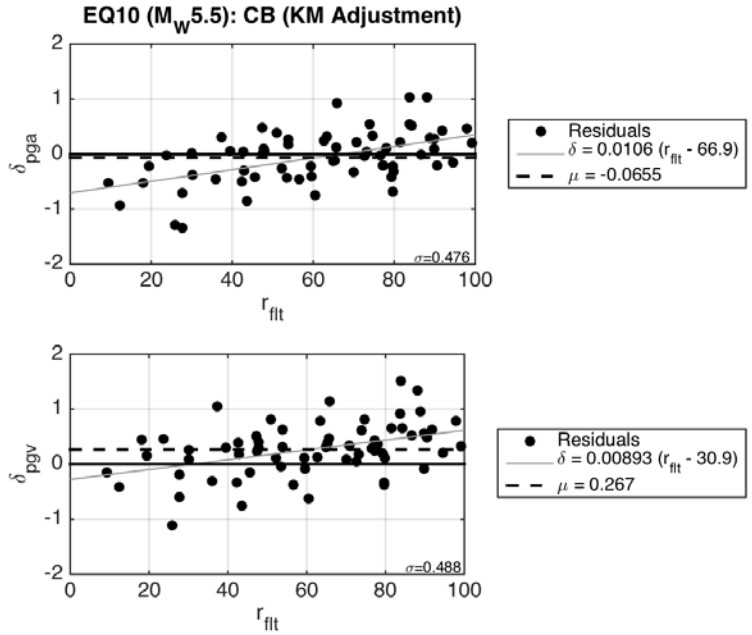

Figure 101: Adjusted delta CB

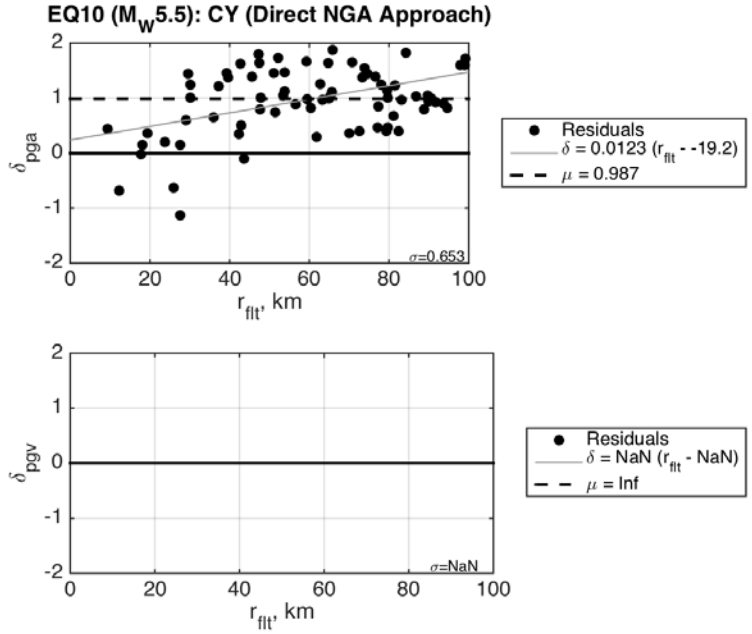

Figure 102: Raw delta CY

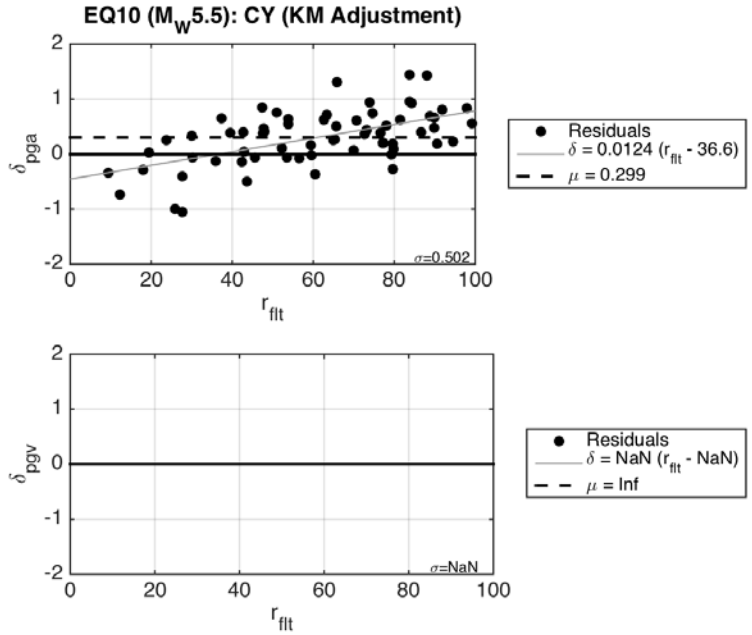

Figure 103: Adjusted delta CY

8 Earthquake 12. 2011 04 13, 10:08 Mw5.9

Figure 104 shows four frames illustrating the geometry of this earthquake.

Figure 105 shows the uncorrected values of peak acceleration as a funciton of distance, and Figure 107 shows the uncorrected values of peak velocity. For comparison, both of these figures show the NGA-West 2 models for Vs30=400 m/s, which is considered to be a reasonable estimate for the network average. Figure 106 shows the adjusted peak accelerations and Figure 108 shows adjusted peak velocities, where the adjustments to the data use Kawase factors and are adjusted to Vs30=760 m/s. Therefore, the NGA curves on these two firgures are for Vs30-760 m/s.

Residuals are shown in Figures 109-116. Raw and adjusted residuals are paired for ease in comparison. To obtain the "raw" residuals, a station-by-station estimate of Vs30 has been used within the NGA models. Since the adjustments are to a common value of vs30, station-by-station adjustments are not needed.

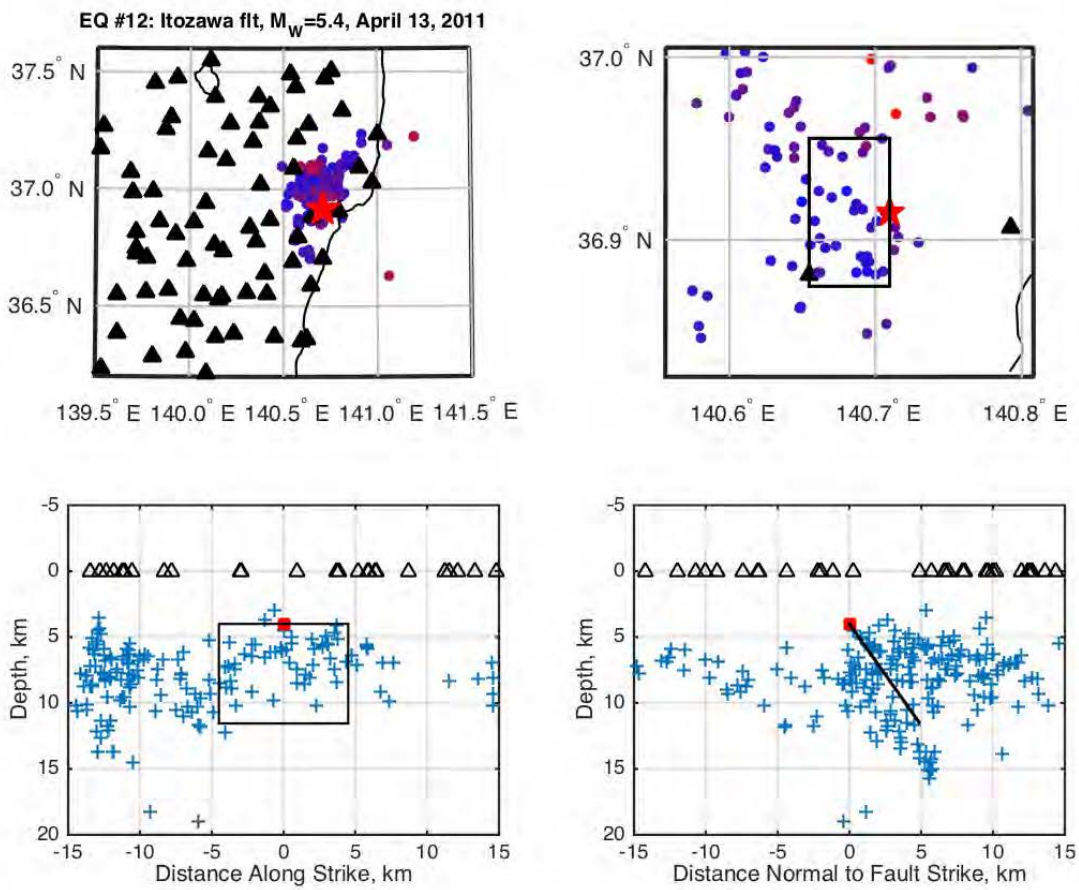

Figure 104: Location and cross section

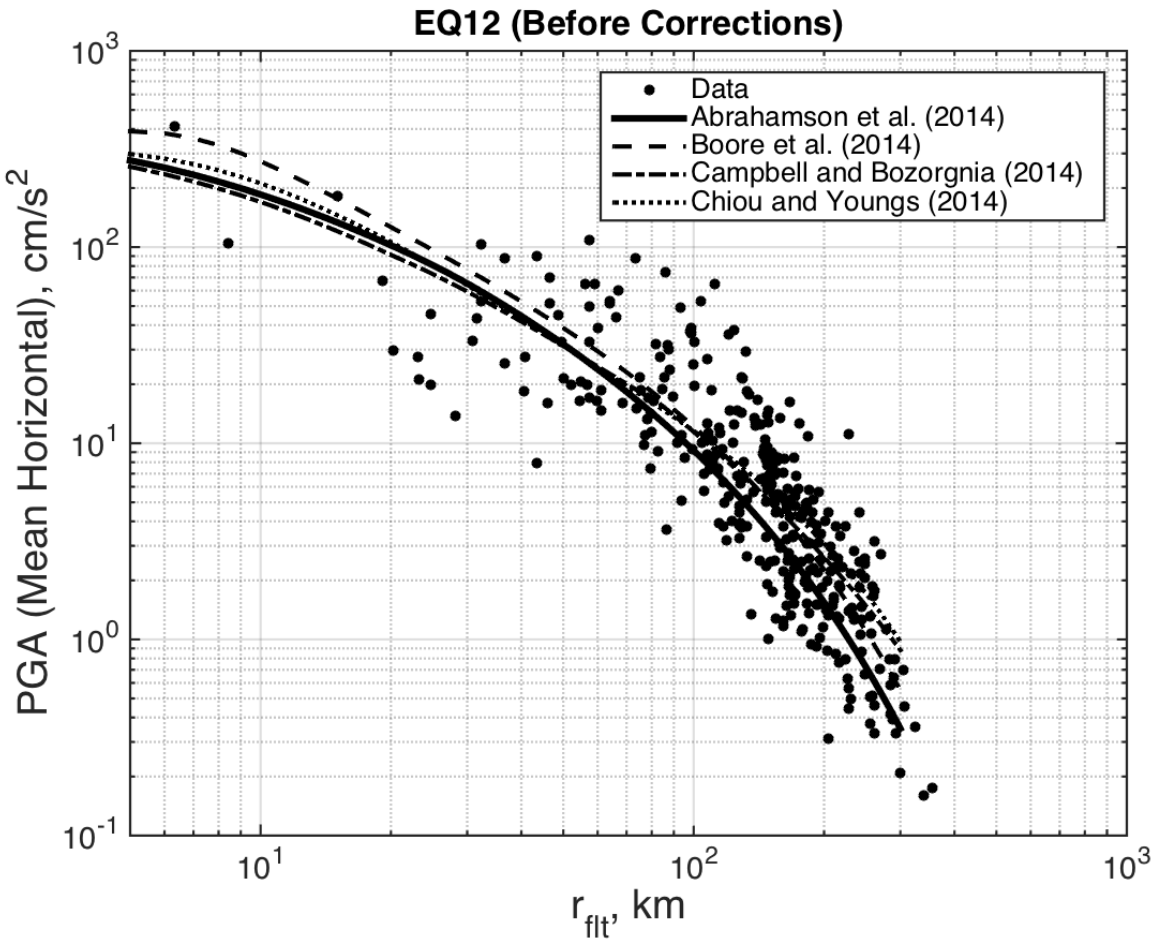

Figure 105: Raw accelerations

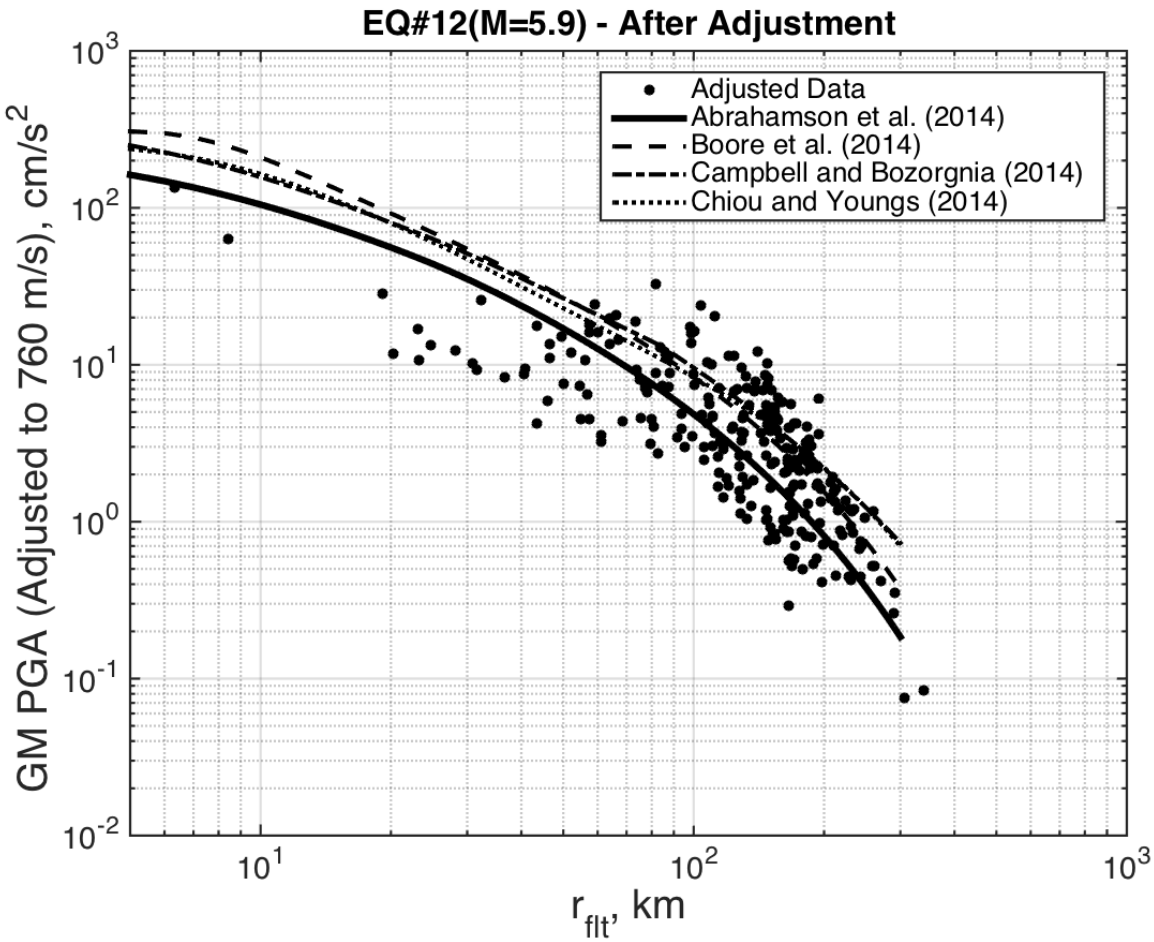

Figure 106: Adjusted accelerations

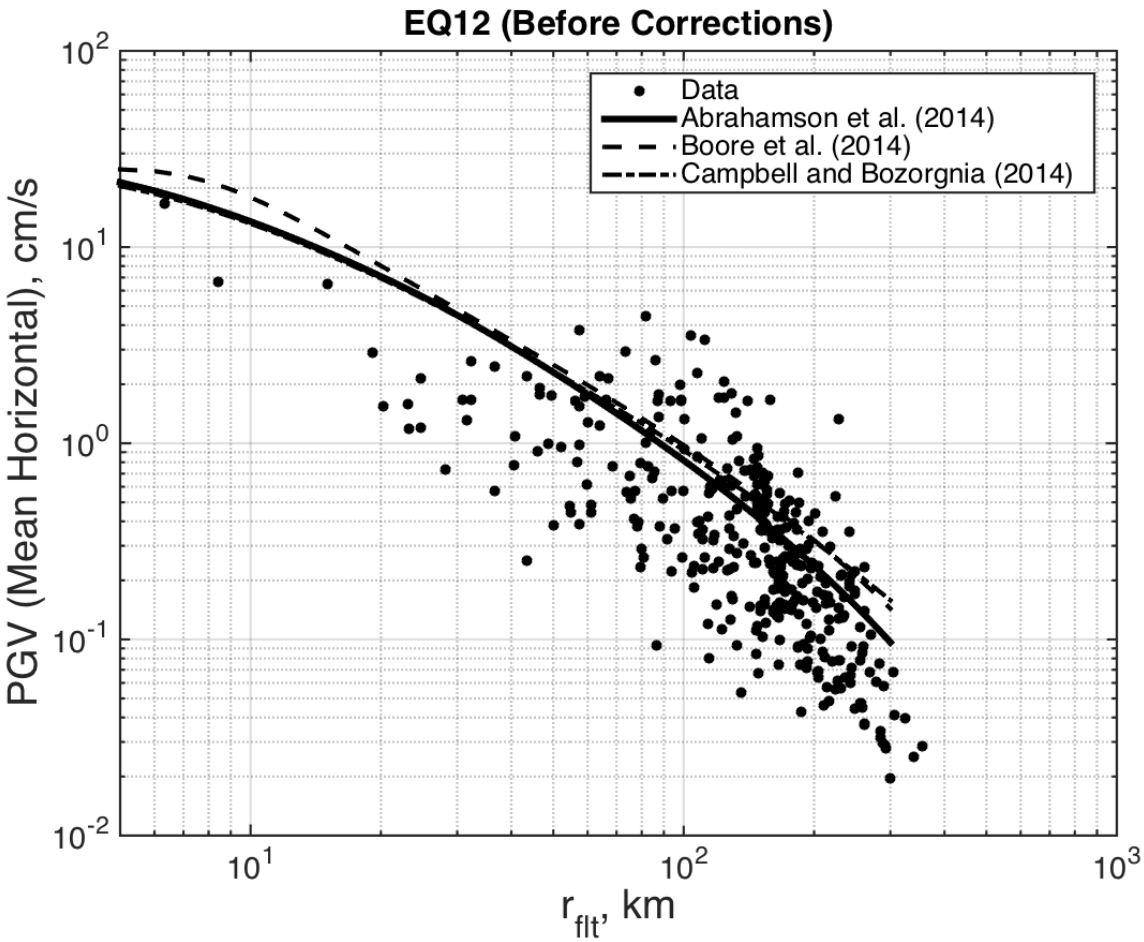

Figure 107: Raw velocities

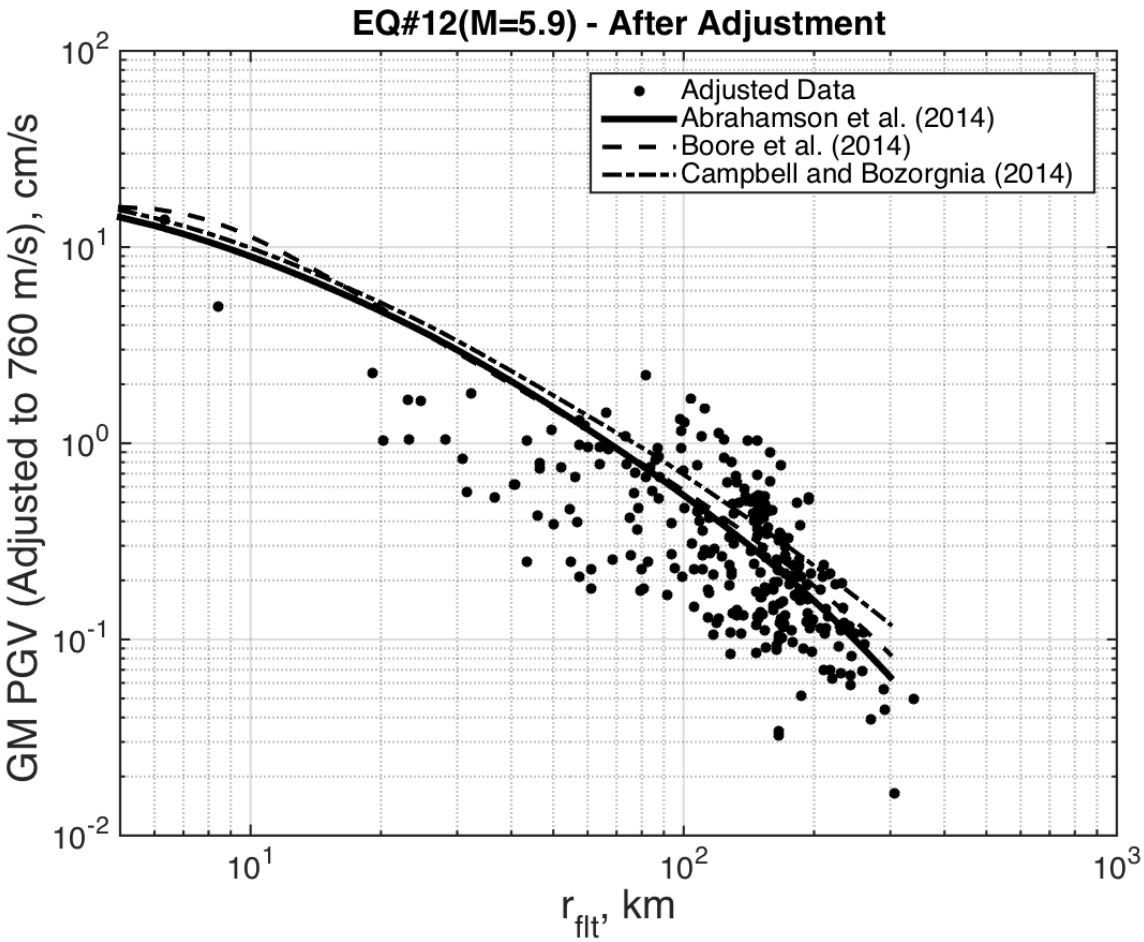

Figure 108: Adjusted velocity

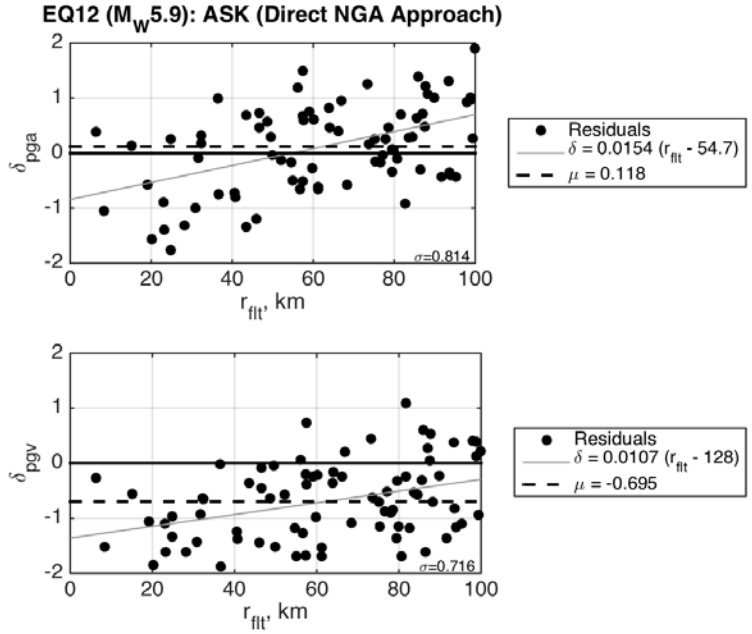

Figure 109: Raw delta ASK

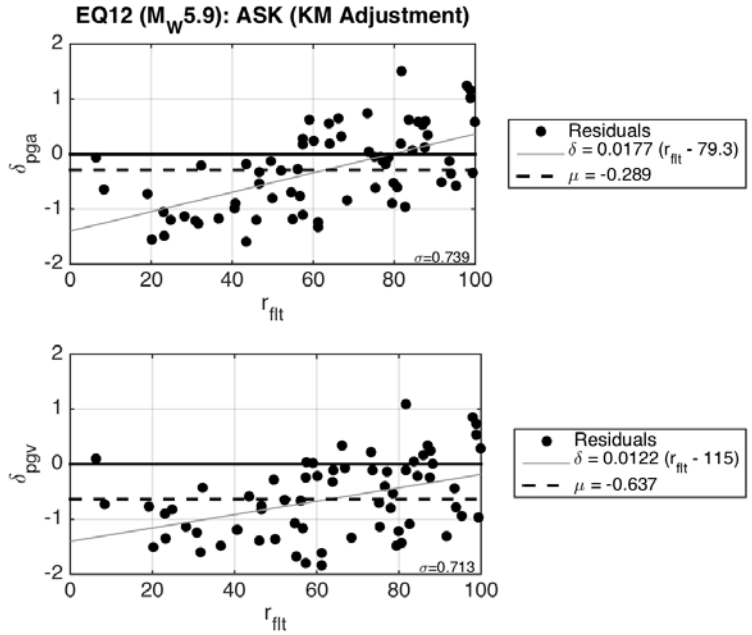

Figure 110: Adjusted delta ASK

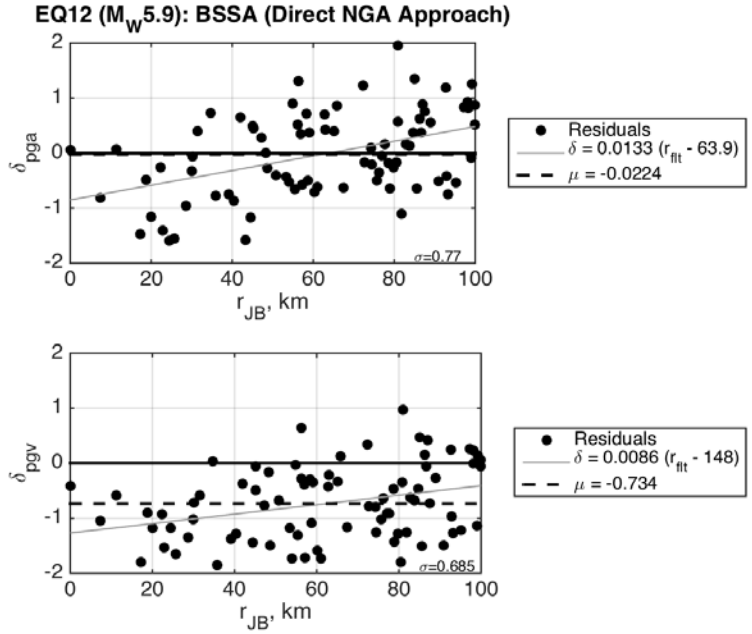

Figure 111: Raw delta BSSA

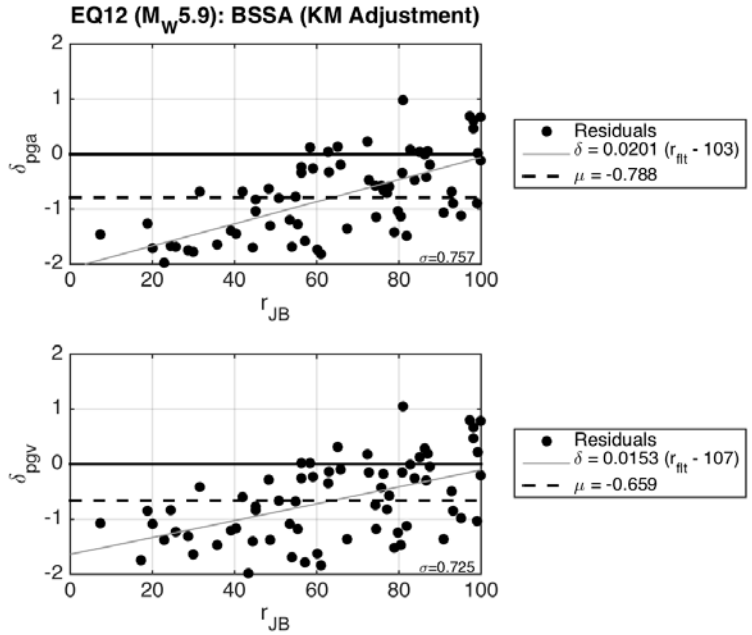

Figure 112: Adjusted delta BSSA

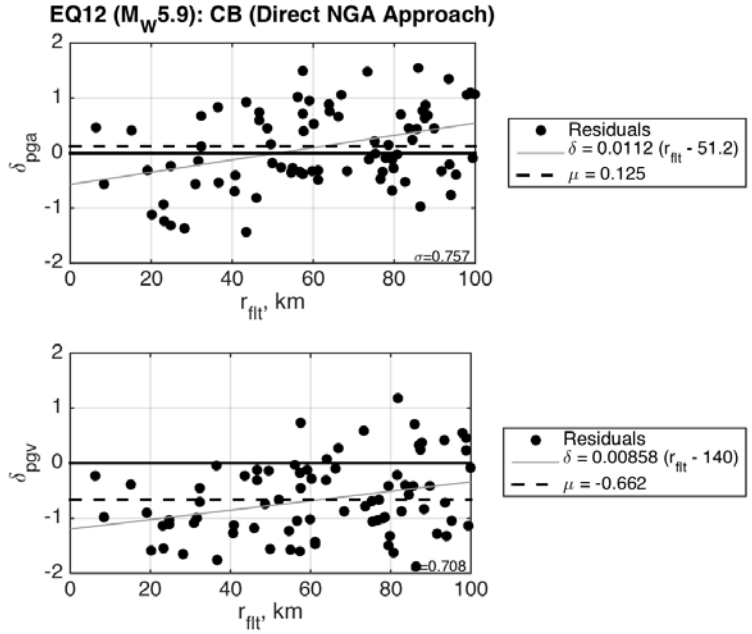

Figure 113: Raw delta CB

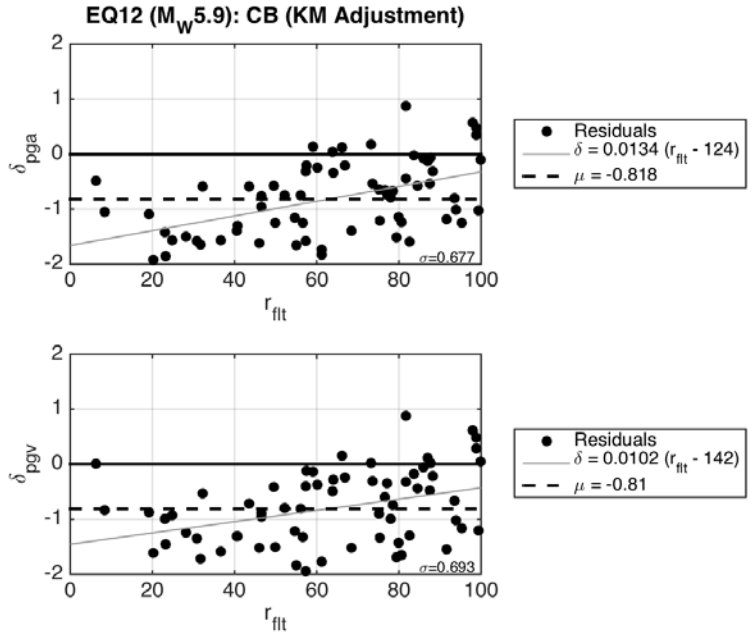

Figure 114: Adjusted delta CB

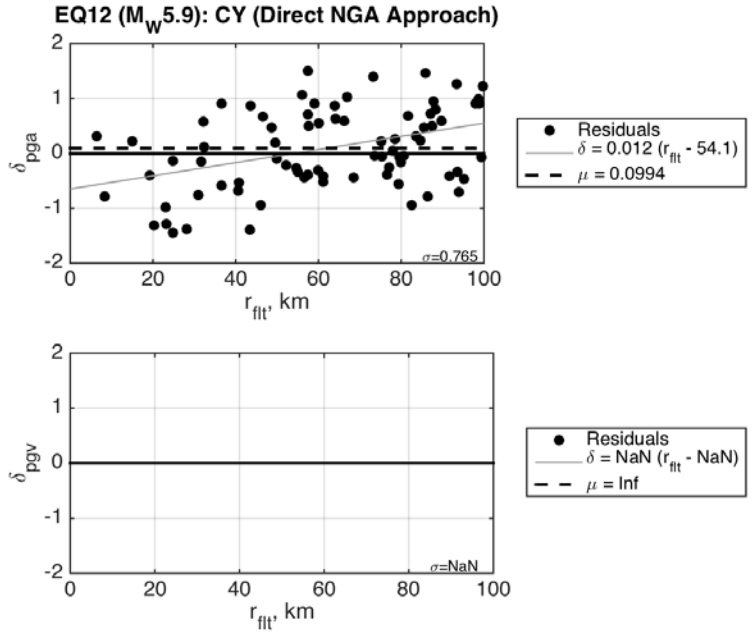

Figure 115: Raw delta CY

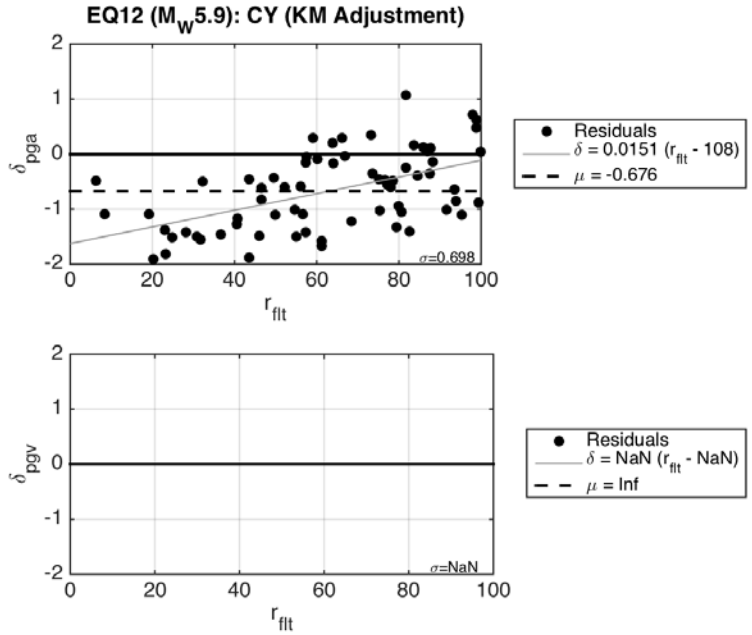

Figure 116: Adjusted delta CY

9 Earthquake 13. 2011 04 14, 13:09 Mw5.0

Figure 117 shows four frames illustrating the geometry of this earthquake.

Figure 118 shows the uncorrected values of peak acceleration as a funciton of distance, and Figure 120 shows the uncorrected values of peak velocity. For comparison, both of these figures show the NGA-West 2 models for Vs30=400 m/s, which is considered to be a reasonable estimate for the network average. Figure 119 shows the adjusted peak accelerations and Figure 121 shows adjusted peak velocities, where the adjustments to the data use Kawase factors and are adjusted to Vs30=760 m/s. Therefore, the NGA curves on these two firgures are for Vs30-760 m/s.

Residuals are shown in Figures 122-129. Raw and adjusted residuals are paired for ease in comparison. To obtain the "raw" residuals, a station-by-station estimate of Vs30 has been used within the NGA models. Since the adjustments are to a common value of vs30, station-by-station adjustments are not needed.

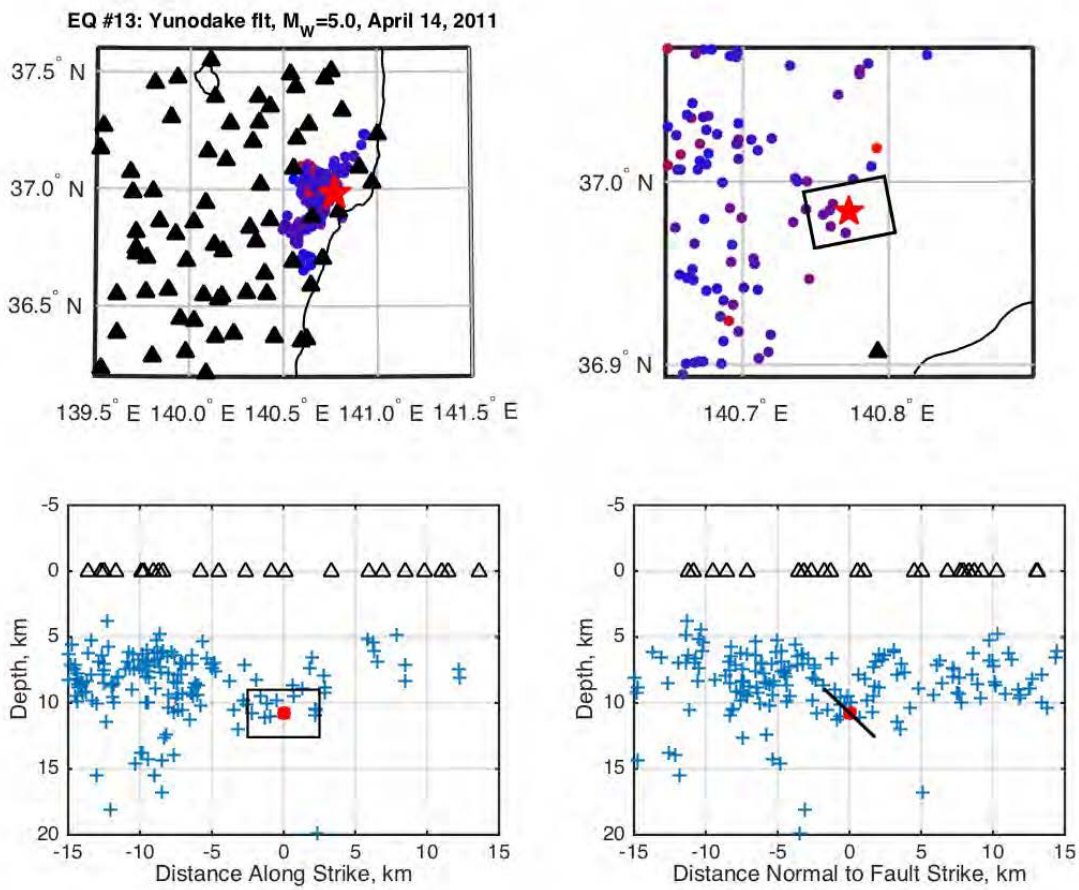

Figure 117: Location and cross section

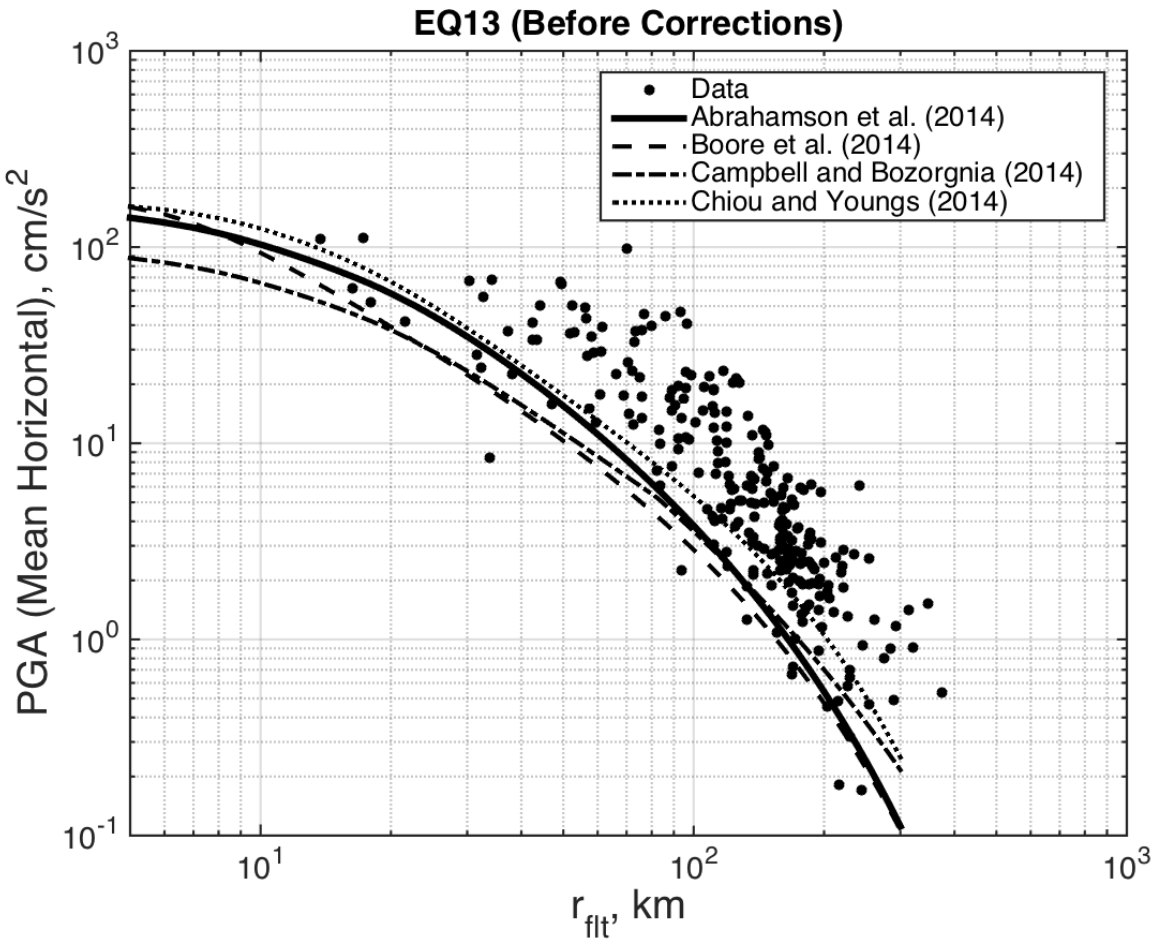

Figure 118: Raw accelerations

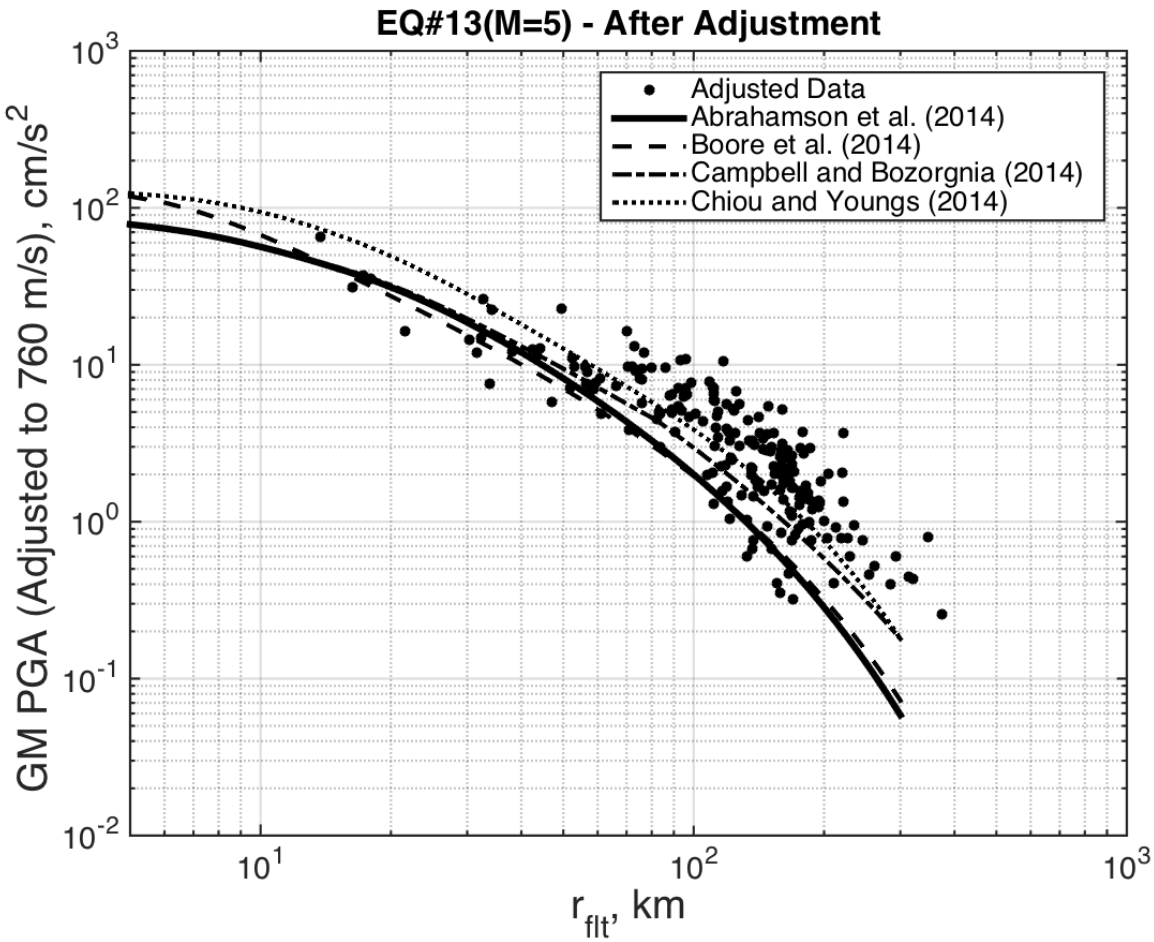

Figure 119: Adjusted accelerations

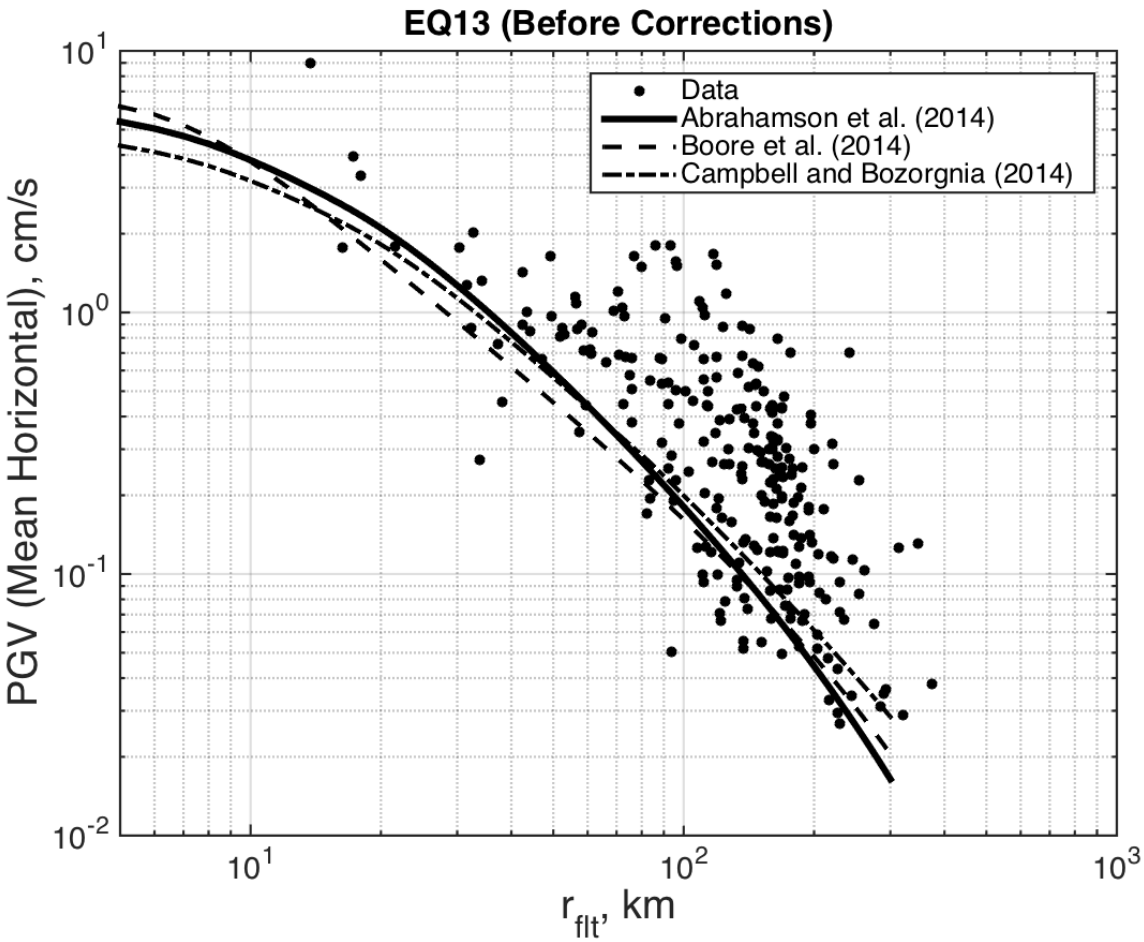

Figure 120: Raw velocities

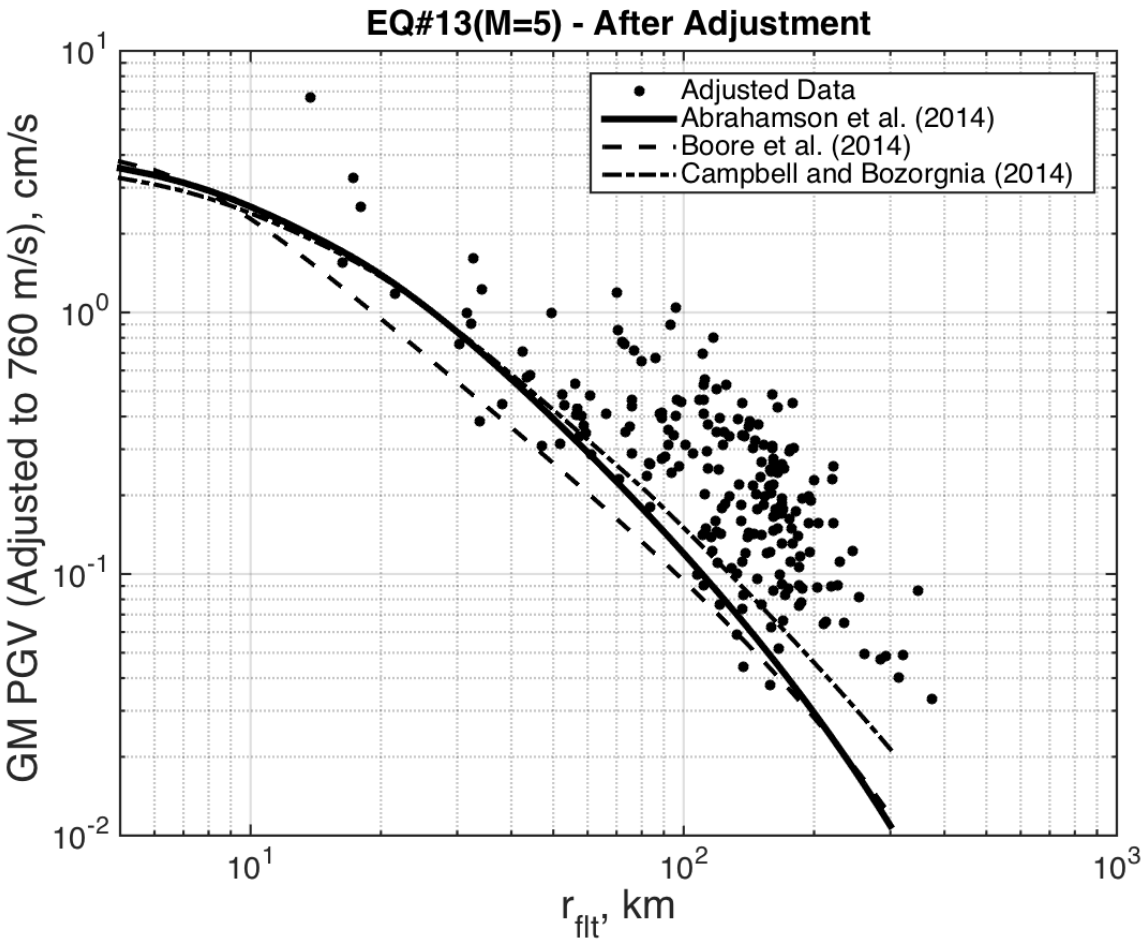

Figure 121: Adjusted velocity

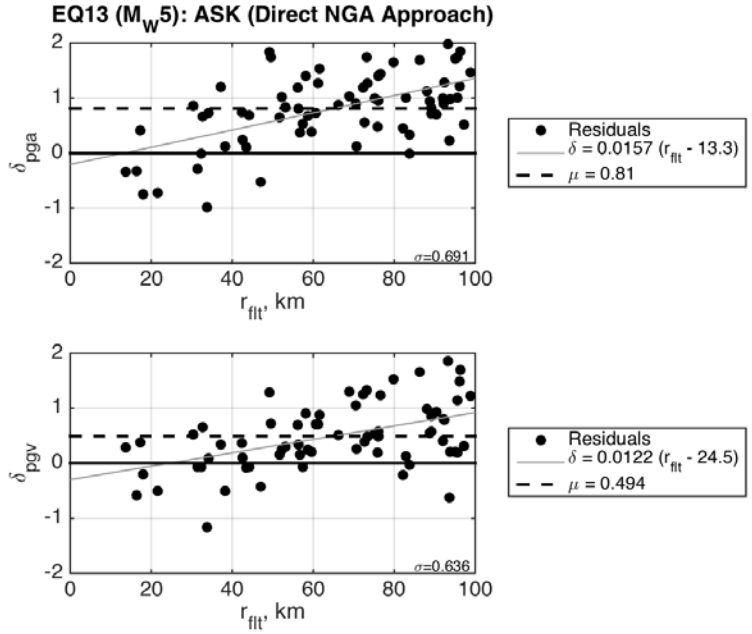

Figure 122: Raw delta ASK

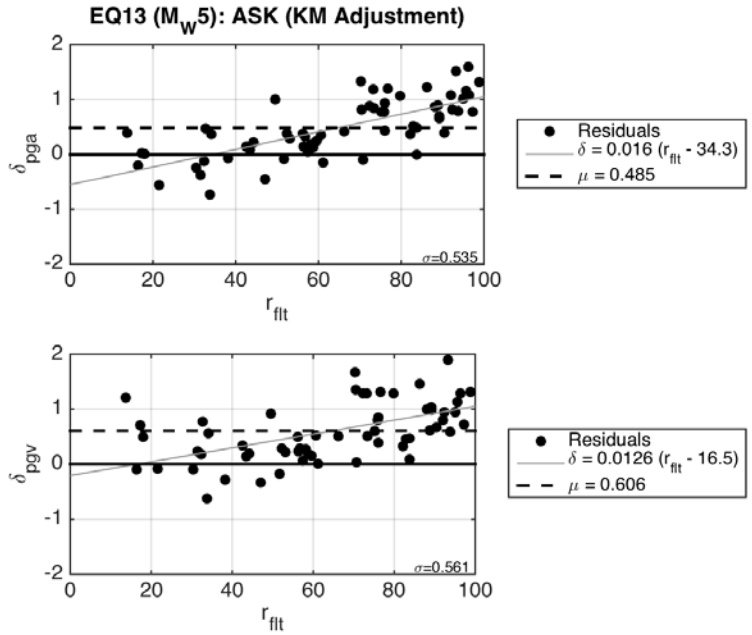

Figure 123: Adjusted delta ASK

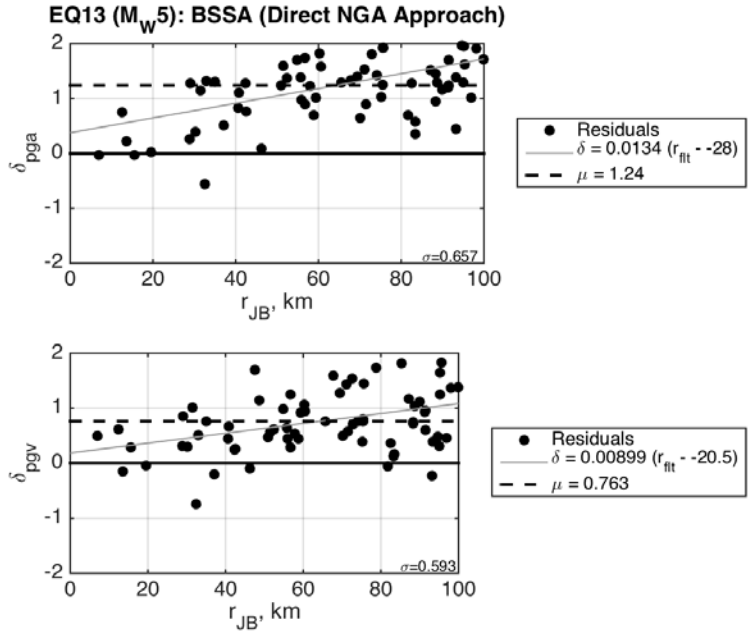

Figure 124: Raw delta BSSA

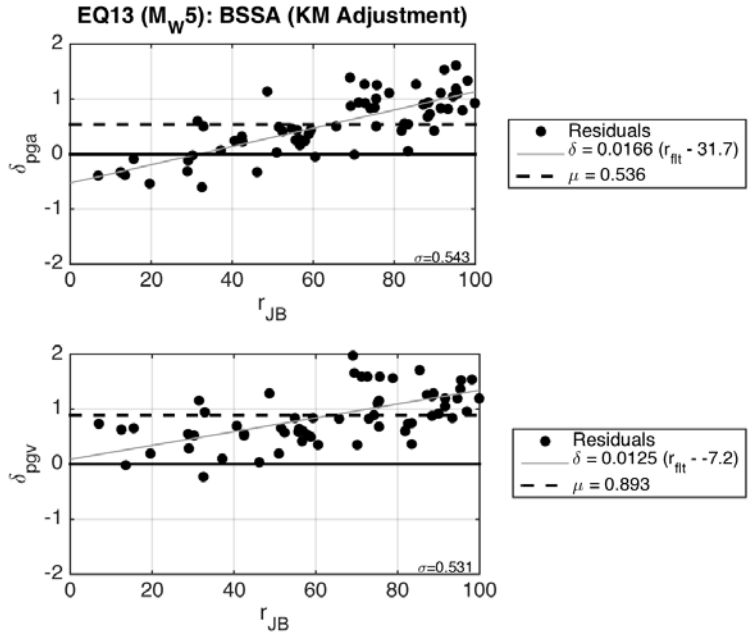

Figure 125: Adjusted delta BSSA

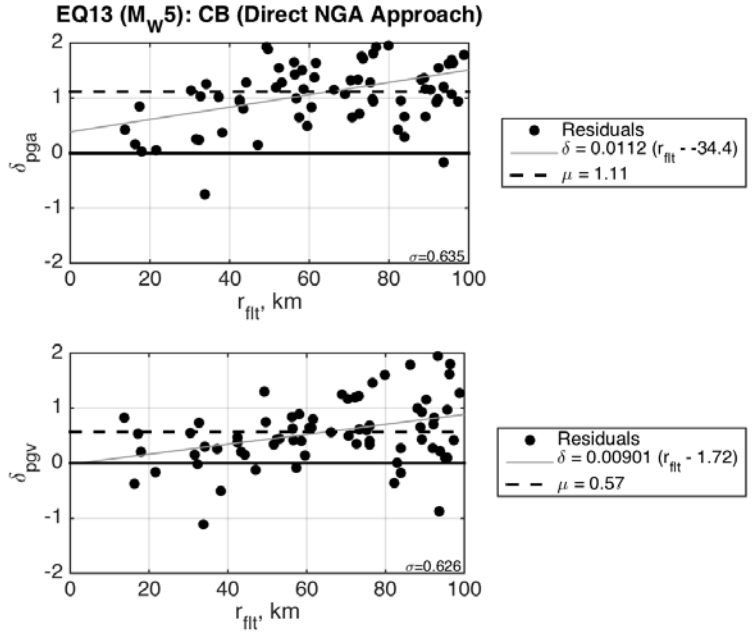

Figure 126: Raw delta CB

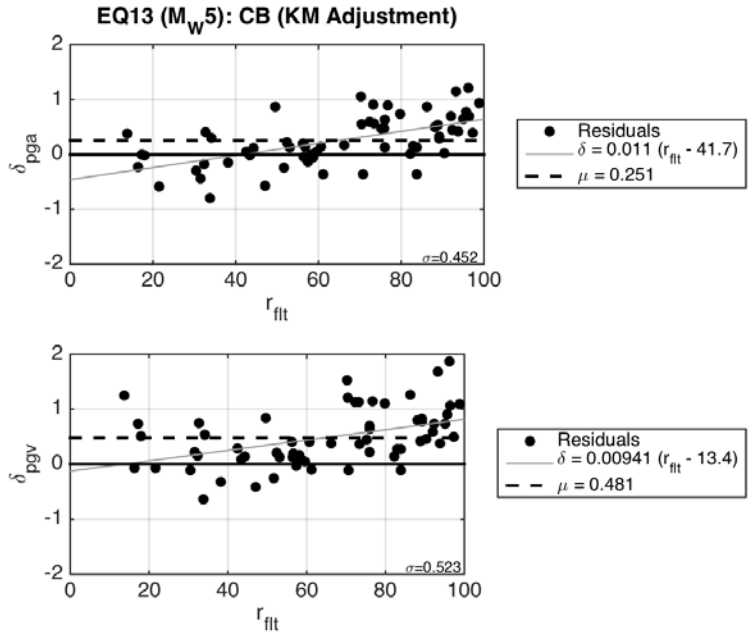

Figure 127: Adjusted delta CB

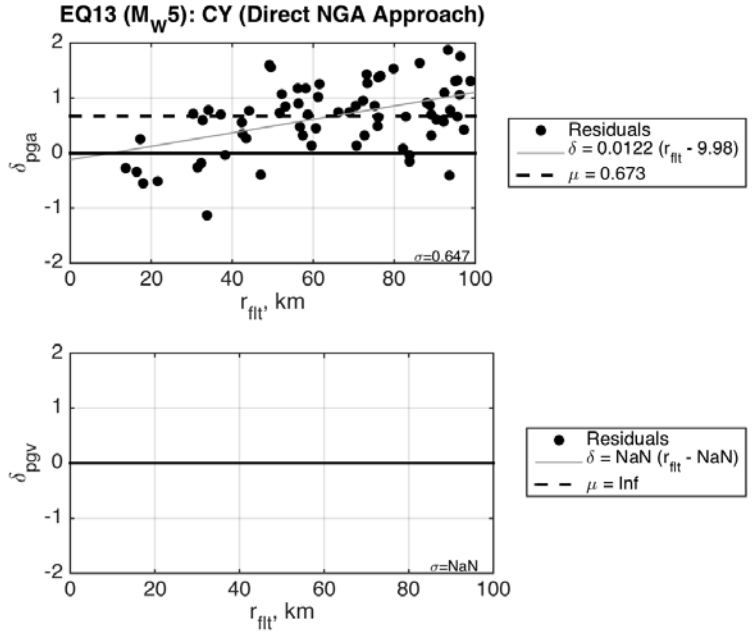

Figure 128: Raw delta CY

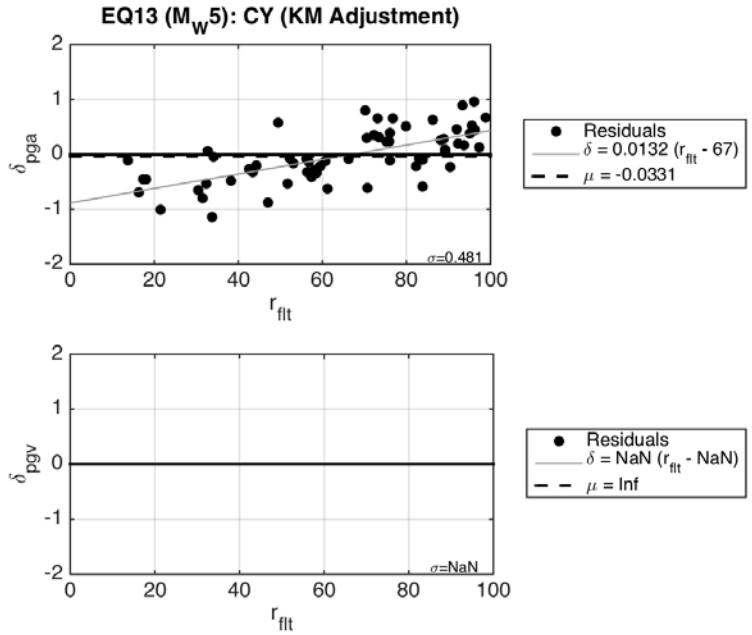

Figure 129: Adjusted delta CY

10 Earthquake 14. 2011 09 21, 22:30 Mw5.1

Figure 130 shows four frames illustrating the geometry of this earthquake.

Figure 131 shows the uncorrected values of peak acceleration as a funciton of distance, and Figure 133 shows the uncorrected values of peak velocity. For comparison, both of these figures show the NGA-West 2 models for Vs30=400 m/s, which is considered to be a reasonable estimate for the network average. Figure 132 shows the adjusted peak accelerations and Figure 134 shows adjusted peak velocities, where the adjustments to the data use Kawase factors and are adjusted to Vs30=760 m/s. Therefore, the NGA curves on these two firgures are for Vs30-760 m/s.

Residuals are shown in Figures 135-142. Raw and adjusted residuals are paired for ease in comparison. To obtain the "raw" residuals, a station-by-station estimate of Vs30 has been used within the NGA models. Since the adjustments are to a common value of vs30, station-by-station adjustments are not needed.

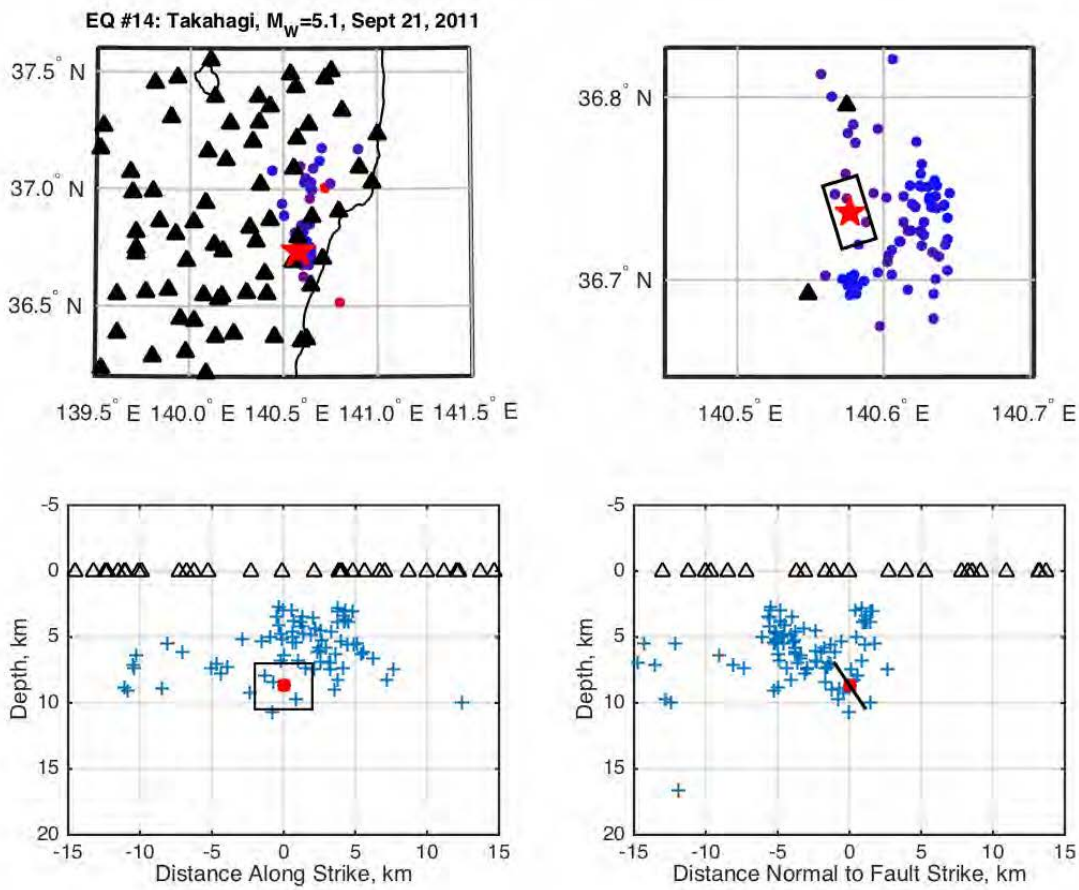

Figure 130: Location and cross section

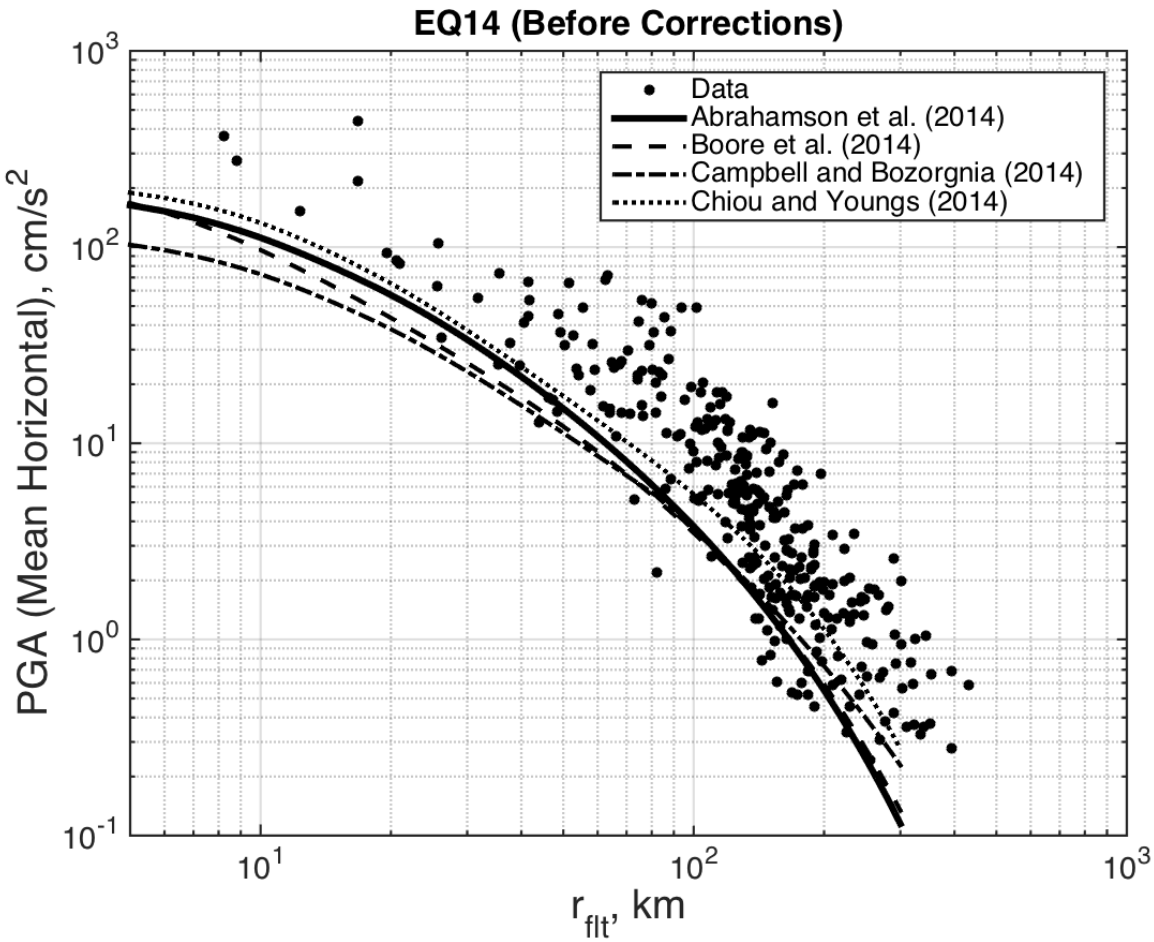

Figure 131: Raw accelerations

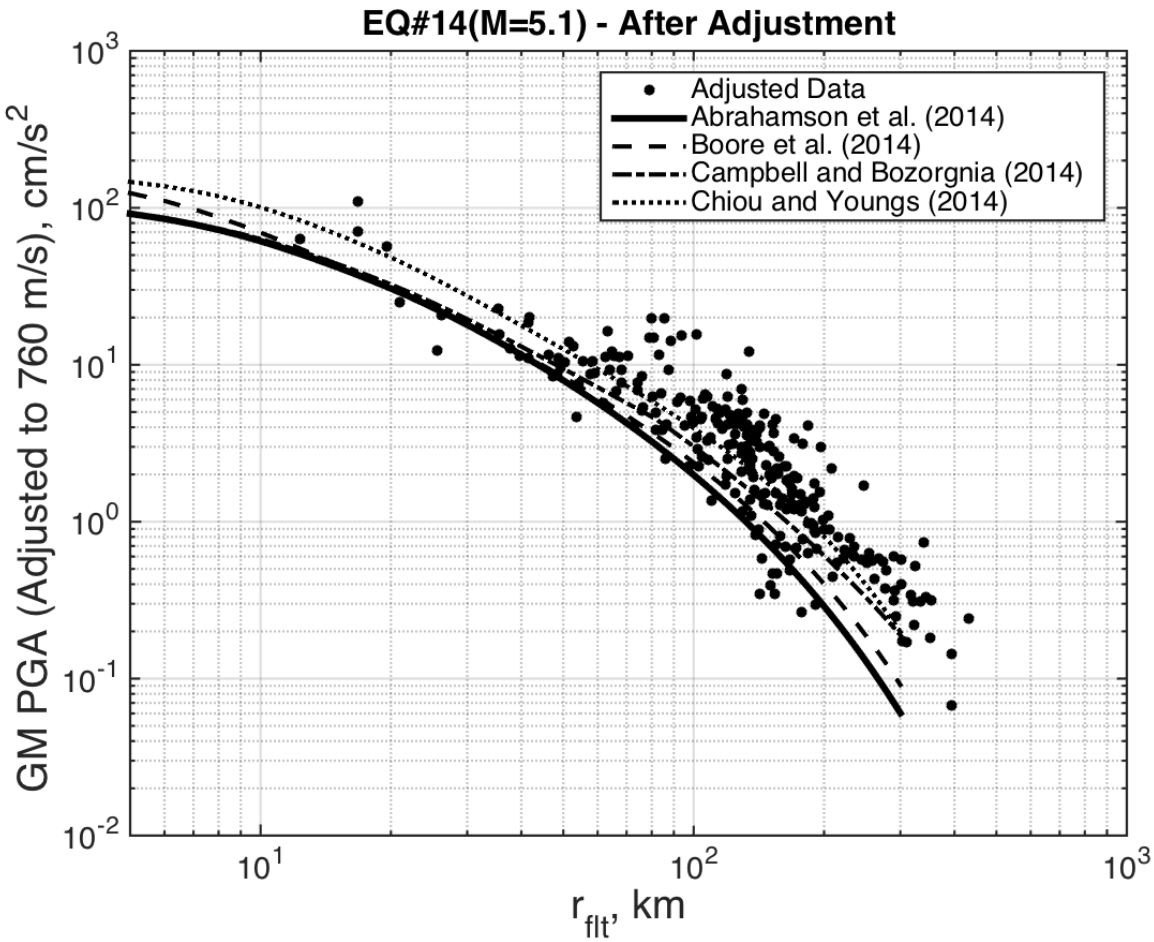

Figure 132: Adjusted accelerations

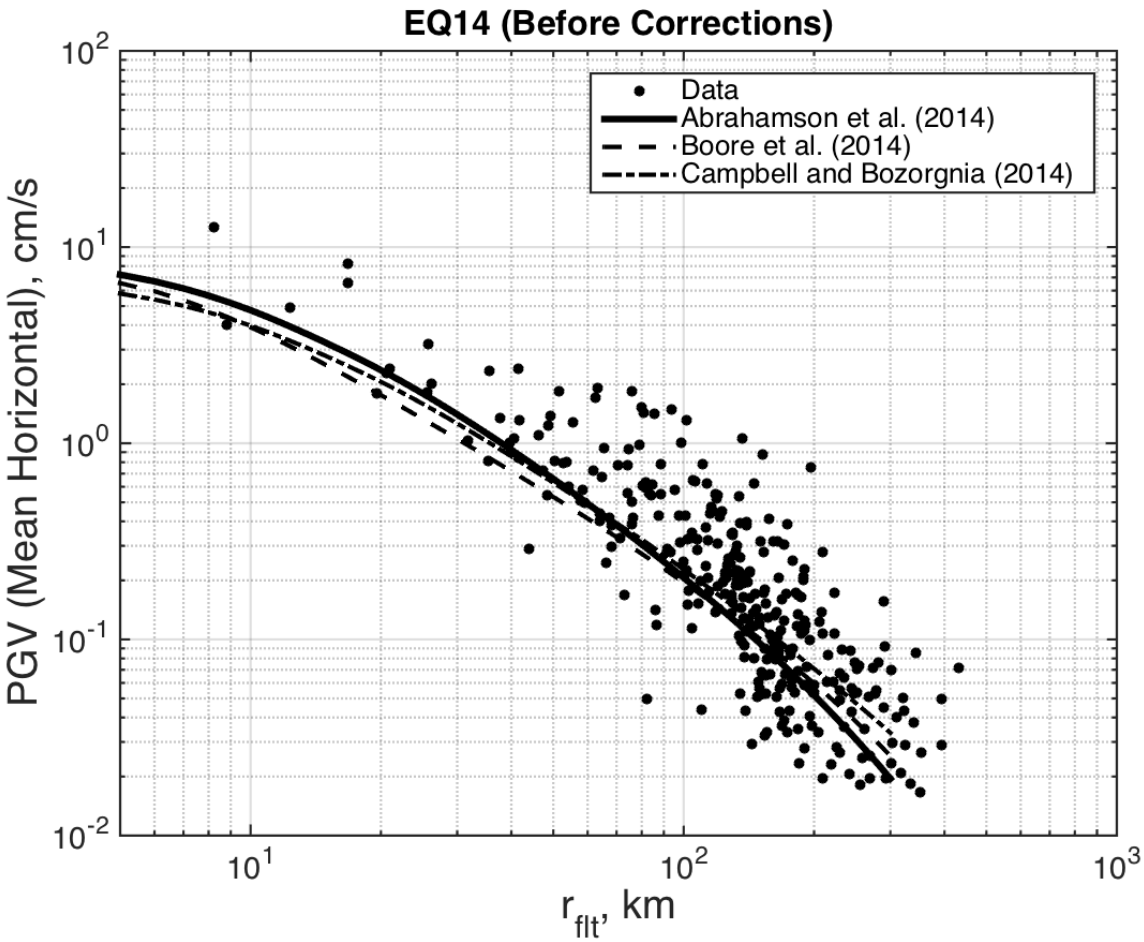

Figure 133: Raw velocities

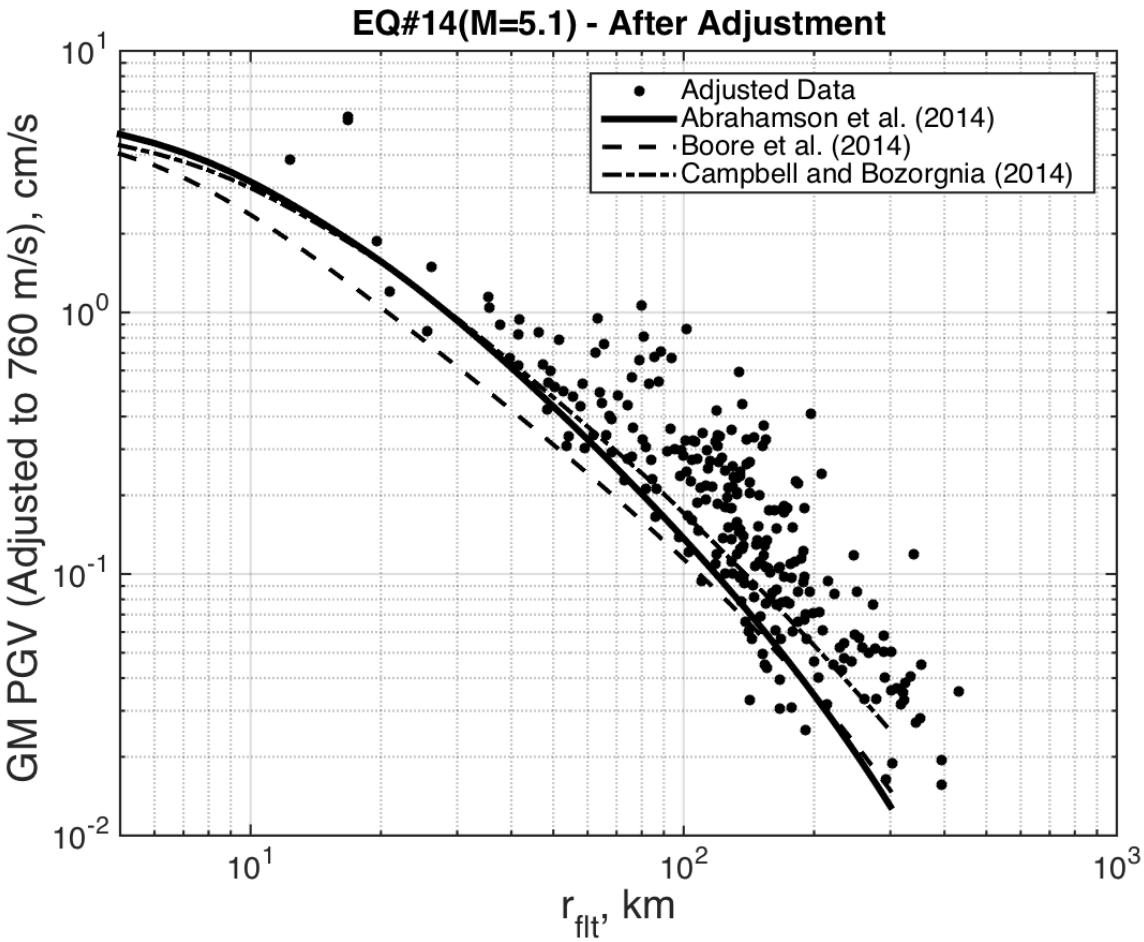

Figure 134: Adjusted velocity

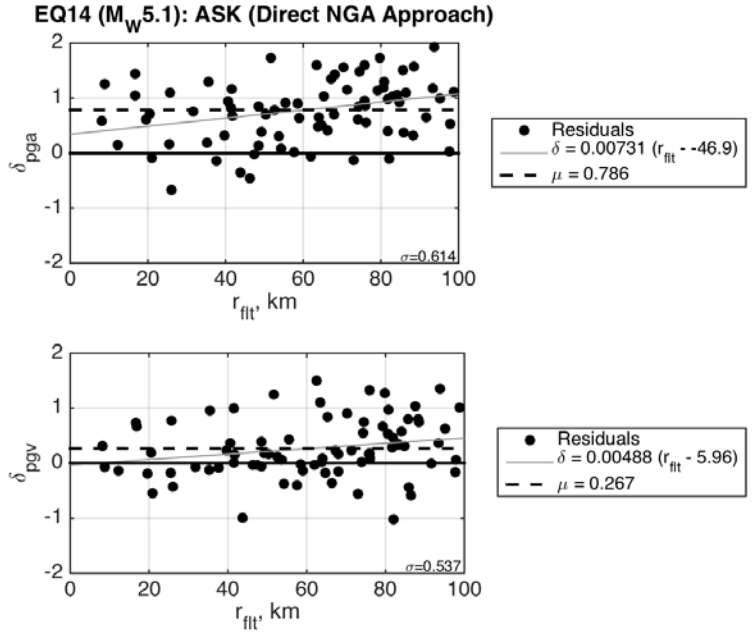

Figure 135: Raw delta ASK

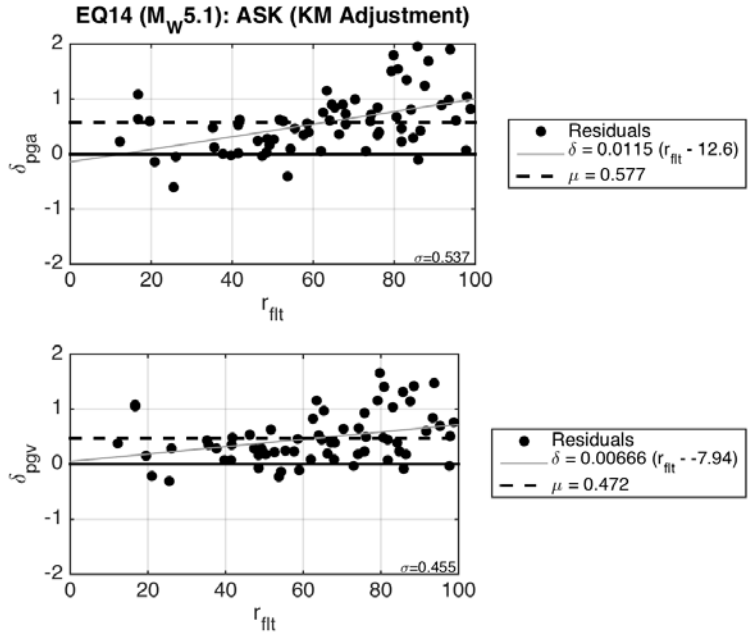

Figure 136: Adjusted delta ASK

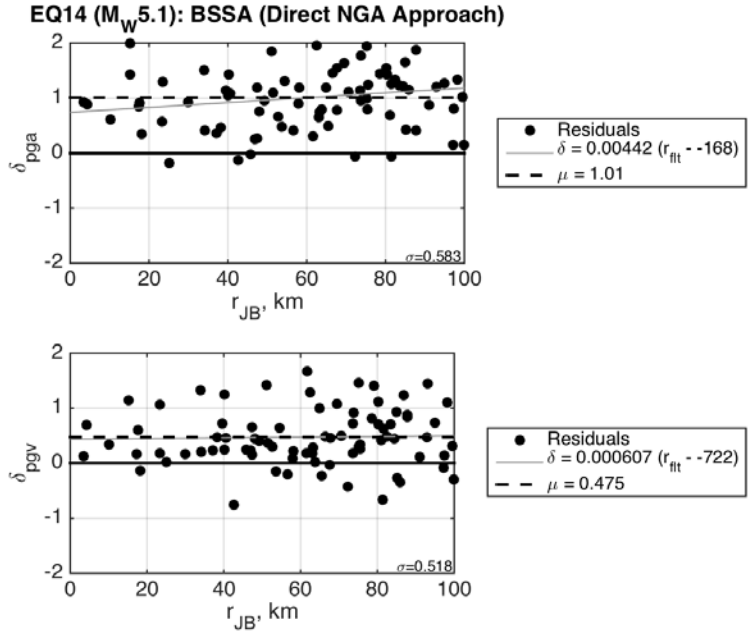

Figure 137: Raw delta BSSA

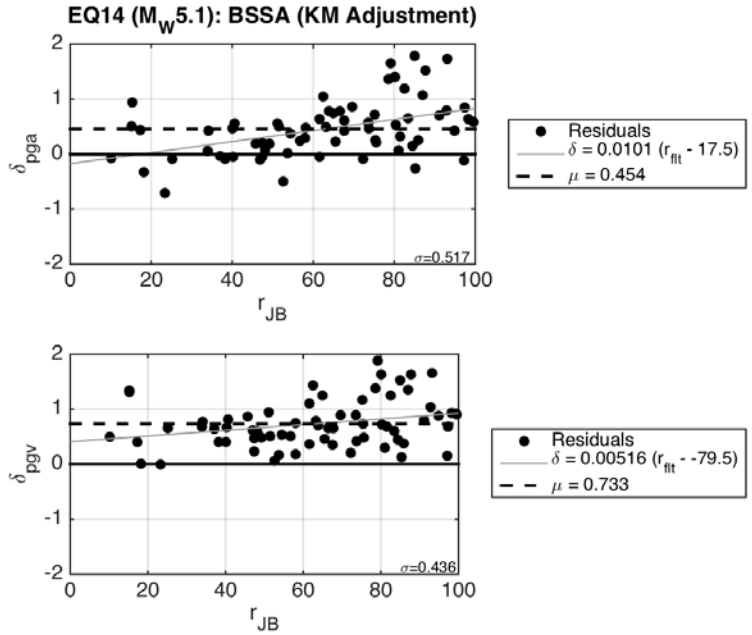

Figure 138: Adjusted delta BSSA

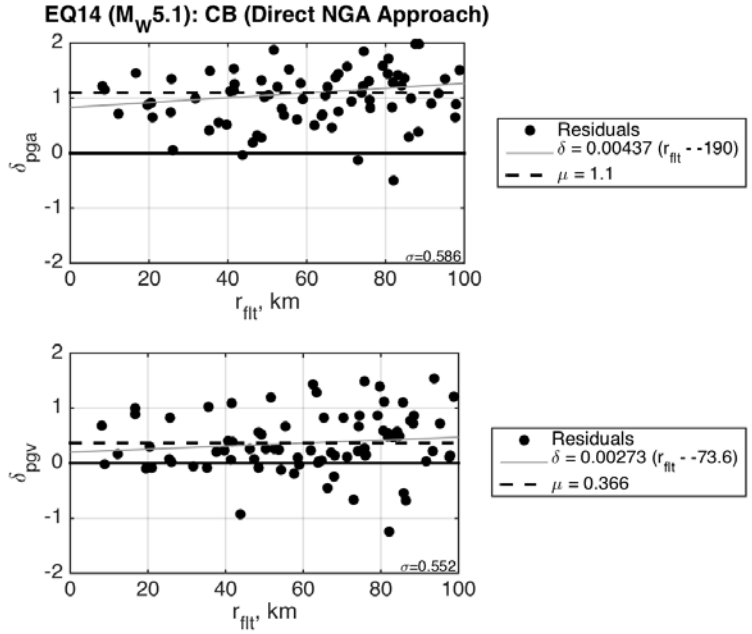

Figure 139: Raw delta CB

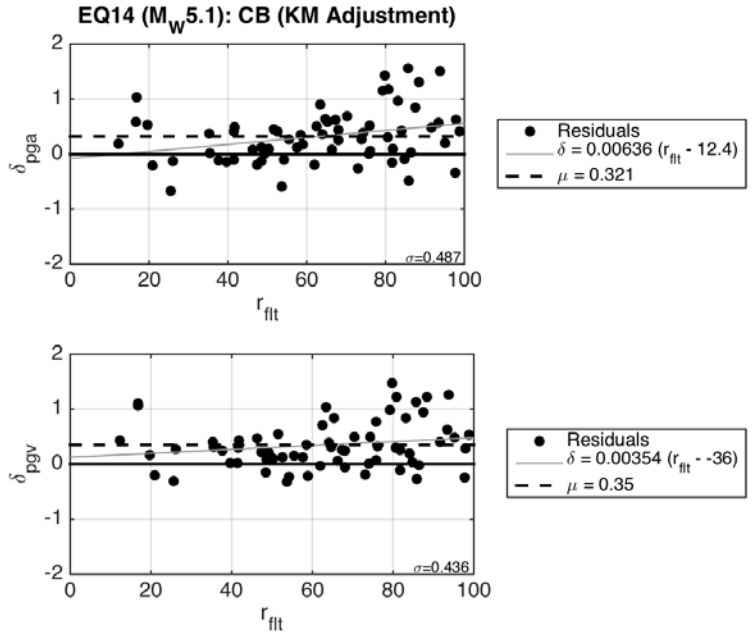

Figure 140: Adjusted delta CB

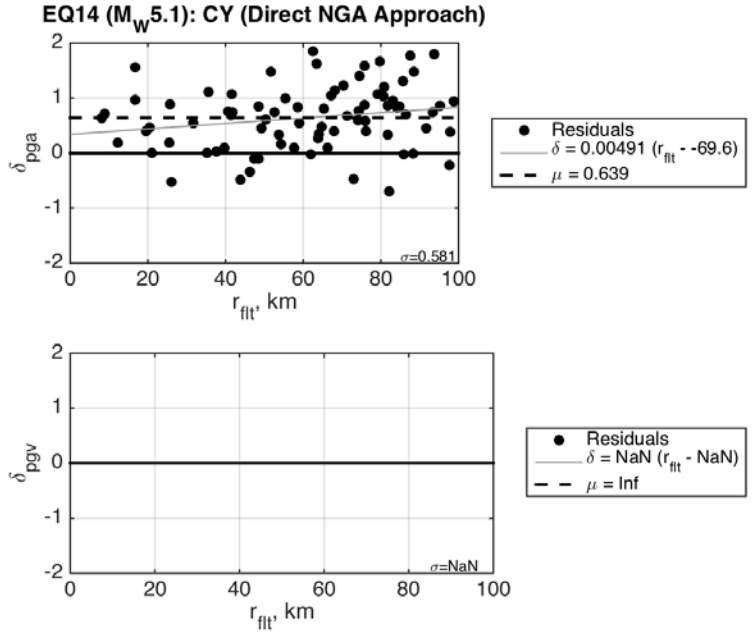

Figure 141: Raw delta CY

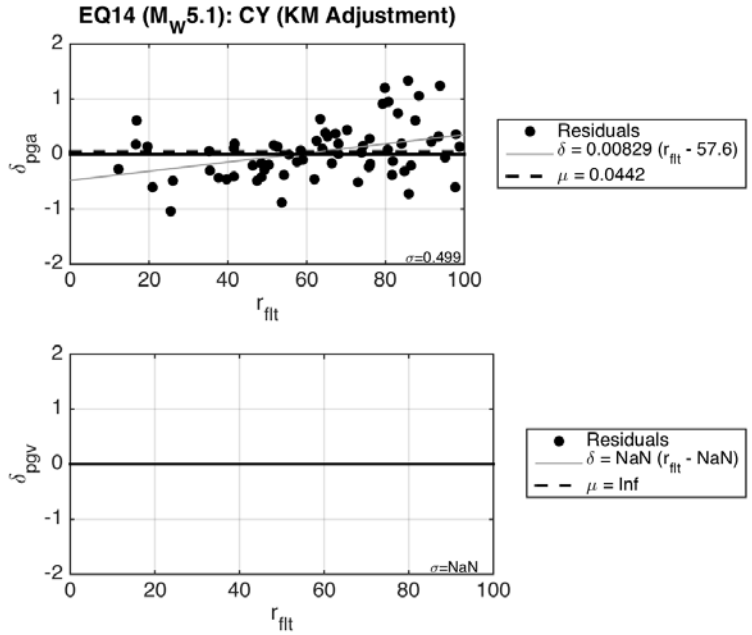

Figure 142: Adjusted delta CY

11 Earthquake 15. 2011 09 29, 19:05 Mw5.1

Figure 143 shows four frames illustrating the geometry of this earthquake. For this earthquake, the northerly-dipping fault plane shown in the lower-right frame, in the view looking along-strike (244°), seems inconsistent with the aftershocks. In three dimenisons, these aftershocks form a v-shaped pattern, and practically all of the relatively sparsely distributed events southwest of the fault, or at distances along strike > 4 km in the view looking at the fault plane (lower-right), are consistent with the chosen plane. Many in the more dense cluster at distances along strike < 4 km seem to occur on a southerly-dipping conjugate plane. However, the southerly-dipping alternative fault plane given by F-net has a dip of only 27°, which is substantially shallower than what the data seem to support. Thus the chosen fault plane is somewhat more reasonable that the alternative.

Figure 144 shows the uncorrected values of peak acceleration as a funciton of distance, and Figure 146 shows the uncorrected values of peak velocity. For comparison, both of these figures show the NGA-West 2 models for Vs30=400 m/s, which is considered to be a reasonable estimate for the network average. Figure 145 shows the adjusted peak accelerations and Figure 147 shows adjusted peak velocities, where the adjustments to the data use Kawase factors and are adjusted to Vs30=760 m/s. Therefore, the NGA curves on these two firgures are for Vs30-760 m/s.

Residuals are shown in Figures 148-155. Raw and adjusted residuals are paired for ease in comparison. To obtain the "raw" residuals, a station-by-station estimate of Vs30 has been used within the NGA models. Since the adjustments are to a common value of vs30, station-by-station adjustments are not needed.

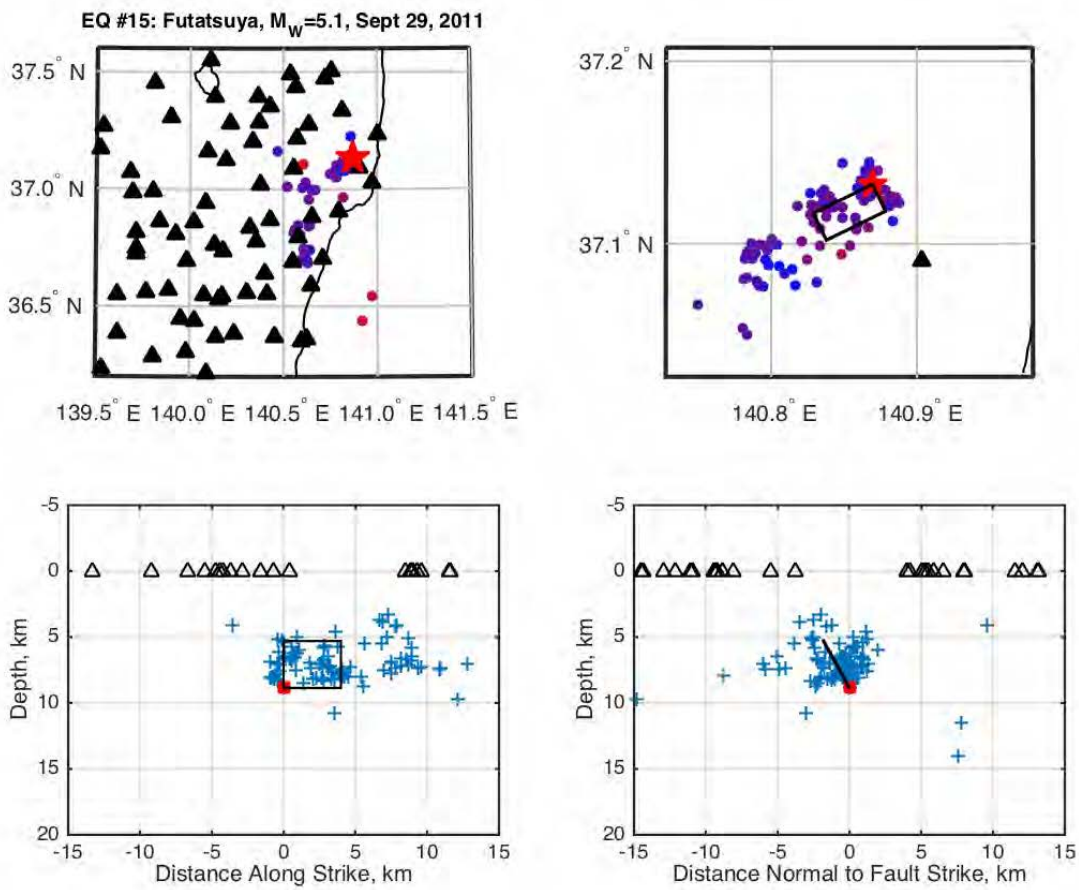

Figure 143: Location and cross section

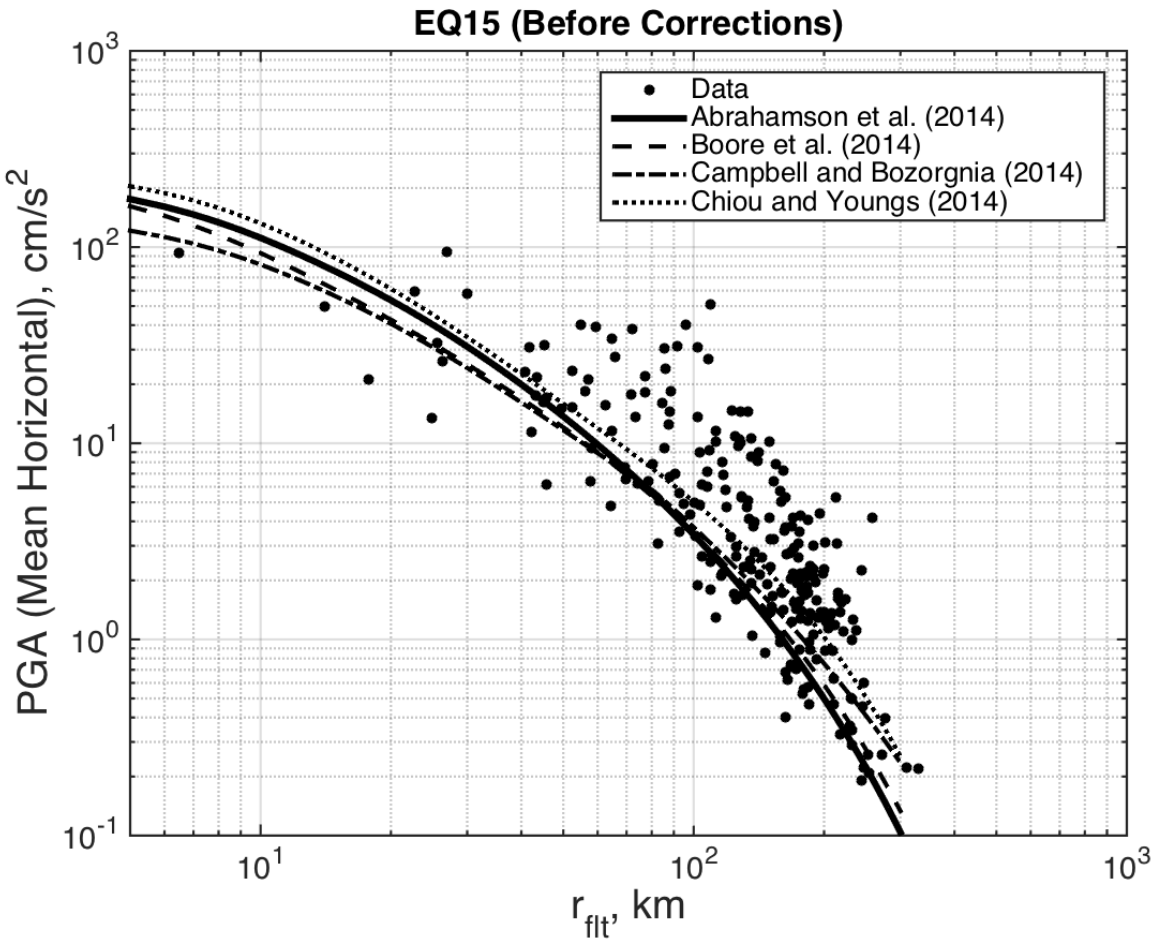

Figure 144: Raw accelerations

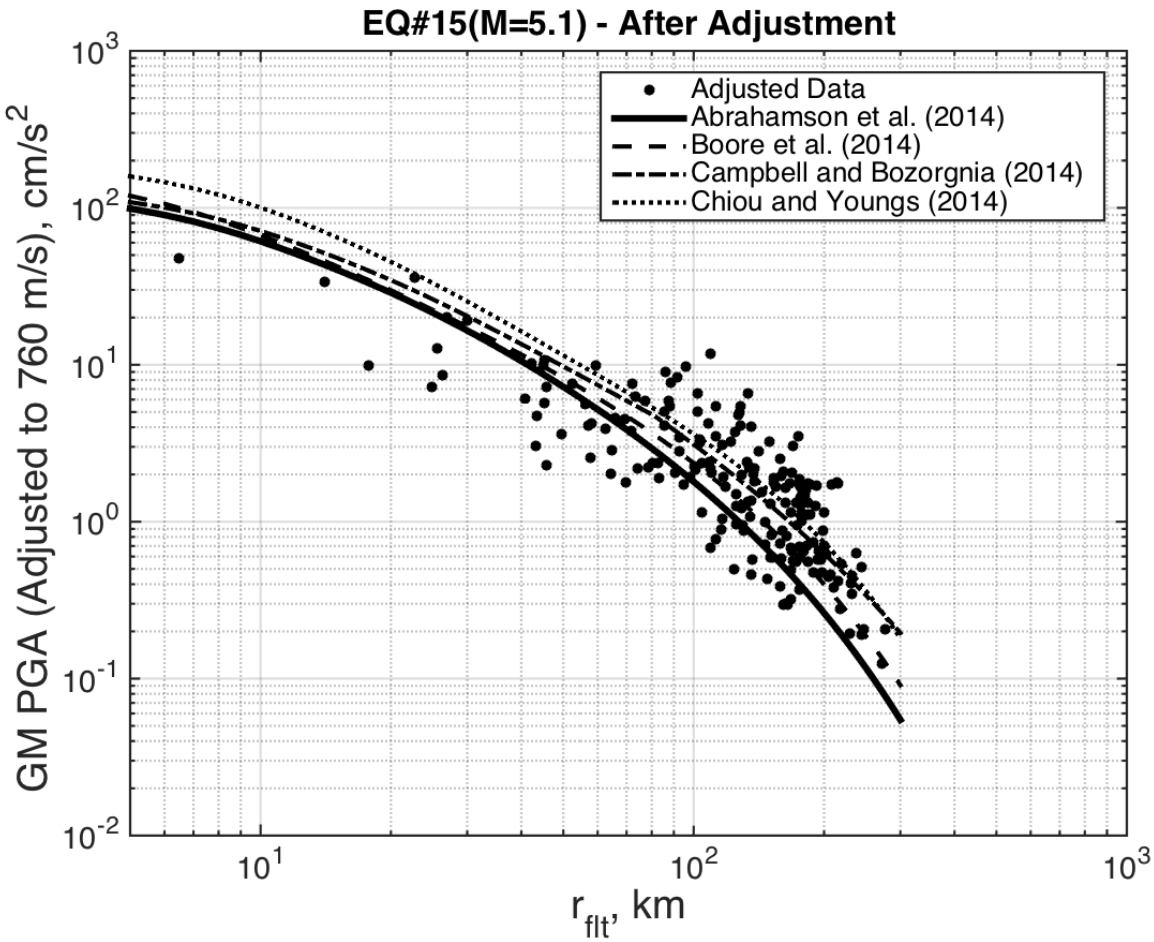

Figure 145: Adjusted accelerations

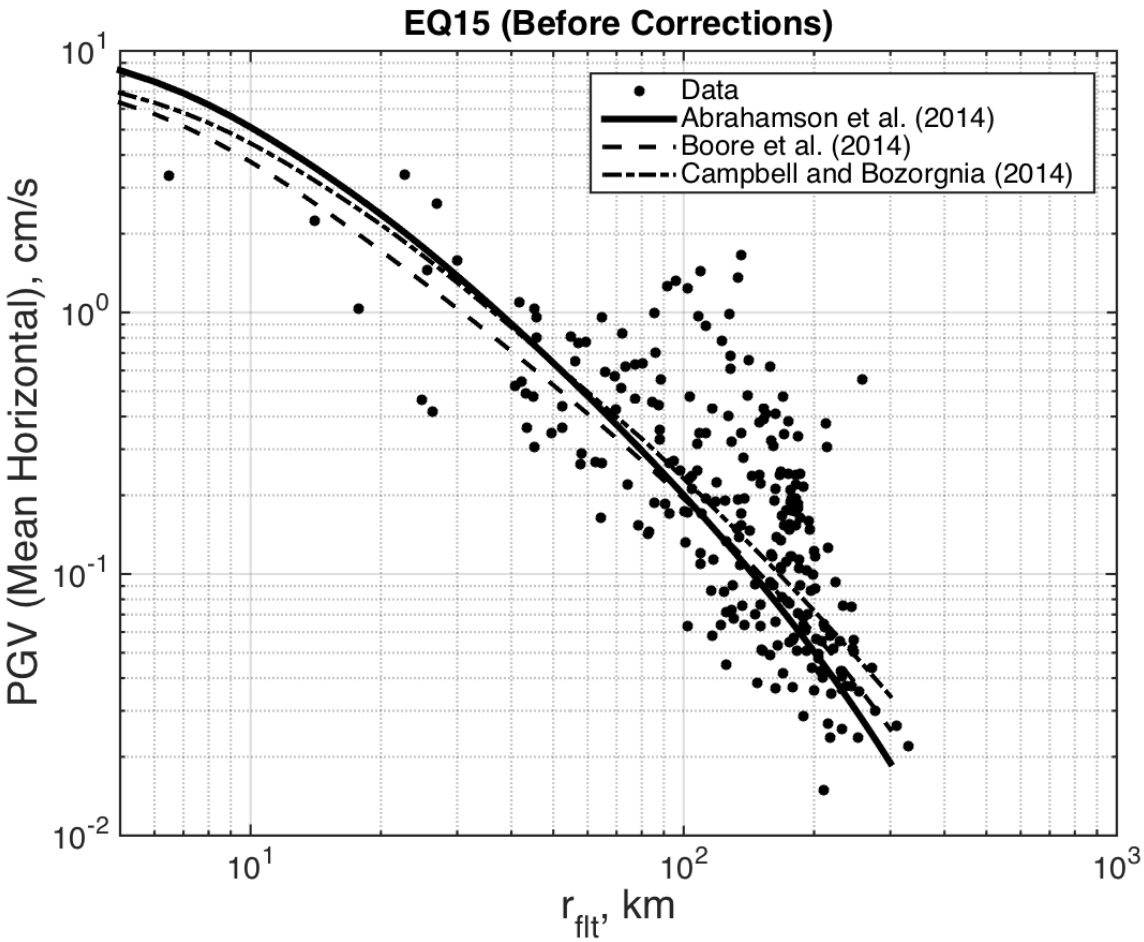

Figure 146: Raw velocities

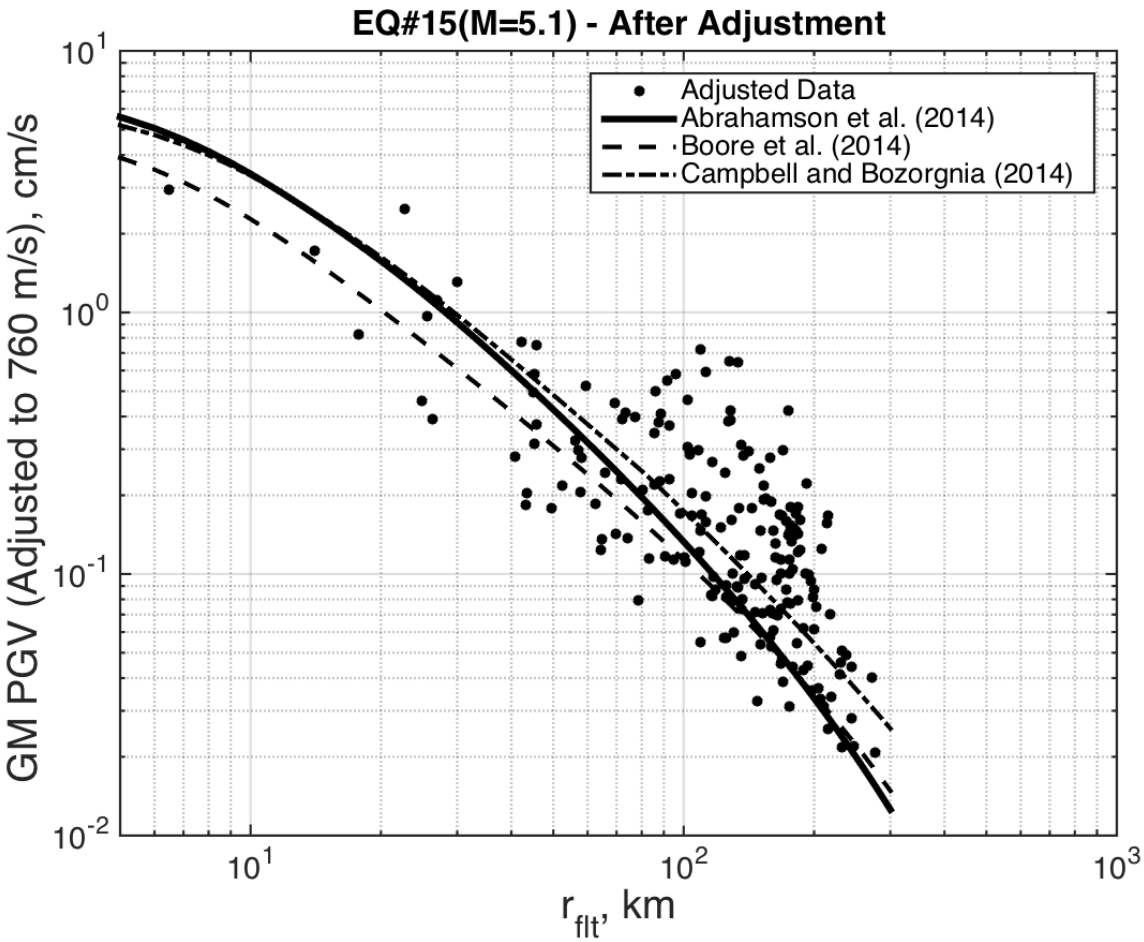

Figure 147: Adjusted velocity

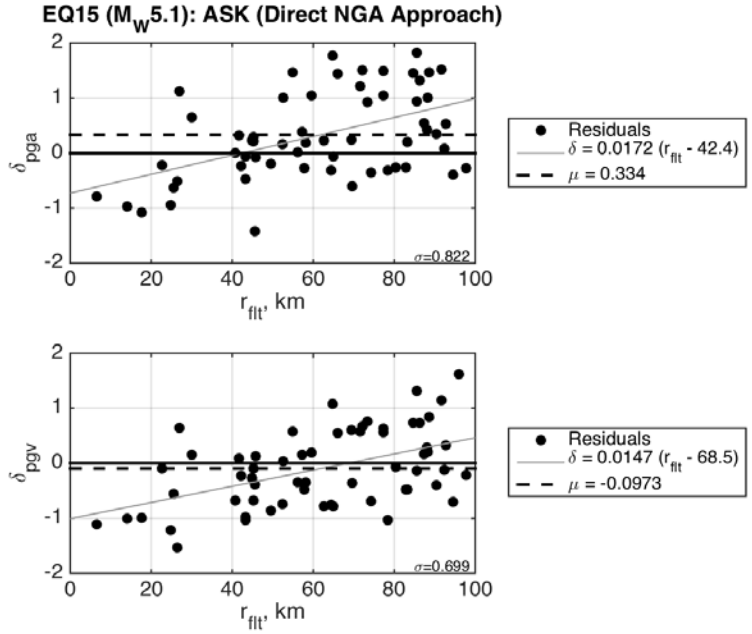

Figure 148: Raw delta ASK

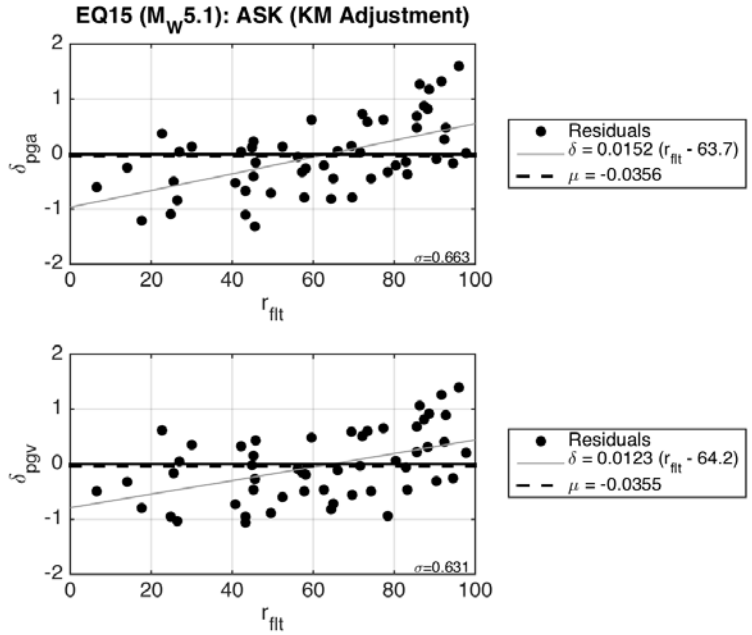

Figure 149: Adjusted delta ASK

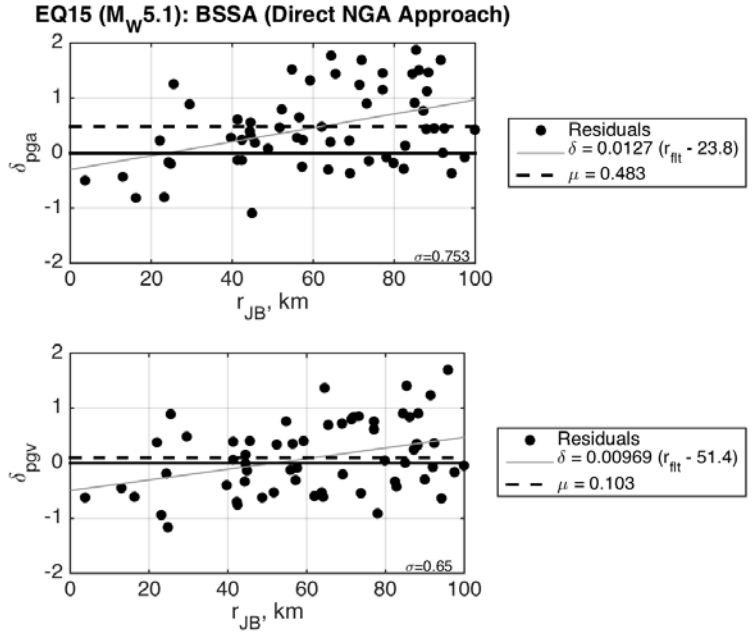

Figure 150: Raw delta BSSA

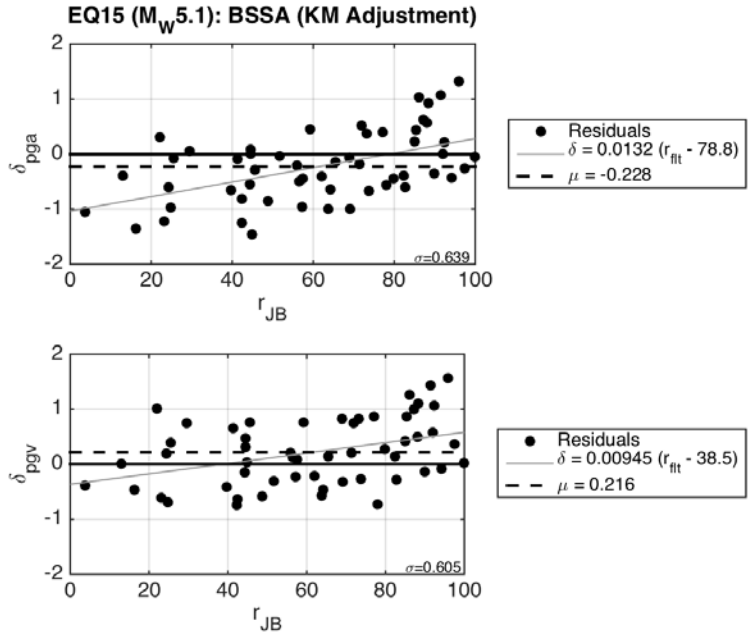

Figure 151: Adjusted delta BSSA

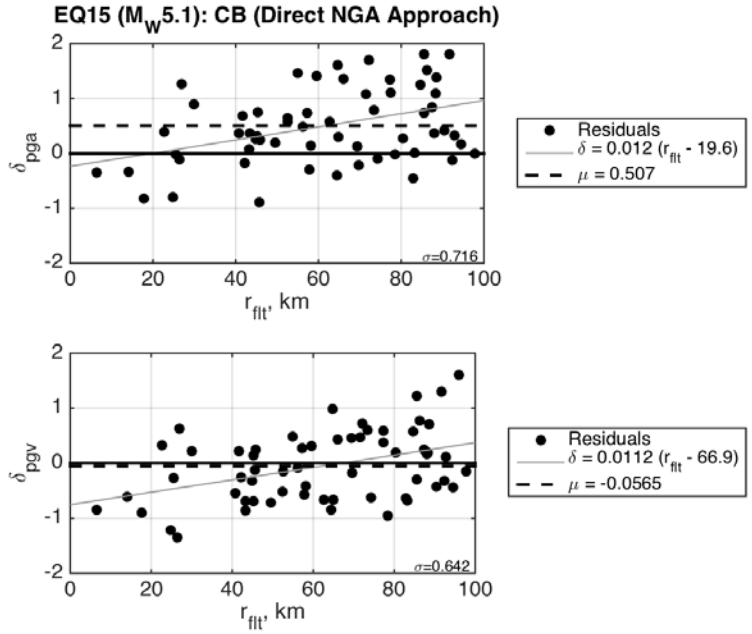

Figure 152: Raw delta CB

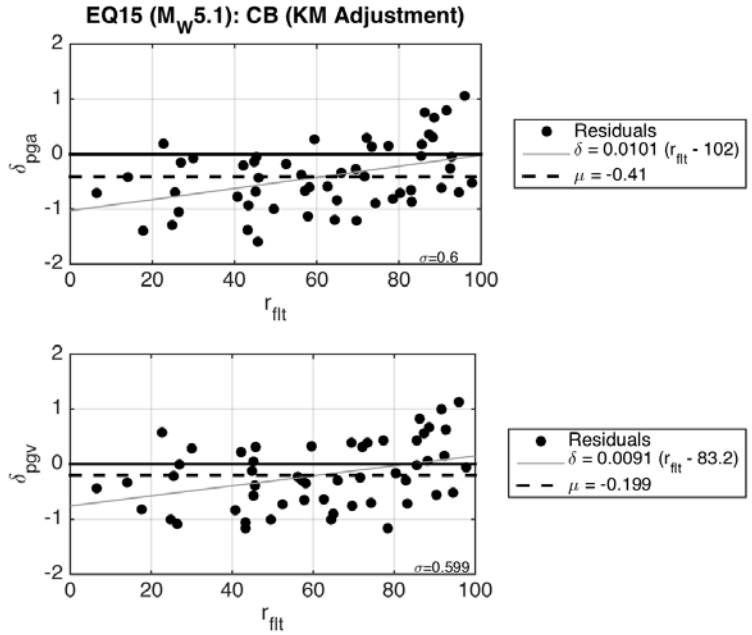

Figure 153: Adjusted delta CB

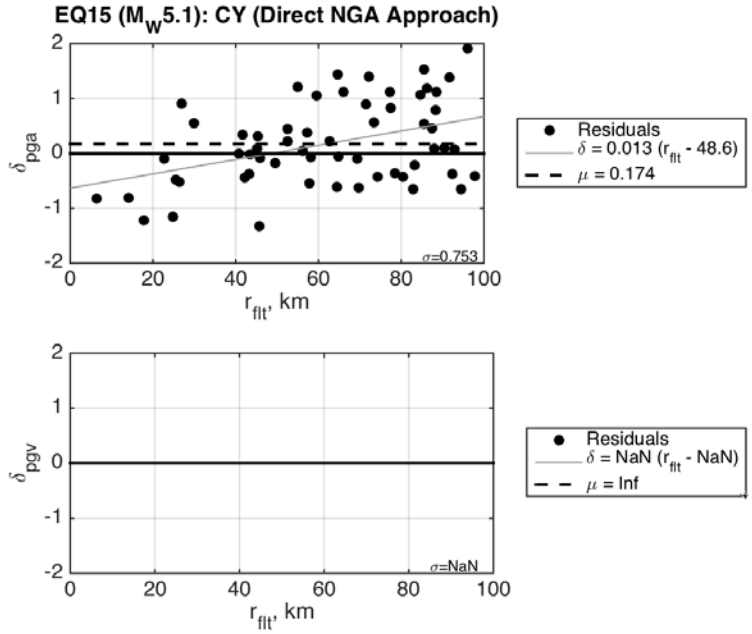

Figure 154: Raw delta CY

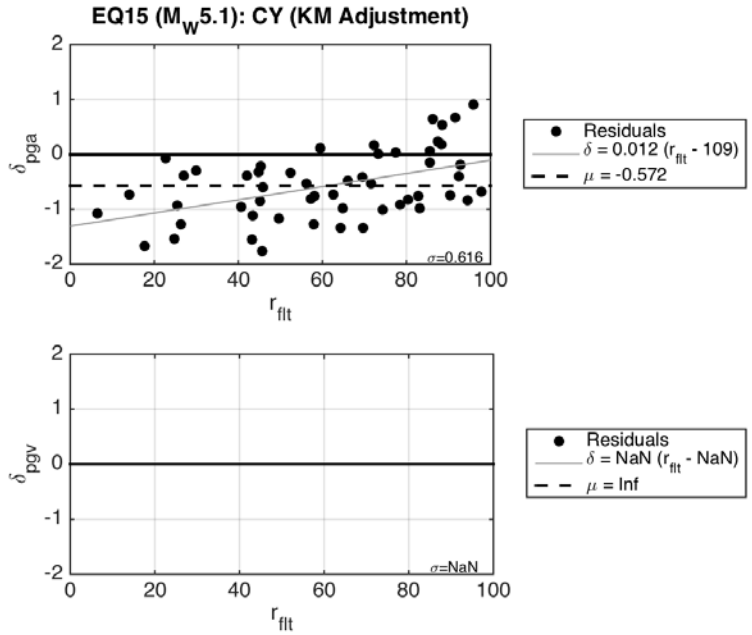

Figure 155: Adjusted delta CY

12 Earthquake 16. 2011 11 20, 10:23 Mw5.0

Figure 156 shows four frames illustrating the geometry of this earthquake.

Figure 157 shows the uncorrected values of peak acceleration as a funciton of distance, and Figure 159 shows the uncorrected values of peak velocity. For comparison, both of these figures show the NGA-West 2 models for Vs30=400 m/s, which is considered to be a reasonable estimate for the network average. Figure 158 shows the adjusted peak accelerations and Figure 160 shows adjusted peak velocities, where the adjustments to the data use Kawase factors and are adjusted to Vs30=760 m/s. Therefore, the NGA curves on these two firgures are for Vs30-760 m/s.

Residuals are shown in Figures 161-168. Raw and adjusted residuals are paired for ease in comparison. To obtain the "raw" residuals, a station-by-station estimate of Vs30 has been used within the NGA models. Since the adjustments are to a common value of vs30, station-by-station adjustments are not needed.

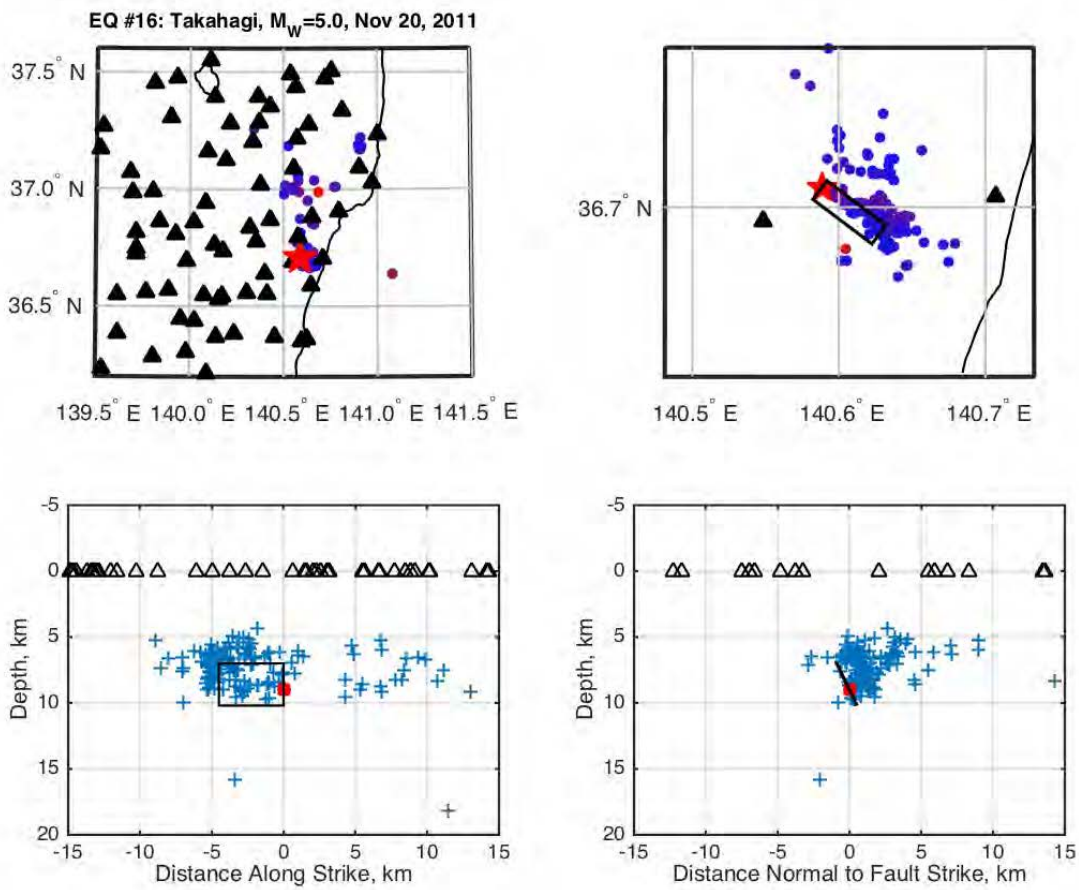

Figure 156: Location and cross section

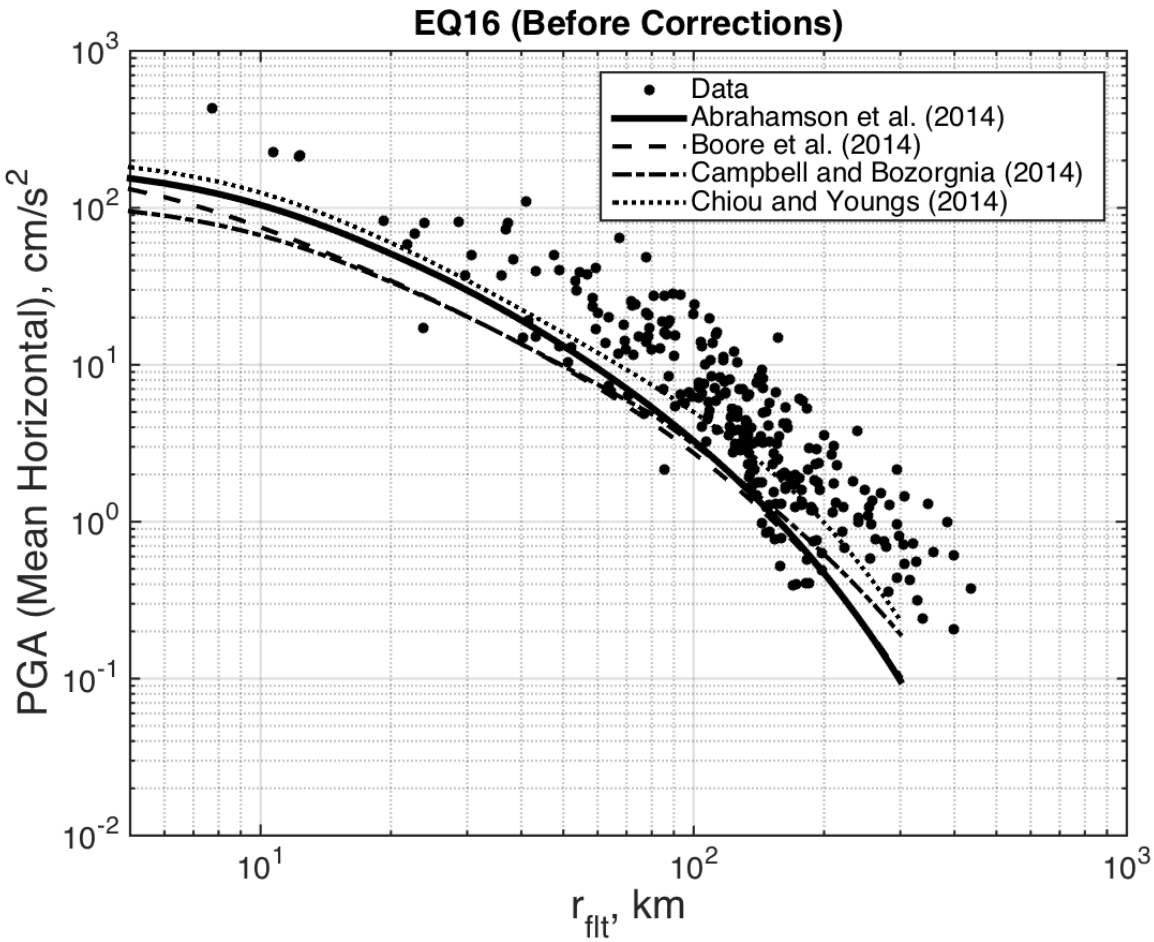

Figure 157: Raw accelerations

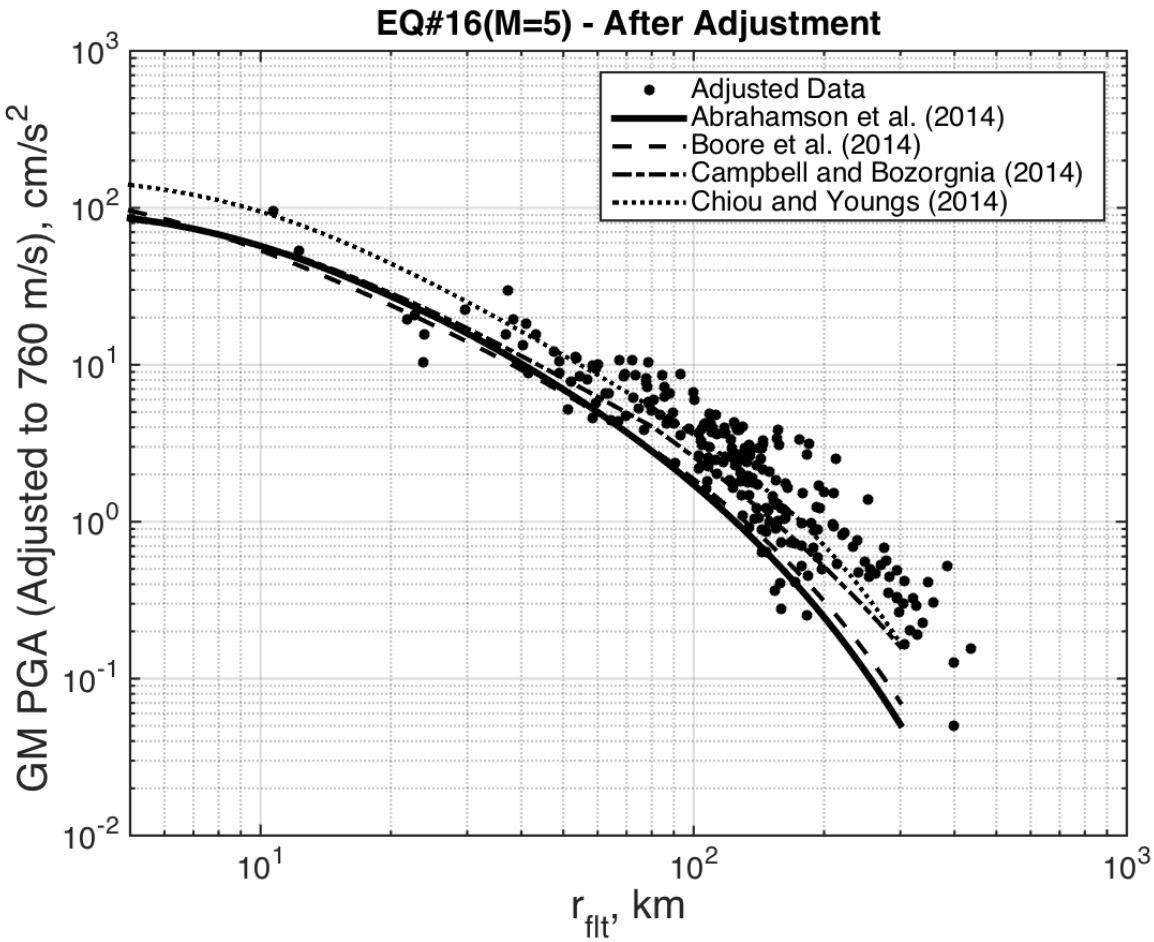

Figure 158: Adjusted accelerations

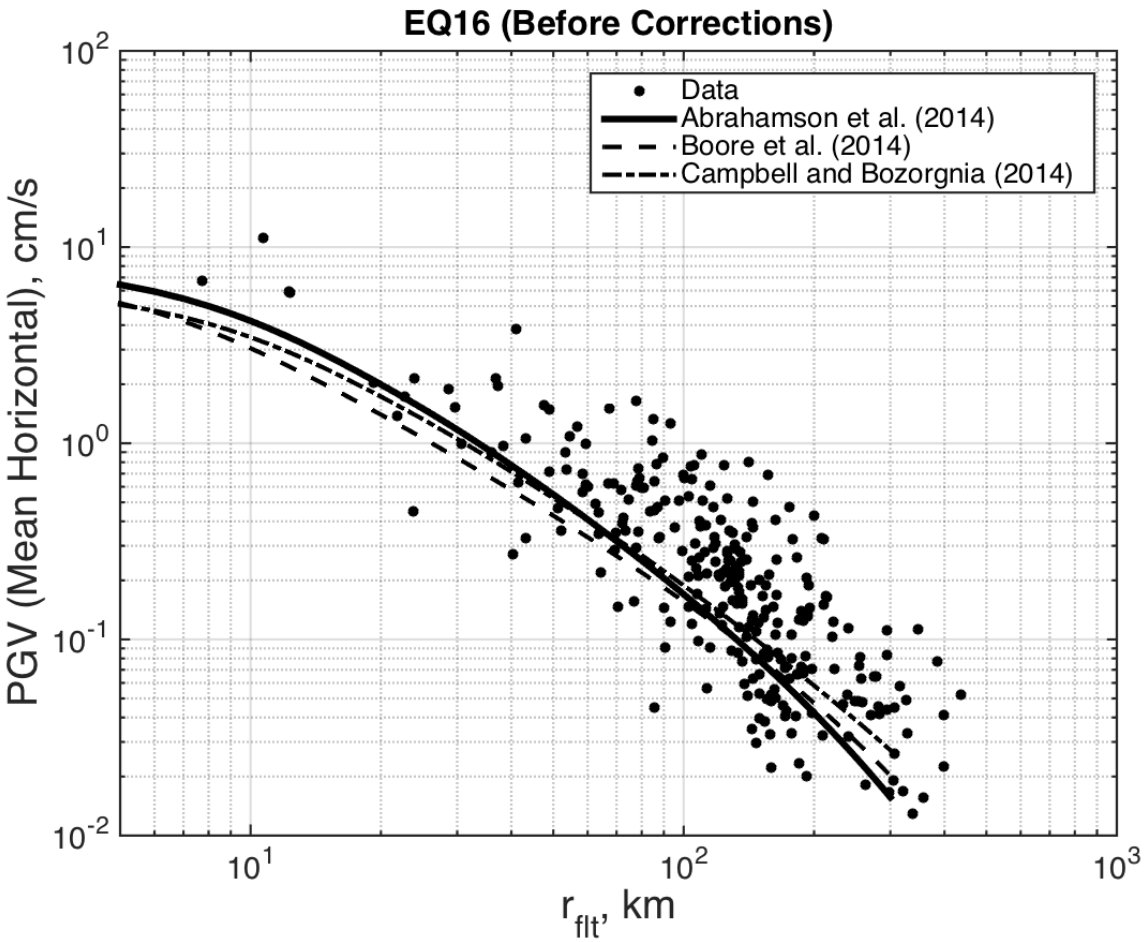

Figure 159: Raw velocities

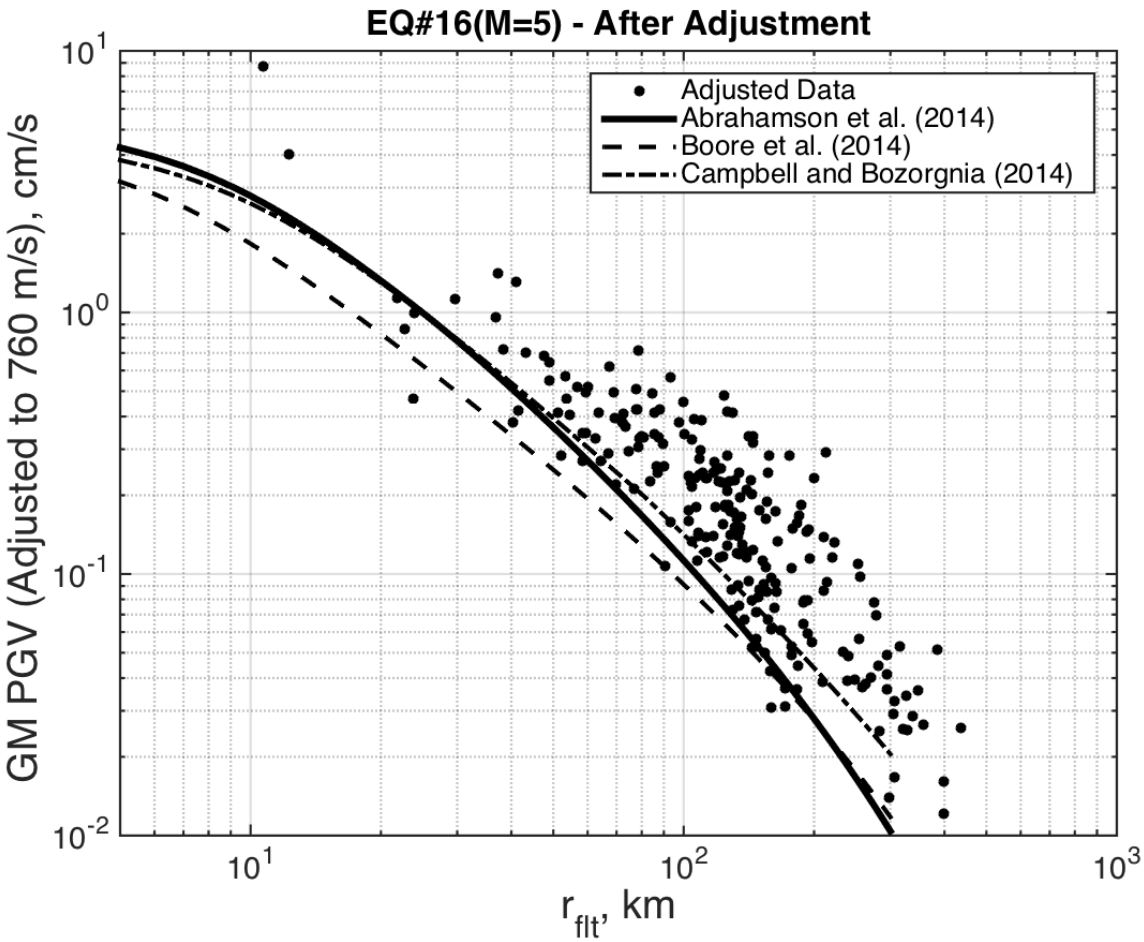

Figure 160: Adjusted velocity

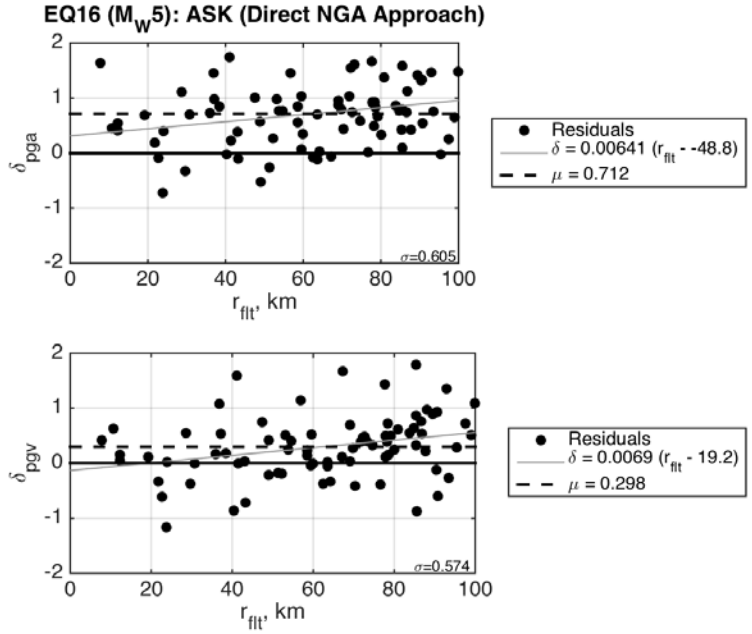

Figure 161: Raw delta ASK

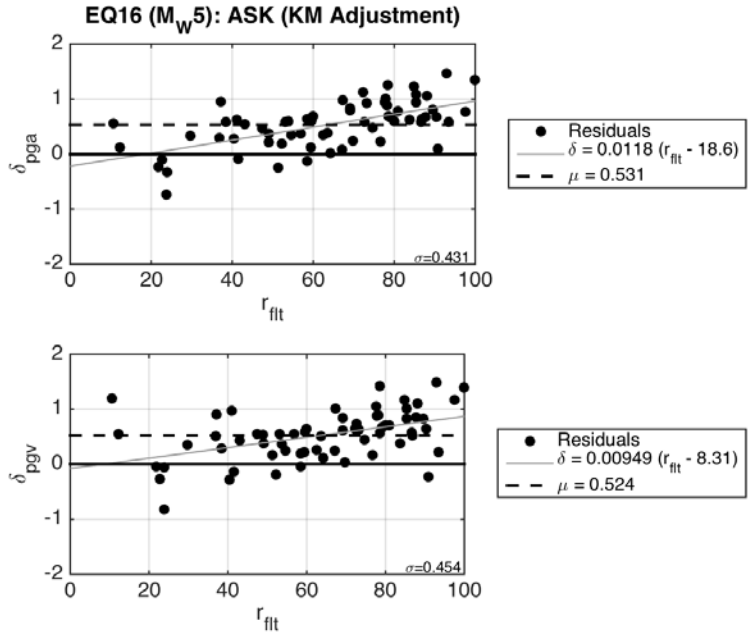

Figure 162: Adjusted delta ASK

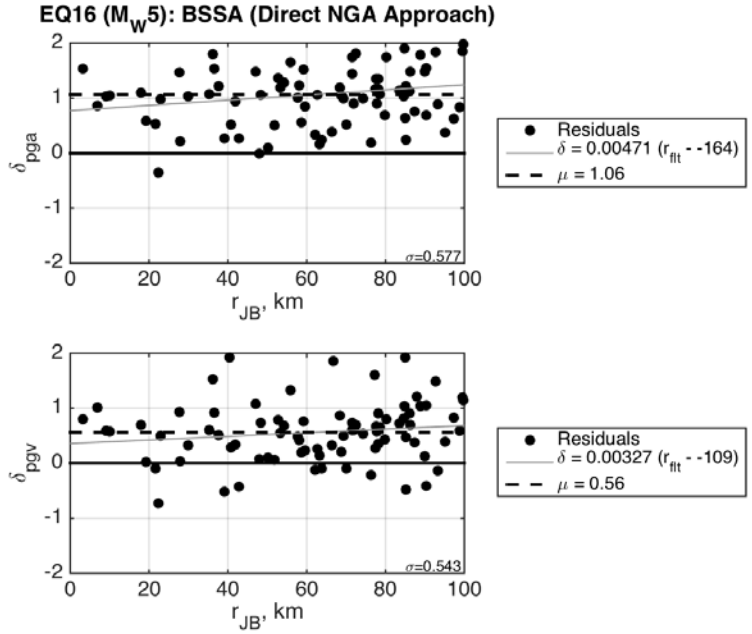

Figure 163: Raw delta BSSA

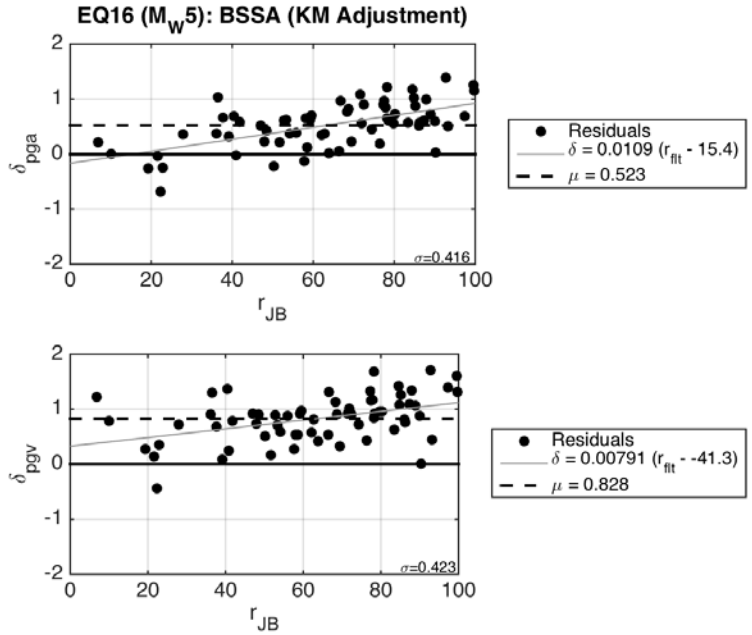

Figure 164: Adjusted delta BSSA

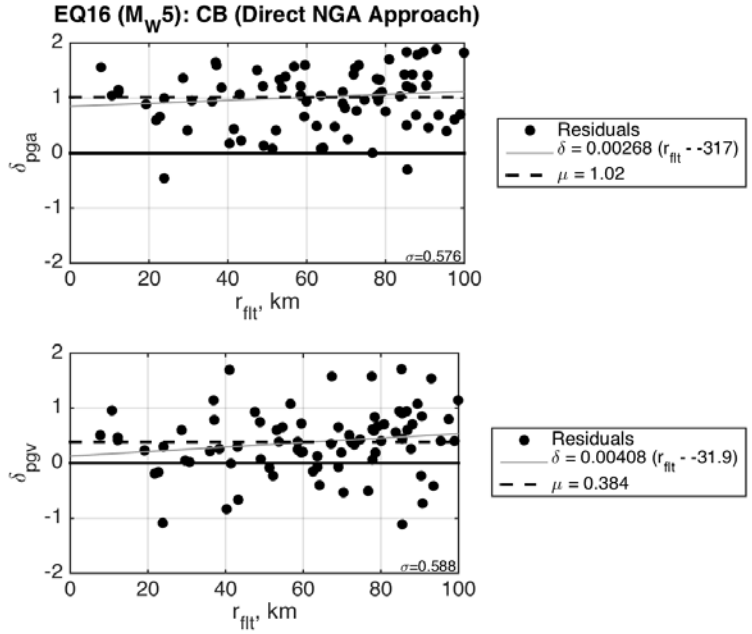

Figure 165: Raw delta CB

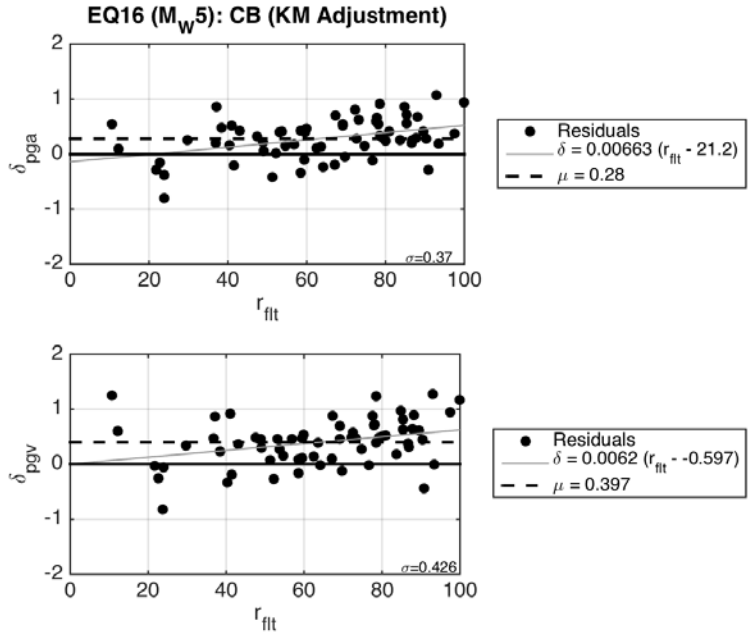

Figure 166: Adjusted delta CB

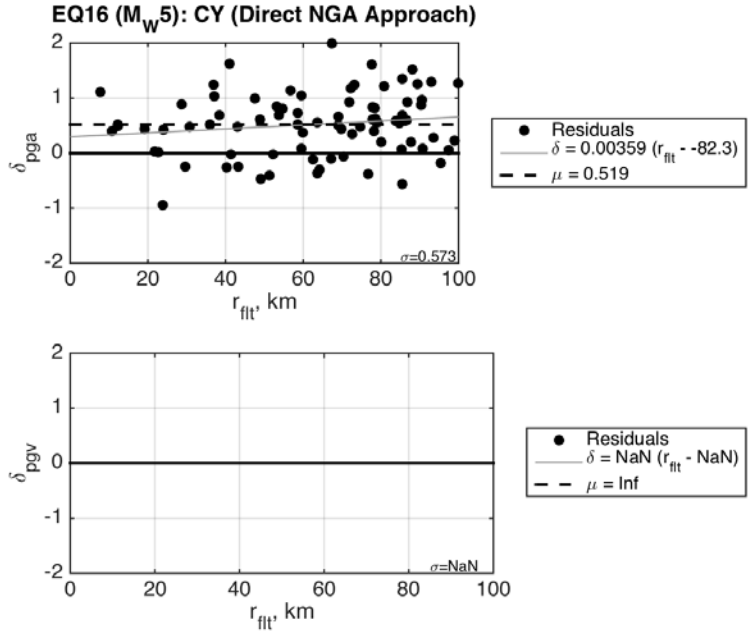

Figure 167: Raw delta CY

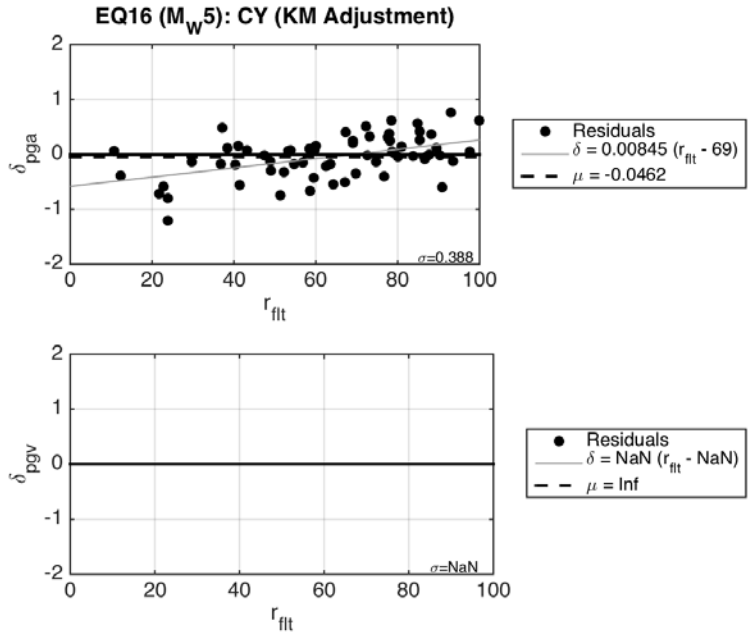

Figure 168: Adjusted delta CY

13 Earthquake 17. 2012 03 10, 02:25 Mw5.2

Figure 169 shows four frames illustrating the geometry of this earthquake.

Figure 170 shows the uncorrected values of peak acceleration as a funciton of distance, and Figure 172 shows the uncorrected values of peak velocity. For comparison, both of these figures show the NGA-West 2 models for Vs30=400 m/s, which is considered to be a reasonable estimate for the network average. Figure 171 shows the adjusted peak accelerations and Figure 173 shows adjusted peak velocities, where the adjustments to the data use Kawase factors and are adjusted to Vs30=760 m/s. Therefore, the NGA curves on these two firgures are for Vs30-760 m/s.

Residuals are shown in Figures 174-181. Raw and adjusted residuals are paired for ease in comparison. To obtain the "raw" residuals, a station-by-station estimate of Vs30 has been used within the NGA models. Since the adjustments are to a common value of vs30, station-by-station adjustments are not needed.

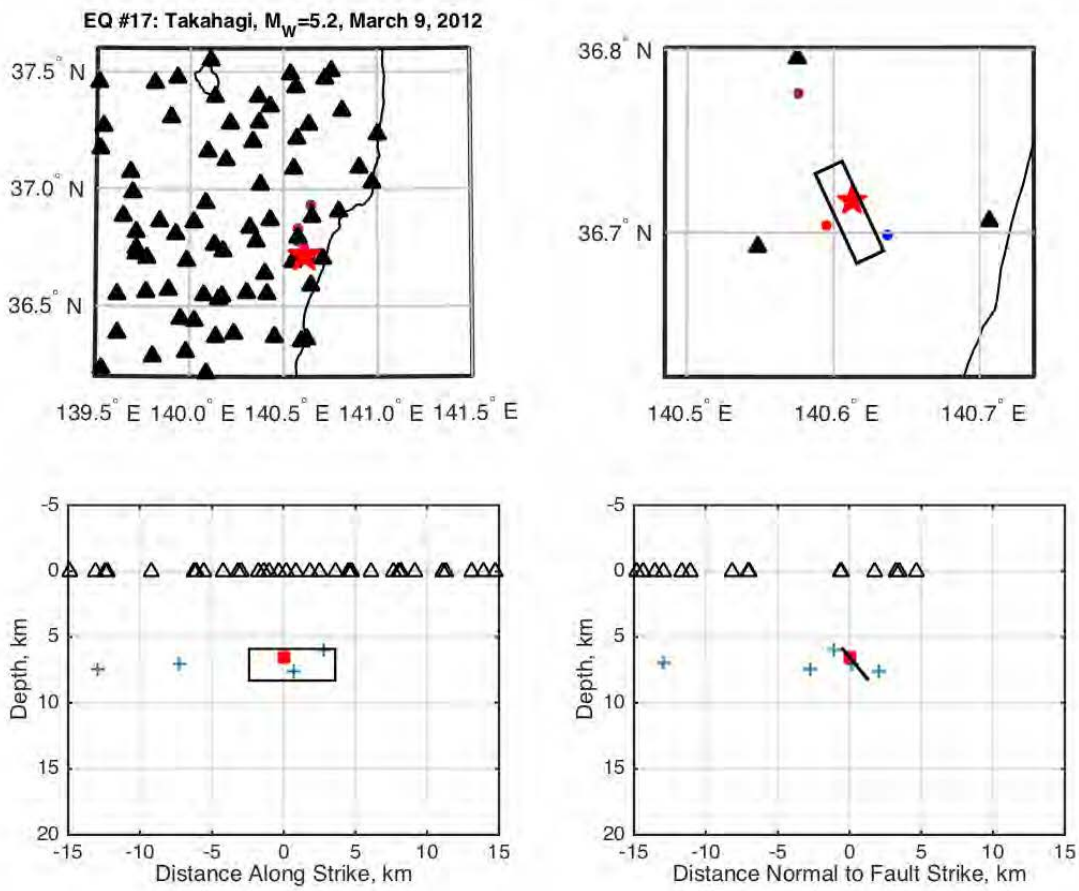

Figure 169: Location and cross section

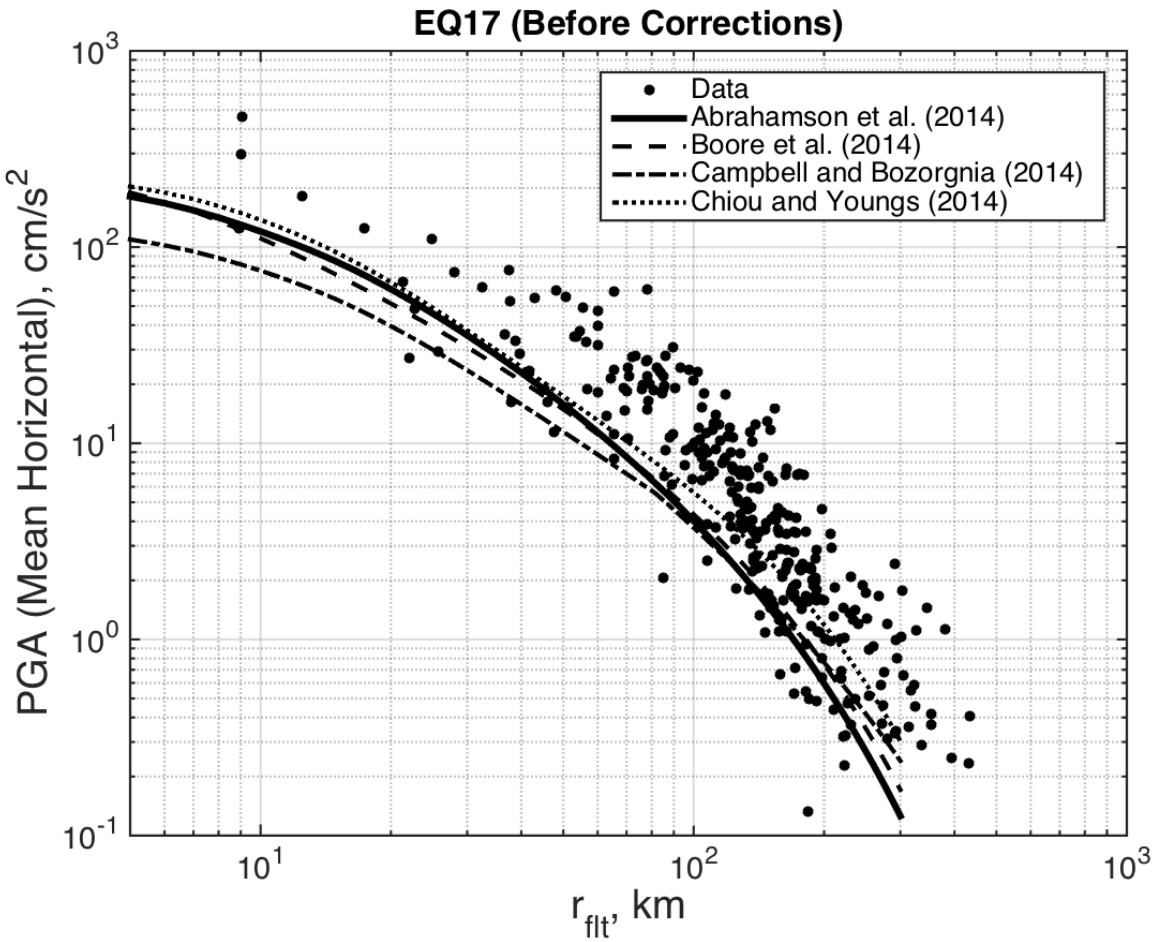

Figure 170: Raw accelerations

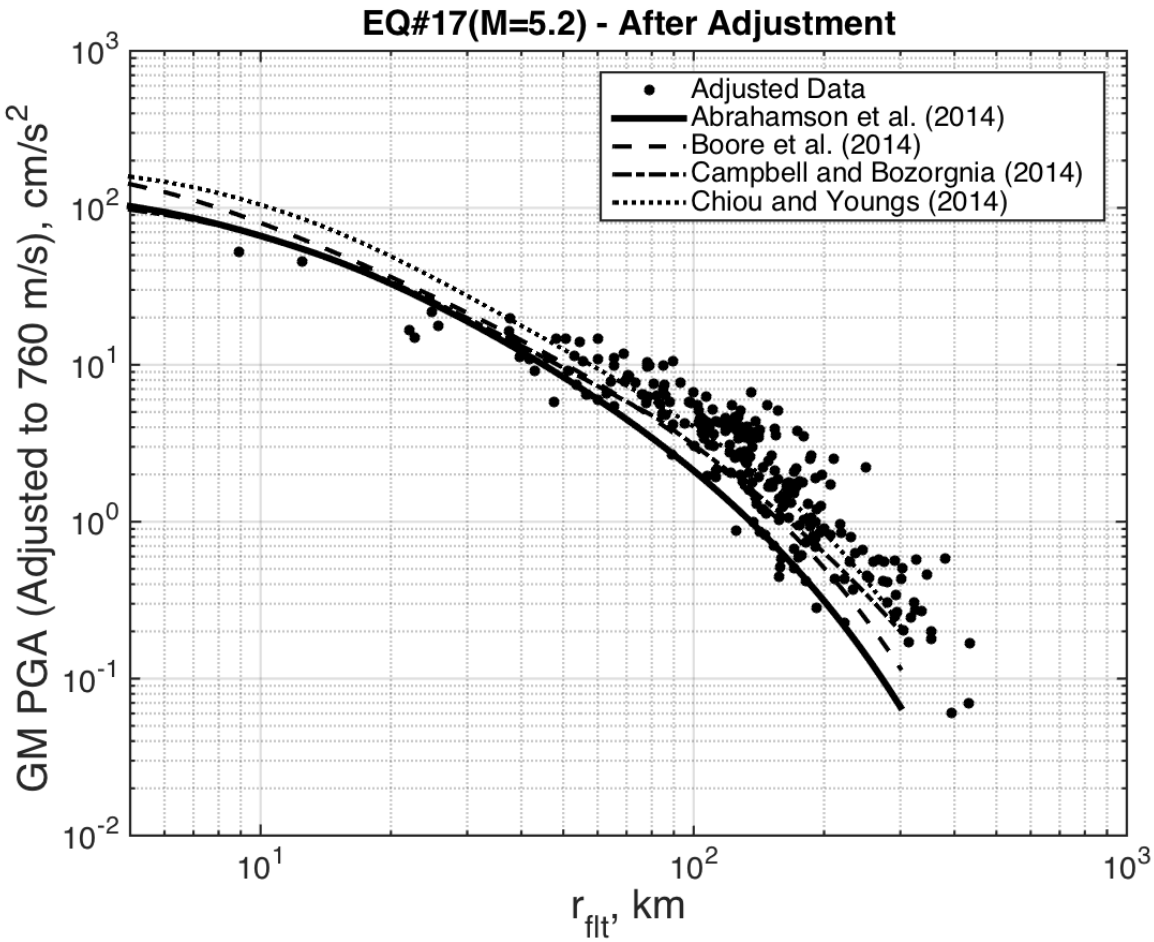

Figure 171: Adjusted accelerations

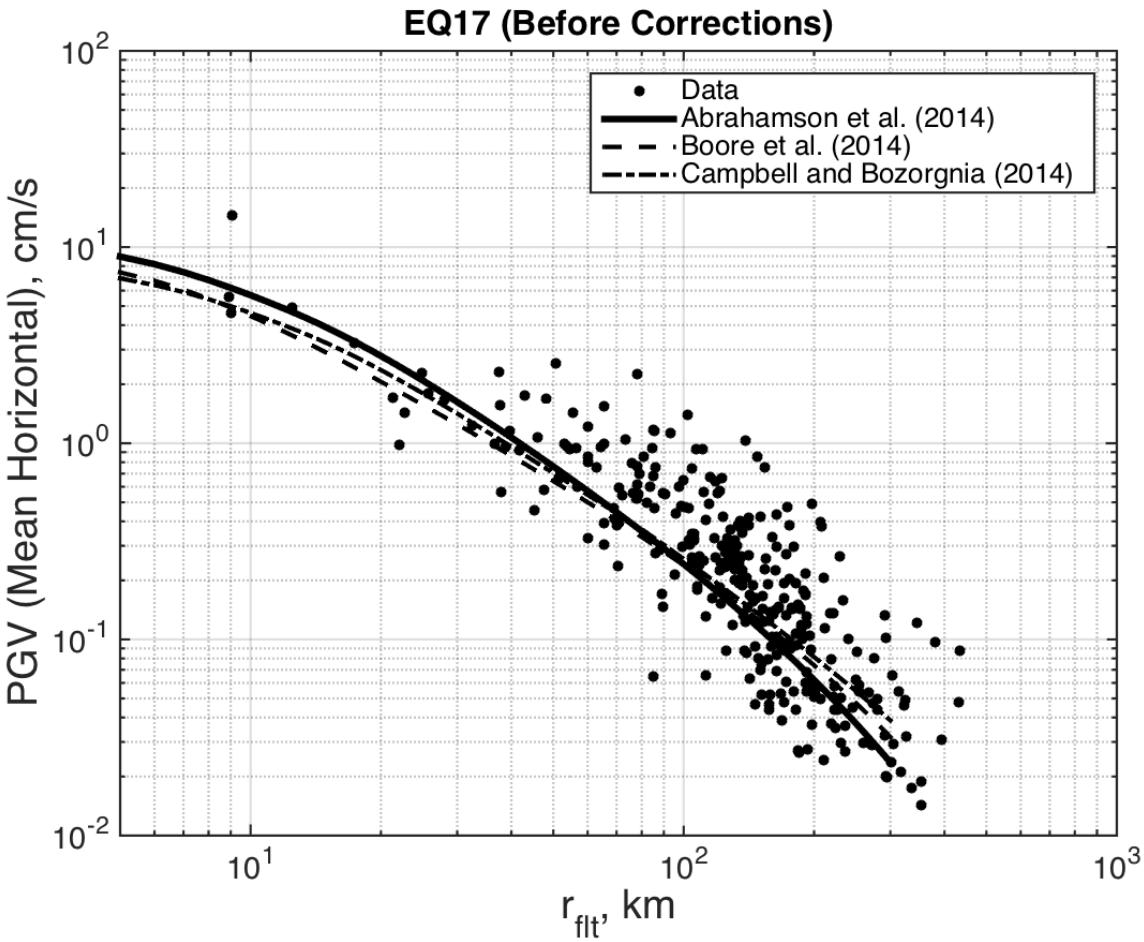

Figure 172: Raw velocities

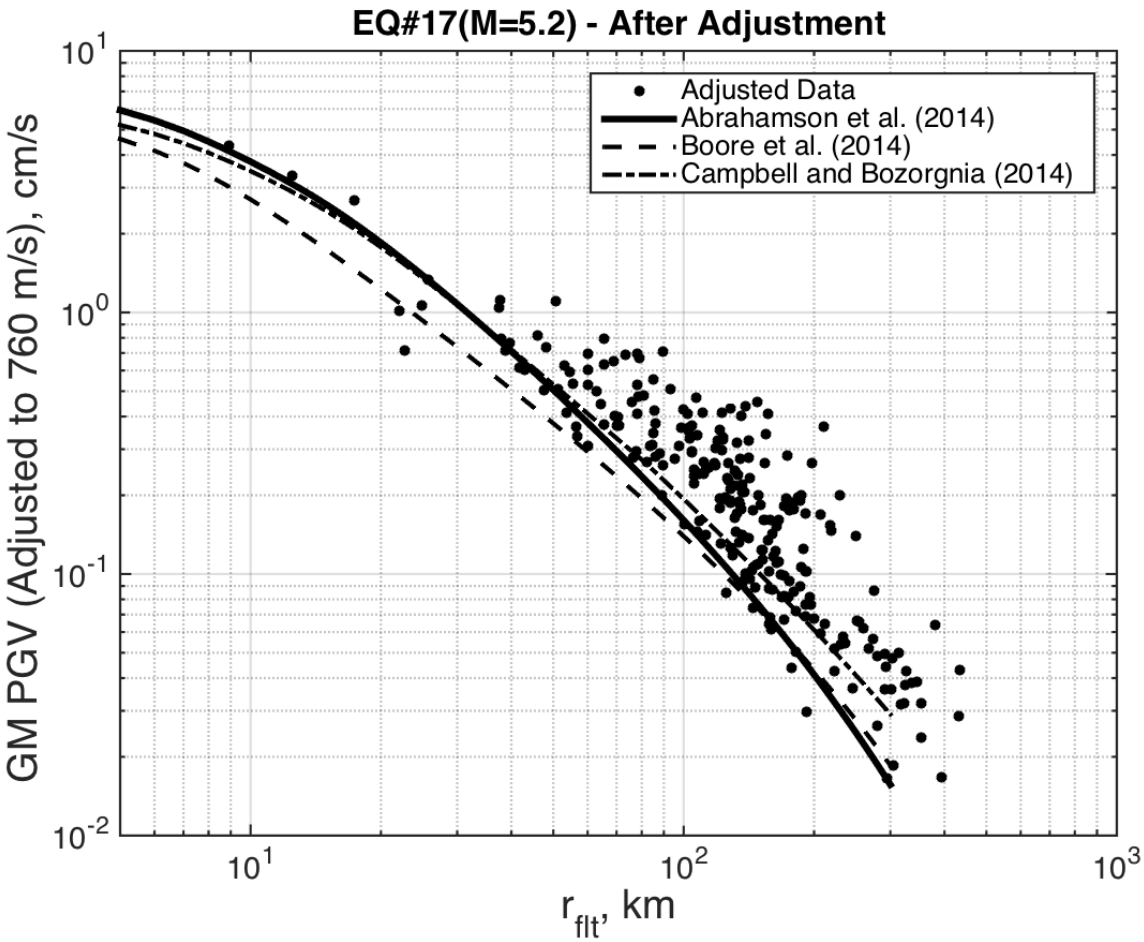

Figure 173: Adjusted velocity

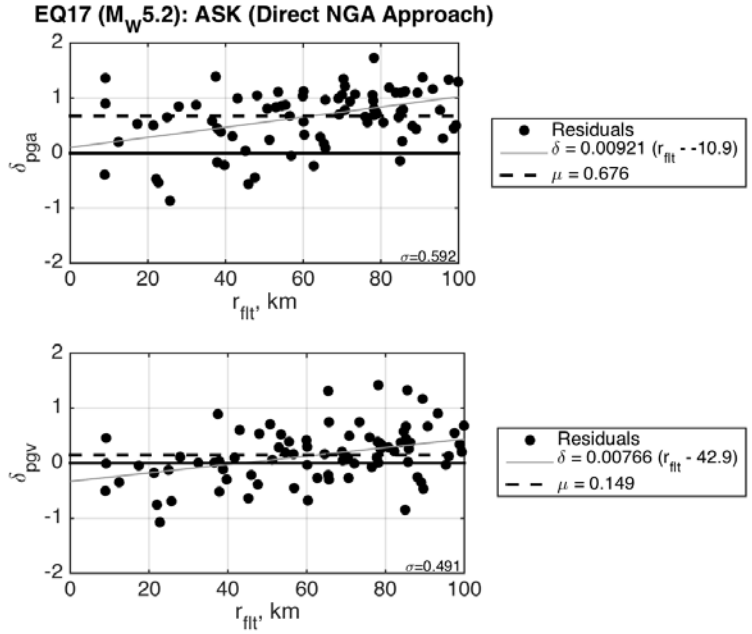

Figure 174: Raw delta ASK

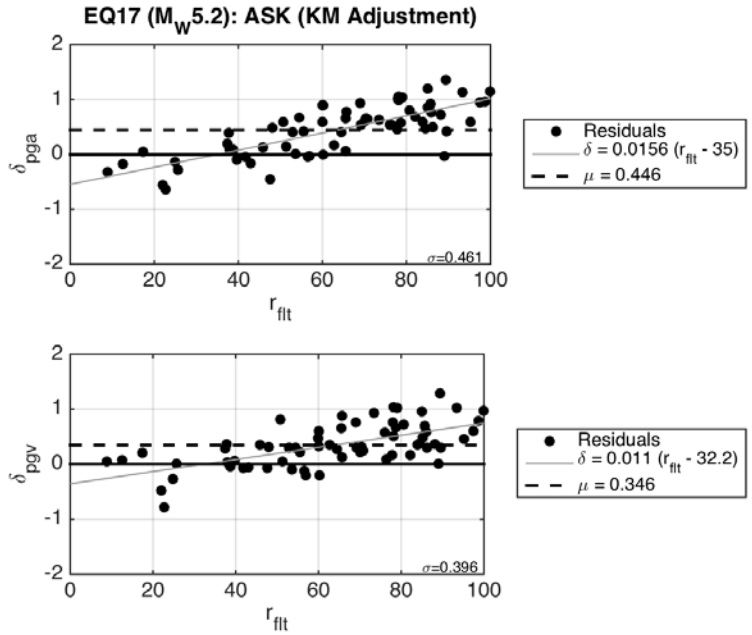

Figure 175: Adjusted delta ASK

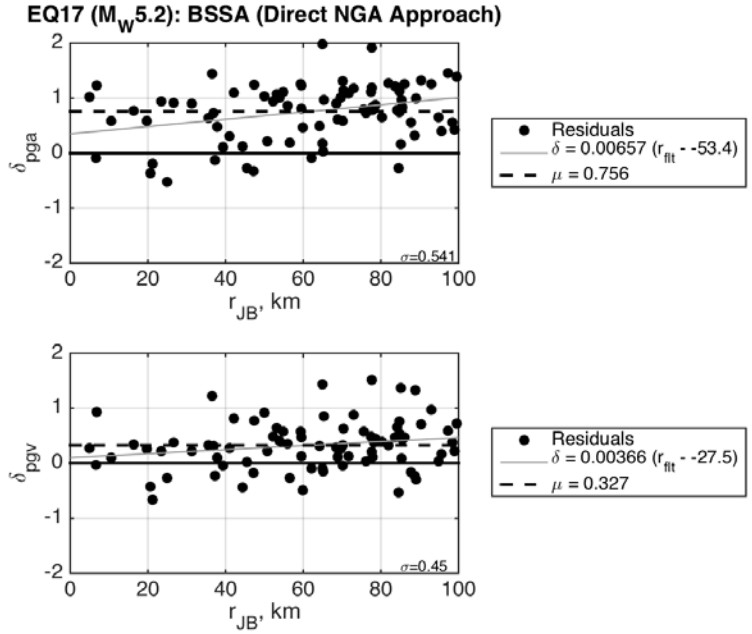

Figure 176: Raw delta BSSA

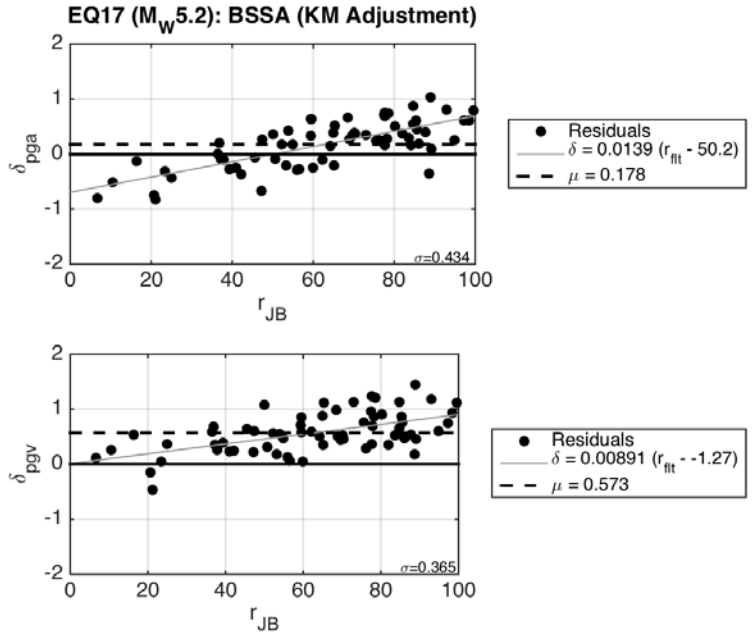

Figure 177: Adjusted delta BSSA

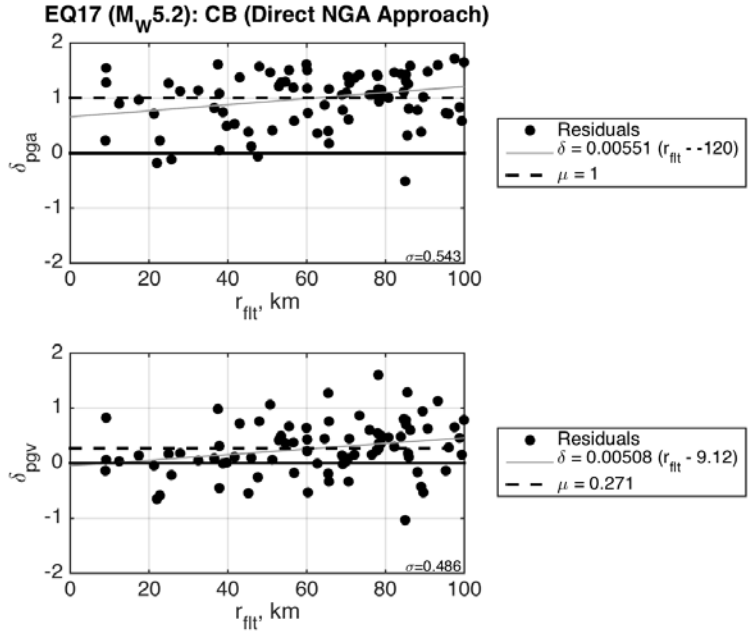

Figure 178: Raw delta CB

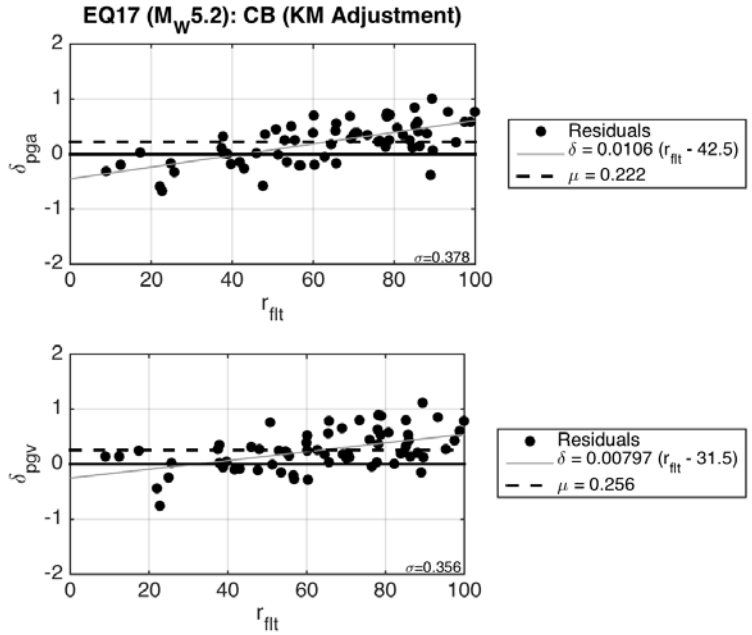

Figure 179: Adjusted delta CB

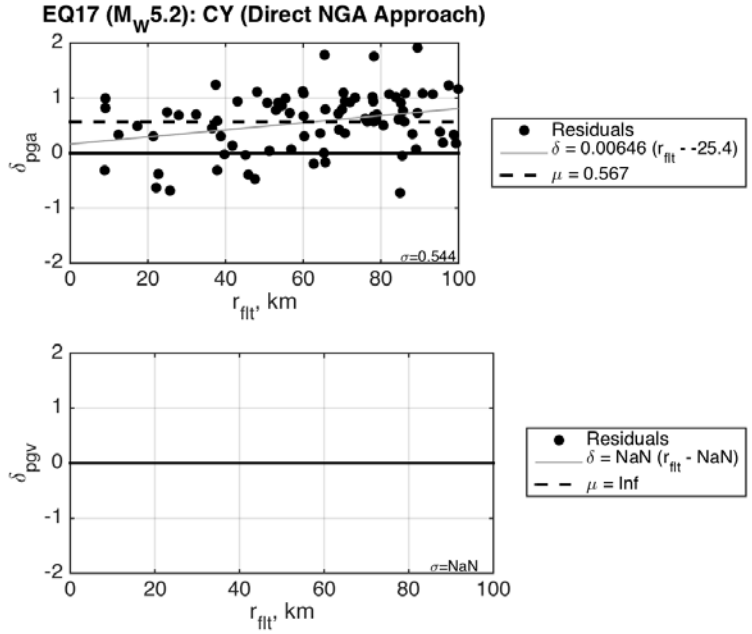

Figure 180: Raw delta CY

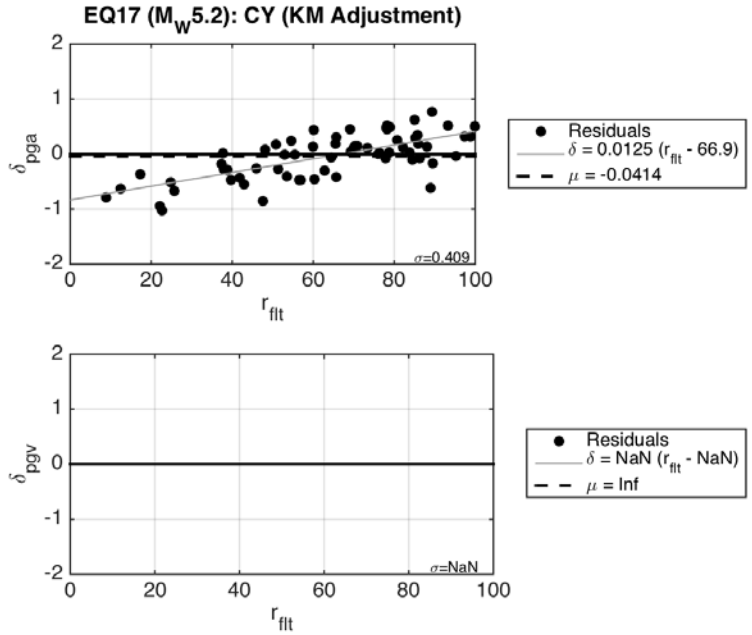

Figure 181: Adjusted delta CY

14 Earthquake 18. 2013 12 31, 10:03 Mw5.1

Figure 182 shows four frames illustrating the geometry of this earthquake.

Figure 183 shows the uncorrected values of peak acceleration as a funciton of distance, and Figure 185 shows the uncorrected values of peak velocity. For comparison, both of these figures show the NGA-West 2 models for Vs30=400 m/s, which is considered to be a reasonable estimate for the network average. Figure 184 shows the adjusted peak accelerations and Figure 186 shows adjusted peak velocities, where the adjustments to the data use Kawase factors and are adjusted to Vs30=760 m/s. Therefore, the NGA curves on these two firgures are for Vs30-760 m/s.

Residuals are shown in Figures 187-194. Raw and adjusted residuals are paired for ease in comparison. To obtain the "raw" residuals, a station-by-station estimate of Vs30 has been used within the NGA models. Since the adjustments are to a common value of vs30, station-by-station adjustments are not needed.

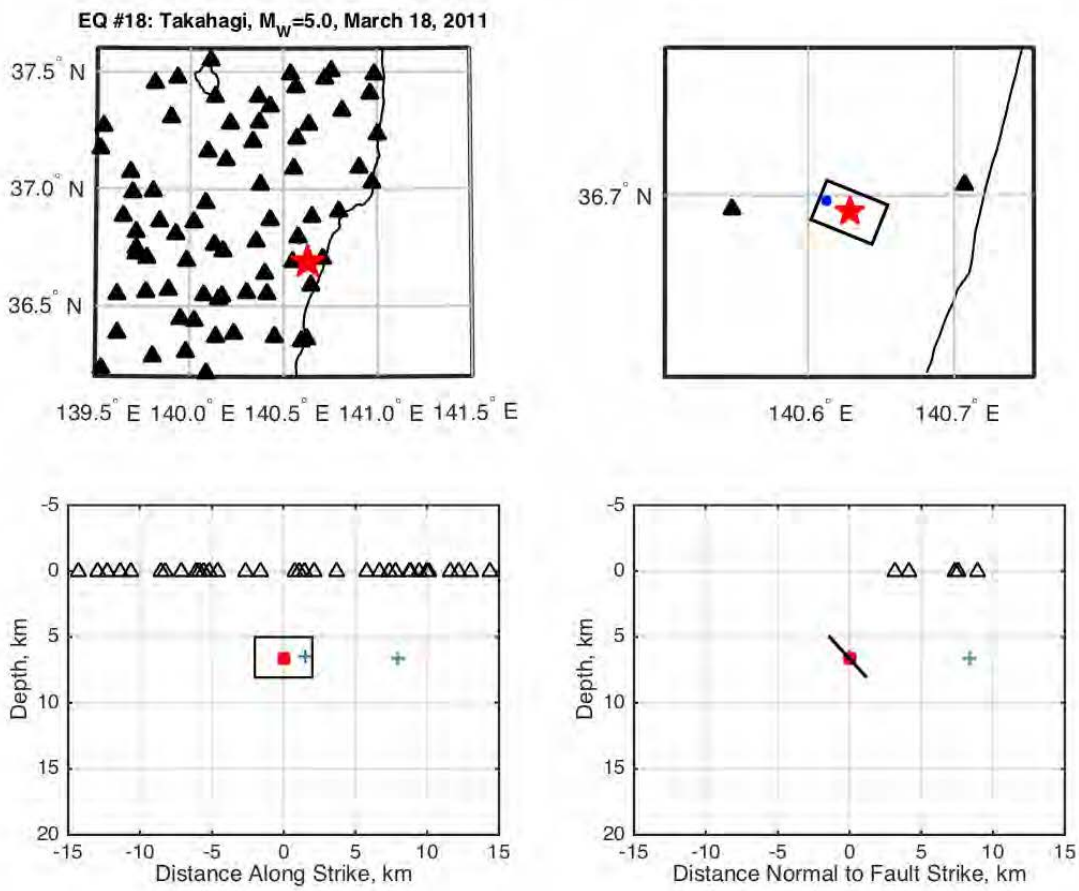

Figure 182: Location and cross section

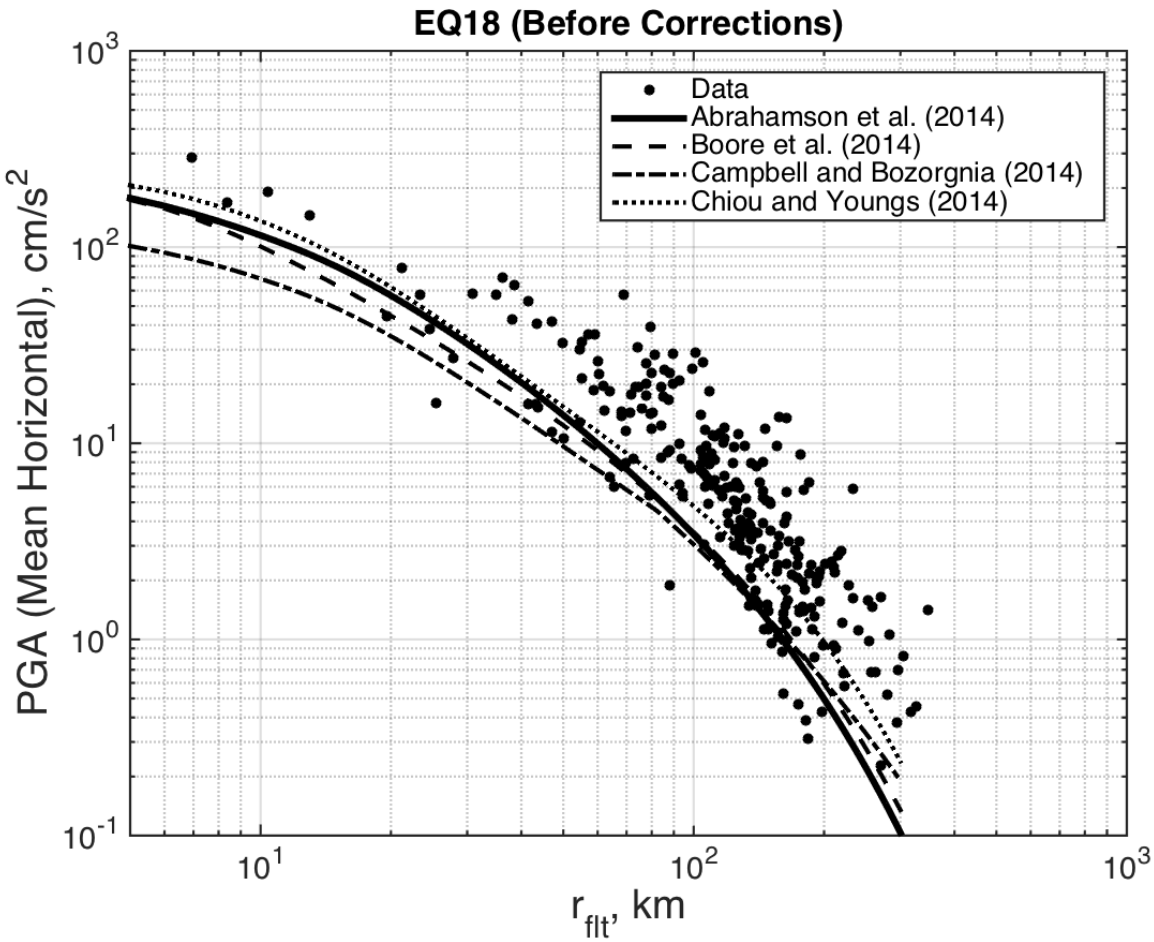

Figure 183: Raw accelerations

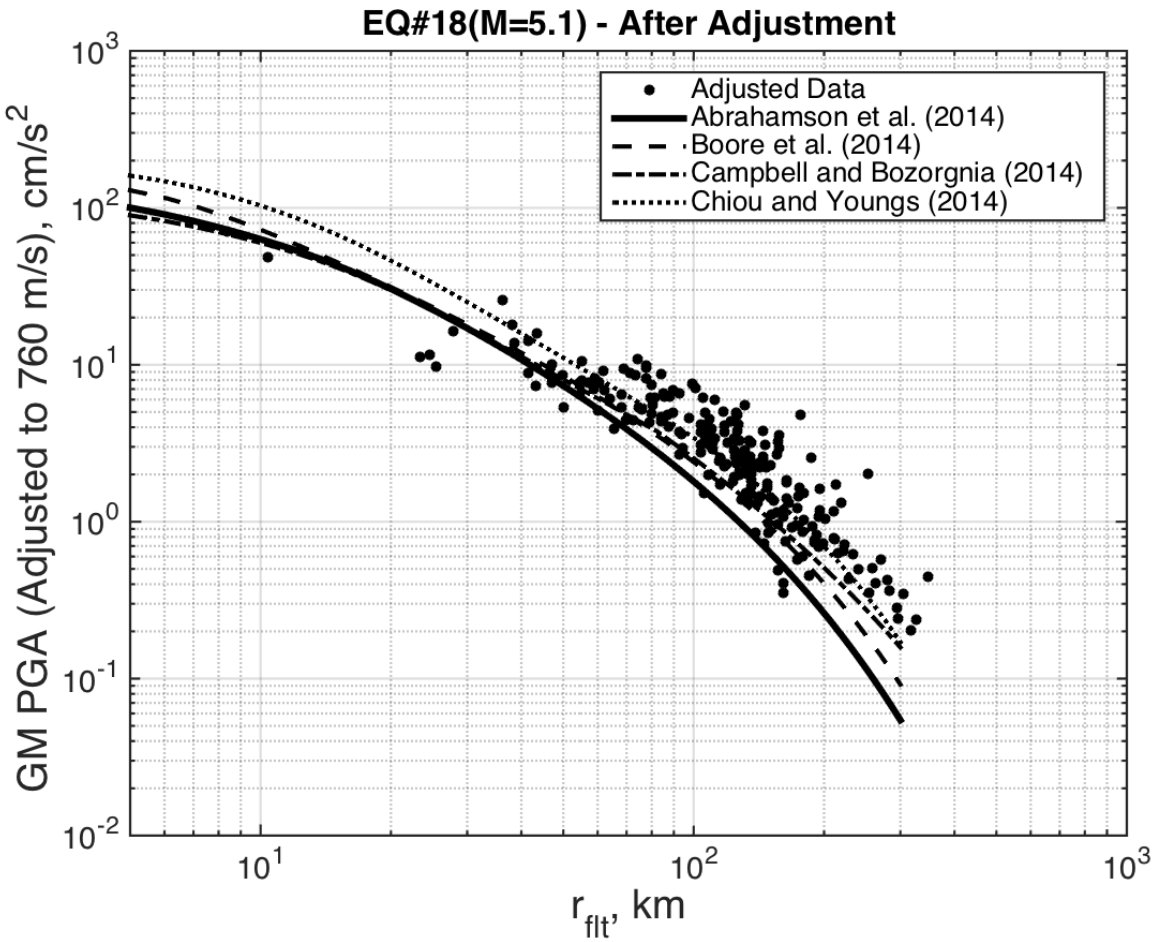

Figure 184: Adjusted accelerations

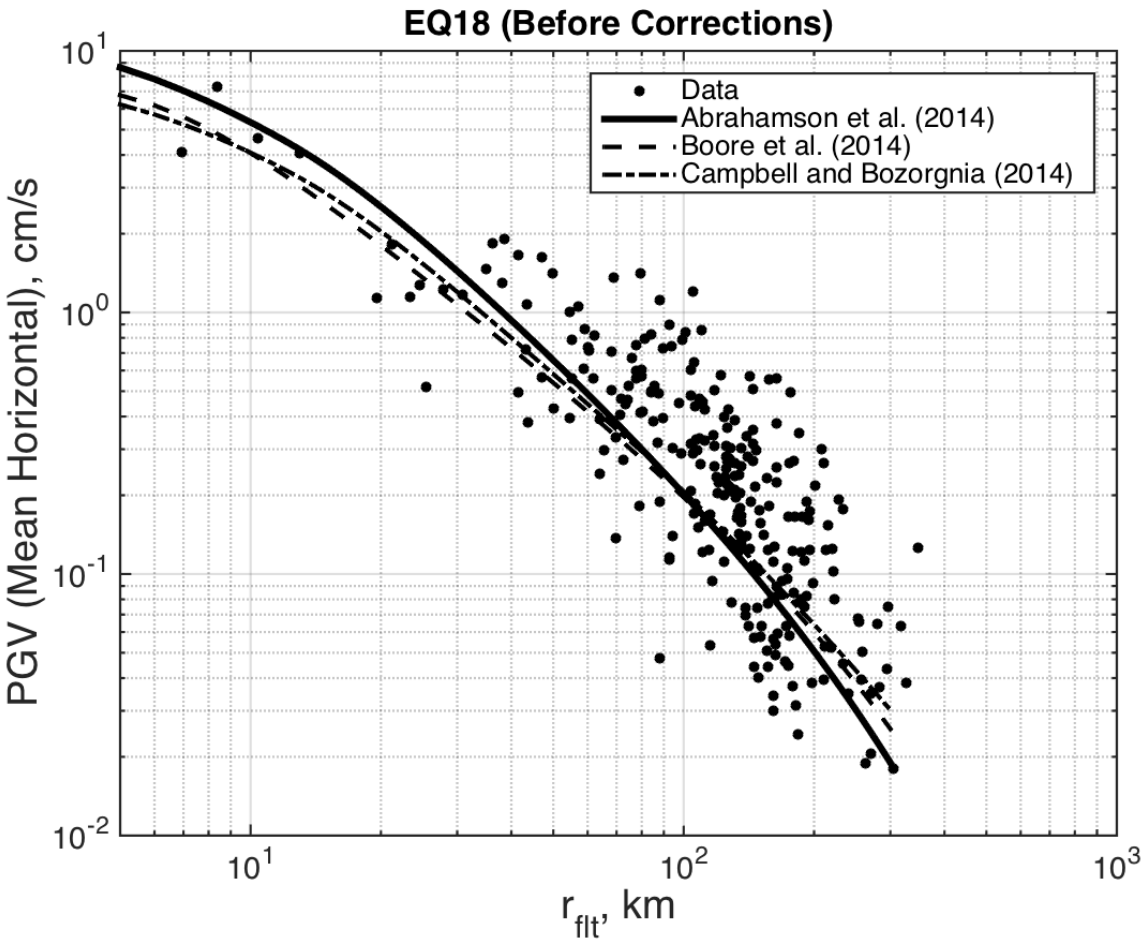

Figure 185: Raw velocities

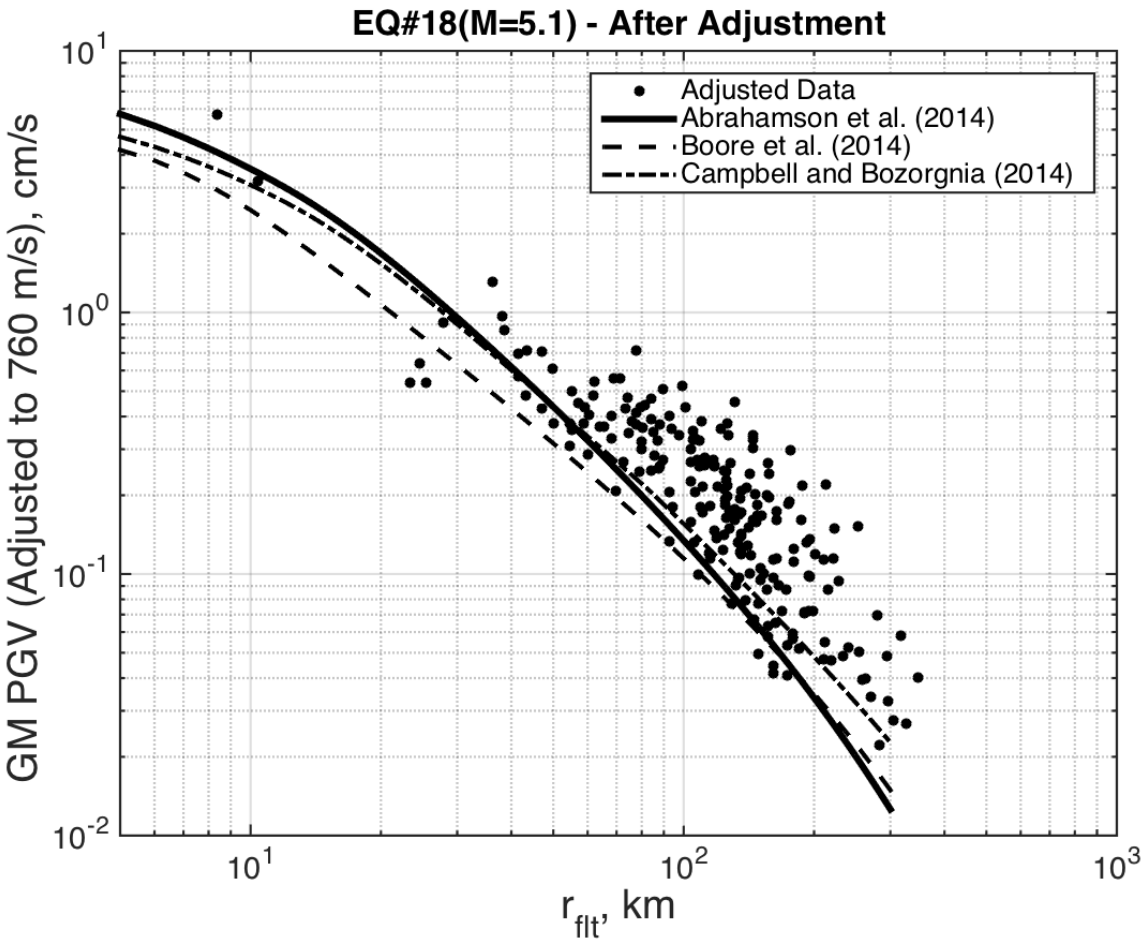

Figure 186: Adjusted velocity

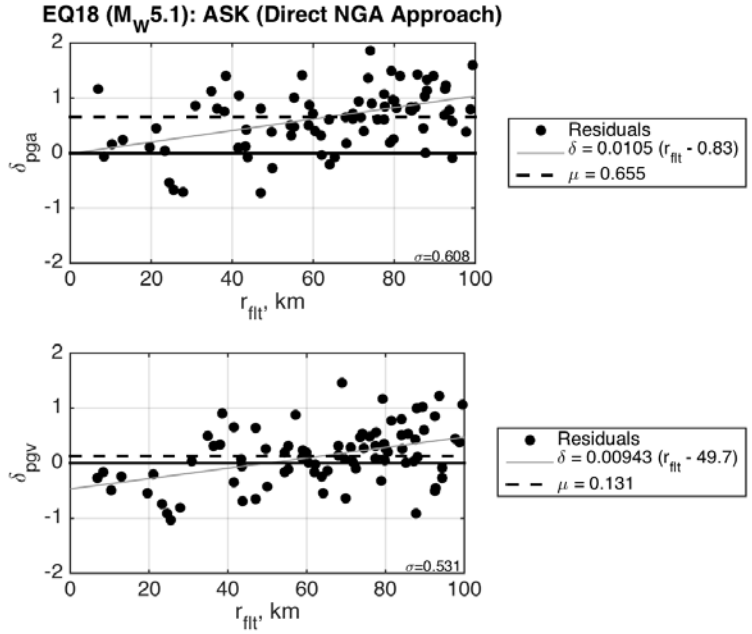

Figure 187: Raw delta ASK

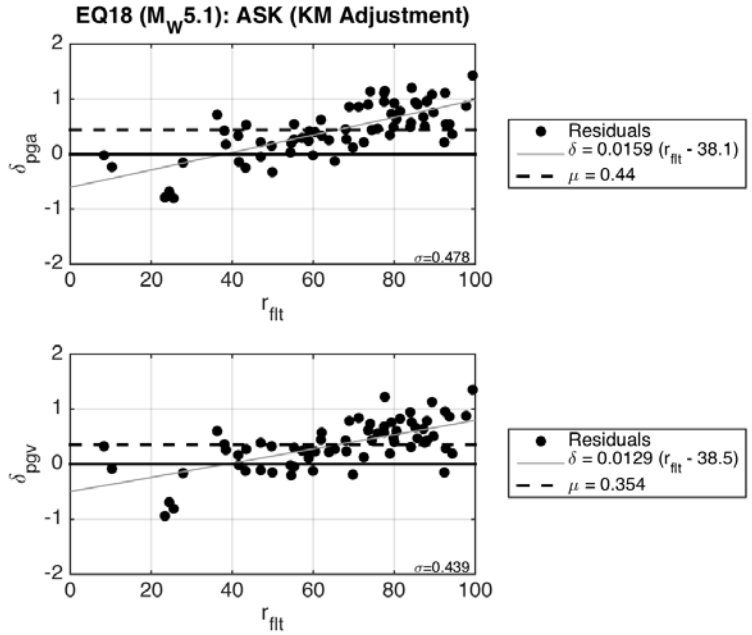

Figure 188: Adjusted delta ASK

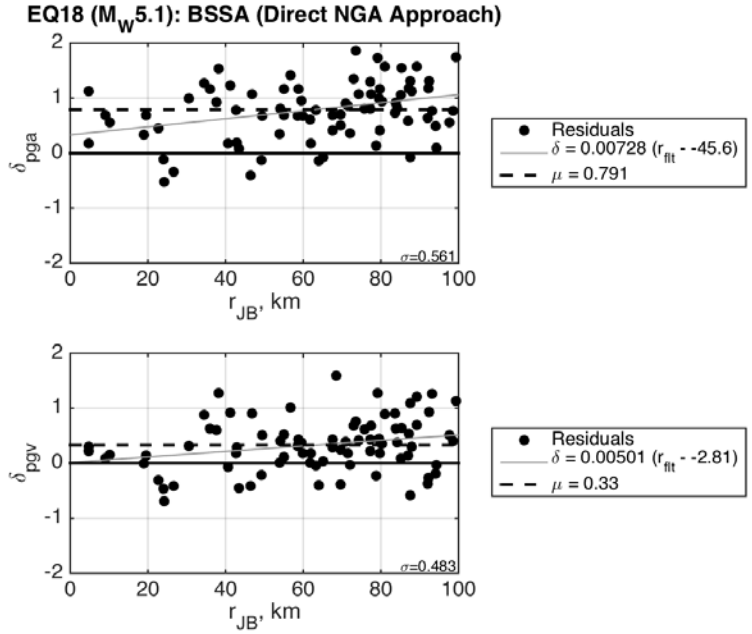

Figure 189: Raw delta BSSA

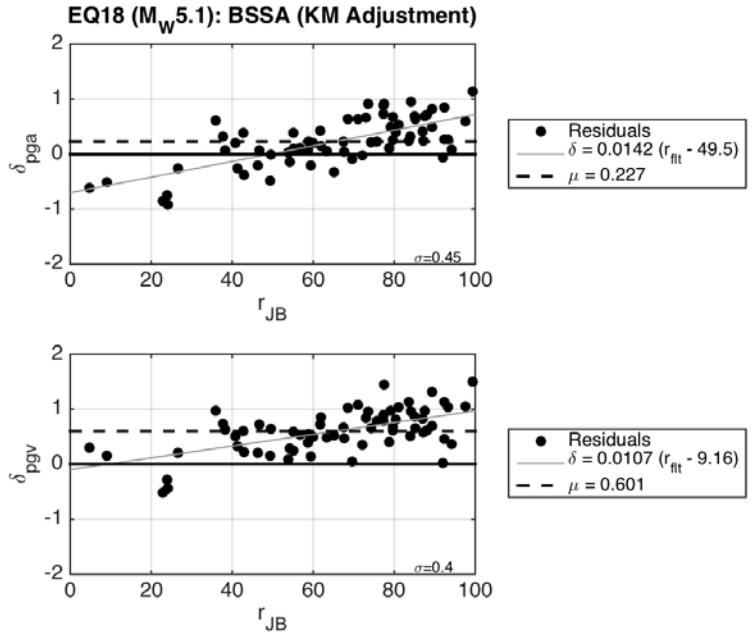

Figure 190: Adjusted delta BSSA

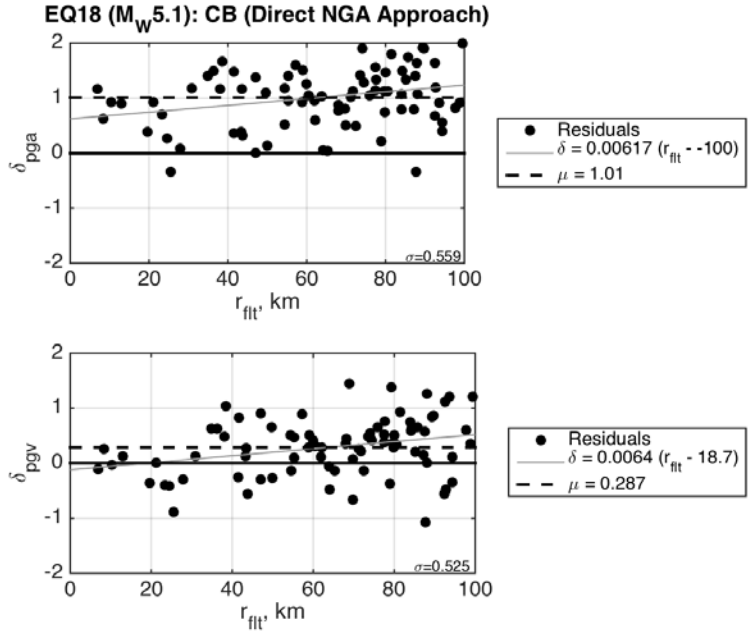

Figure 191: Raw delta CB

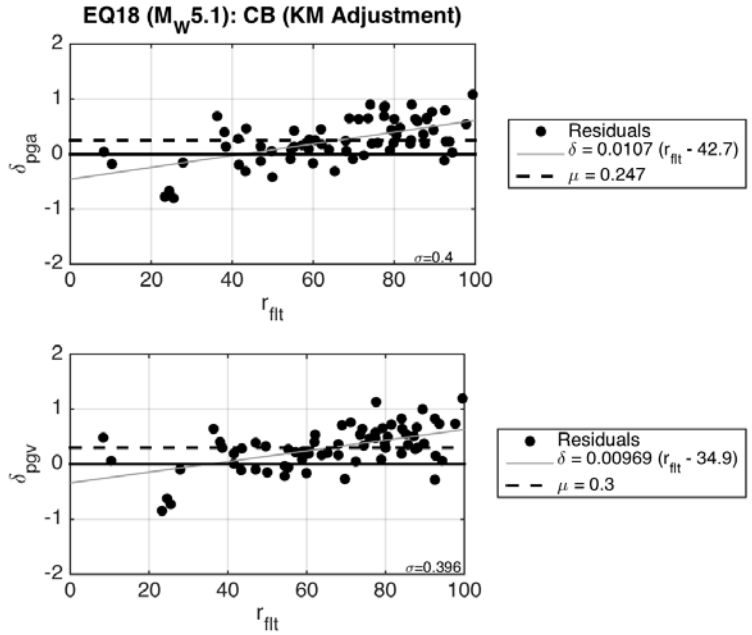

Figure 192: Adjusted delta CB

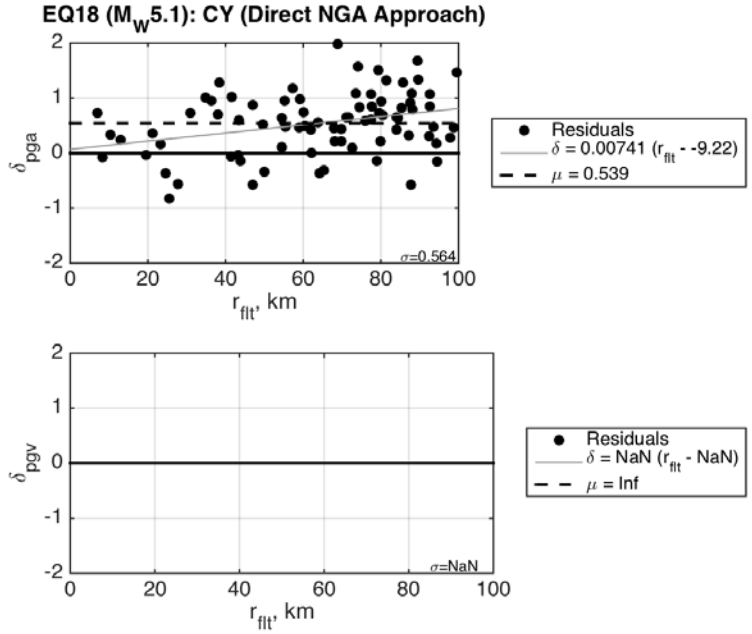

Figure 193: Raw delta CY

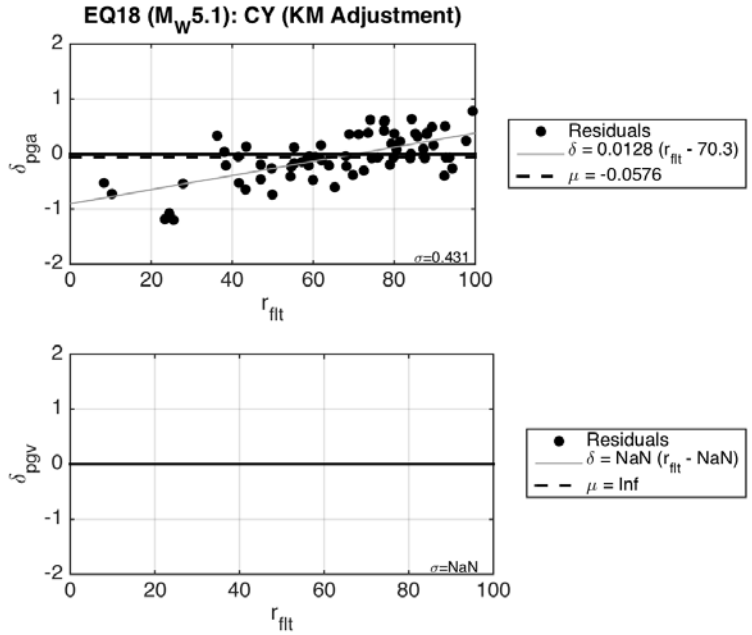

Figure 194: Adjusted delta CY